Damage potential of seismic ground motion considering local site effects

Schadenspotential seismischer Bodenbewegung

unter Berücksichtigung lokaler Standorteffekte

Dissertation

zur Erlangung des akademischen Grades

Doktor-Ingenieur

an der Fakultät Bauingenieurwesen

der

Bauhaus-Universität Weimar

vorgelegt von

Dipl.-Ing. Dominik H. Lang

aus Leonberg/Baden-Württemberg

Weimar 2004

Gutachter: 1. Dr.-Ing. J. Schwarz

2. Prof. Dr.-Ing. habil. C. Könke

3. Prof. Dr. P. Gülkan

Tag der Disputation: 08. Juli 2004

Acknowledgments

Table of contents

1 Introduction

1.1 Influence of local site effects on structural damage

When earthquake phenomena began to receive scientific consideration at the beginning of the twentieth century, the relationship between damage to buildings and properties of subsoil has been expressed in the saying that "earthquake damage is great where the ground is poor" [KANAI, 1983].

Today, it is well known that the extent of earthquake damage depends on different factors, taking into account the effects of the earthquake (source and path effects), the local subsoil and the structure itself than on the subsoil's quality alone.

According to SEED & IDRISS (1982), the factors influencing the characteristics of earthquake ground motion at any site can be summarized as follows:

- magnitude of the earthquake,
- distance of the site from the source of energy release,
- geologic characteristics of the rocks along the wave transmission path from the source to the site,
- source mechanism of the earthquake,
- wave interference effects related to the direction and speed of fault rupture,
- local soil conditions at the site.

Local soil conditions can clearly impinge on the dynamic characteristics of site response during earthquake excitation. The so-called *seismic site effects* can be subdivided into direct seismic site effects and indirect seismic site effects. An explicit definition of both terms is given by WANG & LAW (1994):

Direct seismic site effects   The earthquake resisting behavior of the site and ground soil is weak, resulting in a certain type of ground failure, which is apparently visible and commonly recognized. The main patterns of such a failure are seismic liquefaction of the soil (resulting in settlements and tilting of structures), seismic settlement, collapsible settlement (e.g. earthquake-induced collapse of underground cavity or presence of surface rupture), and seismic landslide provoked by slope instability.

Indirect seismic site effects   The ground soil is strong enough to resist earthquake interference and remains stable. However, seismic waves transmitted through the ground material may be magnified either in amplitude, in frequency content, or in time duration. Examples of this type of site effect are wave-field effects, amplification/filtering effects of soft ground, and resonance effects not only of earthquake excitation and subsoil, but also of the structure.
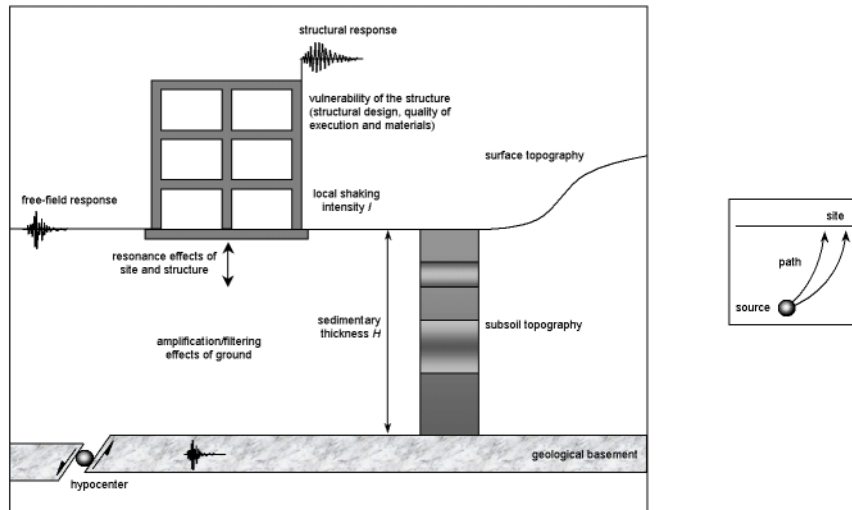
Figure 1.1 Parameters influencing seismic ground motion and thus structural damage.

While direct seismic site effects are obvious, and if they occur, mainly responsible for damage, it could often be observed in the last years that indirect seismic site effects, such as resonance effects between site and structure, were used for damage interpretation in order to divert from structural deficiencies.

Allowing a vast interpretation of earthquake damage, additional aspects concerning the level of local shaking intensity at the site as well as structural design, reflecting the building's vulnerability and structural deficiencies have to be taken into account.
In this context, it should be kept in mind that structural damage occasioned by an earthquake is a final result of the interaction between soil and structure; for this reason the vibrational characteristics of the structure should also be considered (MOORE, 1979).

The main parameters influencing structural damage during earthquakes are illustrated in Figure 1.1. Besides the level of local shaking intensity and the vulnerability of the structure, characteristics of the site and subsoil are presented, strongly affecting the seismic ground motion at the building site. Local shaking intensity embodies all influences on seismic waves between the source and the site of interest, including source, path, and site effects.
Since direct seismic site effects (e.g. soil liquefaction or slope instability), is not the subject of the present work, they are not presented in Figure 1.1.

Local site effects can modify seismic waves in frequency characteristics, amplitude level, and time duration, usually resulting in resonance effects of the site and structure or amplification effects of soft soil layers. Both subsoil topography and surface topography may contribute to the appearance of local site effects. In order to identify these effects, instrumental recordings of seismic ground motion at the site of interest are necessary. By the application of *site response estimation techniques* on the recorded seismic data, an identification of local site effects may be carried out, establishing a link between ground motion characteristics and local structural damage.

The greatest impacts of damage-inducing earthquakes do not automatically appear in the epicentral area. The characteristics as well as the level of amplification of seismic ground motion are strongly influenced by local subsoil conditions. As a result, it is possible that stronger ground motion (higher intensity of shaking) occurs in larger epicentral distances when unconsolidated sediment layers with critical thicknesses are present.

The potential of seismic ground motion to inflict damage to man-made structures, resulting from local site effects, level of ground shaking, and structural deficiencies, is denoted as the *damage potential*. According to RAHNAMA & KRAWINKLER (1991), the damage potential of ground motion depends on both the "severity" of ground shaking and the ability of the structure to resist this shaking. Consequently, assessing the structural vulnerability of damaged buildings is of the utmost importance in terms of establishing the damage potential of seismic ground motion.

The damage potential concept of SEED & IDRISS (1969) is based both on the estimation of forces and motions that are induced in structures of any type during earthquakes, and the effects of this dynamic response on structural performance. The structural damage potential of earthquake ground motion depends on the maximum acceleration and frequency characteristics of the motions, while the frequency characteristics are influenced by soil conditions at the structure site. They also postulate that when analyzing the damage potential of a structure, it is necessary to take its structural characteristics into account, such as the type of framing, quality of materials, and design seismic forces.

1.2 Current state of research

During the past decade, numerous research projects have been initiated dealing with the identification of local site effects (in view of interpreting structural earthquake damage). Special attention has been turned to the development of site response estimation techniques and to the improvement of numerical simulation methods. Although most of the investigations concentrated on earthquake-endangered areas and provide comprehensive data about structural earthquake damage, their outcomes are not explicitly used to interpret the damages. Annex 1 summarizes some of those recent publications, which made an attempt to connect the results of site response estimation techniques with damage to buildings. Table 1.1 briefly compares the main subjects of the selected publications.

Table 1.1 Evaluation of selected publications on site studies and structural earthquake damage.

Author	Topic, subject [1]				
	application of seismic ground motion data (site response estimation techniques)	verification/ identification of local site conditions	experimental investigation of dynamic characteristics of buildings	link between seismic ground motion and structural damage	identification of the damage potential of seismic ground motion
ARAI *et al.* (2000)	●	●	●	●	●
BORCHERDT *et al.* (1989)	●	○	○	◐	○
CHÁVEZ-GARCÍA *et al.* (1990)	●	●	○	◐	○
DUVAL *et al.* (1998)	●	●	○	◐	○
FIELD *et al.* (1992)	●	●	○	◐	○
FUJIWARA *et al.* (2000)	●	○	●	◐	○
JONGMANS & CAMPILLO (1990)	○	●	○	●	◐
NAKAMURA (2000)	●	○	○	●	○
NAKAMURA *et al.* (2000)	●	◐	○	●	○
OHMACHI *et al.* (1991a)	●	○	●	◐	○
OHMACHI *et al.* (1991b)	●	●	○	●	◐
ÖZEL *et al.* (2002)	●	○	●	◐	○
SEO *et al.* (2000)	●	◐	○	◐	○

[1]   ● yes (well)   ◐ coarse (moderate)   ○ no (bad)

It is obvious from Table 1.1 that most of these publications try to identify the effects of site conditions on seismic ground motion and structural earthquake damage, even though their outcomes are neither convincing nor feasible. The one exception to this are ARAI *et al.* (2000), who correlate the results of site studies performed in Gölcük (Türkiye) with the overall damage ratio of buildings, and, with instrumental investigations of individual, multistoried buildings.

One of the main distinguishing aspects of these scientific works appears in the dimension or scale of the investigation. As can be seen in Annex 1, three different types of investigation scales are distinguished:

- site-specific, being concentrated on single sites or damage cases, and thus allowing a more precise investigation of the damaging effects;
- local, referring to small urban areas or districts, possibly leading to an identification of changes in subsoil conditions through ratios of damage occurrence;
- regional, referring to spacious areas, such as large cities or geological basins, and consequently leading to more generalized investigation results.

The different quality levels of reviewed publications were also conducive to the ascertained procedure of the work at hand.
In order to identify the reasons of structural damage during earthquakes, site-specific studies at single damage cases seem to be more successful and target-oriented than investigations on the local or regional scale.

1.3 Strategy and objective

The main objective of the present work is to establish a link between the scientific fields of engineering seismology and structural engineering. Since most of the scientific works dealing with experimental site studies and structural earthquake damage (an assortment was presented in Section 1.2) are misleading with respect to damage interpretation and its practical application for engineering purposes, this work attempts to provide an alternative approach of damage interpretation.

Based on real occurred earthquake damage inflicted to reinforced-concrete frame buildings, the *damage potential of seismic ground motion considering local site effects* was worked out. Comprehensive investigations at selected damage cases in affected regions of Türkiye and Venezuela were therefore carried out. These focus on the following points:

- the documentation of the structural layout, the damage occurrence, and the site conditions,
- instrumental recordings of the free-field site response (earthquakes and ambient noise),
- the experimental identification of the structures' dynamic characteristics, but only in a few cases.

This information allows for the causes of structural earthquake damage to be determined, including the influence of local site effects possibly amplifying the seismic ground motion at the site. Since the studies are concentrated on typical building types representative for the affected regions, this work also tends to future damage predictions or loss scenarios during earthquake disasters.

The present work can be regarded as an interdisciplinary attempt to interpret structural earthquake damage, incorporating all possible influences that come from seismic excitation, site and subsoil conditions, and structural vulnerability in terms of the quality of structural design and building materials. In doing so, the work is structured as follows:

- Since the instrumental site studies are the essential basis of the present work, the characteristics of the applied types of seismic ground motion data are comprehensively presented. Chapter 2 describes their main features, influencing parameters as well as dependencies.

- Chapter 3 displays the methodical basics and an assortment of site response estimation techniques in order to derive the amplification potential of seismic ground motion. In other words, the reliability of selected methods, either analytical or empirical, is investigated with regard to their application for engineering purposes, such as the elaboration of parameters needed for structural design.

- A first practical application of these site response estimation techniques is given in Chapter 4. On the basis of the rough parameters available for soil materials and seismic ground motion data, a hybrid procedure of seismic site assessment is developed. Besides the classification of the site according to a generally accepted scheme, the *Method of an Experimental Seismic Site Assessment, "MESSIAS"* (LANG *et al.*, 2003a), allows for the selection of suitable seismic loads to be made. This assumes that no instrumental records of the damaging event are available at the site. Consequently, MESSIAS provides the basis for a reliable analysis of structural earthquake damage.

- The intrinsic procedure of earthquake damage interpretation is presented in Chapter 5. Information coming from the site, the seismic excitation, and the structure (including the extent and pattern of actual damage) are brought together in order to derive the damage potential of seismic ground motion. Special attention is paid to the identification of both structural performance incorporating the results of experimental investigations on the structural response, and of the nonlinear static "pushover" analysis.

- The procedure to identify the damage potential of seismic ground motion is applied to selected damage cases in Chapter 6. For reasons of reliability, the procedure at first is applied to pure RC frame structures, for which knowledge level of input data is high. However, its applicability to RC frames with masonry infill walls is also prepared. For those damage cases being already available, an evaluation of damage potential of seismic ground motion is carried out on a more superficial level.

1.4 Applied database

The present work requires a broad database not only about cases of structural damage but also about seismic ground motion data. The low seismicity in German earthquake regions, as well as the nonexistence of structural damage data caused by stronger earthquakes, lead to the necessity of collecting data in foreign areas where earthquakes are prevalent. Table 1.2 lists strong earthquake events after which reconnaissance missions led by German TaskForce for Earthquakes took place. In addition to the field missions that happened immediately after the

mainshock, several Post-TaskForce missions were initiated in order to carry out supplementary investigations, including the recordings of ambient seismic noise or dynamic experiments (vibration analysis) on selected RC frame structures.

Except for using small databases from, for example, the European Strong-Motion Database ESMD (AMBRASEYS *et al.*, 2000), all data of seismic ground motion in this paper was collected during TaskForce missions as listed in Table 1.2, as well as by additional field work in Germany (see Chapter 4).

A comprehensive overview of the available databases of seismic ground motion is given in Section 2.4, and in Annex 2.

Table 1.2 Missions of German TaskForce for Earthquakes during which data was collected.

Earthquake event	Date	Reconnaissance mission			Post-TaskForce mission		
		Tasks [1]			Date	Tasks [1]	
		aftershock observation	structural damage analysis	noise recordings		noise recordings	vibration analysis of RC frames
Cariaco (Casanay)	09.07.1997	●	●	○	05.1999	●	●
Adana (Ceyhan)	27.06.1998	●	○	○	10.2000	●	○
İzmit (Kocaeli)	17.08.1999	●	●	○	09.2002 10.2000	● ●	○ ●
Düzce (Bolu)	12.11.1999	●	●	○	10.2000 09.2002	● ●	○ ●
Sultandağı (Afyon)	03.02.2002	●	●	○	09.2002	●	●
Bingöl	01.05.2003	○	●	●	-	-	-

[1] ● performed   ○ not performed

2 Seismic ground motion data

2.1 Ambient seismic noise (*microtremors*)

2.1.1 Terms and descriptions

Regardless of the type of seismic signal one wants to observe, instrumental recordings of ground motion always contain a certain level of ambient seismic noise. This means that the ground is never truly at rest. Since all energy-producing sources excite seismic waves, and because nonhuman sources, such as oceanic and meteorological disturbances, are continuous, a certain level of background noise exists at all times. Therefore any recording of transient waves must be made in the presence of this noise (LAY & WALLACE, 1995).

Ambient seismic noise at any site can be considered as being caused by a set of (surface) sources randomly arranged and with varying amplitude (LACHET *et al.*, 1994). This makes it very difficult to simulate urban noise deterministically.
Scientists had controversial discussions in the past about the types of waves ambient seismic noise consists of. While UDWADIA & TRIFUNAC (1973) showed that noise can be composed of any of the common seismic wave types, KANAI (1983) assumed that mainly vertically incident *S*-waves are contained in noise. Meanwhile, these hypotheses have been dismissed by a number of scientists, showing that noise mainly consists of surface waves (AKI, 1957; BARD, 1998; LERMO & CHÁVEZ-GARCÍA, 1994).
Although we are discussing here which wave types are intrinsically participating, there is no doubt that ambient seismic noise represents oscillations in depth at a site and is not merely a surface phenomenon (CHERRY & SALT, 1971).

The seismic noise recorded at the ground surface is strongly subjected to temporal and seasonal fluctuations. This noise is usually considered as a temporally and spatially variable, while not being uniform at all frequencies.

According to scientific literature, ambient seismic noise is thought to be composed of "microseisms" and "microtremors". Whereas the first represents long-period noise, mainly generated by natural origins, the latter is assigned to short-period noise with artificial origins. Table 2.1 summarizes the different perceptions in order to distinguish between short-period microtremors and long-period microseisms according to different reference points. The limit

between microtremors and microseisms should not be fixed at a single marginal frequency, for example at 1.0 Hz. SEO (1997) already showed that the border line between these two domains may be shifted to longer periods (up to a few seconds). In urban areas characterized by low frequency and high impedance-contrast subsoils, for example, artificial microtremors may be more energetic than natural microseisms even at intermediate periods (up to a few seconds).

Table 2.1 Distinction between long-period and short-period noise according to different authors.

Author, Reference	Marginal frequency, f	Microseisms: long-period noise [1]	Microtremors: short-period noise [1]
AKI, 1957	1.0 Hz		> 1.0 Hz: traffic
ANSARY et al., 1995	1.0 Hz	< 1.0 Hz: R_g- and L_g-waves originating from natural sources, such as sea waves	> 1.0 Hz: generated by artificial noises, such as traffic vehicles, industrial plants, and household appliances
BARD, 1998	1.0 Hz	< 0.3/0.5 Hz: ocean waves at long distances (0.3/0.5)-1.0 Hz: close coastal sea waves and wind	> 1.0 Hz: human activity, reflecting human cycles
CHERRY & SALT, 1971			continuous ground motions whose amplitudes range from between 0.1-1.0 microns; believed to originate primarily from artificial (man-made) sources
FIELD et al., 1990	1.0 Hz	0.2-1.0 Hz: oceanic disturbances	
LERMO & CHÁVEZ-GARCÍA, 1994	0.5 Hz	< 0.5 Hz: atmospheric perturbations over the oceans (propagating as R_g and L_g phases over continental paths)	> 0.5 Hz: R_g waves excited locally from traffic disturbances near the recording site
NAKAMURA, 1989	0.3-0.5 Hz	< 0.3-0.5 Hz: sea waves	> 0.3-0.5 Hz: storm and artificial forces

[1] R_g - Rayleigh wave L_g - Love wave

2.1.2   Influencing parameters

The characteristics of ambient seismic noise are strongly influenced by different parameters that come from temporal, seasonal, and regional variations.

The main aim of microtremor measurements in the context of site response studies is to separate the regional characteristics of the site from temporal and seasonal variations at the time of recording.

(a)   *(b)*
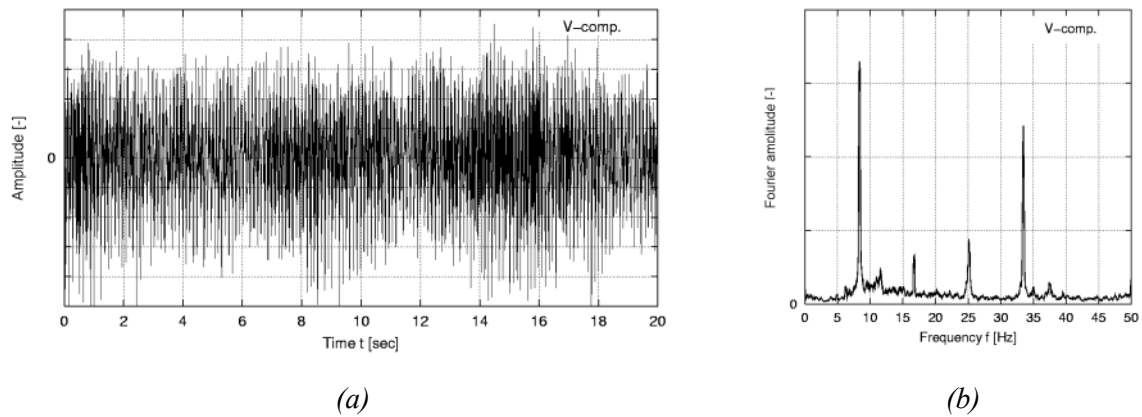
Figure 2.1 Vertical component of a seismic recording close to an electricity aggregate (a), and its corresponding FFT-spectrum (b).

Temporal or seasonal variations of ambient seismic noise can generally be attributed to human activities or meteorological action. While the first leads to an explicit daytime-dependency due to the usual decrease of human or industrial activity during the nighttime ($f >$ 1 Hz), the latter can result in both short-term (e.g. rainfall, wind, storm) and long-term variations (seasonal variations, e.g. stronger oceanic sea disturbance during wintertime).
Other meteorological influences, such as changes of air temperature or atmospheric pressure, were investigated by several scientists. An impact on the stability of ambient seismic noise could not be proved (FRANTTI, 1963; GAULL *et al.*, 1995; BARD, 1998; MUCCIARELLI, 1998).

A more explicitly distinguishing feature is that human activities mainly affect the frequency range above 1 Hz, whereas meteorological variations mainly influence the short-frequency range below 0.5/1.0 Hz.

Besides these temporal and meteorological influencing parameters, noise recordings can be affected by a variety of other factors. Water movements, in general, may influence the short-frequency range of ground motion. As LAY & WALLACE (1995) pointed out, wave surf and standing waves in the ocean are some of the primary sources of seismic noise, mostly affecting frequencies between 0.15 and 0.20 Hz. Thus island sites or sites close to the seashore will be much noisier in this particular frequency range than land sites well removed from the coast.

According to BORCHERDT (1970), care must be taken to avoid nearby cultural noise sources and perturbing signals which have not traveled through the underlying soil. This effect can be observed close to running machines, turbines, electrical generators, or water pumps. Figure 2.1 shows a 20 second cut-out of a seismic recording close to an industrial site and its corresponding Fast-Fourier-Spectrum (*FFT*). The distinct narrow-band peaks of the spectrum indicates the presence of disturbing signals being produced by an adjacent aggregate.
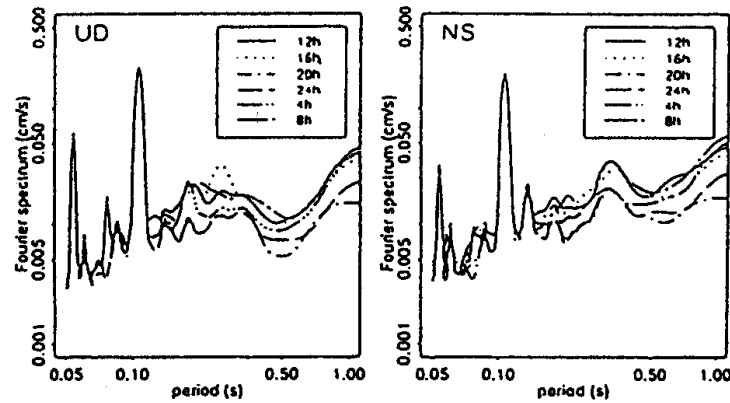
Figure 2.2 Fourier spectra of vertical (left) and horizontal components (right) of ambient noise at different daytimes with a 0.1 second peak caused by machine vibration (ANSARY *et al.*, 1995).

ANSARY *et al.* (1995) also found some narrow-band peaks in Fourier spectra of both horizontal and vertical components of ambient noise (Figure 2.2). They interpreted the peak in the short-period range at about 0.1 sec caused by the vibrations of machinery in a nearby machine room.

In order to ensure a high quality of noise recordings as well as analysis results representing the ground response characteristics, additional aspects have to be regarded. Table 2.2 specifies some of these aspects that depend on three different steps of processing:

-   choice of acquisition system and instrumental parameter settings,
-   selection of recording site and recording date,
-   parameters of data processing.

2.1.3   Practical application

The importance of ambient seismic noise data with regard to its practical application, e.g. for an engineering purpose, is increasing. In comparison to earthquake data, the characteristics of ambient seismic noise do provide two main advantages:

-   Since microtremor measurements do not depend on a certain seismic event, they can be performed at any time and at any place (AKI, 1988; BARD, 1998). This in turn allows for an application of instrumental site studies even in areas of low seismicity (FIELD & JACOB, 1993).
-   Because noise itself is the data, an application even in noisy urban areas or at highly congested sites is possible (KANNO *et al.*, 2000; SATOH *et al.*, 2001a).

Compared to long-term earthquake observations, theoretical studies on the basis of borehole data or seismic prospecting methods, such as reflection or refraction surveys, microtremor measurements are time- and cost-effective (FIELD & JACOB, 1993; KANNO *et al.*, 2000).

Table 2.2 The impact of instrumental settings, conditions at the site during acquisition, and data processing on the quality of noise recordings.

Item	Subject	Prefer	Avoid
1 Instrumental settings			
1.1	type of seismic sensor, digitizer	velocity-proportional sensors (preferably 5- to 10-second seismometers)	accelerometers, due to their low resolution capability in the low-frequency range (BARD, 1998; MUCCHIARELLI, 1998)
1.2	peripheral equipment (cables)	limited cable lengths in order to minimize probable damage	long external wirings, which may also produce mechanical and electronical interferences
1.3	duration of recording	continuous recordings over a couple of days or repeatedly recordings at different daytimes in order to check the daytime-dependent stability of noise	total noise duration less than 30 minutes
1.4	sample frequency	sample frequency should be at least twice as large as the upper cut-off-frequency of the sensor	low sample frequencies, since they negatively affect the spectral resolution
2 Site conditions			
2.1	topographical situation	free field recording sites with plane-like topography	topographical features like hillsides or steep slopes, since they strongly influence the noise wave-field, leading to adverse effects (see Section 3.1.3.3)
2.2	geological situation	natural soil	artificial infills or replenishments
2.3	local base of sensor	consolidated materials closely connecting the sensor (reliability of results increases, if the sensor is placed in a dug-out hole)	paved or tarmac roads
2.4	environmental disturbances	-	mechanical or electronical devices in the close vicinity of the sensor (e.g. electricity cables, high voltage pylons, machines, turbines, pumps, etc.) or elevated structures (e.g. multistoried buildings, towers, masts).
2.5	meteorological disturbances	-	wind gusts and rainfall
3 Data processing			
3.1	type of spectra	Fourier or FFT-spectra, (in some cases: cross correlation spectra, GHAYAMGHAMIAN *et al.*, 1995)	response spectra
3.2	"windowing" (length of FFT-window)	longer time windows, because the analyzable frequency range (regarding the first frequency value > 0) and the spectral resolution increases	-
3.3	averaging, smoothing (filtering techniques)	averaging the spectral curves in order to increase reliability	heavy smoothing at the expense of clarity and plausibility of results

Environmental impairment also does not occur, the importance of which is increasing (BARD, 1998).

One should also bear in mind the negative aspects as well as the application limits of ambient seismic noise. Some of them can be summarized as follows:

- Nonlinear effects are not covered by investigations based on ambient noise data. Only weak-motion site response is provided by these observations.
- The characteristics of ambient seismic noise are very different from site to site. This holds true even at nearby stations and especially in the short-period range. This leads to a large uncertainty in the spectral amplitudes, reflecting more strongly the source and path effects of the signals than the local site conditions (BARD, 1997).
- It is impossible to separate source-path effects of ambient noise from the site effects (AKI, 1988).
- Significant variation in the noise level during the day- and nighttime is present. A careful investigation of noise data therefore requires repeated measurements, making the application of this data type less attractive and more expensive (BARD, 1997).
- In the case of very low resonance frequencies correlated to thick sedimentary structures (f < 0.5 Hz), microtremors alone are not believed to excite the soil structure at such low frequencies (LACHET & BARD, 1994).

2.2   Weak and strong motion data of earthquakes

2.2.1   Earthquakes and seismic waves

Most earthquakes are caused by shear brittle fractures or friction sliding along the tectonic plate boundaries in depths between 5 and 30 km below the earth's surface. About 30% of all earthquake events take place beneath 70 km below the earth's surface, while 8% occur beneath 300 km.

If dovetail connections between the geological structures of two adjoining plates rupture because they were strained beyond the deformational capacity of the type of material involved, a jerky displacement emerges. A fault rupture then occurs, which in some cases spreads from the geological rock to the surface. The type of displacement that occurs on a fault strongly depends on the state of stress between the two plates. In general, three different types of fault ruptures exist (Figure 2.3). Given that horizontal shear stress acts along the fault, lateral motion in the direction of the fault strike occurs, giving rise to a *"strike-slip"*, or lateral fault. When a relative sliding motion acts perpendicular to the fault line, a *"dip-slip"* fault is present. A *"normal fault"* is when the rock mass on the upper side of the fault has a relatively downward movement. Conversely, if the upper rock mass moves upward relative to the lower side, this is called a *"reverse fault"* (CLOUGH & PENZIEN, 1993).
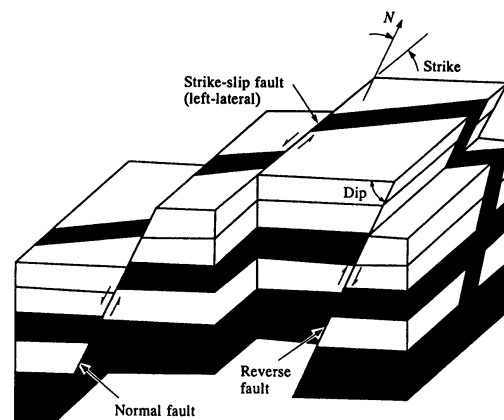
Figure 2.3 Basic types of fault ruptures (adapted from BOLT *et al.*, 1988).

The length of the scarifying fault plane determines the duration of the triggered earthquake. The sudden release of strain energy in the form of seismic waves traveling from the rupture point (*earthquake focus, hypocenter*) in all directions through the earth constitute what is called an earthquake.

Even though earthquakes are in fact predominantly concentrated on plate boundaries, single fractures within heavy burdened plates, or *intra-plate events*, can occur. The proportionate energy of these intra-plate earthquakes are believed to be about 0.5% of the total annual energy release of earthquakes (PLATE & MERZ, 2001). Intra-plate events cause major seismic
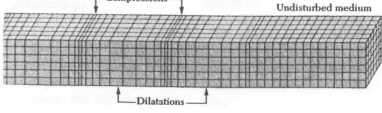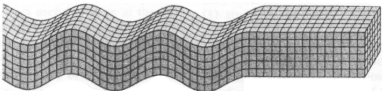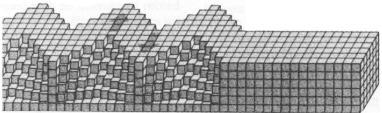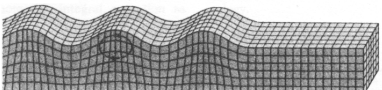
activity and devastating impacts that produce large economic losses, especially for Middle European countries.

Earthquake waves are generally differentiated into *body waves* and *surface waves*. Body waves consist of two types of waves propagating deep within the earth: *P* waves (primary waves, compressional waves) and *S* waves (secondary waves, shear waves). While *P* waves are characterized by material particles moving along the direction of wave propagation (tension and compression deformations), *S* waves constrain the material particles to move perpendicular to the wave propagation path, performing shear deformations. *S* waves can either act in the horizontal (S_H waves) or in the vertical plane (S_V waves).

If the seismic wave energy in form of *P* and *S* waves impinges on the free surface, a type of surface wave is generated due to interference: the *Rayleigh wave* (R_g). If body waves hit a discontinuity in depths below the surface, another type of surface wave is generated: *the Love wave* (L_g). Both can only be observed at recording points situated at a certain distance to the epicenter. While particle motions of soil materials under L_g waves are similar to those under S_H waves, material particles under R_g wave excitation circulate lengthwise.

Illustrations of each of the four different types of seismic waves are given in Table 2.3.

Table 2.3 Seismic wave types and their amplitude and frequency characteristics. The relative propagation velocity decreases from top to bottom (sketches are adapted from BOLT, 1976).

Type	Designation	Schematic particle motion (waves propagating from left to right)	(Amplitude/frequency) characteristics	Ranges of seismic wave frequencies [1]
body waves	*P* wave		- normal stress waves - small amplitudes - high frequencies - vertical comp. mainly (longitudinal partially)	0.02 – 100 Hz (0.01 – 50 sec)
body waves	*S* wave		- shear stress waves - increase in amplitude - shorter frequencies - horizontal comp. mainly (longitudinal, transversal)	0.02 – 100 Hz (0.01 – 50 sec)
surface waves	L_g wave		- shear waves, diminishing rapidly with depth - larger amplitudes - still shorter frequency - transversal component only	0.003 – 0.1 Hz (10 – 350 sec)
surface waves	R_g wave		- tension-compression waves - greatest amplitude, diminishing with depth - regular waveform - vertical and longitudinal component only	0.003 – 0.1 Hz (10 – 350 sec)

[1]   after LAY & WALLACE (1995)

Each of the 4 different wave types possesses different wave propagation velocities, which strongly depend on the stiffness or consistency of the propagation medium (subsoil). Figure 2.4 shows the relation between Poisson's ratio, v, and propagation velocities of primary (v_p), shear (v_s), and Rayleigh (v_R) waves dependent on shear wave velocity, v_s, in a semi-infinite elastic medium. Due to their high propagation velocity, *P* waves travel most rapidly through the subsoil materials and therefore are designated as Primary waves. The Secondary wave designation of *S* waves refers to their slower propagation velocity, leading to their arrival after the *P* waves at any given recording point.

Because both types of surface waves and their slower propagation velocities come from the body waves near the earth surface, their arrival times are accordingly late.
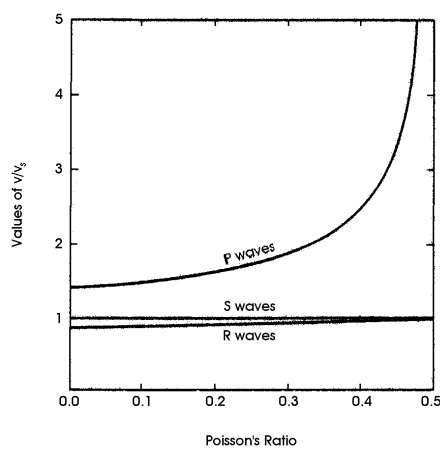
Figure 2.4   Relation between Poisson's ratio, v, and propagation velocities of compression (v_p), shear (v_s), and Rayleigh (v_R) waves in a semi-infinite elastic medium in dependence on shear wave velocity v_s (adapted from RICHART, 1962).

2.2.2   Earthquake ground motion

The impact or characteristics of an earthquake, called *earthquake ground motion*, is different at any given site. The instrumental record of earthquake events can be described in terms of acceleration, velocity, or displacement time-histories.

The ground motion of an earthquake can be characterized by three major elements:

- level of shaking intensity (ground motion intensity),
- frequency content,
- time duration (strong-motion duration).

The application of site response estimation techniques, and especially the frequency content and parameters influencing the spectral characteristics of earthquake ground motion, are of particular interest. The level of shaking intensity at a particular site mainly depends on the size of the earthquake itself, the distance to the seismic source, and the local site conditions. All have significant influence on the frequency content of earthquake ground motion. These parameters will be discussed in more detail below.

In contrast to this, if equal magnitudes are assumed, the time duration of seismic action has only minor significance for frequency characteristics of the seismic records. Nevertheless, strong-motion duration should be regarded in terms of engineering purposes.

As WANG & LAW (1994) pointed out, the longer the duration of ground motion lasts, the lower the ductility of structures and consequently the greater the potential for structural damage during earthquakes. Additionally, the liquefaction potential of soils is directly related to the number of load cycles during earthquake shaking, thus leading to ground failures and also to structural damage.

With respect to local site conditions, the duration of ground motion for the same earthquake at the same epicentral distance will last longer at soft soil sites than at sites with stiff soil or rock conditions. Damage potential due to ground motion duration may therefore be higher at soft soil sites.

It has not been reported that the duration of earthquake shaking influences the spectral characteristics of ground motion at all. This holds only if the whole time-history is regarded, including the period in which surface waves could occur. DOBRY & IDRISS (1978), and HAMPE *et al.* (1990) carried out comprehensive investigations about the relation between the regarded duration of an earthquake's time-history and its corresponding response spectrum for different earthquake records. An example is given in Figure 2.5 to illustrate that even the later time segments of the earthquake's time-history moderately affect the long-period range of response spectra due to the presence of long-period surface waves. The general spectral shape for lower periods is not influenced by the different lengths of the time-history considered in the investigation.

(a) time-history   (b) response spectrum
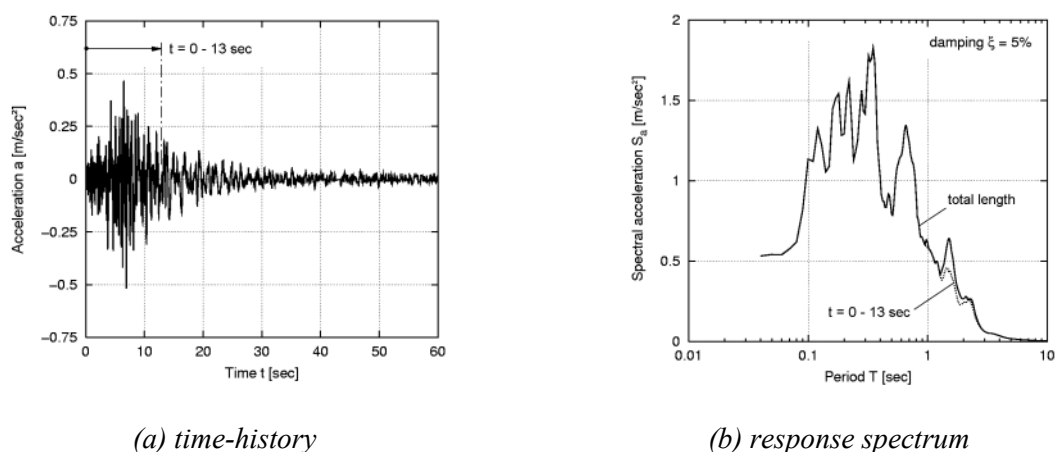
Figure 2.5 Influence of different ground motion durations on the characteristics of response spectra. Long-period waves after the first 13 seconds are responsible for the spectral peak at T = 1.5 sec.

2.2.3 Frequency characteristics of earthquake ground motion

In order to check the frequency characteristics of earthquake ground motion, a transformation of seismic data from time to frequency domain has to be carried out. For this purpose several types of transformation techniques are available, under which the elaboration of Fourier amplitude spectra and elastic response spectra are most commonly used. The latter reflect the maximum elastic response of single-degree-of-freedom systems (*SDOF*) with discrete damping and are excited by the earthquake time-history. (Theoretical backgrounds of both spectrum types will be given in Chapter 3.)

The frequency characteristics of earthquake ground motion are directly influenced by the following:

- magnitude of the earthquake, *M*,
- distance to the seismic source, *d* (epicentral distance, R_e or fault distance, *D*),
- subsoil conditions of the recording site.

These can be denoted as primary parameters. Secondary parameters which exert influence on spectral characteristics of ground motion, such as local shaking intensity or peak ground acceleration, are said to be generated by combinations of the primary parameters.

In order to obtain the most accurate results, the influence of each parameter should be analyzed independently of the other parameters by maintaining their values. The influence of magnitude *M* on frequency characteristics, for example, should be investigated with earthquakes all being recorded at the same site with nearly identical epicentral distances, R_e.

2.2.3.1 *The impact of magnitude, M*

To illustrate the frequency dependence on the level of earthquake magnitude, a set of European strong-motion records was analyzed (European Strong-Motion-Database ESMD; AMBRASEYS *et al.*, 2000). Figure 2.6 shows the average curves of normalized response spectra ($\xi = 5\%$) that are dependent on magnitude range M_s for three different subsoil conditions of the recording sites. All analyzed earthquakes were recorded in epicentral distances $R_e < 20$ km. Regardless of the subsoil conditions, a clear shift of the spectra to longer periods as well as a slight decrease of the highest amplification can be observed when magnitude M_s increases.

Near-field records of both mainshock- and aftershock events of a single strong-motion station confirm these findings (Figure 2.7). Normalized response spectra shifted into the high-period range with increasing magnitudes can be seen especially. A decrease in amplification level for events with stronger magnitudes does not occur, which could probably be explained by the different strong-motion recorders and their sensitivity. (Note: Mainshocks were recorded by SSA 320 instruments (AFET, Ankara), and aftershocks by Kinemetrics ALTUS K2 (GTFE).)

Disregarding the local subsoil conditions and distance to the source, here is a summary of the impacts of magnitude level on the frequency characteristics of earthquake ground motion:

- Normalized response spectra of larger magnitude events have their highest amplification at longer periods, while the peak period for events with smaller magnitudes is shifted into the short-period range.
- The amplification level of the spectral peak increases as the magnitude decreases. This means that the peak amplification level is high for small-magnitude earthquakes and diminishes for larger magnitudes.

Large earthquakes obviously produce larger and longer-period ground motions on the surface than do smaller earthquakes. This might be explained by nonlinear effects occurring in the near-surface soil materials during stronger ground motion (see also Section 3.1.3.2). Since long-period components are usually absent in most aftershock records, this deficiency must be considered when making inferences on site amplification based on weak motions.

The direct application of aftershocks appears to be useful in describing high frequency site responses in areas where the sites experience linear or almost linear responses (TRIFUNAC & TODOROVSKA, 2000).

| (a) soft soil | (b) stiff soil | (c) rock |
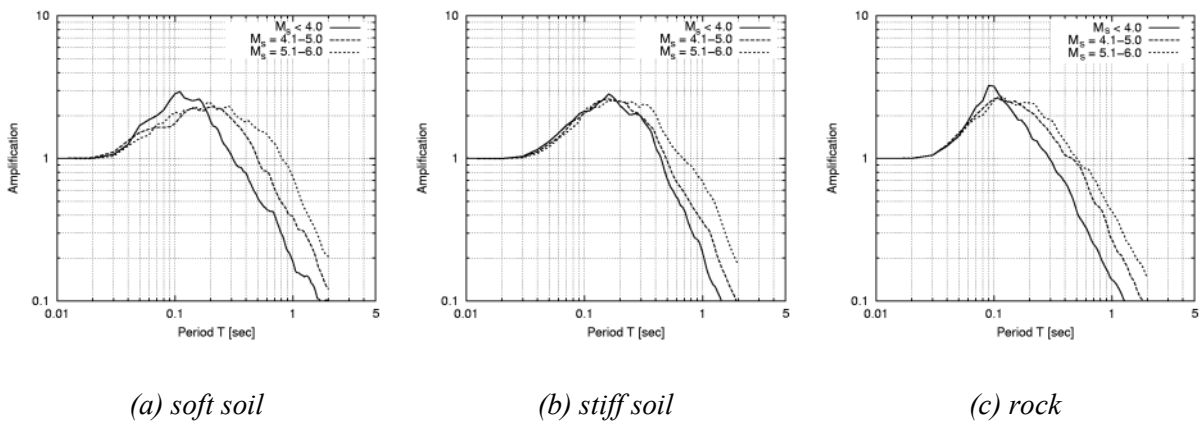
*Figure 2.6 Statistical analysis of near-field strong-motion data (R_e < 20 km) of European Strong-Motion Database ESMD (*AMBRASEYS *et al.,* 2000)*; normalized response spectra dependent on magnitude M_s for different subsoil classes.*
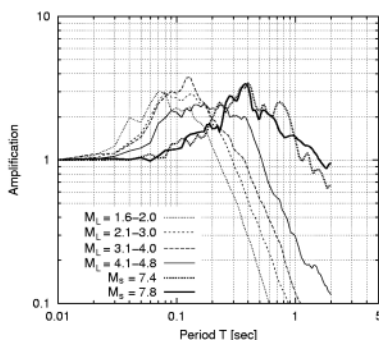
Figure 2.7 Normalized response spectra of both mainshocks and aftershocks for different magnitude ranges recorded at station Düzce DUZ (cf. LANG & SCHWARZ, *2000;* SCHWARZ *et al.,* 2000).

2.2.3.2   The impact of seismic source distance, d

It is well known that amplitude characteristics and frequency content of instrumental earthquake recordings are subjected to the distance between the seismic source and the recording site. Irrespective of possible amplification effects of local subsoil, amplitude level of seismic action decreases as the distance to the seismic source increases. Empirically this field of interest is covered by the elaboration of attenuation laws for peak ground acceleration, *PGA*, or spectral accelerations, S_a, at discrete frequencies.
In contrast to this, the relationship between frequency characteristics and distance to the seismic source is more complex.

It has already been reported that the portion of long-period surface waves in a seismic record enlarges as the distance to the source increases. Therefore frequency characteristics of seismic ground motion at the same site vary in respect to the seismic source distance. This holds true even for constant earthquake magnitudes. An example illustrating this effect is given in Figure 2.8, which shows amplification curves for different earthquake recordings with varying epicentral distance, R_e.

According to WANG & LAW (1994), response spectra become increasingly flat as the epicentral distance, R_e, increases. The peak period corresponding to the maximum acceleration may also changes slightly. Furthermore, the variation of the amplification factor is small for short periods and becomes larger for longer periods (see Figure 2.8).

In order to check the relationship between the predominant period of earthquake ground motion, T_G (i.e. the peak period of Fourier amplitude spectra) and the distance to the seismic source, *d*, SEED *et al.* (1969) analyzed a number of earthquake records at surface rock stations. Results in terms of relation curves for discrete magnitude levels are given in Figure 2.9.
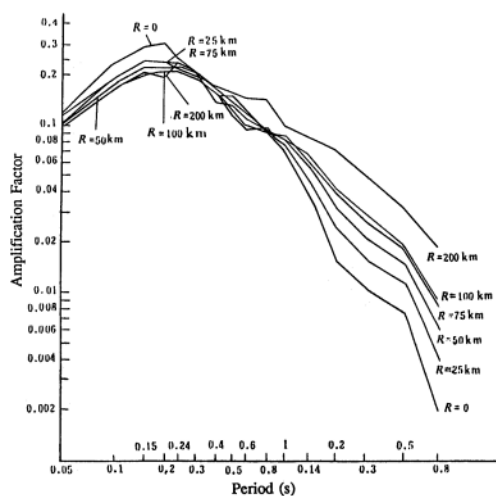
Figure 2.8   Normalized response spectra of earthquakes with different epicentral distances R_e (from WANG & LAW, *1994).*

With regard to the application of long-distance earthquake records with epicentral distances of several hundreds to thousands of kilometers, some other aspects have to be considered as well:

- The signal-to-noise ratio of far-field records is different compared to near-field records, leading to a possible misinterpretation of the ground motion characteristics coming from the earthquake itself.

- Distant earthquake records have little energy at high frequencies, while local earthquakes have higher frequency contents. This leads to different reliabilities concerning the regarded frequency ranges (CHÁVEZ-GARCIA *et al.*, 1990). This can be explained by realizing that the high-frequency components of seismic waves traveling away from a fault, are scattered and absorbed more rapidly than their lower-frequency components (KRAMER, 1996).

- Influence of dispersive effects (for surface waves) increases with increasing distance to the seismic source. Since the velocities of both Rayleigh and Love waves decrease with decreasing frequency (respectively reducing wavelength), the low-frequency surface wave components produced by the earthquake can be expected to arrive at a particular site before their high-frequency counterparts (KRAMER, 1996; HAMPE *et al.*, 1990).
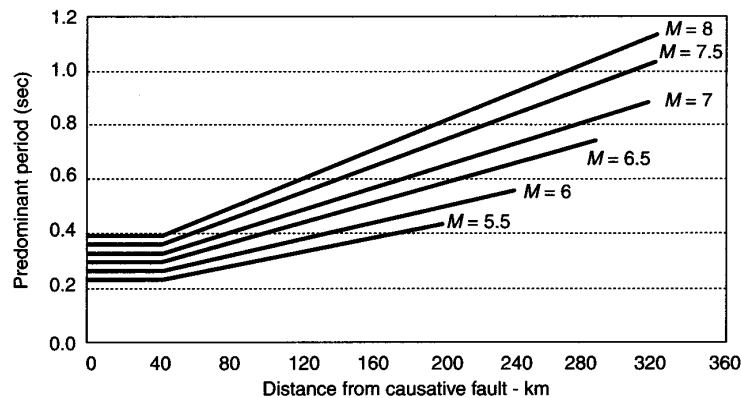
Figure 2.9   Relationships between predominant period of earthquake ground motion, T_G, and fault distance, D, for discrete magnitude levels (from SEED *et al.*, 1969).

2.2.3.3   *Predominant frequency of earthquake ground motion, f_g*

Since the end of the 19th century and, soon after the first seismic instruments were put into practical use, correlations between earthquake ground motion and the queueing subsoil conditions were discovered. Detailed investigations of earthquake records in Tokyo revealed that for every recording site, a certain frequency exists where the amplitude reaches a maximum (KANAI, 1983). As it was already shown by the findings of the preceding sections, investigations showed that this frequency is exposed to variations dependent on the magnitude of the earthquake and the epicentral distance.

Figure 2.10 illustrates the relationship between the level of earthquake magnitude, *M*, and the predominant frequency f_g, respectively the predominant period T_G, for earthquake records at different stations in Japanese prefectures. With regard to the comments by KANAI (1983), the following can be stated:

- For magnitudes smaller than a certain value, the predominant period decreases as the magnitude becomes smaller. In that case, the spectral peak of the highest amplification obviously cannot be ascribed to the characteristics of the site, but rather to the characteristics of the earthquake excitation itself.

- For magnitudes greater than a certain value, the predominant period indicates only small variations around a nearly constant value. Apparently the impacts of large-magnitude earthquakes, especially the long-period components, are able to approach the fundamental site characteristics, i.e. the natural site period, T_s. Because of its independence from the level of magnitude or excitation, the location of the natural site period is not subjected to large variations.

In terms of applying site response estimation techniques to different types of earthquake data, these findings may be of essential importance. The interpretation of the results of site response estimation techniques, such as normalized response spectra of small-size earthquake data, may profit by these perceptions.

It becomes obvious that the predominant frequency of earthquake ground motion, f_g, cannot automatically be ascribed to the subsoil conditions of the site. Variations of the frequency characteristics of earthquake ground motion exist, which mainly depend on the type of earthquake records used.

The connection between the predominant frequency of earthquake ground motion, f_g, and the natural (fundamental) frequency of the site, f_s, will be discussed in more detail in Chapter 3.
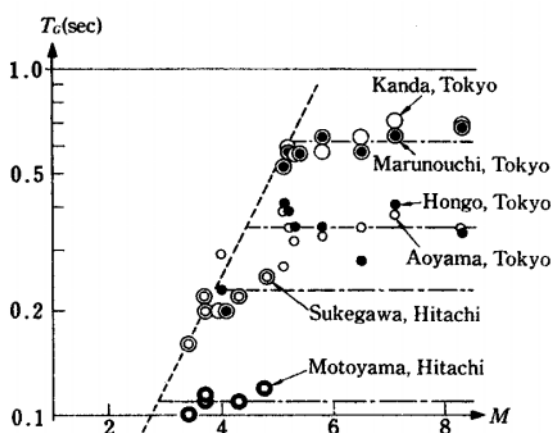
Figure 2.10 Relation between magnitude, M, and predominant period of earthquake ground motion, T_G, for different recording sites in Japan (KANAI, 1983).

2.3 Applicability of seismic ground motion data

The main task of the preceding sections was to characterize the available types of seismic ground motion data, and to elaborate on their limits and possibilities of application for the present work.

It is not intended to evaluate the pros and cons of the different seismic data types, or to make a decision in favor of a single type of seismic ground motion data. As Table 2.4 briefly summarizes, the application of each of the different data types provides certain possibilities (e.g. those concerning the environmental conditions). The quality of the results obtained through analysis may increase if all types of available seismic data are regarded and incorporated into the investigation.

Due to the limited numbers of strong-motion recording stations in most earthquake areas, instrumental records of damaging mainshocks are usually missing for most sites. Instrumental recordings of "alternative" ground motion data that are recorded at the different sites of interest, such as

-   ambient seismic noise, or
-   weak-motion earthquake data (e.g. aftershocks)

seem to be the only chance to provide information on the site's response characteristics.

With regard to the engineering analysis of structural damage and the elaboration of the damage potential of seismic ground motion during earthquakes, it is necessary to check the extent to which these types of instrumental data are useful and reliable. This will be accomplished by applying site response estimation techniques to the different types of seismic ground motion data, as well as by comparing the results of instrumental techniques with those of analytical methods (see Chapter 3).

Table 2.4 Quantification of the pros and cons of noise and earthquake recordings.

Topic, subject	Recordings of [1]	
	Ambient seismic noise (microtremors)	Earthquakes (weak- and strong-motion data)
complexity of measurement	○	●
applicability in low-seismicity regions	●	◑ associated with long observation periods
applicability in noisy areas	●	○
costs of instrumental maintenance (duration of observation period)	○	●
extent of environmental impairment	○	○
identification of source and path effects	○	●
reflecting the nonlinear soil response	○	◑ as far as the threshold shear strain γ is exceeded

[1]   ● yes (high)   ◑ with restrictions (moderate)   ○ no (low)

2.4 Available database and seismic recording stations

An essential part of the present work consists of collecting a comprehensive database of seismic ground motion records during numerous field work assignments (compare to Table 1.2). With regard to Tables 2.5 and 2.6, a differentiation can be made between data recorded by both

-   continuous/temporary operating seismic (broadband) stations, and
-   triggered strong-motion stations.

Table 2.5 lists the different regions where seismic broadband stations were deployed during the work's processing time. It also gives details about the instrumental equipment that was used. Except for the model sites in Germany, which were usually operating for several weeks or even months without pause, stations in Venezuelan and Turkish regions were only recording for several tens of minutes at a time.

Table 2.6 illustrates the earthquake regions of recent TaskForce missions as well as the number of respective strong-motion stations recording both mainshocks and aftershocks. While the mainshocks were mainly recorded by the national seismic networks, aftershock recordings were done by the pool of strong-motion accelerographs temporarily installed by the German TaskForce Group (GTFE).

Details about the different types of strong-motion recorders and their site and subsoil conditions are given by Annex 2, Tables A2-1 – A2-6.

Annex 3 also summarizes all stations that were investigated within the earthquake regions of Venezuela and Türkiye and specifies the available data types, all of which is incorporated into the work at hand.

Table 2.5 Specifications of seismic recording stations from which available noise data was gained during the work's processing time (velocity data).

Country, region	Time of recording	No. of rec. sites	Instrumental equipment	
			digitizer	seismic sensors
Germany, model sites [1]	1999-2003	13	Lennartz M-24 RefTek DAS 72A-06	Lennartz LE-3D Güralp CMG-40T
Northeastern Venezuela, State of Sucre (Cariaco)	05.1999	51	RefTek DAS 72A-06	Mark L4-3D
Southanatolian Türkiye, Adana province	10.2000	10	RefTek DAS 72A-06	Lennartz LE-3D
Northanatolian Türkiye, Kocaeli, Sakarya, Bolu provinces	10.2000 09.2002	50	RefTek DAS 72A-06	Lennartz LE-3D
Aegean Türkiye, Afyon province	09.2002	4	RefTek DAS 72A-06	Lennartz LE-3D
Eastanatolian Türkiye, Bingöl province	05.2003	4	RefTek DAS 72A-06	Lennartz LE-3D

[1]   since seismic stations were continuously operating, all types of earthquake recordings (local, regional, teleseismic) could be recorded during the measurement periods

Table 2.6 Specifications of strong-motion recording stations from which available earthquake data was gained during the work's processing time (acceleration data) [2].

Region, earthquake	Type of events	No. of (free field) stations	No. of identified aftershocks	No. of available recordings [3]	Magnitude (range)
Northeastern Venezuela, Cariaco (Casanay), July 9, 1997	mainshock [4]	2	-	1	M_s 6.8
	aftershocks	12	71	133	M_L 1.6 - 5.1
Southanatolian Türkiye, Adana (Ceyhan), June 27, 1998	mainshock [5]	1	-	1	M_s 6.2
	aftershocks	9	35	146	M_d 2.2 - 3.9
Northanatolian Türkiye, İzmit (Kocaeli), August 17, 1999	mainshock [5]	4	-	4	M_s 7.8
	aftershocks	13	*not definable*	~ 2000	M_L 1.0 - 5.9
Northanatolian Türkiye, Düzce (Bolu), November 12, 1999	mainshock [5]	4	-	4	M_s 7.4
	aftershocks	3	25	66	M_L < 4.3
Aegean Türkiye, Sultandağı (Afyon), February 3, 2002	mainshock [5]	1	-	1	M_s 6.5
	aftershocks	1	48	48	M_L 2.0 - 3.4

[2]   applied strong-motion recorder: Kinemetrics ALTUS K2 (equipment pool of German TaskForce for Earthquakes, GTFE)
[3]   total number of aftershock recordings at the different stations
[4]   data provided by Fundación Venezolana de Investigaciones Sismológicas (FUNVISIS, Caracas)
[5]   data provided by General Directorate for Disaster Affairs (AFET, Ankara)

3 Amplification potential of local subsoil

3.1 Transfer characteristics of local subsoil

Numerous observations in earthquake-affected areas have shown that the local intensity of earthquake shaking and the amount of structural damage due to seismic impact are in some way influenced by the local subsoil. Due to impedance contrasts, resonance or absorption phenomena, traveling waves of an earthquake are either amplified or attenuated by the local subsoil, which in some cases only affects discrete frequencies (BUDNY, 1984).

Neglecting the source and path of a dynamic signal, the same is influenced by the sedimentary layers overlying the geological bedrock. The differences between earthquake motion at the ground surface and geological basement (bedrock) are known as the *transfer characteristics of the local subsoil*, expressed by the transfer function, *TF*. The ability of a soil deposit to amplify or deamplify each frequency of the bedrock input motion is known as the *soil amplification potential*.

The soil amplification potential of a site can be investigated by different approaches: either analytically or instrumentally. While the latter presumes reliable seismic data to be recorded at least at the ground surface and possibly at an additional reference site, the first requires detailed information about the site's subsoil stratigraphy and geotechnical soil parameters.

If sufficient information about the soil-describing parameters is available, an analytical site investigation can be carried out, using different numerical methods, some of which are presented in Section 3.2.

To simplify matters, most of the analytical methods are based on idealized subsoil models, such as one-dimensional subsoil profiles, and do only apply linear-elastic soil parameters. The analytical investigation of the transfer characteristics of local subsoil, effects of surface and subsoil topography, and nonlinear effects of soil materials that strongly influence soil amplification potential have not been accounted for yet. These different influencing effects and the model-based characterization of subsoil will be discussed in more detail in the following sections.

3.1.1   Soil-describing parameters

The subsoil characteristics at a given site are determined, to put it simply, by its geological stratigraphy and the mechanical and dynamic parameters of the soil materials. Detailed knowledge of the consistency and thickness of the queueing soil layers overlying the geological basement (halfspace) is important for the evaluation of the site's dynamic response characteristics.

Each soil material can be described in terms of stiffness, mass and damping (HAMPE *et al.*, 1990). While the mass of a soil material can be clearly specified by its mass density ρ (identified by laboratory tests on intact soil probes or in-situ tests in boreholes), the damping used for engineering practice can be described by the equivalent damping factor, ξ. The latter is either determined by laboratory testing (inelastic material properties) or by seismic in-situ measurements (observation of energy loss/amplitude decline of the seismic signal with distance).

The stiffness of a soil material can be characterized by the following different (dynamic) parameters (in the range of small shear strains, γ):

-   (dynamic) modulus of elasticity (Young's modulus), E_{dyn} ,
-   (dynamic) shear modulus, G_{dyn} ,
-   compression wave velocity, v_p ,
-   shear wave velocity, v_s ,
-   Poisson's ratio, v .

To some extent these soil-describing parameters are ascertainable by means of each other. A variety of the prevailing formula relationships, for example, is given in BUDNY (1984), FLESCH (1993), and LÜDELING (1976). A brief summary of the basic relationships between the soil-describing parameters is given in Table 3.1. The definitions of the parameters used here are as follows:

Modulus of elasticity (Young's modulus) E
The modulus of elasticity E is a measure of elongation with respect to the total length of the burdened soil specimen under unidirectional impact. For soil materials it can be calculated thus:

$$E = (2.0 \ldots 3.0) \cdot G \qquad\qquad (3.1)$$

Shear modulus G_{dyn}
The shear modulus, G, stands for the material resistance of a test piece under shear deformation. Experimentally it can be assessed by the ratio of shear stress τ and shear strain γ.

P wave and S wave velocity, v_p and v_s

Both types of velocities describe the propagation velocity of the respective body wave (*P* or *S* wave) within the elastic solid. They depend on the stiffness of the soil material with respect to the types of deformation induced by each wave. For soil materials the *P* wave velocity exceeds the *S* wave velocity by an amount that depends on the compressibility (reflected in Poisson's ratio, *v*) of the solid (KRAMER, 1996). Here is the ratio between v_p and v_s :

$$\frac{v_p}{v_s} = \sqrt{\frac{(2 - 2 \cdot \upsilon)}{(1 - 2 \cdot \upsilon)}} \tag{3.2}$$

Poisson's ratio v

Poisson's ratio, *v*, is a parameter without dimension that represents the load-dependent ratio between the specimen alterations in transversal and longitudinal direction. The values of Poisson's ratio for soil materials vary between 0.2 (rock) and $\approx$ 0.5 (water-saturated loose sediments).

Table 3.1 Formula relationships between different soil-describing parameters.

Parameter		Formula in terms of parameters			
		G, v, ρ	*E, G, ρ*	*E, v, ρ*	*ρ, v_p, v_s*
modulus of elasticity	*E*	$2 \cdot G \cdot (1 + \upsilon)$	-	-	$\rho \cdot v_s^2 \cdot \dfrac{3 \cdot v_p^2 - 4 \cdot v_s^2}{v_p^2 \cdot v_s^2}$
shear modulus	*G*	-	-	$\dfrac{E}{2 \cdot (1 + \upsilon)}$	$\rho \cdot v_s^2$
P wave velocity	v_p	$\sqrt{\dfrac{G \cdot (2 - 2 \cdot \upsilon)}{\rho \cdot (1 - 2 \cdot \upsilon)}}$	-	-	-
S wave velocity	v_s	$\sqrt{\dfrac{G}{\rho}}$	$\sqrt{\dfrac{G}{\rho}}$	$\sqrt{\dfrac{E}{2 \cdot \rho \cdot (1 + \upsilon)}}$	-
Poisson's ratio	*v*	-	$\dfrac{E - 2 \cdot G}{2 \cdot G}$	-	$\dfrac{v_p^2 - 2 \cdot v_s^2}{2 \cdot (v_p^2 - v_s^2)}$

In order to obtain a soil's deformation behavior under dynamic load, both the deformation modulus (shear modulus *G*, elasticity modulus *E*) and the damping are most significant. Both depend on the shear strain amplitude, *γ*. With increasing shear strain *γ*, shear modulus *G* decreases while damping factor *ξ* increases. Both can be described as a function of shear strain *γ*. For a small set of different soil materials, see Figure 3.1.

As can be seen in current literature (see Figure 3.1), the characteristic curves of shear modulus *G* or damping factor *ξ* for a particular soil material can vary broadly.
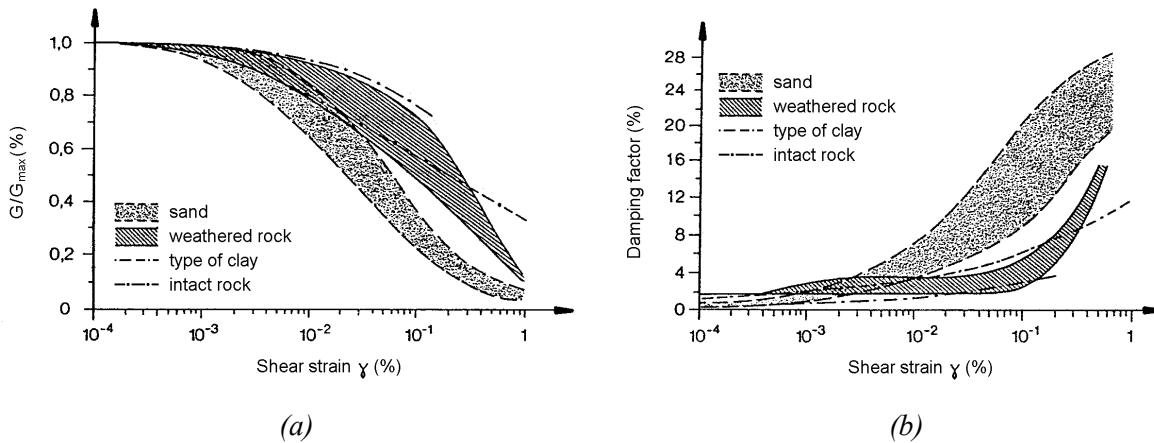
Figure 3.1 Behavior of (a) shear modulus, G, and (b) damping factor, ξ, dependent on shear strain γ (STUDER & ZIEGLER, 1986).

The curves of *G/G$_{max}$* and damping factor *ξ* show that already in the range of small deformations soil materials follow a strong nonlinear behavior. In order to consider the level of seismic impact, the soil dynamics parameters *(G, D)* have to be determined according to the value of shear strain *γ* reached during seismic action.

For most cases in engineering practice the use of equivalent linear values of the shear modulus and damping factor is sufficient.

3.1.2   Model-based characterization

Depending on the detailed knowledge of the local site and subsoil conditions, a characterization of the site can be performed in terms of a one-, two- or three-dimensional subsoil model. Ground response analyses based on one-dimensional models have shown ground response to agree to measured response in many cases. Since the generation of two- or three-dimensional subsoil models requires extensive data of boreholes or seismic exploration procedures, one-dimensional modeling is preferred.

Regardless of the dimensions of the ground model elaborated upon here, reliability of analysis results, for example analytical methods (see Section 3.2), strongly depends on the grade of accuracy of subsurface stratigraphy and the geotechnical parameters of the soil materials.

The generation of a one-dimensional subsoil profile representing the subsurface conditions of a given site basically assumes that:

- all boundaries between two different soil layers are horizontal, and
- soil and bedrock surface extend infinitely in horizontal directions.

Analysis results based on one-dimensional soil models therefore do not consider any effects that come from inhomogeneities in the surface or subsoil topography. The reported effects of surface topography occurring on rock ridges or steep soil slopes cannot be accounted for by one-dimensional soil profiles.

3.1.3   Influencing effects

As was already noted, the seismic amplification potential or the transfer characteristics of a site are influenced not only by the geological conditions of bedrock and overlying stratum, but also by effects coming from the surface and subsoil topography, and the nonlinear behavior of soil materials during strong cyclic loads. Since most of the commonly used analytical procedures for site estimation cannot account for these effects, their possible impacts on the transfer characteristics will be discussed here.

3.1.3.1   *Presence of sedimentary soil layer(s)*

The presence of a single or a package of sedimentary soil layers overlying the geological bedrock is the primary reason for soil amplification effects. Due to the impedance contrast between the "solid" bedrock and the "soft" overlying sediments, a trapping of the seismic waves occurs, leading to an amplification of the seismic wave amplitudes.

For each soil material i, the product of mass density, ρ_i, and shear wave velocity, v_s, is defined as the impedance $(\rho_i \cdot v_{s,i})$. The impedance ratio α_z between bedrock and overlying sediments can be calculated by equation (3.3), whereas $(\rho_r \cdot v_{s,r})$ is the impedance of the bedrock, and $(\rho_s \cdot v_{s,s})$ that of the overlying sediments.

$$\alpha_z = \frac{\rho_r \cdot v_{s,r}}{\rho_s \cdot v_{s,s}} \tag{3.3}$$

The interferences between the trapped waves lead to resonance patterns, which are characterized by various spectral peaks in the frequency domain (BARD, 1997). The resonance frequencies at which strong amplification occurs solely depend on the geometry (in particular thickness, H) and dynamic soil properties (in particular shear wave velocity v_s) of the sedimentary soil layer(s). The i th resonance frequency of the soil profile is given by

$$f_i = (2i+1) \cdot \frac{v_s}{4H} \qquad\qquad i = 0, 1, 2\ldots, \infty \tag{3.4}$$

where: v_s -   shear wave velocity of the overlying sediments [m/sec]

                 H -   total thickness of overlying sediments [m].

For $i = 0$ the lowest resonance frequency is determined, called the fundamental or natural site frequency, f_s. Frequency values calculated for $i > 0$ represent higher harmonics of the natural site frequency, f_s.

(a)   *(b)*
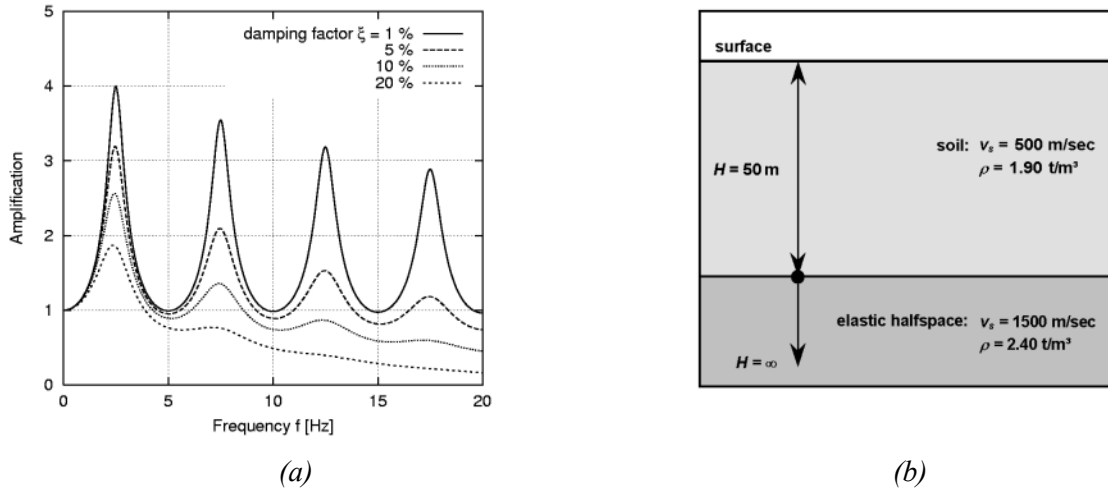
Figure 3.2   Influence of damping factor, ξ, on amplification characteristics of a homogeneous soil layer overlying elastic halfspace (geological bedrock).

Since soil damping affects the amplification in the frequency range of higher harmonics more than at lower frequencies, the fundamental site frequency, f_s, will roughly reveal the greatest amplification factor. This effect is illustrated by Figure 3.2, which shows the influence of different damping factors, ξ, on the amplification characteristics of a single soil layer over an elastic halfspace. It can be seen that the various spectral peaks exactly occur at frequencies that are uneven multiples of the frequency of the lowest spectral peak, representing the higher harmonics of the fundamental site frequency, f_s. The different damped curves, each of which describes the ratio of displacement amplitudes between the top and the bottom of the soil layer, are characterized as the transfer functions of the site. The detailed derivation of transfer functions, which are complex mathematical functions, will be given in Section 3.2.

To briefly summarize the effects of soil layers overlying the geological bedrock on the transfer characteristics of the site, the following can be stated:

- The amplification of the seismic waves amplitudes is strongly dependent on the impedance contrast α_z between rock and overlying soil layers. If the contrast between the consistencies of both media is high, large amplification of the seismic signals are more likely to occur. A high impedance contrast, α_z, can either be aroused by decreasing impedance of the overlying soil layers or by increasing impedance of the underlying rock; cf. equation (3.3).
- An additional amplification of seismic wave amplitudes takes place at the natural site frequencies f_s due to resonance effects. The fundamental site frequencies and their higher harmonics essentially depend on the thickness and consistency of overlying sediments; (cf. equation (3.4)). In order to illustrate this effect, fundamental site period T_s (reciprocal value of frequency f_s) as a function of layer thickness, H, and shear wave velocity, v_s, is given by Figure 3.3 (DURVILLE *et al.*, 1985).

- The level of amplification is controlled mainly by the damping factor, ξ, of the soil layers. Its impact increases as higher harmonics of the natural site frequency are concerned (cf. Figure 3.2).

It must be explicitly pointed out that the findings and formula relationships presented herein are more complex if two- or three-dimensional subsoil models are concerned.
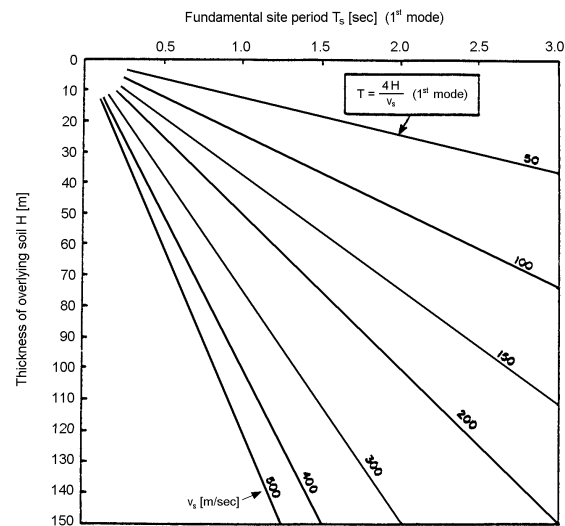
Figure 3.3 Fundamental site period, T_s, as a function of soil thickness, H, and shear wave velocity, v_s, (DURVILLE *et al.*, 1985; figure taken from BARD, 1997).

3.1.3.2 Nonlinear behavior of soft soils

The application of weak-motion data in terms of interpreting structural earthquake damage, such as small-magnitude earthquakes or ambient seismic noise, leads to the consideration of possible nonlinear effects that are induced by strong earthquake shaking. According to ÖZEL *et al.* (2002), nonlinear site effects are one of the most important and controversial problems and does not allow seismologists to apply weak-motion data to strong-motion prediction. However, the determination of the threshold acceleration or shear strain γ, beyond which soil nonlinearity becomes observable, is quite difficult. Since the effect of soil nonlinearity is largely a function of soil type (VUCETIC & DOBRY, 1991), each having different stress-strain relationships under seismic excitation, the designation of a distinct threshold value may not be helpful.

Since the early 1970's, nonlinear soil effects have been regarded by geotechnical engineers and are accounted for in several code provisions. The pioneering work of HARDIN & DRNEVICH (1972) illustrated the strong nonlinear behavior of soft soils during seismic excitation, characterized by a simultaneous decrease of shear modulus G and increase of material damping ξ. They found that the stress-strain relationship was hysteretic and that the soil materials behaved either like elastic-plastic or elastic-viscous plastic (PAVLENKO, 2001).

It could be proved on the basis of laboratory findings that if the earthquake shaking is strong enough to cause large strain above a certain threshold, a nonlinear behavior of the soil can be observed, influencing shear modulus and material damping dependent on shear strain γ (YANG et al., 2000).

Nonlinear behavior in soil materials can generally be described by a nonlinear relation between shear stress, τ, and shear strain, γ:

$$\tau = G(\gamma) \cdot \gamma \tag{3.5}$$

The strain-dependent shear modulus, $G(\gamma)$, is expressed by the Hardin-Drnevich relation (HARDIN & DRNEVICH, 1970):

$$G(\gamma) = \frac{G_{max}}{1 + |\gamma| / \gamma_{ref}} \tag{3.6}$$

where: G_{max} -   shear modulus for smallest shear strains

           γ_{ref} -   reference shear strain

As it was already mentioned in Section 3.1.1, curves of G/G_{max} can be described by hyperbolic relationships between shear modulus, G, and shear strain, γ. In order to give a more general form of the relationship between G and γ, equation (3.7) was introduced by BUDNY (1984):

$$\frac{G}{G_{max}} = \frac{1}{1 + \alpha \cdot \gamma^{\beta}} \tag{3.7}$$

where: α, β -   constants, depending on the type of soil material

Since less investigations have been carried out on the relationship between damping ξ and shear strain γ, equation (3.8) provides a reliable estimate of damping factor ξ:

$$\frac{\xi}{\xi_{max}} = 1 - \frac{G}{G_{max}} \tag{3.8}$$

As shown in Figure 3.1, the curve characteristics of G/G_{max}, and their respective damping factors ξ, reflect the restriction with which equation (3.8) can be applied for the smallest shear strain γ, which results in $\xi/\xi_{max} = 0$; and thus $\xi \rightarrow 0$ (BUDNY, 1984).

It can be seen that a soil site's ability to show a nonlinear behavior under earthquake shaking depends largely on the local soil consistency, i.e. its stress-strain dependency. There are many other factors, however, that play a role in the nonlinear behavior of a soil site during an earthquake:

- the intensity of earthquake shaking,
- the seismic source distance,
- the subsurface topography,
- the spectral composition of the incident seismic wave, and
- the dispersion and absorption properties of the medium (AKI, 1988; ÖZEL *et al.*, 2002; PAVLENKO, 2001; YANG *et al.*, 2000).

In order to exclude possible misinterpretations of results based on strong-motion data, the possible effects of soil nonlinearity on the spectral characteristics of earthquake ground motion should be accurately investigated. The nonlinear behavior of soft soils may induce:

- a slight increase of the predominant period T_G, and/or the fundamental site period T_s,
- a decrease of amplification level over the whole period range,
- a decrease of peak ground acceleration *PGA*, as damping effects are more pronounced in the high-frequency range.

To illustrate these effects, Figure 3.4 compares the results of a linear analysis with those of a nonlinear analysis. Using the program *ProShake (Version 1.1)*, the response of a 2-layer soil profile (overlying elastic bedrock) under seismic excitation (El Centro, M_s 6.7) was investigated. Figure 3.4a shows the first eight seconds of the acceleration time-histories at the ground surface for both the elastic and the inelastic case, whereas Figure 3.4b compares their corresponding response spectra.

| (a) | (b) |
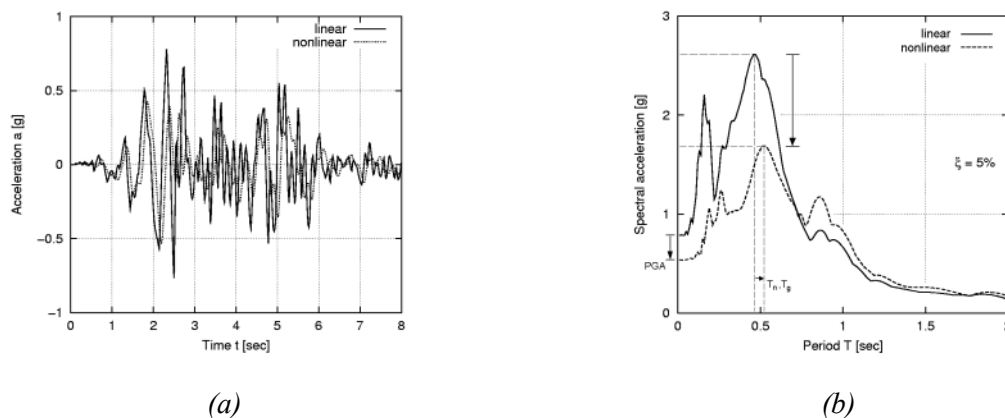
Figure 3.4   Comparison of the linear and nonlinear response of a soft soil site under seismic excitation in (a) time- and (b) frequency domain (program used: ProShake, Version 1.1).

The decrease of peak ground acceleration *PGA* due to a particular soil's nonlinearity has been investigated by several authors. They correlate the peak ground acceleration on soft soil sites to that on rock sites. Figure 3.5 illustrates approximate relationships of different groups. The nonlinear soil behavior and thus the increase of soil damping becomes observable as the soil curves fall below the rock curve. Both illustrations confirm the controversial discussions about the acceleration level beyond which nonlinear soil behavior becomes visible.

The investigations of SILVA (1991) showed that the total thickness of sedimentary layers also has significant influence on the level of peak ground acceleration (Figure 3.6). The impact of thick sedimentary soil layers undoubtedly agrees with that of strong seismic input signals, leading to an increase of damping effects and thus to a decrease of the high-frequency components of ground motion. Conversely, thin sedimentary layers have the same effects as weak-motion input signals that cause large signal amplifications especially in the high-frequency range (PAVLENKO, 2001).

As a matter of principle, these results are reflected in the concept of subsoil- and geology-dependent spectra of DIN 4149 (DIN, 2002). The influence of sedimentary thickness on the high-frequency ground amplification is taken into account by the value of soil parameter, *S*.

(a)   (b)
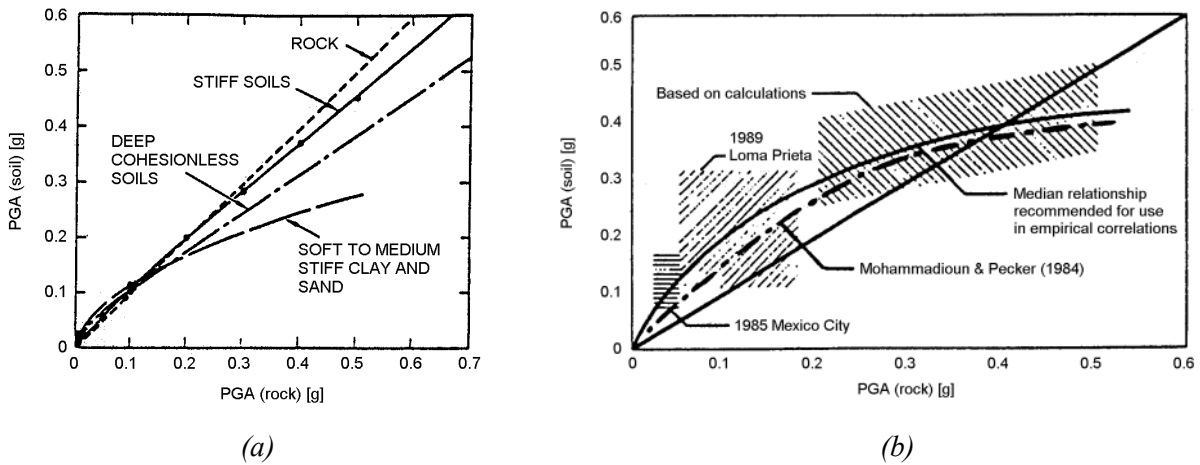
Figure 3.5   Relationships between peak ground accelerations on soft soil sites and rock sites to illustrate the nonlinear soil effects: (a) SEED & IDRISS, 1982; *(b)* IDRISS, 1990 *(figure taken from* BARD, 1997).
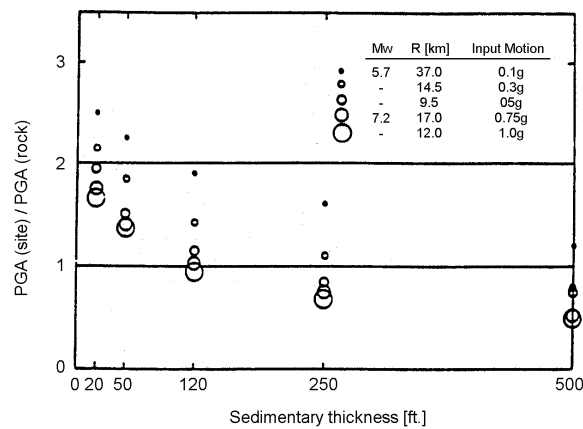
Figure 3.6 Influence of sedimentary thickness on the ratio of peak ground acceleration between soil and rock (SILVA, 1991; figure taken from BARD, 1997).

The consideration of possible nonlinear effects may be important for the application of weak-motion data (e.g. small earthquakes, microtremors) to predict strong ground motion at a given soil site. As was shown, nonlinear effects of soil materials have significant influence on the spectral feature of earthquake ground motion (cf. Figure 3.4).

It must be proved to which extent soil nonlinearity can be considered by the current site response estimation techniques, especially by those using only weak-motion data. According to different scientific groups, the influence of soil nonlinearity may be overridden during the application of spectral H/V-techniques (see Section 3.3.4). Own investigation results were confirmed by the results of THEODULIDIS & BARD (1995), who found that nonlinear effects are most likely eliminated by spectral H/V-ratios. This assumes that they are almost comparable in horizontal and vertical motion, thus leading to nearly identical amplification functions for weak- and strong-motion seismic data.

3.1.3.3 *Surface and subsurface topography*

Even though it is well known in the scientific community that surface topography can have considerable influence on the frequency and amplitude characteristics of earthquake ground motion and thus on the extent of local structural earthquake damage, it received only minor attention for a long time.

Two general types of topography have to be distinguished:

- surface topography, mainly characterized by mountainous features, such as the presence of rock ridges or steep soil slopes,
- subsurface (or subsoil) topography, either caused by lateral heterogeneities of the subsoil layers or by sharp basin geometry (FÄH *et al.*, 1996; MAYER-ROSA & JIMÉNEZ, 2000); the curvature of a sediment-filled basin structure in particular can capture body waves and cause some incident body waves to propagate through the alluvium as surface waves resulting in stronger shaking effects and longer duration of strong ground motion (KRAMER, 1996).

In contrast to subsoil topography, more serious effects are reported to be caused by surface topography. According to numerous reconnaissance studies after strong earthquakes, an increase of damage to buildings can be observed on steep slope situations which extend towards the plateau (Figure 3.7). Recent damaging events in Türkiye (Bingöl earthquake of May 1, 2003) and Algeria (Northern Algerian earthquake of May 21, 2003) displayed heavy damage concentrations along the top of steep slopes (SCHWARZ *et al.*, 2004; pers. comm. WENK, 2003). Since both earthquakes caused damage to different types of buildings, as well as direct seismic site effects (e.g. soil liquefaction or slope instability) can be excluded as damage-contributing factors, topographic effects alone may be responsible for the increase of damage.
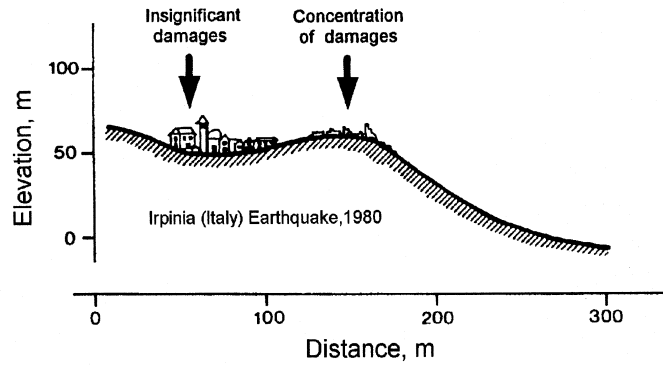
Figure 3.7   Scheme illustrating the heaviness of damage occurrence at topographic features (figure taken from ATHANASOPOULOS *et al.*, 1998).

As BARD (1997) pointed out, it has to be proved if the damage extent can really be ascribed to amplification effects caused by the topographic shape of the ground surface or to the dynamic triggering of land- and rockslides during strong earthquake shaking.
In order to concentrate on the effects that surface topography has on the amplification potential of seismic ground motion, the latter cause of damage will be neglected below.

There is no question that surface topography has great influence on strong-motion earthquake data. Its influence on weak-motion data (e.g. ambient seismic noise), however, is still not clarified. Own microtremor recordings on the base, the ridge, and the plateau range of steep slopes displayed no clear results (see Section 3.3.4.1).
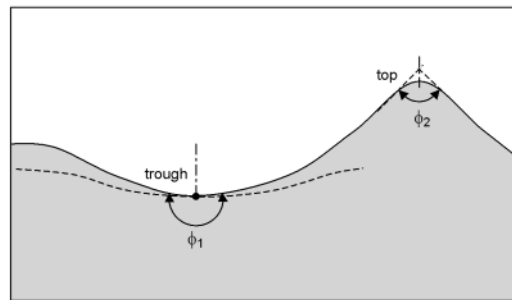
Figure 3.8   Cases of surface topography; capability to amplify or deamplify the seismic signal strongly depends on the aperture angle φ.

According to different scientific groups (AKI, 1988; BARD, 1995, 1997; GÉLI *et al.*, 1988) that deal with instrumental and theoretical investigations of surface topography on ground motion characteristics, the following can be stated:

-   Mountain tops or ridge crests, and more generally, convex topographies (such as cliff borders), lead to an amplification of seismic ground motion, while valleys or foothills (concave topographies) tend to deamplify the seismic signals (Figures 3.7 and 3.8).
-   The effects of surface topography are larger on horizontal components than on vertical ones, thus indicating that *S* motion is more affected by surface topography than *P* motion.

- The influence of surface topography on ground motion is directly related to the sharpness of topography. Figure 3.9 illustrates this effect on the basis of two topographic features having different wedge angles. According to this theoretical model, amplification of incoming seismic waves increases as the wedge angle becomes sharper.
- Amplification and deamplification of seismic ground motion on topographic features are apparently both frequency-dependent and band-limited: maximum effects can be observed for wavelengths that approximately agree with the horizontal dimensions of the topographic shape.

(a) *(b)*
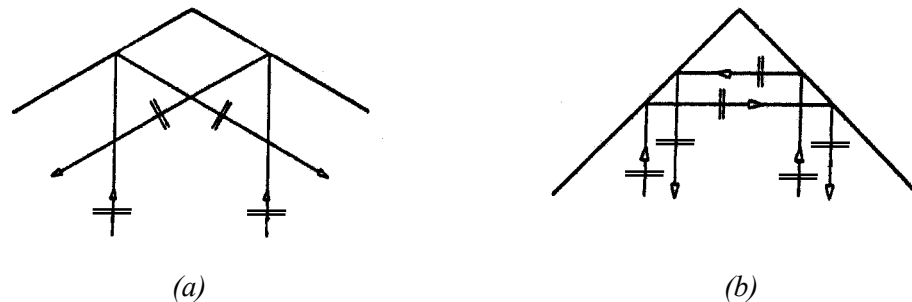
Figure 3.9 Theoretical response of two topographical models having different wedge angles, ϕ, to vertically incident S_H waves (after BARD, 1997).

Although recent results on the basis of theoretical models roughly match with observed instrumental results at sites being characterized by surface topography, a quantitative determination of its effects is not possible.

In terms of interpreting instrumental results, recording sites close to topographic features should be obviated. Own investigations showed that topography strongly influences ambient seismic noise, resulting in spectral H/V-ratios not suitable for subsoil classification (see Section 3.3.4).

Amplification effects of earthquake ground motion at topographic features are incorporated in several building code provisions, e.g. in the French earthquake code AFPS (1990). Depending on the slope of the angle, the situation within the slope, or the distance to the slope ridge, a topographic amplification factor, τ, is defined, raising the spectral accelerations S_{as} *(T)* for potential building design (Figure 3.10).

valid for: $H \geq 10$ m

$\tan \beta \leq 0.33 \cdot \tan \alpha$

$S_a(T) = \tau \cdot S_{as}(T)$

whereas: τ - topographic amplification factor

$\tau = 1.0$	for $I\text{-}i \leq 0.40$
$\tau = 1.0 + 0.8\ (I\text{-}i\text{-}0.4)$	for $0.40 \leq I\text{-}i \leq 0.90$
$\tau = 1.4$	for $I\text{-}i \geq 0.90$

wheras: $I = \tan \alpha$
           $i = \tan \beta$
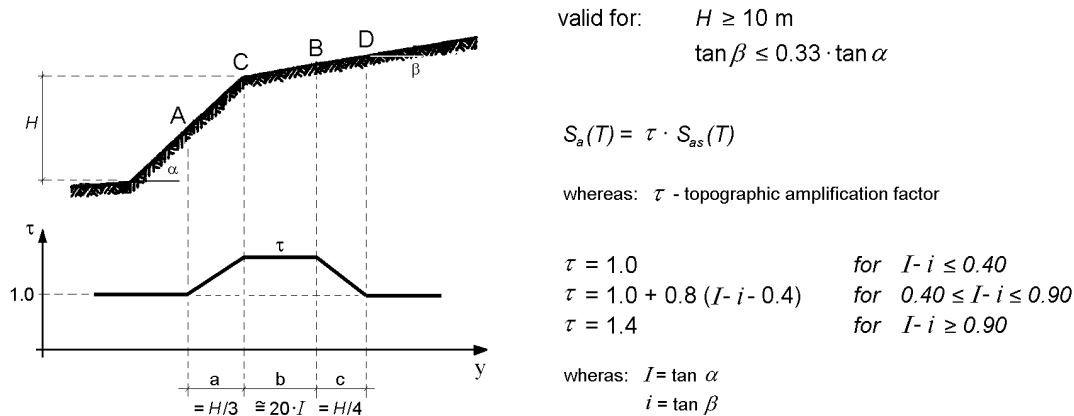
Figure 3.10   Consideration of amplification effects at topographic features following the earthquake code provision of France (AFPS, 1990).

3.2 Analytical methods (theoretical)

For the theoretical estimation of the site response or its dynamic transfer characteristics, a variety of numerical analysis methods are available. A rough classification of these methods can be done either on the dimension of the ground model (one-, two-, or three-dimensional), or on the consideration of linear or nonlinear material (soil) behavior.

The quality of results derived from theoretical site response estimation methods strongly depends on the detailed knowledge of the following:

- the subsurface stratigraphy, including the single layer thicknesses, the total sedimentary thickness, and the depth of the geological basement (rock horizon),
- the geotechnical properties of the soil materials (mechanical and dynamic parameters).

Furthermore, the reliability of theoretical results increases as they are compared with results of other techniques, such as those using different types of instrumental recordings.

Two different theoretical methods will be described in more detail below, both elaborating a frequency-dependent transfer function of one-dimensional soil models.

3.2.1   Theoretical transfer function of one-dimensional subsoil profiles

In order to describe the influence of local subsoil conditions on the amplification characteristics of a site, the frequency-dependent transfer function of a one-dimensional soil profile can be seen as the most commonly used one. With regard to the detailedness of available information of the local site geology, also 2D or 3D techniques that refer to the dimension of the ground motion can be applied.

The transfer function describes the resonance characteristics of the subsoil profile, which in turn is described by its geological stratigraphy (single soil thicknesses h_i, total sedimentary thickness H), and mechanical (ρ, υ) or dynamic parameters (E_{dyn}, G_{dyn}, v_p, v_s) of the single soil materials. Waves passing through the sedimentary layers are modified in frequency and amplitude due to conditions at the layer boundaries and transfer processes of the different soil materials.

The theoretical transfer function provides information about the factor with which amplitudes of the harmonic particle motions are amplified due to the local soil conditions.

The one-dimensional transfer functions determined here are based on the following assumptions (ELTON & MARTIN II, 1989; MAYER-ROSA & JIMÉNEZ, 2000; WEISSENBURG, 1995):

- the structural soil model consists of horizontally stratified soil layers, each being homogeneous and isotropic, and extend to infinity,
- the ground surface is level, which means that no effects coming from surface topography can occur,
- only plane horizontal shear wave motions are addressed, as vertically propagating S_H waves have the greatest influence on the dynamic site period and soil behavior,
- each soil layer is described by its respective thickness h, shear modulus G, mass density ρ, and damping factor ξ.

The approaches and algorithms incorporated into the different programs (e.g. ProShake, SIRESPO) to calculate the transfer functions can be taken from numerous references (e.g. KRAMER, 1996; WEISSENBURG, 1995) and will not be repeated here in detail.

The transfer function can generally be regarded as the amplitude ratio of the ground motion between the free surface u_s and the (elastic) halfspace u_r. It reflects the dynamic transfer characteristics of the soft sediment soil layers. Consequently, distinct peaks of the transfer functions mark the individual mode frequencies of the soil profile. Equations (3.9) and (3.10) describe the transfer function $F(\omega)$ for a single soil layer over elastic halfspace.

$$F(\omega) = \frac{u_s}{u_r} = \frac{2}{(1+\alpha_z^*) \cdot e^{i \cdot k_s^* \cdot H} + (1-\alpha_z^*) \cdot e^{-i \cdot k_s^* \cdot H}} \qquad (3.9)$$

Since the transfer function $F(\omega)$ is a complex function, it can be rewritten using Euler's law:

$$F(\omega) = \frac{u_s}{u_r} = \frac{1}{\cos(k_s^* \cdot H) + i \cdot \alpha_z^* \cdot \sin(k_s^* \cdot H)} \qquad (3.10)$$

where: $\alpha_z^* = \dfrac{G_s^* \cdot k_s^*}{G_r^* \cdot k_r^*}$ - complex impedance ratio,

k_s^*, k_r^* - complex wave numbers of the sediment or bedrock motion,

H - total thickness of the sedimentary soil layer(s).

To verify the applicability of available computer programs and thus to illustrate the possible differences in transfer functions $F(\omega)$, one-dimensional transfer functions were calculated for selected soil profiles provided in literature and compared to each other. Table 3.2 lists the soil parameters of model profiles investigated by FIELD *et al.* (1992). Respective transfer functions $F(\omega)$ are compared in Figure 3.11. For results calculated by different programs, only small deviations occurred, which consequently confirms the reliability of the method.

Table 3.2 One-dimensional model parameters of model sites S1 and S3 in FIELD *et al.* (1992).

Layer	Site S1				Site S3			
	h [m]	v_s [m/sec]	ρ [t/m³]	ξ [%]	h [m]	v_s [m/sec]	ρ [t/m³]	ξ [%]
1	6.1	90	1.6	3.1	159	384	2.0	3.1
2	164	384	2.0	3.1	-	-	-	-
Halfspace	∞	1200	2.4	0.5 [1)]	∞	1200	2.4	0.5 [1)]

[1)] damping factor, ξ, for halfspace was subsequently amended

(a) (b)
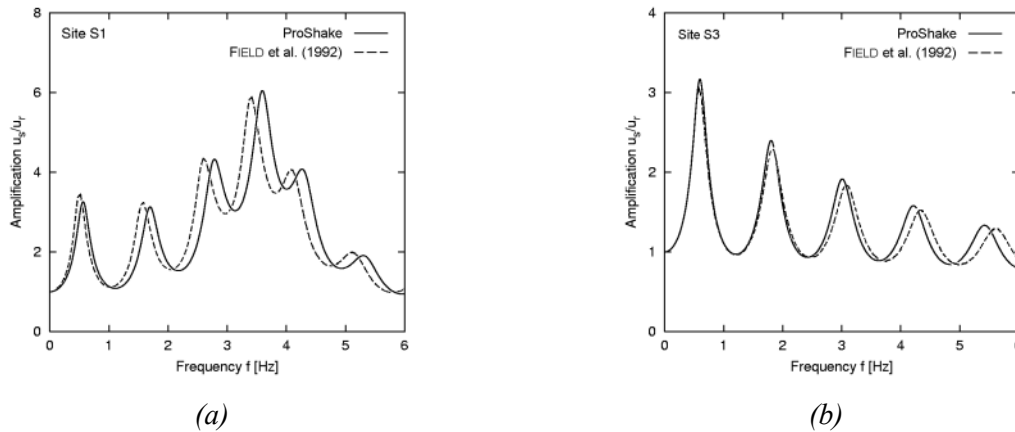
Figure 3.11 Transfer functions of model sites S1 and S3 as determined by FIELD *et al.* (1992) *compared with calculation results using the program ProShake* (EDUPRO CIVIL SYSTEMS, INC.).

3.2.2 Theoretical H/V-ratio of Rayleigh waves

Another way to identify the fundamental site frequency on the analytical way, insists on elaborating the dispersion function of Rayleigh waves, and thus of the corresponding H/V-spectra, also known as the Rayleigh ellipticity curve.

In contrast to conventional transfer functions of vertically propagating S_H waves as described in the previous chapter, the transfer characteristics for P and S_V waves representing the Rayleigh wave motion at the surface or soil layer boundaries are sought. Concerning the response characteristics of a given soil profile, the elaboration of theoretical H/V-ratios is a common tool which is also applied by different scientific groups (e.g. FÄH *et al.*, 2001; NAKAMURA, 2000). All theoretical H/V-spectra incorporated in the present work were calculated using a program sequence which was developed by ENDE (2000). The following paragraphs briefly present the integral steps of this procedure in order to work out the dispersion function of Rayleigh waves and the theoretical H/V-ratio.

In order to carry out the procedure, certain assumptions are needed:

- horizontally stratified soil layers,
- homogeneous soil materials (soil properties are constant over the whole layer) with elastic behavior (Hooke's law can be adopted since small displacements are considered),
- underlain by an elastic deformable halfspace, meaning that only waves can descent into the halfspace but not allowed to emerge out of it.

(a)   *(b)*
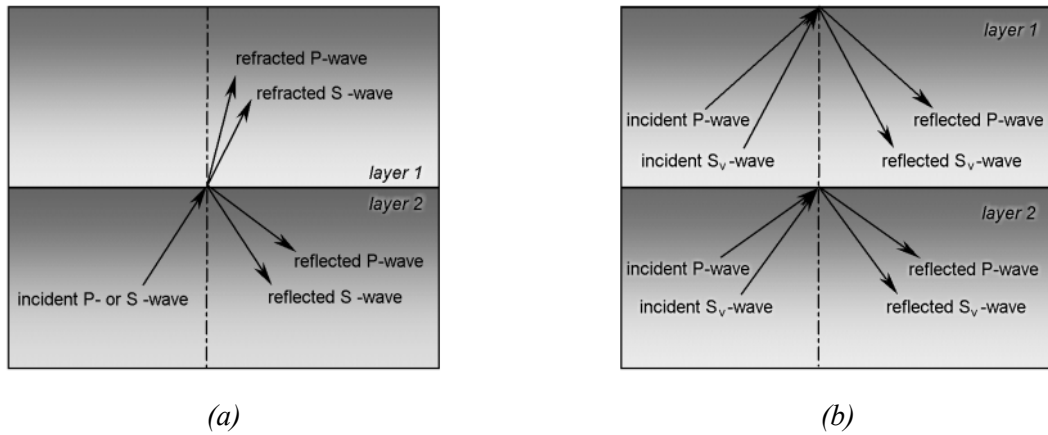
Figure 3.12   (a) Principal scheme of refraction and reflection of incident P or S_V waves at a layer boundary; (b) basic model of the analysis (after ENDE, 2000).

Figure 3.12 schematically illustrates the basic model of the analysis, showing both incident and reflected waves. Assuming that the whole layer package is excited, both, *P* and S_V waves are present in each layer. The refracted waves indicated in Figure 3.12a will not be explicitly regarded in the basic model (Figure 3.12b), since these waves exist in the upper layer.

The displacement equation of corresponding *P* and S_V waves moving upward and downward at one layer boundary can be written thus:

$$v(x,z,t) = \begin{Bmatrix} u^* \\ w^* \end{Bmatrix} = P\downarrow \cdot \begin{Bmatrix} k \\ m \end{Bmatrix} \cdot e^{i\cdot(kx+mz-\omega t)} + P\uparrow \cdot \begin{Bmatrix} k \\ -m \end{Bmatrix} \cdot e^{i\cdot(kx-mz-\omega t)}$$

$$+ S\downarrow \cdot \begin{Bmatrix} n \\ -k \end{Bmatrix} \cdot e^{i\cdot(kx+nz-\omega t)} + S\uparrow \cdot \begin{Bmatrix} -n \\ -k \end{Bmatrix} \cdot e^{i\cdot(kx+nz-\omega t)} \tag{3.11}$$

where: *P, S* -   propagator term either in the upward- (↑) or downward (↓) direction

      k, m, n -   wave numbers in *x*- (*P* & S_V wave), *z*- (*P* wave), and *z*-direction (S_V wave)

Factoring out the term $e^{i(kx-\omega t)}$, leads to the below

$$V(z) = \begin{Bmatrix} u \\ w \end{Bmatrix} = P\downarrow \cdot \begin{Bmatrix} k \\ m \end{Bmatrix} \cdot e^{-imz} + P\uparrow \cdot \begin{Bmatrix} k \\ -m \end{Bmatrix} \cdot e^{-imz} + S\downarrow \cdot \begin{Bmatrix} n \\ -k \end{Bmatrix} \cdot e^{inz} + S\uparrow \cdot \begin{Bmatrix} -n \\ -k \end{Bmatrix} \cdot e^{-inz} \tag{3.12}$$

$$v(x,z,t) = V(z) \cdot e^{i\cdot(kx-\omega t)} = V(z) \cdot e^{ikz} \cdot e^{i\omega t} \tag{3.13}$$

This transformation leads to a time- and location independence of the equation. Furthermore, only the propagation in the vertical plane at one location is regarded.

To solve these equations, different boundary conditions have to be defined:
  (1) stresses at the surface $\sigma_{zz0} = \tau_{zx0} = 0$
  (2) at the layer boundaries, the wave numbers in *x*-direction k = const., and in *z*-direction $m = n \neq$ const.
  (3) referring to the elastic halfspace, propagator terms for upward-moving waves $P\uparrow, S\uparrow$ $= 0$, and for downward-moving waves $P\downarrow, S\downarrow \neq 0$.

In the next step, strains and stresses at each boundary are calculated using Hooke's law, finally leading to the stress motion vector:

$$\vec{r}(z) = \begin{Bmatrix} u \\ w \\ \sigma_{zz} \\ \tau_{zx} \end{Bmatrix} = E \cdot a(z) = \begin{bmatrix} k & k & n & -n \\ m & -m & -k & -k \\ 2Gi(n^2-k^2) & 2Gi(n^2-k^2) & -iknG & iknG \\ 2Gimk & -2Gimk & Gi(n^2-k^2) & Gi(n^2-k^2) \end{bmatrix} \cdot \begin{Bmatrix} P\downarrow e^{imz} \\ P\uparrow e^{-imz} \\ S\downarrow e^{inz} \\ S\uparrow e^{-inz} \end{Bmatrix} \quad (3.14)$$

This equation system describes the stresses and displacements at a certain location in depth *z*. In order to incorporate the link of neighboring layer boundaries, equation (3.14) has to be supplied with certain modifications and extensions. Therefore matrix *E* and vector *a(z)* have to be converted in the following manner:

$$E = \begin{bmatrix} 1 & 0 & 0 & 0 \\ 0 & 1 & 0 & 0 \\ 0 & 0 & iG & 0 \\ 0 & 0 & 0 & iG \end{bmatrix} \cdot \begin{bmatrix} k & k & n & -n \\ m & -m & -k & -k \\ 2(n^2-k^2) & 2(n^2-k^2) & kn & kn \\ 2mk & -2mk & (n^2-k^2) & (n^2-k^2) \end{bmatrix} = G \cdot H \quad (3.15)$$

$$a(z) = \begin{bmatrix} e^{imz} & 0 & 0 & 0 \\ 0 & e^{-imz} & 0 & 0 \\ 0 & 0 & e^{inz} & 0 \\ 0 & 0 & 0 & e^{-inz} \end{bmatrix} \cdot \begin{Bmatrix} P\downarrow \\ P\uparrow \\ S\downarrow \\ S\uparrow \end{Bmatrix} = \Lambda(z) \cdot w \quad (3.16)$$

where: *G* - shear modulus

Consequently, stress motion vector $\vec{r}(z)$ can be written as below:

$$\vec{r}(z) = G \cdot H \cdot \Lambda(z) \cdot w \quad (3.17)$$
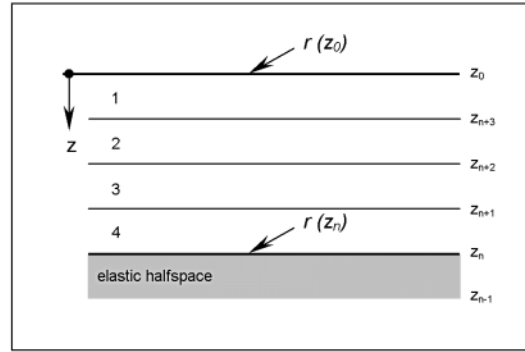
Figure 3.13 Multi-layered soil profile resting on an elastic deformable halfspace (after ENDE, 2001).

Since $\Lambda(z)$ is the only term containing soil depth z, the connection between all boundaries can be established. Regarding a multi-layered soil profile overlying both an elastic halfspace (Figure 3.13) and boundary condition (2) already described above, a new equation system representing the whole layer package with an elastic halfspace can finally be generated:

$$\vec{r}(z) = \begin{Bmatrix} P\downarrow \\ P\uparrow \\ S\downarrow \\ S\uparrow \end{Bmatrix} = \begin{bmatrix} P_{11} & P_{12} & P_{13} & P_{14} \\ P_{21} & P_{22} & P_{23} & P_{24} \\ P_{31} & P_{32} & P_{33} & P_{34} \\ P_{41} & P_{42} & P_{43} & P_{44} \end{bmatrix} \cdot \begin{Bmatrix} u_0 \\ w_0 \\ \sigma_{zz0} \\ \tau_{zx0} \end{Bmatrix} \Rightarrow \vec{r}(z) = \begin{Bmatrix} P\downarrow \\ 0 \\ S\downarrow \\ 0 \end{Bmatrix} = \begin{bmatrix} P_{11} & P_{12} & P_{13} & P_{14} \\ P_{21} & P_{22} & P_{23} & P_{24} \\ P_{31} & P_{32} & P_{33} & P_{34} \\ P_{41} & P_{42} & P_{43} & P_{44} \end{bmatrix} \cdot \begin{Bmatrix} u_0 \\ w_0 \\ 0 \\ 0 \end{Bmatrix} \quad (3.18)$$

Considering boundary conditions (1) and (3) leads to the version of equation (3.18) shown on the right-hand side. The system can be solved as follows:

$$\begin{matrix} P_{21} \cdot u_0 + P_{22} \cdot w_0 = 0 \\ P_{41} \cdot u_0 + P_{42} \cdot w_0 = 0 \end{matrix} \quad \Rightarrow \quad \det \begin{vmatrix} P_{21} & P_{22} \\ P_{41} & P_{42} \end{vmatrix} = 0 \quad (3.19)$$

Given that soil parameters z, ρ, v_s, v of each layer are available, the dispersion function can be calculated for each ω-k-combination, which fulfills equation (3.19). Even though infinite solutions exist, only the dispersion functions ω-k and phase velocity functions v_Φ-k for the first, second, and third mode of the pictured model soil profile are illustrated in Figure 3.14.

As a by-product of the left-hand part of equation (3.19), a theoretical H/V-function can be calculated for each mode as follows:

$$\frac{u_0}{w_0} = -\frac{P_{22}}{P_{21}} \quad (3.20)$$

Corresponding H/V-functions for the first three modes are given in Figure 3.14b. In the following chapters, only the theoretical H/V-function of the first mode will be applied in order to characterize the transfer function of any soil profile.

(a)

(c)

(b)

(d)
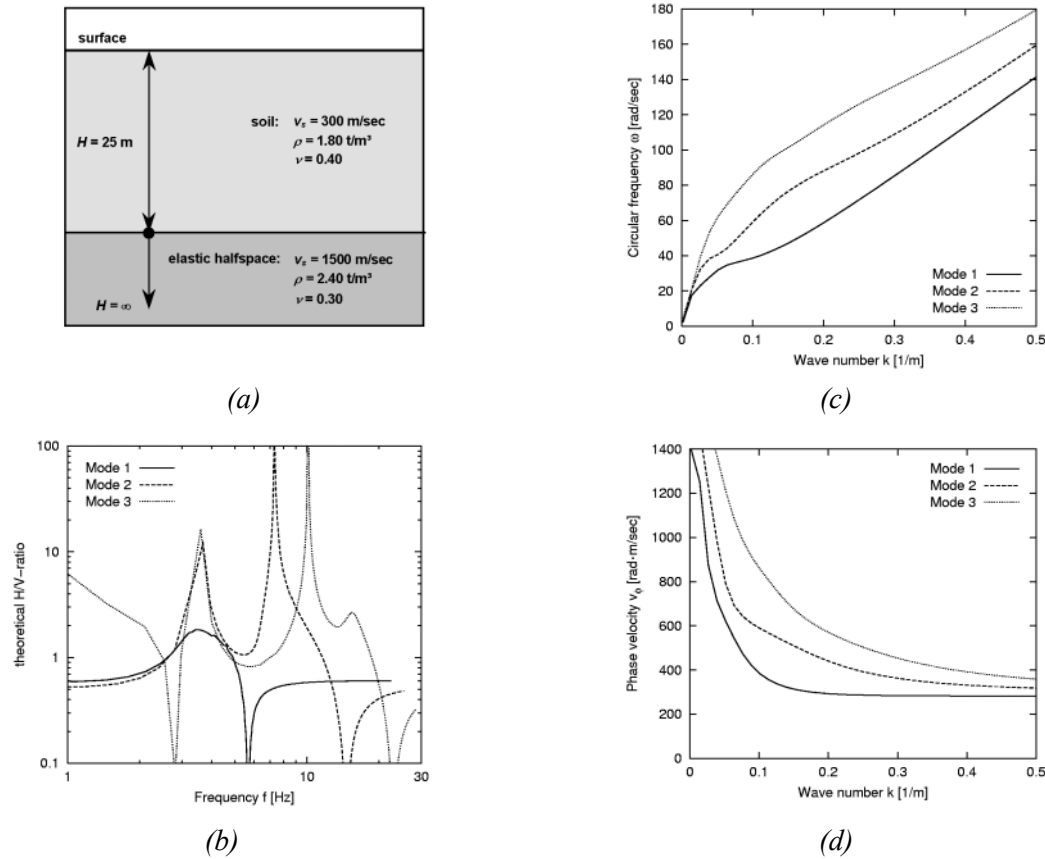
Figure 3.14 Calculation results of the first, second, and third mode of Rayleigh wave motion traveling through a given soil profile (a), theoretical H/V-functions (b), dispersion functions ω-k (c), and phase velocity functions v_Φ-k (d).

3.3 Instrumental methods (experimental, empirical)

3.3.1   Spectral amplification function method (S_a/a) on earthquake data

One of the most convenient ways of obtaining amplification characteristics of a given recording site from instrumental data is to regard the spectral amplification functions of earthquake data.

Most of the current site response estimation techniques refer to the intrinsic frequency content of the seismic signals. For example, the quasi-transfer function of the investigated site is determined by regarding the absolute shape of Fourier amplitude spectra alone or by considering relations between Fourier spectra of different sites (e.g. sediment to rock site) or components (e.g. horizontal to vertical component).

In contrast to these methods, which will be discussed in the succeeding sections of this work, the spectral amplification function, S_a/a, of earthquake data basically relies on the calculation of response spectra normalized with respect to the peak value of acceleration $S_a(T)$/a (peak ground acceleration *PGA*), velocity $S_v(T)$/V, or displacement $S_d(T)$/d of ground motion. Since strong-motion data in most cases is available in terms of ground acceleration, the calculation

of normalized response spectra with respect to peak ground acceleration $S_a(T)/a$ is most commonly used.

For the direct estimation of the expected structural demand under earthquake excitation, the calculation of response spectra has become an important tool in earthquake engineering practice. A response spectrum describes the maximum response induced by the ground motion (due to the earthquake) in oscillators with a single-degree-of-freedom (SDOF). These have different fundamental periods, but possess the same degree of internal damping ξ (KRAMER, 1996; PETERSEN, 1996).

In order to eliminate the absolute level of earthquake ground motion and to establish a common basis that can compare the amplifications of different events, a normalization of the response spectrum has to be carried out. Figure 3.15 illustrates the normalization of an acceleration response spectra ($\xi = 5$ %) by its value of peak ground acceleration. For all normalized spectra, the zero ordinate indicates unity, and different amplification functions can be compared.

For many years, the shapes of all response spectra for a given class of soil condition were assumed to be identical to the level of peak ground acceleration as the only distinguishing criterion. As more instrumental records of earthquakes become available, the spectral shape's dependency on both the magnitude as well as the source distance was quickly recognized. These influencing factors were intensely discussed in Section 2.2.3. According to these findings, spectral investigations of earthquake data do not necessarily reflect the local site conditions only, but also the type of the earthquake record itself. Dependencies on the magnitude level and/or the distance to the seismic source exist, leading to certain ranges of variation with respect to the frequency band of maximum amplification (predominant frequency) and to the amplification level itself.

In order to avoid misinterpretations, the use of normalized response spectra to obtain information about the local site characteristics should therefore be based on a variety of earthquake records covering smaller and larger magnitudes. Taking into account the findings compiled in Section 2.2.3, identifying the fundamental site frequency f_s by regarding the spectral shapes (response or Fourier spectra) of earthquake data is only possible if earthquakes are strong enough to excite the fundamental frequency f_s of the site. However, in earthquake engineering practice, near-distance records of strong earthquakes having magnitudes able to fulfill this prerequisite are seldom.

Investigations at single stations, where a sufficient amount of earthquake records are available (e.g. station DUZ, Figure 2.7) confirm the sharp discrepancy between the spectral shapes of small- to medium-magnitude and large-magnitude earthquakes. In the case that amplification functions calculated for the magnitude $M_s\,7.4$ and $M_s\,7.8$ earthquakes indicate a predominant period $T_G = 0.4$ sec, the fundamental site period T_s can only be discovered if additional investigations are performed.

(a)   *(b)*
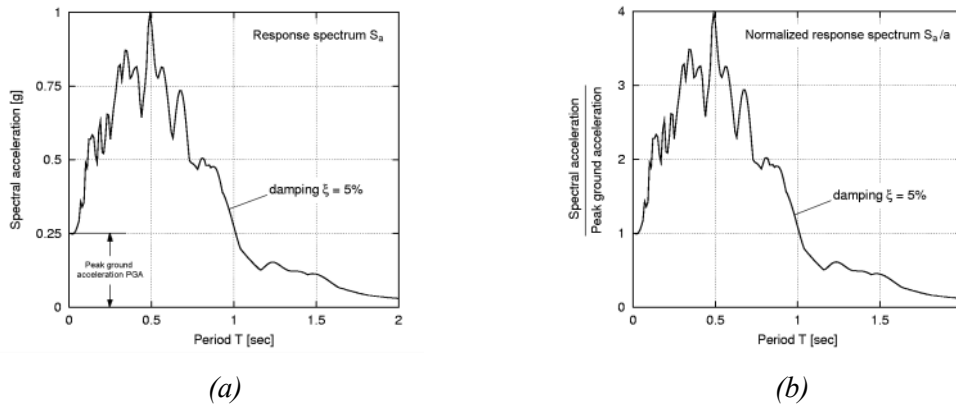
Figure 3.15   Normalization procedure of an acceleration response spectra with respect to its peak (maximum) ground acceleration.

In addition to the application within the investigation of the recording site characteristics, the concept of normalized response spectra is taken up in most of the international earthquake code provisions regarding the elaboration of subsoil-dependent design spectra. Shapes of normalized response spectra for each site class are simplified by using average or envelope curves. In this context, Figure 3.16 shows elastic design spectra dependent on different subsoil classes according to Eurocode 8 (CEN, 2002) and the national earthquake code of France AFPS-90 (AFPS, 1990).

Tests illustrate that soft soils and thick sedimentary layers introduce larger portions of long-period components, while their level of amplification decreases as the thickness of soil layers or their softness increases (SEED & IDRISS, 1982).

Even though amplification functions S_a/a of earthquake data alone are not suited to clearly identify the predominant site frequency, f_s, or detailed information about the subsoil conditions at the recording site, they are important components within the description of seismic ground motion characteristics (see also Chapter 4). If records of strong (damaging) earthquakes are missing, smaller events more likely to occur (e.g. aftershocks) can be applied to reconstruct the ground motion characteristics induced by the mainshock.
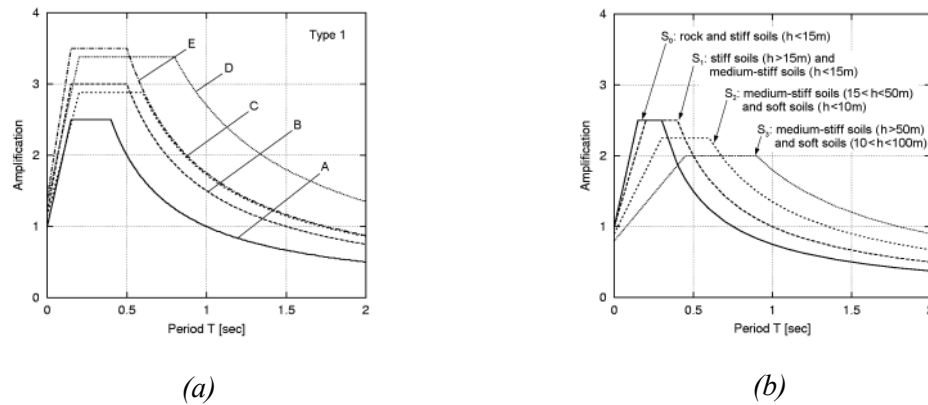
Figure 3.16 Elastic design spectra based on normalized response spectra for different subsoil classes as applied in (a) Eurocode 8, prEN 1998-1 (CEN, *2002*) *and (b) the French earthquake code* (AFPS, *1990*).

3.3.2   Fourier amplitude spectra method (FAS) on microtremor data

In 1954, KANAI introduced the application of the Fourier amplitude spectra method (*FAS*) on microtremor data. Although a variety of shortcomings of the technique were reported by different scientists, absolute noise spectra are still adducted in terms of investigating the site response (ANSARY *et al.*, 1995; FUKUWA & TOBITA, 2000; GUTIERREZ & SINGH, 1992; DE HERNÁNDEZ & DE BARCIA, 1999; LEE *et al.*, 1995; LERMO *et al.*, 1988; NAKAMURA, 1989; OHTA ET AL, 1978; SAKAJIRI, 2000).

The first application of this technique insisted on deriving a "qualitative soil index" (BARD, 1998) based on the average spectrum of ambient noise recorded at the site of interest. Thus a short predominant period indicates a rather stiff or rock-type recording site, while larger periods were attributed to soft soil sites. The idea that a lengthening of the period is associated with an increase of the amplitude was considered in a more refined version of the method.

While not regarding the quality of results obtained by the Fourier amplitude spectra method, the operability of this method strictly depends on two main assumptions (KANAI *et al.*, 1954):

-   ambient seismic noise solely is composed of vertically incident shear waves (*S* waves);
-   the source spectrum of microtremors is characterized by white noise, which means that its power spectral density is constant with frequency.

It can be proved that both assumptions do not correspond to the truth, because

-   microtremors are mainly composed of surface waves (see Section 2.1.1), and
-   each spectrum based on free field noise data is not white, being influenced by band-limited perturbing signals and temporal variations (see Section 2.1.2).

Regardless of the validity of KANAI's assumptions, the Fourier amplitude spectra method on microtremor data sometimes lead to satisfactory results. The grade of stability of Fourier

amplitude spectra, as well as their limits of application, are listed in Table 3.3. They rely on the investigations of different scientific groups. According to these findings, stability of most amplified frequency peaks can be observed especially on soft soil sites in the long-period range ($T > 1.0$ sec). Based on this, predominant frequencies of simple Fourier amplitude spectra have often been regarded as the fundamental resonance frequency of the site. Site effects are clearly strong enough to withstand the source effects under certain conditions. According to BARD (1998), these effects are strongly related to the impedance contrast at depth: "When this ratio is high, surface and/or body waves are trapped and there is a conspicuous spectral peak at the resonance frequency, whatever the origin of the noise waves. When this ratio is low, the trapping in not efficient enough, and noise spectra reflect mainly the source spectra."

Even though stable results may occur under these circumstances, it has to be clarified whether the predominant peaks reflect the influence of long-period microseisms instead of the fundamental resonance frequency of the subsoil.

In order to demonstrate some of the problems which can occur when dealing with the Fourier amplitude spectra method, an example is given in Figure 3.17. At 3-hour intervals over a 24-hour period and at two different sites (A and B), TOKIMATSU (1995) investigated the variation of Fourier spectra of the horizontal and vertical motions on microtremors. Their respective subsoil characteristics are described by the v_s- and v_p-functions with depth H. While spectra at site A show a stable predominant peak at around 0.35 sec in both directions (horizontal, vertical), both Fourier amplitude spectra for the horizontal and the vertical component at site B are not stationary. This leads to an ambiguous identification of predominant peaks.

It can be proved that the fundamental periods at both sites cannot be estimated either from the horizontal or from the vertical Fourier amplitude spectra. Based on the given shear structures in Figure 3.17, the fundamental site periods are 1.39 sec for site A and 0.21 sec for site B.

In some cases the findings of most authors dealing with the Fourier amplitude spectra method on microtremor data confirm that direct spectral amplitudes are misleading when estimating site effects (LERMO & CHÁVEZ-GARCIA, 1994; TOKIMATSU, 1995). Here the probability of exploring the exciting function of the source rather than the site response characteristics is given.

The application of the conventional Fourier amplitude spectra method as described before must be carried out in a very cautious manner. It is strongly recommended to mirror the results of the method with those of other, dependable site response estimation techniques.
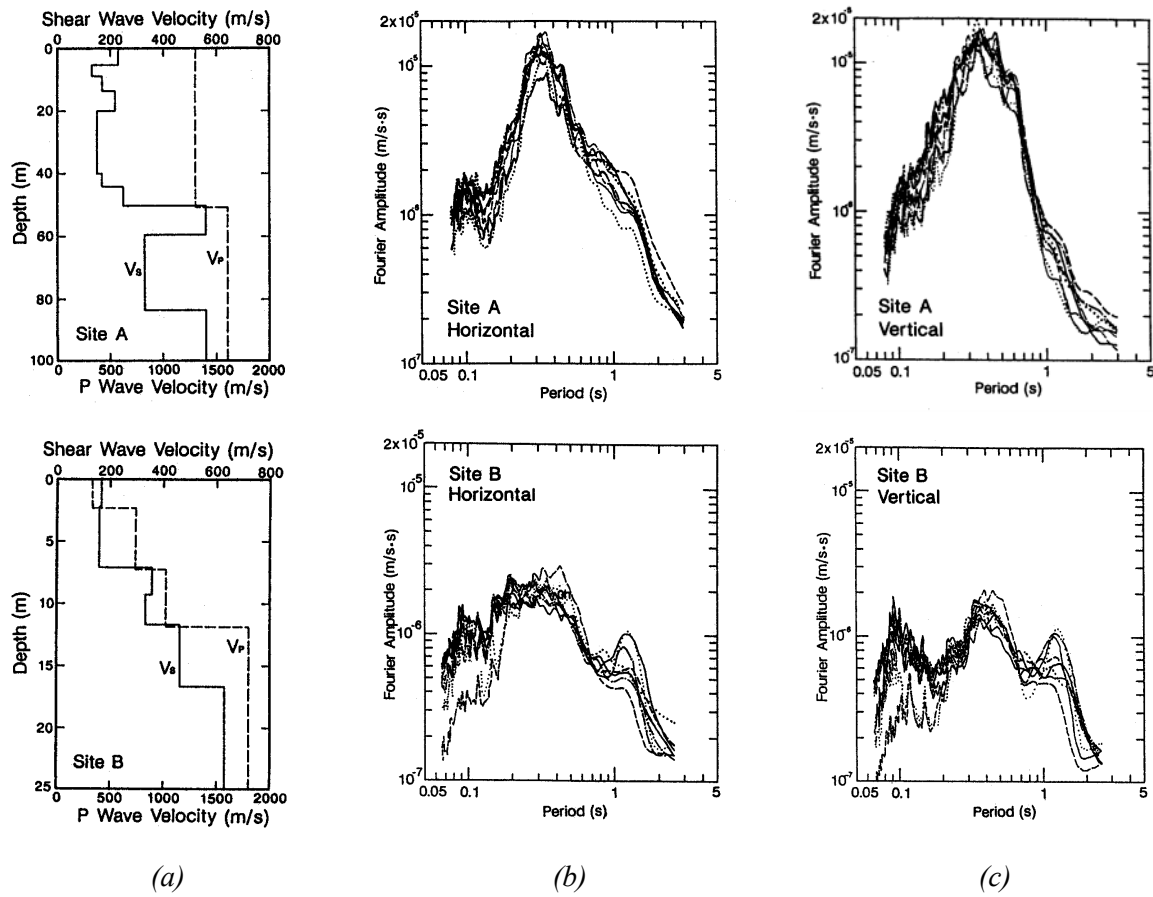
Figure 3.17 Seismic velocity models with depth (a), horizontal (b), and vertical Fourier spectra (c) of microtremors at study sites A (top) and B (bottom); (TOKIMATSU, 1995).

Table 3.3 Grade of stability and limits of application of microtremor Fourier amplitude spectra according to different scientific groups.

Author, Reference	Grade of stability [1] of FAS in the period range T		Comments
ANSARY *et al.*, 1995	◑	> 0.4 sec	FAS influenced by perturbing signals even in the short-period range
FUKUWA & TOBITA, 2000	●	> 1.0 sec	FAS show strong variations in the short-period range
GUTIERREZ & SINGH, 1992	◑	> 2.5 sec	FAS influenced by microseisms
DE HERNÁNDEZ & DE BARCIA, 1999	○		minor quality of results
LERMO & CHÁVEZ-GARCÍA, 1994	◑	*n.s.*	quality of results are case-dependent
LERMO *et al.*, 1988	●	> 0.5 sec	FAS strongly daytime-dependent in the short-period range
OHTA *et al.*, 1978	● (if long-period seismic excitation)	> 1.0 sec	-
SAKAJIRI, 2000	● (if impedance contrast is high)	> 1.0 sec	-
SEO *et al.*, 2000	● (for soft soil sites)	> 1.0 sec	FAS show strong daytime-dependency
TOKIMATSU, 1995	● (for soft soil sites)		FAS show daytime-dependency in the short-period range (see Fig. 3.4)

[1] ● high/good   ◑ moderate/medium   ○ low/minor

3.3.3 Standard spectral ratio method (sediment-rock spectral ratio *SRSR*)

3.3.3.1 *Application of SRSR to earthquake data*

The most applied site response estimation technique on earthquake data, called standard spectral ratio method, was introduced by BORCHERDT (1970). Its main background consists of computing the ratio of horizontal Fourier amplitude spectra between a sediment (soft) recording site (target site) and a nearby recording site on rock (reference site).

The applicability of the technique depends on two basic assumptions:

- The source and paths effects at both sites are similar.
- The reference site has a negligible site response, that is, its spectrum is flat.

The first assumption requires that the distance between both sites is limited in order to have a similar wave field (with similar incidence angles and azimuths) arriving at the two sites. This effect can also be reached with increasing source-receiver distance compared to the distance between the two recording sites (FIELD *et al.*, 1992).
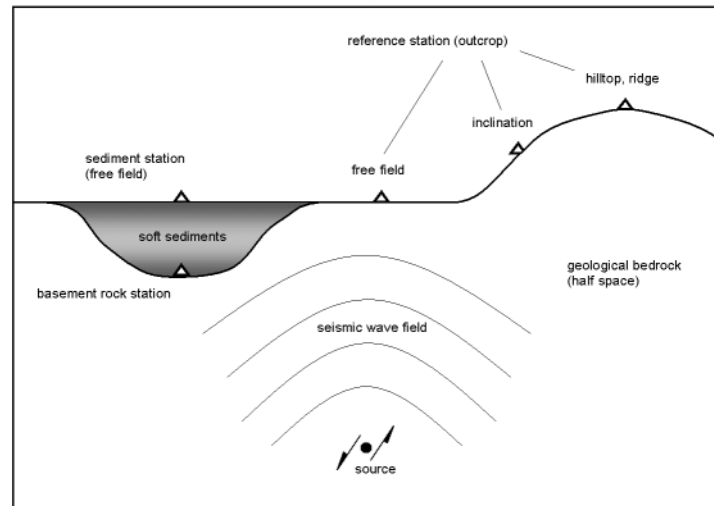
Figure 3.18 Schematic diagram displaying the principles of the sediment-rock spectral ratio technique (SRSR).

The second assumption implies that the record on the rock site, which usually is a free field station on the ground surface, is equivalent to the input motion at some depth (basis of sediment layers), not taking into account the free-surface effects (LERMO & CHAVEZ-GARCIA, 1994). Assuming that the reference site itself has no site response will surely be restrictive in practice. If the bedrock site exhibits a site response apart from a flat spectrum, one could run the risk of an underestimation of the site response. If that is the case, FIELD *et al.* (1992) suggest considering the estimate as a "relative site response".

Apart from the theoretical background, one of the major problems when applying the standard spectral ratio method is making the identification of a pure bedrock site meeting the mentioned pre-requisites.
The investigations of MENKE *et al.* (1990) showed that recordings on different hard-rock sites were statistically coherent (at the 95% confidence level) only when the distance between the stations was less than one third to one half of the wavelength.

The topography of a rock site also plays an important role. TUCKER *et al.* (1984) pointed out that sites on outcrops situated on a ridge can amplify incident motion by as much as a factor of eight over a narrow frequency band. Different rock sites on or in topographic features, such as hilltops or inclinations (compare to Figure 3.18), affect frequencies inversely proportional to the characteristic dimension of that feature.

Own field studies showed, however, that even pure outcrops of geological bedrock close to sediment basins or soft alluvial sites, as well as unweathered outcrops at the ground surface, are very hard to find (e.g. RAPTAKIS *et al.*, 1998).

The standard spectral ratio method was applied to earthquake data by different scientific groups with varying success. The different quality of investigation results (stability and plausibility of spectral curves) may depend on the following factors:

- the type of recording instruments,
- the recorded data type (acceleration, velocity, displacement),
- the types of applied earthquake records (source distance, magnitude range),
- the local site conditions at the recording stations.

Table 3.4 confronts the applied data type of recordings with the quality of results, as well as their grades of conformity with results of other applied site response estimation techniques according to different scientific groups. The quality level of the results can be seen to act independently of the type of seismic data. Interestingly, if the results of the SRSR technique are of high quality, their grade of conformity with the results of other site response estimation techniques also increases.

In order to check the level of the results' dependence on the type of earthquake data, a compilation of selected data sets is given in Figure 3.19. While the chart on the left shows the magnitude-epicentral distance relationships of earthquake events leading to high-quality investigation results, the chart on the right indicates those leading to minor quality levels. The suitability of earthquake recordings for standard spectral ratio technique does not depend on the level of magnitude M or the range of epicentral distance R_e. It could be demonstrated that SRSR does not depend on epicentral distance, focal depth, or magnitude (GUTIERREZ & SINGH, 1992). The same holds for azimuth and, source and path effects (LERMO & CHÁVEZ-GARCÍA, 1993).

In contrast to this, CHÁVEZ-GARCÍA *et al.* (1990) stated that spectral ratios on data coming from distant earthquakes are only valid in the frequency band 1 to 10 Hz. This is true because such a small amount of wave energy exists at high frequencies. Spectral ratios from local earthquakes, however, can be assumed to be reliable between 1 to 15 Hz.

Only small differences between *SRSR* for *P*, *S* and coda waves segments were found by SAKAJIRI (2000), and SATOH *et al.* (2001b).

When dealing with the sediment-rock spectral ratio method, local site conditions at the recording stations tend to exert the largest influence on the level of results. For example, ROVELLI *et al.* (1991) attribute variations in *SRSR* to probable topographic effects at reference stations situated on an elevation.

Table 3.4 Types of applied data and quality of results according to different scientific groups applying Standard Spectral Ratio method (SRSR).

Author, Reference	Data type	Quality of results [1]	Comparison of SRSR with other SRET	Grade of conformity [1]
BORCHERDT *et al.*, 1989	vel. acc.	○ ○	transfer function of *P*, S_V, S_H-waves	○
CHÁVEZ-GARCÍA *et al.*, 1990	vel.	○	-	-
CHÁVEZ-GARCÍA & CUENCA, 1998	acc., vel.	●	HVSR, HVNR (+ RSR)	●
CRUZ *et al.*, 2000	acc.	○	HVNR	○
DUVAL *et al.*, 1994	*n.s.*	○	HVNR	○
FIELD *et al.*, 1992	vel.	●	1-D transfer function	●
FIELD *et al.*, 1995	acc.	◐	HVNR	○
GUTIERREZ & SINGH, 1992	acc.	◐	FAS	○
LERMO & CHÁVEZ-GARCÍA, 1993; 1994	acc., vel.	●	HVSR, HVNR	●
LERMO *et al.*, 1988	acc.	●	FAS	●
ÖZEL *et al.*, 2002	acc., vel.	●	HVSR	●
RAPTAKIS *et al.*, 1998	acc.	●	HVSR, 1-D transfer fct.	◐
RODRIGUEZ & MIDORIKAWA, 2000	acc.	●	HVNR	◐
ROVELLI *et al.*, 1991	vel.	○	SRNR, 1-D transfer fct.	○
SAKAJIRI, 2000	vel.	◐	FAS	◐
SATOH *et al.*, 2001B	vel.	●	HVSR, HVNR	●
TABER, 2000	vel.	◐	HVSR, HVNR	◐
THEODULIDIS & BARD, 1995	acc.	○	HVSR	○
YAMANAKA *et al.*, 1993	vel.	◐	SRNR	○
ZASLAVSKY *et al.*, 1998	vel.	●	HVSR, HVNR	●

[1]   ● high/good   ◐ moderate/medium   ○ low/minor

(a)   *(b)*
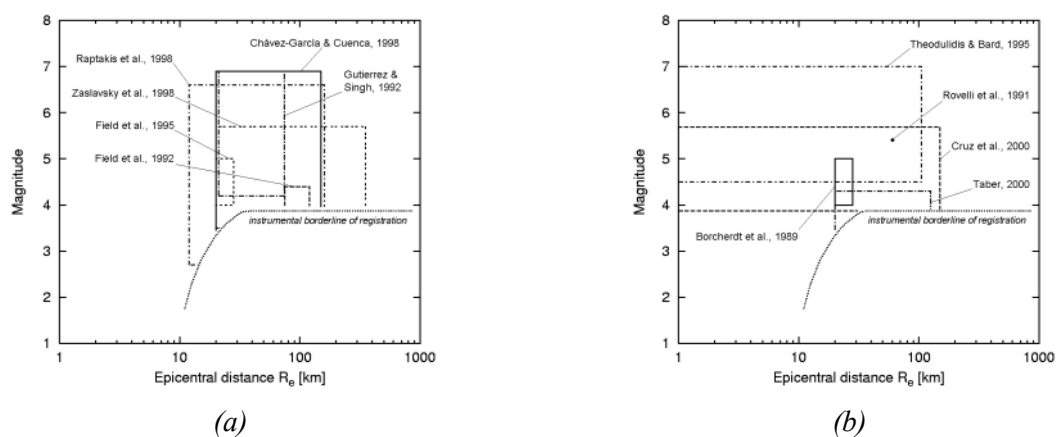
Figure 3.19 Magnitude-distance relationships of earthquake data sets used for standard spectral ratio technique leading to (a) high-quality and (b) low-quality results. Restricted by the instrumental borderline of registration after SMIT, *1996. (Note: Only those data sets are shown for which sufficient information was available.)*

In order to check the applicability and reliability of the standard spectral ratio method, case studies could be carried out with aftershock data recorded by a densely distributed network of German TaskForce in the Southanatolian earthquake region of Adana (Türkiye). More details of the recording stations and their geological conditions can be seen in Annex 2, Table A2-2.

Results for aftershock data with duration magnitudes M_d 2.2 - 3.9 and epicentral distances R_e = 0 - 60 km illustrate, that the reliability of the method depends on the subsoil conditions of the sediment site (magnitudes and localization of aftershocks provided by AFET, 1998). Stable results could be acquired especially for sites with very soft sediments, as at the stations Abdioğlu and Yerdelen (Figure 3.20). If recording sites have stiffer soil conditions, variations in the spectral ratios for different aftershock events are higher (see station Sagkaya, Figure 3.20c).

Since recording stations and locations of aftershock epicenters are distributed within a relatively small area, a more exact investigation of the standard spectral ratio technique could be carried out. A possible factor influencing the stability of results may be the incidence angles of seismic waves arriving at both recording stations. Because seismic waves propagate in radial motions from their source, a more feasible analysis of the method would be to compare the longitudinal and transversal components at both stations.

The "geographic" components of recorded ground acceleration (*NS*, *EW*-comp.) can easily be transformed into transversal and longitudinal components, as long as epicentral coordinates are available. Depending on the azimuth angle, longitudinal and transversal components of ground motion consist of distinct portions of both geographical components. Figure 3.21 compares the average mean curves for different components of ground motion. The types of components regarded here also do not affect the sediment-rock spectral ratios explicitly.
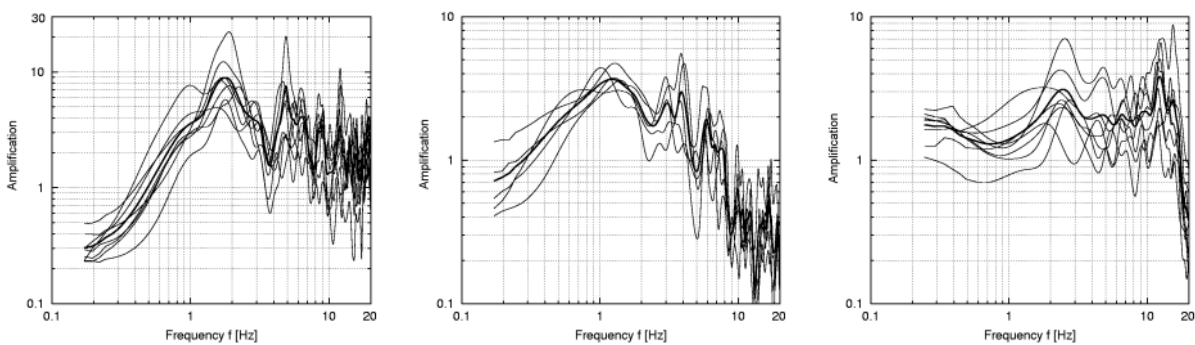
(a) Abdioğlu ABD / Cotlu COT   (b) Yerdelen YER / Sarihuğlar SAR   (c) Sagkaya SAG / Cotlu COT

Figure 3.20   Sediment-rock spectral ratios of aftershocks for different couples of recording sites around Adana, Southanatolian Türkiye. (Note: spectral ratios were calculated for the NS-component of registrations; bold lines represent the mean-value curve.)
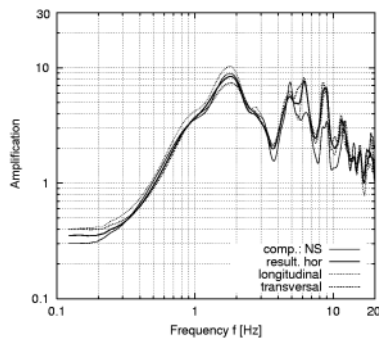
Figure 3.21 Average mean curves of SRSR between station Abdioğlu (ABD) and Cotlu (COT) for different components of ground motion (thin solid line: single NS-comp., thick solid line: resulting horizontal ($\sqrt{NS^2+EW^2}$) comp., thin broken line: longitudinal comp., thick broken line: transversal comp.).

Since the application of the standard spectral ratio technique on weak- or strong-motion data requires a densely distributed array of recording stations, and in the case of minor or moderate seismicity a long observation period, the use of microtremor data was taken up with growing interest among the scientific community.

3.3.3.2   Application of SRSR to microtremor data

The elaboration of sediment-reference spectral ratios of noise data is performed in a similar way as that of earthquake data. In addition to the basic assumptions, one main aspect has to be considered: The applicability of standard spectral ratio method on microtremors implicitly assumes that noise sources at both sites are either common or else statistically similar (HOUGH *et al.*, 1992). The reliability of the method on noise data will depend on the degree to which the prerequisite of similar source and path effects is satisfied.

An important question still remains: Is it necessary to perform noise recordings simultaneously at both stations? In order to identify the same wavefield arriving at both sites, one solution would be to select absolute time windows to correspond to the different shapes of the seismograms. An alternative would be to average many windows at each site, assuming that this represents its ground characteristics at any given time (LERMO & CHÁVEZ-GARCÍA, 1994).

However, although several scientific papers deal with the use of standard spectral ratio techniques on microtremors, questions remain concerning its reliability (FIELD *et al.*, 1990; FIELD *et al.*, 1995; HOUGH *et al.*, 1992; LERMO & CHÁVEZ-GARCÍA, 1993; ROVELLI *et al.*, 1991; ZHAO *et al.*, 2000).

3.3.4   Horizontal to vertical spectral ratio method (H/V)

3.3.4.1   *Application of H/V-method to microtremor data (HVNR)*

Since the early seventies, one of the most debated approaches to site amplification estimates has been applied by scientists all over the world. The so-called spectral H/V-technique (single-station method) on microtremor data was first introduced by NOGOSHI & IGARASHI (1971). Later it was enhanced by NAKAMURA (1989), who suggested that spectral H/V-ratios on microtremors (*HVNR*) represent the *"Quasi-Transfer Spectrum"* of the recording site. Even though the given theoretical background of the technique is questionable to many scientists till today, the stability as well as plausibility of results are almost convincing. There are two interpretations of the method's background that are agreed upon by most of the scientific community.

NOGOSHI & IGARASHI (1971) showed through their investigations, that H/V-ratios on microtremors are directly related to the ellipticity curve of Rayleigh waves because of the predominance of Rayleigh waves in the vertical component. Later they supposed that the frequency-dependent ellipticity leads to conspicuous peaks and troughs in the H/V-ratio, the first being generated by the vanishing of the vertical component around the fundamental *S* wave resonance frequency. According to their statements, results are also valid in the case of present Love waves, since Love waves do not impact the vertical component.

In contrast to this, NAKAMURA (1989) proposed that the H/V-ratio on microtremors can be esteemed as the site response function to *S* waves. Dividing the horizontal component of surface ground motion by the vertical, a removal of the source as well as the Rayleigh wave effects can be obtained. NAKAMURA received many criticisms in response to this statements, leading him to alter his assumptions (NAKAMURA, 1996; NAKAMURA, 2000). Although, NAKAMURA (2000) still assumes that the H/V-ratio is mainly determined by S_H waves, his theoretical background is hardly plausible. He rules out the possibility of Rayleigh waves being responsible for the generation of the spectral peak, since Rayleigh wave energy is very small for this particular frequency range.

Regardless of this fact, which of the proposed theories underlies the spectral H/V-technique on microtremors, results by many scientific groups dealing with this technique show high levels of stability.

It is widely accepted in the scientific community that the spectral H/V-ratio method on microtremors can identify the fundamental frequency of the site, f_s (BARD, 1998; FIELD & JACOB, 1995; LACHET & BARD, 1994; NAKAMURA, 1989; a.s.o.), whatever the theoretical background may be. According to TOKIMATSU (1995), the fundamental site frequency could be as much as 10-20 % smaller than the peak frequency of H/V-ratio, or approximately equal to half the frequency of the H/V minimum. He supposes that the H/V peak frequency of

microtremors may not implicitly correspond to the fundamental site frequency, but may reflect the second one or the depth of the interface between two layers with the highest impedance ratio.

With regard to the whole spectral shape of H/V-ratios, there are clearly differences of opinion as to what the "true" *S* wave amplification function is.

In contrast to the ability of spectral H/V-ratio in identifying the fundamental site frequency, there is no ultimate correlation between the H/V peak amplitude and the maximum spectral amplification of the site. There might be some local relationships for a limited area (BARD, 1998). However, amplification values of spectral H/V-ratios should only be regarded as a relative indicator of local site amplification, since applied instruments or instrumental settings may also exert influence.

Another limit of application, which is reported in numerous publications, is that the H/V-ratio method only provides a reliable estimate of the site characteristics if a significant impedance contrast between overlying stratum and halfspace exists. This in turn means that H/V-ratios on rock sites usually will not exhibit a clear frequency peak, if any, in the high-frequency range. Even though a clear threshold of impedance contrast is in most cases not explicitly given, there is still an obvious correlation between the generation of a clear H/V frequency peak and the stiffness of overlying sedimentary layers. Own investigations of noise recordings directly on outcropping rock sites confirm these effects. That H/V frequency peaks are correlated to stiffness in overlying sedimentary layers leads to the conclusion that spectral H/V-ratios are not amplified over the whole frequency range or characterized by a clear peak in the high-frequency range above 10 Hz. This is illustrated in Figure 3.22, which shows spectral H/V-ratios on microtremors at two outcropping rock sites in Southanatolian Türkiye and Venezuela.

(a) Çakalkuyusu CAK   (b) El Cordon COR
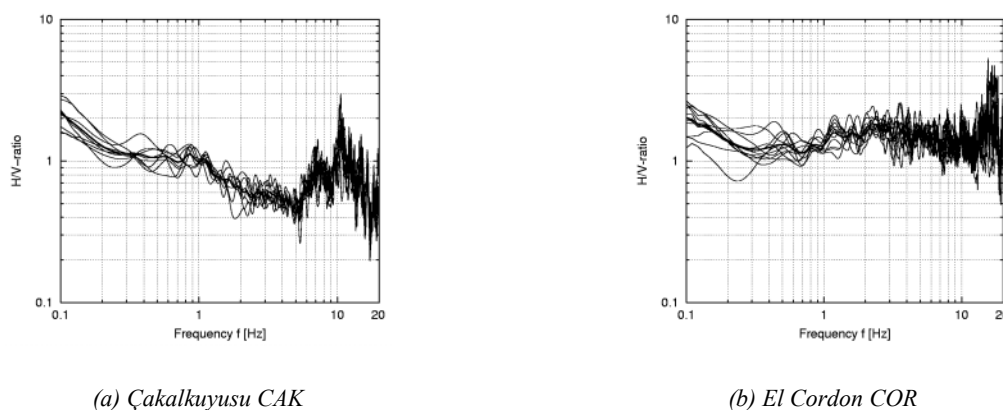
Figure 3.22 Spectral H/V-ratios on microtremors at outcropping rock sites in Southanatolian Türkiye and Venezuela. (Note: Bold lines indicate arithmetic mean curves.)

The successful application of the H/V-ratio method on microtremors premises a good performance of noise measurements. Section 2.1.2 already specified the important aspects in order to gain high-quality noise records. Applicability of the spectral H/V-method or stability of results also depend on several criteria:

- *the type of the seismic sensor and digitizer:*
  GUILLIER *et al.* (2002) made comprehensive checks on the applicability of different instrumental equipment for the spectral H/V-method, showing that reliability and reproducibility of spectral H/V-ratios does not depend on the type of acquisition system (digitizer), but strongly on the type of seismic sensor. According to GUILLIER *et al.* (2002), accelerometers in general and velocity sensors (seismometer, geophones) with natural frequencies higher than 1 Hz should be avoided.

- *the topographical site conditions:*
  Topographical features should be avoided, since they unfavorably alter the H/V-spectra. With respect to the shape of spectral H/V-ratios on microtremors recorded on a steep slope or on a small hilltop, an unusual generation of distinct peaks and troughs can occur. Figure 3.23 schematically illustrates the cross-section of a slope in the city of Bingöl, Eastanatolian Türkiye, with locations of microtremor recording sites (A, B). *HVNR* (Figure 3.23b) show large differences in the low-frequency range ($f < 1$ Hz). Even though local subsoil conditions can be expected to be similar at both sites, the predominant peak at $f = 0.7$ Hz, which seems to represent the fundamental site frequency, can only be observed at site B.

  LERMO & CHÁVEZ-GARCÍA (1993) observed a systematic peak of amplification (at 5 Hz) on the spectral H/V-ratios of ambient seismic noise. The recording equipment was installed at the top of a hill, indicating that the peak was caused by the topographical site conditions.

  To relate this topographical feature with the code provisions of France (AFPS, 1990; cf. Figure 3.10), ordinates of elastic design spectrum, $S_{as}(T)$, at recording site A should be increased by topographic amplification factor, τ ($1.0 < \tau \leq 1.4$). This implies that there are seismic loads up to 40% higher at site A than at site B, located only 50 m away.

| (a) | (b) |
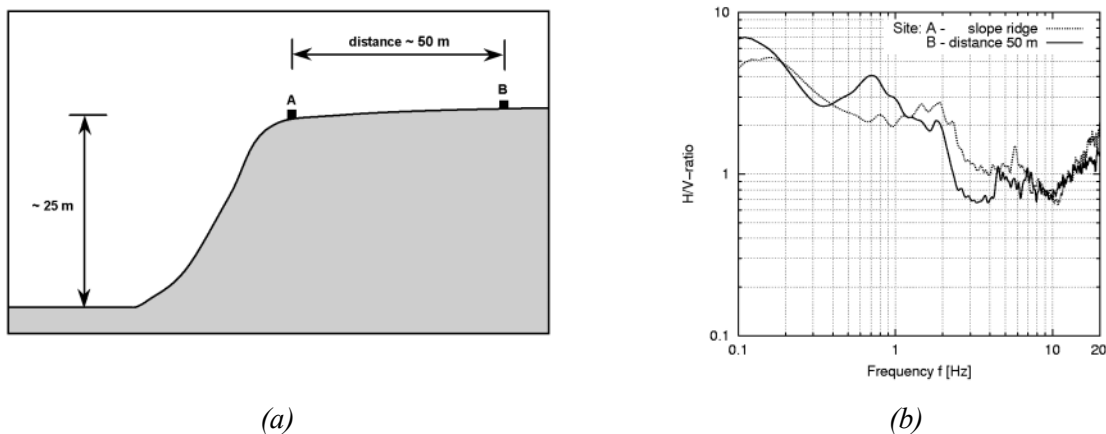
Figure 3.23   Microtremor measurements at a topographic feature in the city of Bingöl (Türkiye): (a) schematic cross-section of the slope, (b) averaged spectral H/V-ratios of recording sites A and B.

- *the local base of the sensor:*
  Shape of spectral H/V-ratios is affected by the material of the local base; compared to natural soil or concrete foundations, investigations on paved or tarmac roads provide negative results; probable damping effects of the local material may modify the seismic signals.

- *the environmental disturbances:*
  Although the spectral H/V-ratio method is believed to nullify the source and path effects of disturbing signals, strong interfering frequencies coming from nearby can change the spectral H/V-ratios significantly; Figure 3.24 illustrates the influence of occasionally interspersing signals coming from machinery near the recording equipment.

- *the meteorological disturbances:*
  Wind gusts and rainfall have an observable influence on the stability of H/V-ratios, while no changes could be observed due to variations in temperature or atmospheric pressure conditions (see also MUCCHIARELLI, 1998); the results of own investigations on the stability of Fourier amplitude spectra and of spectral H/V-ratios under varying meteorological conditions are listed in Table 3.5.

(a) weekend	*(b) workday*
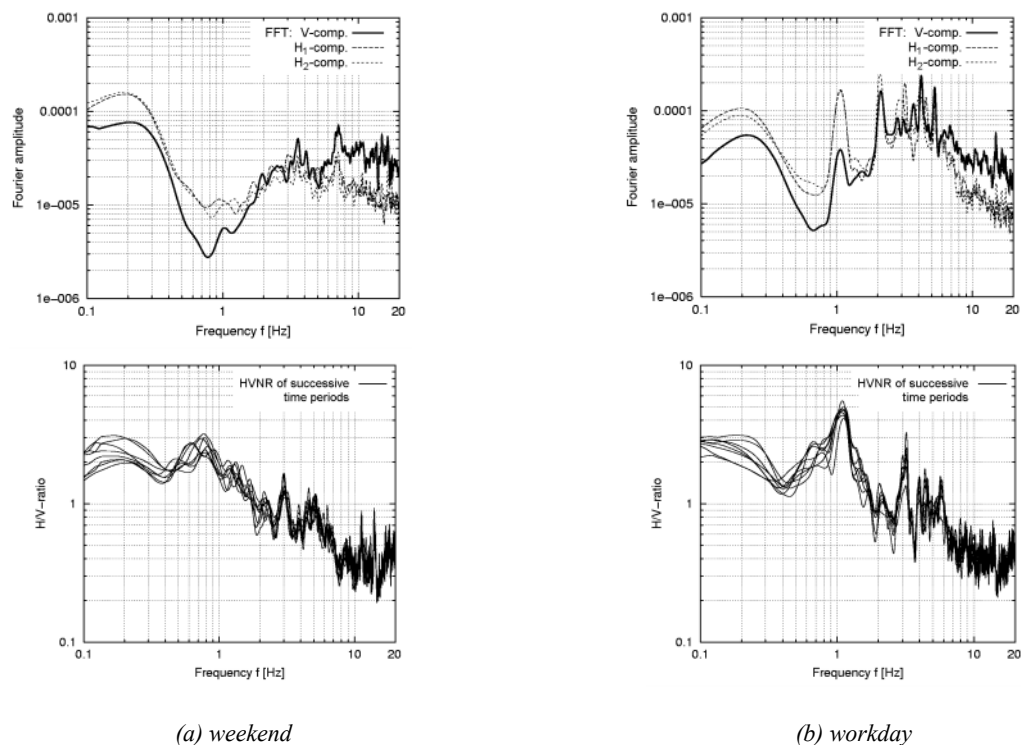
Figure 3.24 Influence of disturbing signals on spectral H/V-ratios on microtremors recorded at the same industrial site on different weekdays. Fourier amplitude spectra (see figures on the top) illustrate the influence of a strong disturbing frequency at ~ 1.1 Hz, which only appears during workdays, thus falsifying the corresponding H/V-spectra.

Table 3.5 Influence of meteorological disturbances on the spectral characteristics (FFT, HVNR) of microtremors (based on long-term observations at a German industrial site; see also ENDE, 2001*).*

Influence on	Meteorological disturbance [1]		
	wind	rainfall	air temperature
Fourier amplitude spectra (*FFT*)	●[2]	●[2]	◐
Spectral H/V-ratios (*HVNR*)	●[3]	●[2]	○

[1]   ● large   ◐ little   ○ no influence
[2]   especially in the low-frequency range (*f* < 1 Hz)
[3]   only around the fundamental site frequency f_s

The reliability of the spectral H/V-ratio technique and its results also depends on several parameters related to the instrumental settings and to the procedure of analysis. Table 3.6 compiles some of these parameters, set by different scientific groups which exert influence on spectral H/V-ratios. All of the authors referred to in this work and who deal with the spectral H/V-ratio technique on microtremors used velocity-type seismometers and based their investigations on Fourier amplitude spectra (FFT).

Table 3.6 shows that most of the depicted spectral H/V-ratios are calculated in the frequency range between 0.1 and 20 Hz. In the case of recording sites with very thick sedimentary layers (*H* > 100 m), it is suggested that the lower cut-off-frequency be determined at 0.04 Hz in order to capture the site's whole amplification characteristics. Spectral resolution in the low-frequency range (around the lower frequency border) can be improved as sample rate and length of analyzed time window increases. Detailed investigations of these effects were carried out by IBS-VON SEHT (1996) and many others.

Averaging the spectral H/V-ratios on microtremors is strongly recommended to allow a clear identification of the single predominant peaks while minimizing large amplitude variations. In addition to conventional averaging, spectral resolution can also be influenced by a variety of filter techniques, tapering the time-history, or smoothing the spectrum.

A careful and convenient coordination of all these influencing parameters, combined with a sophisticated illustration of results (double logarithmic scale is preferred), leads to an enhancement of quality (see also Table 3.6).

Table 3.6 Parameters of data acquisition and processing according to different scientific groups that apply the spectral H/V-ratio method on microtremors (HVNR).

Author, Reference	Sample rate [Hz]	Recording duration	"Windowing"	Frequency range [Hz]	Quality of results [1]
ABEKI *et al.*, 1998a; 1998b	*n.sp.*	3 min each h	5 x 20.48 s	0.2 - 20	●
ANSARY *et al.*, 1995	100	24 h	120 s each h	1.0 - 20	●
ARAI *et al.*, 2000	100	5 min	10 x 20.48 s	0.5 - 20	●
ARAI & TOKIMATSU, 1998	*n.sp.*	*n.sp.*	*n.sp.*	0.2 - 20	●
BOUDEN-ROMDHANE *et al.*, 2000	125	few min	65.54 s	0.1 - 20	○
CHÁVEZ-GARCÍA & CUENCA, 1998	100	2 x 1min	4-6 x 20 s	0.6 - 20	●
CRUZ *et al.*, 2000	*n.sp.*	*n.sp.*	*n.sp.*	0.3 - 20	○
DUVAL *et al.*, 1994	*n.sp.*	several min	8-32 s	0.12 - 20	●
DUVAL *et al.*, 1995	125	10 min	5 x 16 s	0.5 - 20	●
DUVAL *et al.*, 1998	125	10/15-min	5 x 16.38 s	0.12 - 20	◑
ENOMOTO *et al.*, 2000	100	16 h	10 min each h	0.05 - 50	◑
FIELD *et al.*, 1995	*n.sp.*	9 min	*n.sp.*	0.2 – 6	◑
FUKUWA & TOBITA, 2000	100	23 min	64 x 20.48 s, 8 x 163.84 s	0.1 – 10	◑
DE HERNÁNDEZ & DE DEBARCIA, 1999	200	11 x 30 s	*n.sp.*	0.1 – 100	○
JAFARI, 2000	100	60 s	20 s	0.02 – 25	○
KIND *et al.*, 2000	*n.sp.*	*n.sp.*	*n.sp.*	0.1 – 10	●
LERMO & CHÁVEZ-GARCÍA, 1993	*n.sp.*	*n.sp.*	*n.sp.*	0.1 – 20	●
LERMO & CHÁVEZ-GARCÍA, 1994	*n.sp.*	*n.sp.*	*n.sp.*	0.1 – 10	●
MARUYAMA *et al.*, 2000	100	*n.sp.*	*n.sp.*	0.5 – 50	○
NAKAJIMA *et al.*, 2000	*n.sp.*	24 h	6 x 20.48 s each h	0.2 – 20	◑
NAKAMURA, 1989	100	30 h	20.48 s each h	0.15 – 20	●
OHMACHI *et al.*, 1991a	100	3 x 40.96 s	3 x 10.24 s	0.2 – 40	◑
OHMACHI *et al.*, 1991b	100	3 x 40.96 s	3 x 10.24 s	0.2 – 40	◑
RODRIGUEZ & MIDORIKAWA, 2000	*n.sp.*	*n.sp.*	3 x 20.48 s	0.5 – 10	○
SATOH *et al.*, 2001b	50	15 min	81.92 s	0.2 – 10	●
SEO *et al.*, 2000	*n.sp.*	*n.sp.*	*n.sp.*	0.1 – 10	○
TABER, 2000	100	*n.sp.*	*n.sp.*	0.1 – 10	○
TOKIMATSU, 1995	*n.sp.*	*n.sp.*	*n.sp.*	0.3 - 12.5	●
ZASLAVSKY & SHAPIRA, 1998	*n.sp.*	tens of sec	*n.sp.*	0.6 – 10	◑
ZASLAVSKY *et al.*, 1998	*n.sp.*	30 s	*n.sp.*	0.6 – 10	◑

[1] ● high/good   ◑ moderate/medium   ○ low/minor

With regard to the parameter setting of different scientific groups shown in Table 3.6, the performance of spectral H/V-ratio technique for the present work follows a fixed scheme. Table 3.7 depicts the types of instrumental equipment used in the investigations, their parameter settings, and the parameters of data processing (compare with Section 2.1.2). These are presented in respect to the type of noise recording (temporary or continuous measurements).

Table 3.7 Applied instrumental equipment, parameters of recording and data processing
for H/V-ratio technique on microtremor data (HVNR).

Parameter, setting	Type of noise recording	
	temporary	continuous
type of seismic sensor	Lennartz LE-3D/5sec Mark L4-3D/1sec	Lennartz LE-3D/5sec Güralp CMG-40T/30sec
type of digitizer	RefTek DAS 72A-06 (24/16bit)	Lennartz M-24 (24bit) RefTek DAS 72A-06 (24/16bit)
sample frequency	100 Hz	100 Hz (50 Hz)
recording duration	~ 30 min	over several weeks, months
windowing (length of FFT-window)	8,192 values (81.92 sec) 16,384 values (163.84 sec) [1]	
tapering (of time-history data)	not applied	
smoothing (of spectral data)	moving average	
calculation of H/V-ratio	$\dfrac{H_1(NS)}{V(UD)}$ $\dfrac{H_2(EW)}{V(UD)}$ $\dfrac{H_1(NS)+H_2(EW)}{2 \cdot V(UD)}$	
averaging of H/V-ratios	mean value curve of several ratios	
frequency range of interest	0.1 - 20 Hz 0.04 - 20 Hz [1]	

[1] in those cases where sites have very thick sedimentary layers

3.3.4.2 *Application of H/V-method to earthquake data (HVSR)*

Before NAKAMURA introduced his H/V-technique on microtremors in 1989, LANGSTON already calculated spectral H/V-ratios of weak- and strong-motion data by the end of the 1970's (LANGSTON, 1977; LANGSTON, 1979). In order to determine the velocity structure of the crust and upper mantle, he discovered that the vertical component of ground motion is (assumed to be) relatively uninfluenced by the local structure, whereas the horizontal component contains *P* to *S* wave conversions from structural discontinuities below the site. Therefore, by deconvolving the vertical component from the horizontal, an estimate of the impulse response function, or *"receiver function"* below the site is obtained (FIELD & JACOB, 1995).

Meanwhile, numerous authors began applying the spectral H/V-method on earthquake data to investigate the site response for all kinds of earthquake recordings. The results of some of these publications are summarized in Table 3.8. The magnitude-distance relationships of earthquake databases applied to the spectral H/V-method can be taken from Figure 3.25.

Table 3.8 Types of applied data and quality of results according to different scientific groups applying spectral H/V-ratio method to earthquake data (HVSR).

Author, Reference	Data type	Quality of results [1]	Conformity [1] to the results of					
			HVNR		SRSR		SBSR	
			freq.	ampl.	freq.	ampl.	freq.	ampl.
CHÁVEZ-GARCÍA & CUENCA, 1998	acc., vel.	●	●	●	●	●	-	-
LACHET *et al.*, 1994	acc.	◑	-	-	-	-	●	○
ÖZEL *et al.*, 2002	acc., vel.	●	-	-	●	●	-	-
RAPTAKIS *et al.*, 1998	acc.	●	-	-	◑	●	-	-
SATOH *et al.*, 2001b	vel.	●	●	●	◑	●	-	-
TABER, 2000	vel.	◑	◑	●	●	○	-	-
THEODULIDIS & BARD, 1995	acc.	○	-	-	○	●	-	-
TSUBOI *et al.*, 2001	acc.	◑	-	-	-	-	◑	●
ZASLAVSKY & SHAPIRA, 1998	vel.	●	●	●	-	-	-	-
ZASLAVSKY *et al.*, 1998	vel.	●	●	●	◑	●	-	-

[1]   ● high/good   ◑ moderate/medium   ○ low/minor
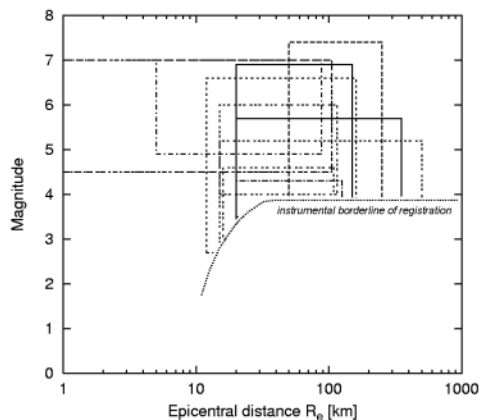
Figure 3.25 Magnitude-distance relationships of earthquake data sets (from Table 3.8) used for spectral H/V-method. Restricted by the instrumental borderline of registration after SMIT, 1996. *(Note: Only those data sets are shown for which sufficient information was available.)*

In order to evaluate the results of HVSR of different scientific groups, Table 3.8 shows the conformities to the results of other site response estimation techniques with respect to frequency and amplitude agreements. Focussing on the spectral H/V-technique, correlations between *HVSR* and *HVNR* are of special interest. Spectral H/V-method on earthquake data may depend on several criteria, such as:

- the recording equipment (type of seismic sensor) determining the type of seismic data (acceleration, velocity),
- the type of earthquake recording (concerning magnitude or epicentral distance) and possible nonlinear effects in the case of strong earthquakes,
- the analyzed parts of the seismogram, e.g. *P* wave or *S* wave window,
- the characteristics of the recording site itself.

Influence of recording equipment

According to Table 3.8, in most cases both velocity and acceleration data show stable results of *HVSR*, which lead to high conformities in predominant frequency peaks and amplitudes compared to other site response estimation techniques. At first sight, the quality of the results does not depend on the type of seismic sensor. However, in order to receive reliable seismic data, one must also consider the spectral transfer characteristics of the seismic recording equipment. To illustrate this effect, Figure 3.26 shows H/V-ratios of two local earthquakes recorded at the same site with different seismometers. It can be seen that the *HVSR* of the event recorded by a short-period seismometer (Lennartz LE-3D/1sec) is not amplified in the whole frequency range below 1 Hz, while the *HVSR* based on the recording of a long-period seismometer (Lennartz LE-3D/5sec) displays a clear frequency peak at about 0.15 Hz.
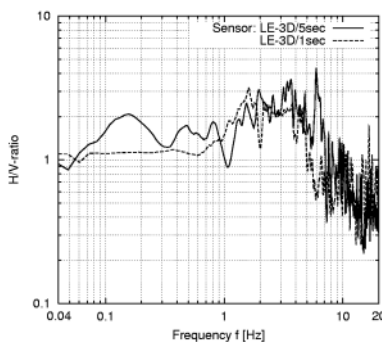
Figure 3.26 Spectral H/V-ratios of two local earthquakes recorded with different seismic sensors (recording site: deep soft sediments).

Findings like these confirm that even the results of high-sensitive seismometers should be checked according to their frequency-dependent transfer characteristics. As a result, reliable assertions concerning HVSR results should only be stated in the frequency range ensured by the transfer characteristics of the recording equipment.

The investigations of earthquake data recorded by high-frequency strong-motion accelerometers clearly exhibit these effects in the short-frequency range. As Figures 3.27 and 3.28 indicate, correlations between spectral H/V-ratios on microtremors (*HVNR*, recorded by broad-band seismometer) and aftershocks (*HVSR*, recorded by strong-motion accelerograph) occur only if the fundamental site frequency is below 1 Hz.

In case of predominant site frequencies in the short-frequency range (as described by *HVNR* in Figure 3.29), the *HVSR* of aftershocks are not able to confirm the frequency peak below 1 Hz. Frequency peaks of *HVSR* in the higher frequency range may exhibit higher harmonics of site characteristics.

A valid objection against these assumptions is that small-magnitude earthquakes (e.g. aftershocks) with short epicentral distances cannot excite the low-frequency range of subsoil due to their high-frequency characteristics (compare to Section 2.2). This would mean that strong earthquakes (e.g. mainshocks) are applicable even at sites with soft sedimentary layers of large thicknesses, indicating the fundamental site frequency in the low-frequency range. In order to vitiate this supposition, spectral H/V-ratios of three different mainshock recordings are compared to *HVNR* on microtremors, recorded during recent Post-TaskForce missions to Venezuela and Türkiye. Mainshock records were performed by different types of strong-

motion accelerographs (station UDO: SMA-1, station CYH: SMA-2, station BOL: SSA-320); data was provided by the national seismic networks (FUNVISIS, Caracas; AFET, Ankara). Tests clearly confirm that agreement between *HVNR* and *HVSR* only occur if the fundamental site frequency is situated in the frequency band of the strong-motion sensor, as at station UDO Cumaná (Figure 3.29a).

Almost every publication checked in Table 3.8 is concentrated on the frequency range above 1 Hz. Thus the level of conformity between *HVNR* and *HVSR* is high. It can be hypothesized that the quality of results decreases, since sites with softer subsoil conditions or larger sediment thicknesses having fundamental frequencies below 1 Hz will be investigated.

(a) Düzce DUZ   *(b) Çaybaşi CAY*   *(c) Gölyaka GOY*
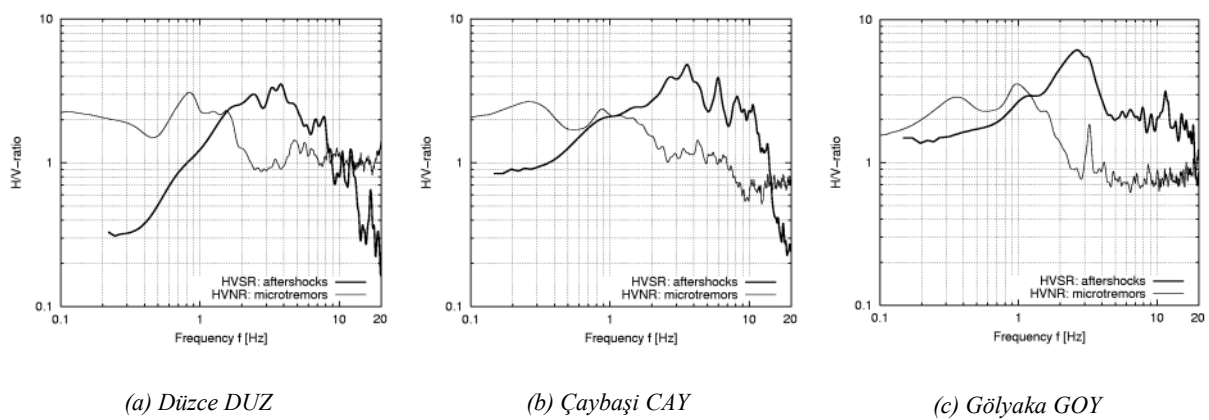
Figure 3.27 Averaged spectral H/V-ratios of aftershocks (M_L 2.0-3.0) and microtremors at sites with fundamental frequencies below ~ 1 Hz (bad compliance between HVSR and HVNR).

(a) Abdioğlu ABD   *(b) Yerdelen YER*   *(c) Akyazi AKY*
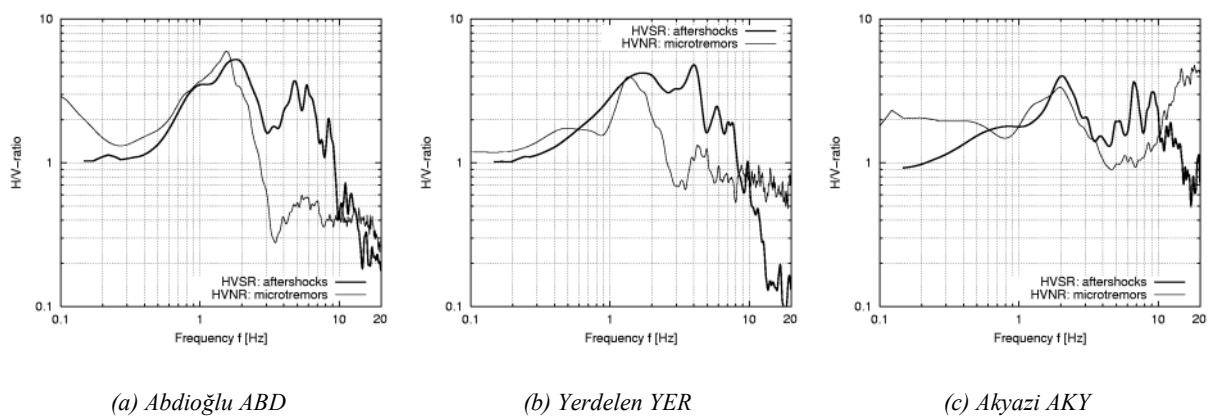
Figure 3.28 Averaged spectral H/V-ratios of aftershocks (M_L 2.0-3.8) and microtremors at sites with fundamental frequencies above ~ 1 Hz (good compliance between HVSR and HVNR).

(a) Cumaná Univ. de Oriente UDO
(1997 Cariaco earthquake, M_w 6.9)

(b) Ceyhan CYH
(1998 Adana earthquake, M_s 6.2)

(c) Bolu BOL
(1999 Düzce earthquake, M_s 7.4)
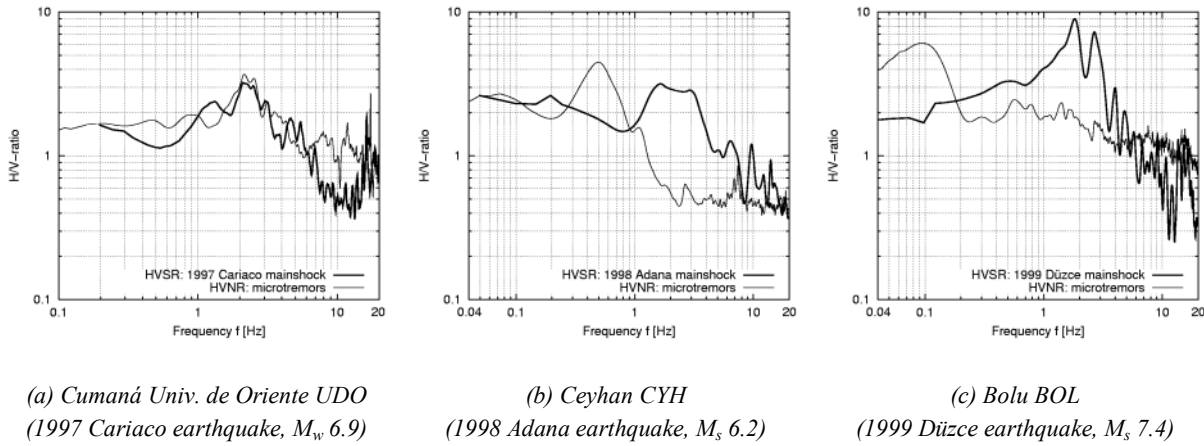
Figure 3.29   Spectral H/V-ratios of mainshock recordings and microtremors at three different sites (data provided by: FUNVISIS Caracas *(a),* AFET Ankara *(b)(c)).*

Influence of earthquake characteristics

To check the dependence of *HVSR* stability on earthquake characteristics such as epicentral distance, R_e, or earthquake magnitude, *M*, own investigations of near-source events ($R_e \leq 50$ km) were carried out. In the case of small- to medium-magnitude events it can be shown that *HVSR* does not depend on magnitude or epicentral distance. Figure 3.30 illustrates *HVSR* average curves of arranged aftershocks dependent on local magnitude, M_L, and epicentral distance, R_e, at three strong-motion recording stations in Northanatolian Türkiye (LANG *et al.*, 2002). Although the magnitude range fell between 1.0 and 5.0, only small deviations occurred.

The question whether nonlinear effects are already comprised in these medium-magnitude events cannot be answered. If they were, it could be concluded that *HVSR* are unaffected by nonlinear effects. In order to check this phenomenon, comprehensive investigations even of strong earthquake recordings with higher levels of ground acceleration would be necessary. Figure 3.31 compares *HVSR* of available mainshock- and aftershock records at one single station in Northanatolia. It can be seen that *HVSR* of both magnitude 7 mainshocks are slightly shifted in the short-frequency range and are more amplified below 2 Hz than *HVSR* of aftershocks. Two possible explanations for the differences in *HVSR* of mainshocks and aftershocks could be given: the influence of nonlinear effects or the transfer characteristics of the different strong-motion sensors.

However, results indicate that even on the basis of mainshock records, no information about the spectral amplification below 1 Hz can be obtained. With regard to Figure 3.31, it is supposed that the influence of nonlinear effects in spectral H/V-ratio technique can be neglected. In all likelihood, a lack of agreement between *HVSR* curves in Figure 3.31 can be assigned to the different transfer characteristics of applied strong-motion recorders.

(a) Akyazi AKY   *(b) Çaybaşi CAY*   *(c) Gölyaka GOY*
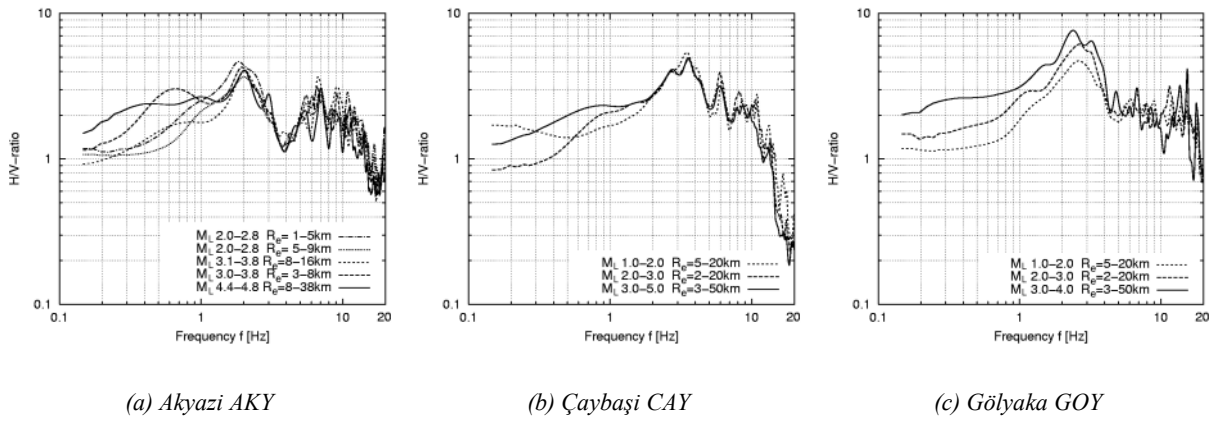
Figure 3.30 Averaged spectral H/V-ratios of aftershocks dependent on ranges of magnitude, M_L, and epicentral distance, R_e (Lang et al., 2002).
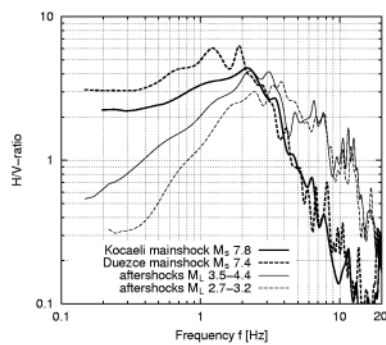
Figure 3.31   Comparison between HVSR of mainshocks and averaged aftershock records for different ranges of magnitude at station Düzce DUZ (DZC).

Influence of different wave types

Recent publications recommend taking only the intense *S* wave part of the seismogram (accelerogram) for spectral H/V-analysis. In the case of near-source events, a separate analysis of the *P* and *S* wave part of the seismogram is nearly impossible. All *HVSR* given in previous figures were calculated for the whole accelerogram and comprised all wave types.

A comprehensive investigation was done in this context by Satoh et al. (2001b), who calculated *HVSR* of *P*, early *P* coda, *S*, and late *S* coda wave-trains, and showed that the *P* wave part of a seismogram cannot be applied to spectral H/V-technique. As can be seen in Figure 3.32, spectral H/V-ratios for the *P* wave part are completely different from H/V-ratios for the other parts of the seismogram. According to Satoh *et al.*, these results can be interpreted as surface waves becoming important with the beginning of *P* coda as time progresses, because microtremors are considered to be mainly composed of surface waves. A more perspicuous explanation would be to interpret microtremors consisting of *S* waves, thus leading to the spectral agreements of the curves. Figure 3.33 illustrates spectral H/V-ratios for separate *P* and *S* wave windows of two teleseismic recordings compared to the H/V-spectra on microtremors just before the *P* wave arrival, called pre-noise. Results confirm the observations of Satoh *et al.* (2001b): While clear correlations between H/V-ratios on microtremors and *S* wave parts exist, spectral shape of the H/V-ratio for *P* wave parts are sizably lower in the frequency range up to 2 Hz.

In order to make use of long-distance or teleseismic recordings in terms of spectral H/V-analysis, it is recommended to neglect the *P* wave part of the seismogram and concentrate solely on the *S* wave windows.
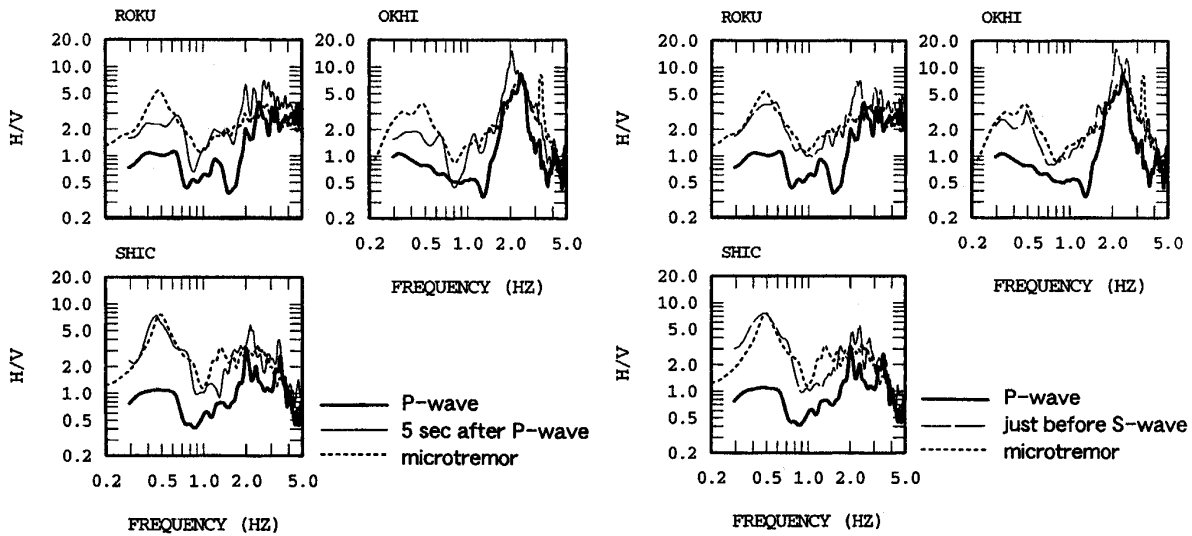
Figure 3.32   Averages of spectral H/V-ratios for microtremors and different wave windows of earthquakes at three recording sites in Japan (SATOH *et al.*, 2001b).
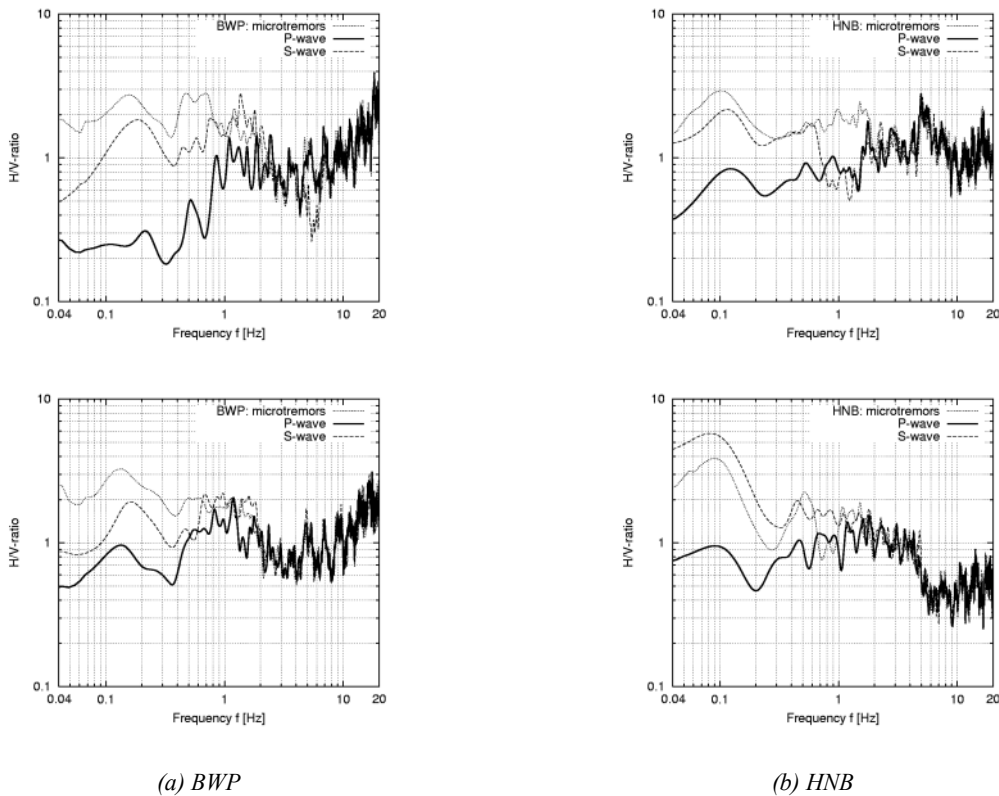
(a) BWP   *(b) HNB*

Figure 3.33   HVSR for microtremors, P and S waves of selected teleseismic events at two German seismic stations with comparable site conditions (top: Fiji Islands Region, 19.8.2002, M_s 7.5; bottom: Russian-Chinese border, 26.6.2002, m_b 7.5).

3.3.5   Surface-borehole spectral ratio method (SBSR) on earthquake data

One of the most reliable instrumental techniques for site response estimation is the surface-borehole spectral ratio technique (SBSR). In contrast to the sediment-rock spectral ratio method, which is based on surface recordings of ground motion, the SBSR technique accounts for the simultaneous measurements of seismic signals on the ground surface and at a certain depth. Because the latter requires the availability of a seismic instrumented borehole that, at best reaches the geological bedrock, this technique could only be tested at very few sites (e.g. BOUDEN-ROMDHANE *et al.*, 2000; LACHET *et al.*, 1994; SEO *et al.*, 2000; TSUBOI *et al.*, 2001).

Its basic procedure of analysis is identical to that of the sediment-rock spectral ratio technique, assuming that the borehole station deep in the ground acts as the reference station. KUDO & WANG (1992) showed that spectral results of the SBSR technique are less scattered than those of the SRSR method, even though the average mean curves for both techniques are nearly the same. Figure 3.34 compares *SBSR* and *SRSR* curves for several earthquake events.

<p align="center">(a) SBSR   (b) SRSR</p>
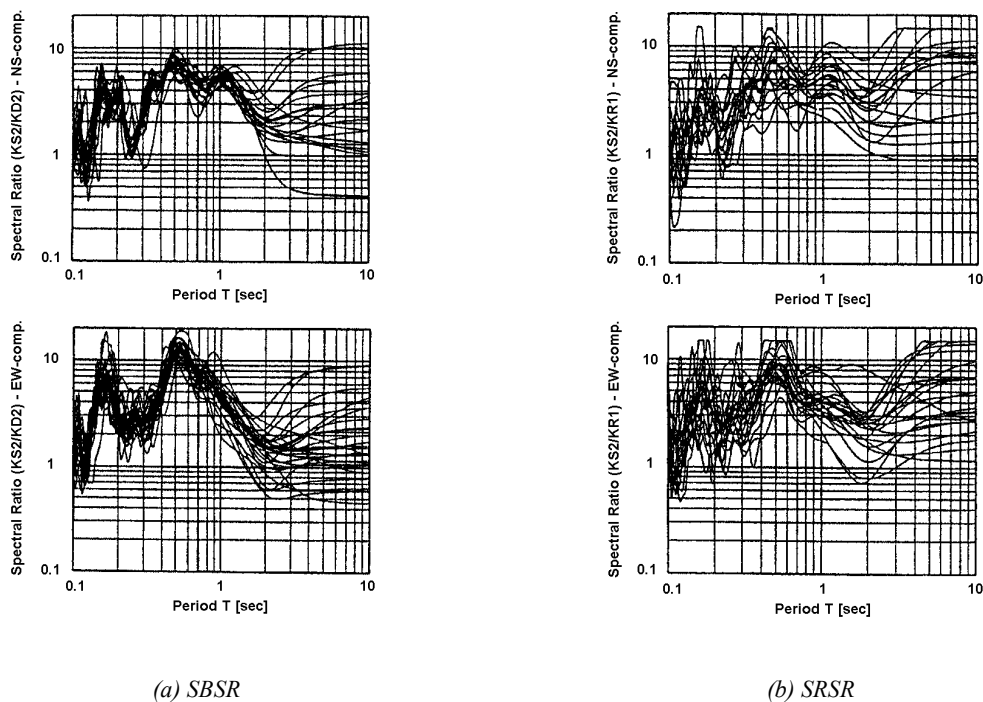
Figure 3.34 Spectral ratios of a sediment surface station (KS2) to a borehole station (KD2, - 97 m) and to a rock surface station (KR1) (reproduced from KUDO & WANG, 1992; KUDO, 1996).

Since earthquake data from instrumented boreholes is hard to obtain, applicability of the SBSR method is constricted. Own investigations on the plausibility of the method using earthquake data of two different borehole sites in California (Treasure Islands, La Cienega) showed that results strongly agree with theoretical transfer functions of the corresponding soil profiles (Figure 3.35, cf. SCHWARZ & MAIWALD, 2003). In contrast to theoretical transfer functions, *SBSR* are characterized by high amplification levels, which can be explained by the different ground motion amplitudes at the ground surface and at a certain depth.
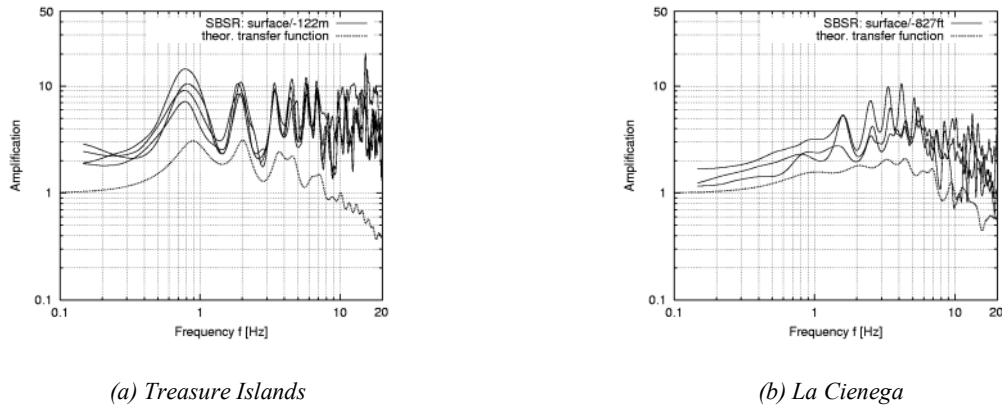
(a) Treasure Islands   (b) La Cienega

Figure 3.35 Surface-to-borehole spectral ratios on different earthquake recordings compared with theoretical transfer functions of the respective site (data provided by CSMIP; GRAIZER *et al.*, 2000).

3.4 Evaluation of the different site response estimation techniques

The theoretical and empirical (instrumental) site response estimation techniques described so far represent only an extract of the total number of available methods. Nevertheless, the techniques discussed here can be regarded as the most commonly applied methods. Except for the SRSR and SBSR methods, the instrumental techniques are mainly concentrated on the single-station methods or on methods using seismic signals recorded at the ground's surface (Table 3.9).

As the importance of economical aspects increases, those analysis methods providing a high degree of simplicity concerning measurement and data processing are being used. In this regard, analysis methods based on seismic data recorded in boreholes (e.g. surface-borehole spectral ratio method SBSR), or using instrument arrays (e.g. spectral-analysis-of-surface-waves SASW on microtremors), imply high efforts and thus increased costs. Even though the quality and detailedness of these results are usually higher compared to the simpler methods, their benefit for reaching the defined targets should be balanced.

As noted in Section 1.2, a major problem when dealing with microzonation studies and the application of empirical site response estimation techniques is the inability to interpret the results and how to use these results for engineering purposes. In any case, since most of the methods presented here lead to frequency-dependent curves (spectra), it has to be clarified whether they represent

- the characteristics of the site's subsoil or
- the characteristics of the exciting function of the source.

Table 3.9 Classification of empirical methods discussed in this section.

Method	Abbr.	Applied on [1]		No. (type) of observation points	Component motions of interest [2]
		noise data	earthquake data		
Spectral amplification functions	S_a/a	○	●	1 (surface)	H
Fourier amplitude spectra	FAS	●	○	1 (surface)	H (V)
Standard spectral ratio	SRSR	●	●	2 (surface)	H
Horizontal-vertical spectral ratio	HVSR, HVNR	●	●	1 (surface)	H and V
Surface-borehole spectral ratio	SBSR	○	●	1 (surface & downhole)	H (V)

[1] ● applicable ○ not applicable
[2] H - horizontal V - vertical component of seismic motion

Spectral ratios between different components of seismic motions (e.g. *HVNR*, *HVSR*) or different recording sites (e.g. *SRSR*, *SBSR*) are more suitable to reflect the subsoil characteristics, as source and path effects are nullified. In contrast, methods elaborating absolute spectra of the seismic data (e.g. *FAS*, S_a/a) reproduce the characteristics of the exciting function, such as the noise wavefield or a strong seismic event.

The results of the different empirical techniques may indicate the following:

- (ranges of) predominant site frequencies, f_s,
- level of site amplification,
- transfer function of the local subsoil conditions, *TF*,
- site response to earthquake excitation.

It must be stressed that the predominant site frequency, also denoted as natural site frequency, f_s, is related only to the subsoil and its physical properties. Because of the nonlinear soil behavior and its strong dependence on the level of ground shaking, one should concentrate on a certain range of natural site frequencies, f_s, rather than on a single fixed value (HAMPE *et al.*, 1991; LANG *et al.*, 2002). Its actual significance lies in giving information about the frequency range of the highest expected soil amplification, and thus can be an important parameter for structural design.

Predominant site frequencies, f_s, particularly those relying on ambient seismic noise or weak-motion earthquake data, can only reflect the elastic soil behavior. As was shown in Section 2.2.3, incorporating the intensity of strong ground motion is hard to obtain and can only be realized as the case arises. Though spectral ratio techniques on strong ground motion tend to neglect the nonlinear behavior of soil (see Section 3.3.4.2), care has to be taken while extrapolating results based on weak-motion data to the level of (damaging) strong ground motion. This holds especially when referring to absolute spectral values (e.g. spectral amplification functions S_a/a).

The ability of different site response estimation techniques to identify the natural site frequency f_s, the corresponding amplification level, the whole transfer function including the detection of higher modes, or the earthquake site response is qualitatively evaluated in Table 3.10.

The spectral H/V-ratio technique on microtremors is most reliable when used to define the local subsoil characteristics. Since the recording of ambient seismic noise provides some advantages to earthquake recording, spectral H/V-ratio method on microtremors will preferably be applied for further site and subsoil classification.

As is proposed by most scientists dealing with the methods on instrumental data described in this work, results of different empirical techniques and different types of input data should be compared in order to increase their reliability. In this context, BARD (1998) strongly recommends that we not "rely only on microtremor measurements" (..), but further to install "a few temporary stations in order to obtain several earthquake recordings, at least for a local 'calibration' of noise results." Given that information on the local subsoil conditions are available, theoretical analyses should also be carried out.

Table 3.10 Qualitative evaluation of different empirical methods on instrumental seismic data according to scientific literature.

Method	Type of data	Ability to identify [1]			
		predominant site frequency	level of site amplification	site transfer function	earthquake site response
S_a/a	earthquake	◑	◑	○	●[3]
FAS	noise	○	○	○	○
SRSR	noise	○	○	○	○
SRSR	earthquake	●	◑[2]	◑	○
HVNR	noise	●	●	●	○
HVSR	earthquake	●	●	◑	○
SBSR	earthquake	●	◑[2]	●	○

[1]   ● with high accuracy (exact)   ◑ with moderate accuracy (rough, to some extent)   ○ impossible
[2]   amplification levels are usually too high
[3]   reliability of results decreases as only weak-motion earthquake data is applied

It also must be checked how these results could be applied for engineering purposes. It is of great interest to which extent the results of empirical methods help to deduce parameters needed for seismic design (i.e. generation of elastic design spectrum of the site). Figure 3.36 schematically illustrates the "EC 8-type" elastic design spectrum, as well as the parameters determining its shape.

The elastic design spectra representing the smoothed shape of actual earthquake response spectra can clearly be compared with normalized response spectra, S_a/a. It should still be analyzed whether any dependencies between results of the estimation techniques and parameters describing the elastic design spectrum exist.

This may concern two points:

- the (range of) natural site frequency, f_s (and respective natural site period, T_s) with corner periods T_B and T_C, describing the plateau range of the highest spectral amplification,
- the level of site amplification with soil parameter, S.

With respect to results based on spectral H/V-ratio technique on microtremors, tendentious contiguities exist between the amplification level of H/V-ratios and soil parameter, S, as quantified in DIN 4149 (DIN, 2002), for example. Conversely, the fundamental site period, T_s, does not correlate with corner periods, T_B or T_C. Even though there is a trend that corner period(s), (T_B) and T_C, are shifted into the longer period range as soil consistency becomes softer and/or total sediment thickness increases (and natural site period T_s also moves into the long-period range), a dependency between both cannot be stated.
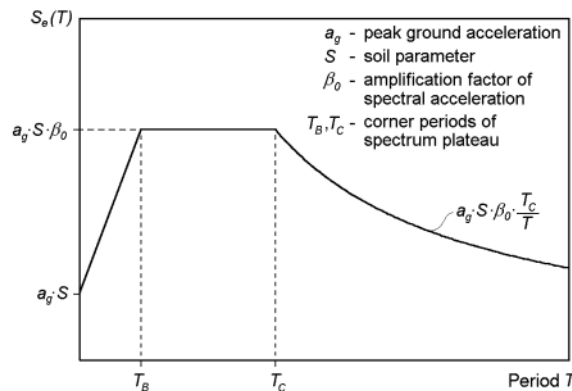
Figure 3.36 Principle description of elastic design spectrum (EC 8-type).

Concerning the applicability of results of both empirical and analytical site response estimation techniques, the following can be summarized in terms of deriving parameters useful for structural design:

- investigated spectral ratio methods are suitable to detect the (range of) natural site frequency, f_s, and to some extent, the level of site amplification;
- because spectral H/V-ratios on microtremors provide the highest level of both stability and reliability, further applications (site classification) are concentrated mainly on this technique;
- there are only rough correlations between parameters describing the elastic design spectrum of a site and the results of the spectral ratio methods;
- a description of an elastic design spectrum can only be supported by normalized response spectra on earthquake data, S_a/a.

4 Experimental seismic site classification

4.1 Purpose of site classification

In order to provide reliable seismic design loads for a selected site, the identification of its amplification potential, among other things, has to be carried out. Seismic site amplification depends on the characteristics of local subsoil rather than on the level of seismic excitation. A reliable categorization of site conditions should therefore be ensured.

A variety of classification schemes are generally given in different international earthquake codes. Many of them are based largely on the soil consistency of the upper 30 m (100 ft) of the soil profile, which in turn assumes that dynamic or geotechnical material parameters of the soil layers are available. The definition of typical soil categories expressed by lithologic terms - rock, consolidated sediments, and soft soils - is common practice. By allocating different shapes of elastic design spectra for each soil class, their influence on amplification and frequency characteristics can be considered. In earthquake resistant design codes, the effects of local soil conditions are generally taken into account by the corner periods of the highest site amplification and the soil amplification factor relative to the bedrock amplification.

The consistency of the near-surface subsoil layers has significant influence on the transfer and amplification characteristics of seismic waves. To keep matters simple, a more or less detailed generalization of subsoil conditions and their distribution into several site classes must be performed.
It therefore must be proved whether the site classification schemes of most current code provisions are powerful enough to consider all possible aspects of soil amplification. In addition to soil consistency and total depth of sedimentary layers, soil amplification characteristics could also be influenced by other parameters, such as surface topography or nonlinear soil effects (see Section 3.1).

The importance of a seismic site assessment lies not only in the description of seismic loads in terms of interpreting or estimating the amount of structural damage, but also in different scientific fields of engineering seismology. Since local soil conditions may have a considerable influence on the characteristics of seismic waves, the importance of a reliable seismic site assessment is increasing. By combining sites of similar soil conditions into several site classes, a kind of simplification as well as a basis for comparability between different soil types can be achieved.

A variety of some of the most popular and innovative site classification schemes is presented in the following section.

4.2 Site classification schemes

According to current site classification schemes as applied in international earthquake resistant design codes or scientific publications, a rough subdivision into the following groups can be observed:

- stiffness-related classification schemes,
- stiffness-and-depth-related classification schemes,
- hybrid classification schemes.

While stiffness-related classification schemes are mainly based on the soil parameters, and more precisely on the soil material stiffness of the uppermost 20 or 30 m of the near-surface soil layers, stiffness-and-depth-related classification schemes also consider the extent of the sedimentary layers at depths. The latter distinguishes between sites having the same consistency of near-surface soil layers but different depths, i.e. different total thickness of sedimentary soil layers. Both site classification schemes are based primarily on the available information coming from borehole data and soil laboratory tests.

In contrast, hybrid procedures of site classifications rely on the principles of stiffness-and-depth-related site classification schemes endorsed by the results of experimental site investigations. Examples of this include spectral H/V-ratios on microtremor data recorded at the ground surface.

The main characteristics of the different classification schemes, as well as some of their limits of application, are summarized in Table 4.1. The backgrounds of the classification systems will be given in the following sections.

Table 4.1 Characteristics of the different types of site classification schemes.

	Classification scheme [1]			
	Stiffness-related		Stiffness-and-depth-related	Hybrid
	N_{SPT}	$v_{s,30}$, G_{dyn}	v_s, H	v_s, H, *exp.data*
regarding dynamic soil properties	○	●	●	●
regarding total depth of soil layers	○	○	●	●
identification of natural site frequency f_n	○	○	●	●
identification of relative site amplification	○	○	◑	●
identification of liquefaction susceptibility (water-saturation)	●	○	○	◑

[1]   ● yes   ◑ to a certain extent   ○ no

A more simplified scheme of site classification, disregarding any parameter of the soil materials (such as shear wave velocity, v_s, or dynamic shear modulus, G_{dyn}) can be found in the Geomatrix classification system (GEOMATRIX CONSULTANTS, 1993). This will not, however, be discussed in detail here. Its different site classes separating rock and shallow soil sites from deep soil sites are listed in Table 4.2. Because this classification scheme requires little detailed site information in order to classify a site, it is commonly used in the United States (RATHJE *et al.*, 2003).

Table 4.2 The Geomatrix classification system (GEOMATRIX CONSULTANTS, 1993).

Site class	Site class description	Comments
A	Rock	Soil depth $H < 6$ m.
B	Shallow soil	Soil depth $H < 20$ m.
C	Deep soil, narrow canyon	Soil depth $H > 20$ m, canyon < 2 km wide.
D	Deep soil, wide canyon	Soil depth $H > 20$ m, canyon > 2 km wide.
E	Soft soil	$v_s < 150$ m/sec

4.2.1 Stiffness-related classification schemes

The stiffness-related site classification schemes are always constricted to a certain range of soil depth below the ground surface. Most of the schemes are limited to the uppermost 30 m (100 ft) of the soil profile (e.g. AMBRASEYS *et al.*, 1996; HOSSER & KLEIN, 1983; ICBO, 1997). Being inconsiderate of the soil medium below, either mechanical (e.g. values of standard penetration resistance of the soil, N_{SPT}) or dynamic parameters (e.g. average shear wave velocity $v_{s,30}$, shear modulus G_{dyn}) of the 30 m of soil profile act as the main criteria for site classification.

Table 4.3 compares the classification schemes according to AMBRASEYS *et al.* (1996) and HOSSER & KLEIN (1983), which are only based on the average shear wave velocity, $v_{s,30}$, of the uppermost 30 m of the soil profile.

Table 4.3 Comparison between different site classification schemes.

Grade of soil stiffness	AMBRASEYS *et al.* (1996)		HOSSER & KLEIN (1983)	
	Site class	Shear wave velocity, $v_{s,30}$ [m/s]	Site class [1]	Shear wave velocity, $v_{s,30}$ [m/s]
very low	very soft	$v_{s,30} < 180$	*not defined*	
low	soft	$180 < v_{s,30} < 360$	A	$v_{s,30} < 400$
medium	stiff	$360 < v_{s,30} < 760$ (800)	M	$400 < v_{s,30} < 1100$
high	rock	$v_{s,30} > 760$ (800)	R	$v_{s,30} > 1100$

[1] A – alluvium,   M – medium,   R – rock

Types of stiffness-related site classification schemes were also adopted by several international earthquake resistant code regulations (those of the United States and Venezuela, for example).

While the site classification of the Venezuelan earthquake regulation COVENIN (Provisional) 1756-82 (MDU, 1990) is based only on the shear wave velocity $v_{s,30}$ of the upper 30 m of sedimentary soils (Table 4.4), the classification of the 1997-UBC of the United States (ICBO, 1997) can be done either regarding the average shear wave velocity, $v_{s,30}$, or the average standard penetration resistance, N_{SPT}, of the uppermost 30 m (Table 4.5).

Table 4.4 Stiffness-related site classification of the Venezuelan earthquake regulation COVENIN (Provisional) 1756-82 (MDU, 1990).

Grade of soil stiffness	COVENIN (Provisional) 1756-82 (MDU, 1990)		
	Site class	Shear wave velocity, $v_{s,30}$ [m/s]	Description
very low	S3	$v_{s,30} < 250$	Loose granular soils and/or soft to medium-cohesive soils with $H > 10$ m.
low	S2	$250 < v_{s,30} < 450$	Medium-dense to dense sands and gravel, stiff to very stiff sands or clays, or mixed types.
medium	S1	$300 < v_{s,30} < 700$	Hard and/or dense soils with $H < 50$ m.
high	S1	$v_{s,30} > 750$	Rock.

Table 4.5 Site classification according to the 1997 Uniform Building Code (ICBO, 1997).

Site class	Site class description	Average soil properties for uppermost 30 m of soil profile		
		Shear wave velocity, $v_{s,30}$ [m/s]	Standard penetration test, N [blows/ft]	Undrained shear strength, u_s [kPa]
A	Hard rock, eastern United States sites only	> 1500	*not applicable*	*not applicable*
B	Rock	760 – 1500	*not applicable*	*not applicable*
C	Very dense soil and soft rock	360 – 760	$N \geq 50$	$u_s \geq 100$
D	Stiff soils	180 – 360	$15 \leq N \leq 50$	$50 \leq u_s \leq 100$
E	Soft soil, profile with more than 3 m of soft clay defined as soil with plasticity index $PI > 20$, moisture content $w > 40\%$	< 180	$N < 15$	$u_s < 50$
F	Soils requiring site specific evaluations: 1. Soil vulnerable to potential failure or collapse under seismic loading, e.g. liquefiable soils, quick and highly sensitive clays, collapsible weakly cemented soils. 2. Peats and/or highly organic clays: layers 3 m thick or more. 3. Very high plasticity clays: layers 8 m thick or more, with $PI > 75$. 4. Very thick soft/medium stiff clays: layers 36 m thick or more.	*not specified*	*not specified*	*not specified*

4.2.2   Stiffness-and-depth-related classification schemes

Since the stiffness-related classification procedures are restricted to the uppermost soil layers (e.g. 30 m), the influence of the total sedimentary soil thickness on the amplification characteristics of the site will not be covered. The amplification of ground motion is significantly affected by the natural period of the site, T_s, which depends not only on the dynamic stiffness of the soil materials (expressed by shear wave velocity, v_s, and material density, ρ), but also on their total thickness, H.

A stiffness-and-depth-related classification procedure subdividing the soil profile into different layers of thickness is incorporated into several earthquake resistant code provisions, e.g. into France's, Türkiye's and Germany's. As Table 4.6 illustrates, the classification scheme of the Turkish earthquake code (TMPS, 1998) is based on the definition of different soil groups (A)-(D). A further arrangement of soil groups (A)-(D) put into local site classes Z1-Z4 in dependence on the total layer thickness, h, has also been achieved (Figure 4.1).

Table 4.6 Site classification according to the Turkish code provision (TMPS, 1998).

Soil group	Site class description	Average soil properties		
		Shear wave velocity, v_s [m/s]	Standard penetration test, N [blows/ft]	Unconf. compression strength [kPa]
(A)	1. Rock (massive, unweathered, metamorphic, stiff cemented)	> 1000	-	> 1000
	2. Very dense sand, gravel	> 700	> 50	-
	3. Hard clay, silty clay	> 700	> 32	> 400
(B)	1. Soft/weathered rocks	700-1000	-	500-1000
	2. Dense sand, gravel	400-700	30-50	-
	3. Very stiff clay, silty clay	300-700	16-32	200-400
(C)	1. Highly weathered soft rocks	400-700	-	< 500
	2. Medium dense sand and gravel	200-400	10-30	-
	3. Stiff clay, silty clay	200-300	8-16	100-200
(D)	1. Soft, deep alluvial layers with high water table	< 200	-	-
	2. Loose sand	< 200	< 10	-
	3. Soft clay, silty clay	< 200	< 8	< 100
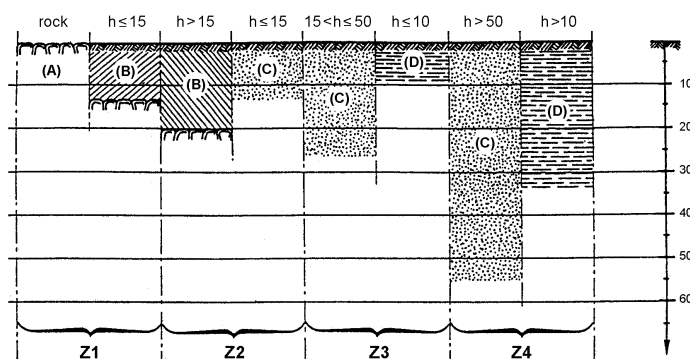
Figure 4.1 Local site classes as defined in the Turkish earthquake code regulation (TMPS, 1998).

Another site classification scheme regarding the influence of a globally described subsoil and the geological profile at a certain depth is comprised in the current German earthquake code DIN 4149 (DIN, 2002). A twofold classification has been carried out, distinguishing between the type of soil materials and their total thicknesses above bedrock. Soil material types are represented by three different soil condition classes: 1, 2, and 3 (Table 4.7). Geological subsoil classes (A, B, C) consider the geological subsurface conditions, and hence stand for the thickness of overlying sediments.

Geological subsoil class A can be characterized by missing or overlying sediments with maximum thicknesses of 25 m, whereas class C is described by deep, mostly Quaternary alluvial layers reaching depths between 100 and 1000 m. Geological subsoil class B represents the transition zones between classes A and C, as well as shallow basin structures with thicknesses of sedimentary layers between 25 and 100 m.

The geological conditions within Germany's earthquake regions admit only some possible combinations between the different geological subsoil classes and soil condition classes. These six, respectively seven different combinations of the so-called site-specific subsoil classes (*SC*) are illustrated by Figure 4.2 (SCHWARZ *et al.*, 1999 proposed a subdivision into seven different site-specific subsoil classes complementing class C2).

It should be stressed that these soil profiles represent the idealized variants of nearly homogeneous material stiffness over the total soil depth (SCHWARZ *et al.*, 1999).

Table 4.7 Definition of the different soil condition classes of German earthquake code
DIN 4149 (DIN, 2002).

Grade of soil stiffness	DIN 4149 (DIN, 2002)		
	Soil condition class	Shear wave velocity, v_s [m/s]	Description
low	3	$v_s < 350$	fine-grained soil (fine sands, *loesses*)
medium	2	$350 < v_s < 800$	loose soil (gravel to coarse sands, marls)
high	1	$v_s > 800$	firm to medium-firm soil
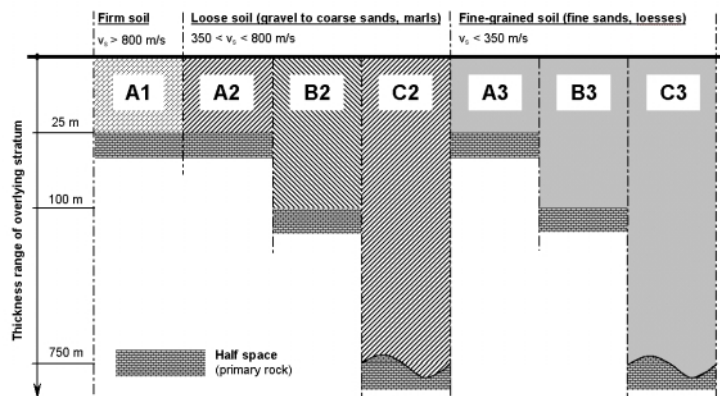
Figure 4.2 Possible combinations of site-specific subsoil classes (SC) following the principles of the national German earthquake code DIN 4149 (DIN, 2002). (Note: SC C2 is not considered in the present draft of DIN 4149. Modified figure taken from LANG et al., 2003a.)

4.2.3 Hybrid site classification schemes

With regard to the aforementioned restrictions of the stiffness-related site classification schemes, local site conditions can be described more accurately if the total thicknesses of their sedimentary layers are considered. Both types of site categorization however are based on geotechnical information about soil materials. This in turn assumes that data has to be obtained by geotechnical (boreholes) or seismic exploration methods (surface reflection/refraction), which usually are time- and cost-consuming. As a result, a reliable seismic site assessment on the basis of these "conventional" procedures can only be performed if sufficient information about the local subsoil conditions is available.

For this reason, hybrid site categorization methods have been developed that consider the predominant site frequency, f_s, as an additional differentiating factor. Since site response estimation techniques are suitable for deriving the quasi-transfer function of the site and thus the fundamental site frequency, f_s, from seismic data recorded at the ground surface, an alternative site classification can be achieved even when information on geotechnical subsoil is missing.

An innovative example for a hybrid site classification scheme that meets both the characteristics and demands of a stiffness-and-depth-related classification scheme, as well as the specification of ranges for fundamental site frequency, f_s, is presented by BRAY & RODRÍGUEZ-MAREK (1997). The proposed classification following the 1997-UBC scheme (ICBO, 1997) is summarized in Table 4.8, primarily subdividing the 1997-UBC site classes into different soil depths, H. A further sub-classification of the soft soil classes is made by accounting for the depositional age (Holocene or Pleistocene) and the soils' cohesive level.

Although indicated ranges for fundamental site frequencies seem to be determined by using the results of theoretical calculations for possible combinations between average shear wave velocities, v_s, and total sediment thicknesses, H, a site classification based on instrumental techniques could be carried out.

A practical application of a hybrid site classification is described by LEE *et al.* (2001), who used response spectra shape and horizontal-to-vertical spectral ratio of earthquake records for classification of strong-motion sites in Taiwan. Categorization of response spectra was done by using the mean acceleration spectral shapes from SEED *et al.*, 1976 (Figure 4.3a), while *HVSR* were classified according to the regulations of the Japanese code (JAPAN ROAD ASSOCIATION, 1980). The latter distinguishes between four different period ranges for the fundamental site period, T_s (Figure 4.3b).

Table 4.8 Hybrid site classification on the basis of 1997-UBC simplified geotechnical site categories (BRAY & RODRÍGUEZ-MAREK, 1997; *table reproduced from* RODRÍGUEZ-MAREK *et al.*, 2001).

Site	Site class description	Site frequency, f_s [Hz]	Comments
A	Hard rock	≥ 10.0	Hard, strong, intact rock: $v_s > 1500$ m/s.
B	Rock	≥ 5.0	Most "unweathered" California rock cases: $v_s \geq 760$ m/s or $H < 6$ m of soil.
C-1	Weathered/soft rock	≥ 2.5	Weathered zone: $H = 6 - 30$ m; $v_s > 360$ (700) m/s.
C-2	Shallow stiff soil	≥ 2.0	Soil depth: $H = 6 - 30$ m.
C-3	Intermediate depth stiff soil	≥ 1.25	Soil depth: $H = 30 - 60$ m.
D-1	Deep stiff holocene soil, either sand or clay	≥ 0.7	Soil depth: $H = 60 - 200$ m. Sand has low fines content ($< 15\%$) or non-plastic fines ($PI < 5$). Clay has high fines content ($> 15\%$) and plastic fines ($PI > 5$).
D-2	Deep stiff pleistocene soil, sand or clay	≥ 0.7	Soil depth: $H = 60 - 200$ m. See D-1 for sand or clay sub-categorization.
D-3	Very deep stiff soil	≥ 0.5	Soil depth: $H > 200$ m.
E-1	Medium depth soft clay	≥ 1.4	Thickness of soft clay layer: $H = 3 - 12$ m.
E-2	Deep soft clay layer	≥ 0.7	Thickness of soft clay layer: $H > 12$ m.
F	Special, e.g. potentially liquefiable sand or peat	≈ 1.0	Holocene loose sand with high water table ($z_w < 6$ m) or organic peat.
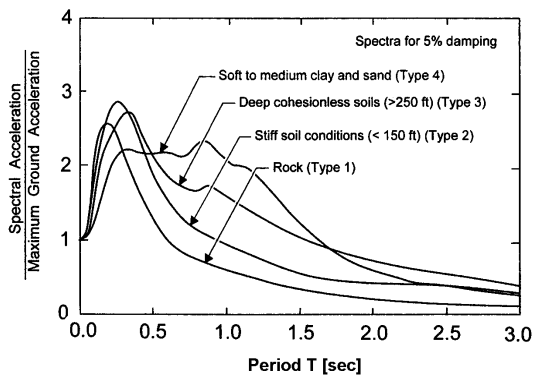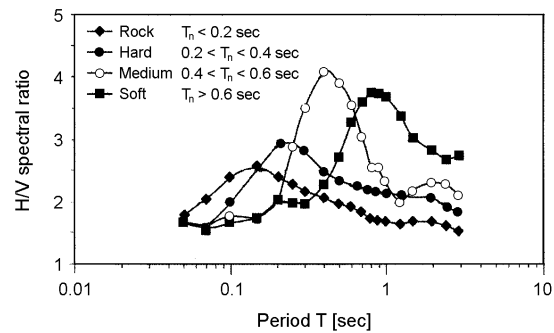
(a)   *(b)*

Figure 4.3 Normalized response spectra (a) and H/V spectral ratio (b) for hybrid site classification as proposed by LEE *et al., 2001 (figures taken from (a)* SEED *et al., 1976 and (b)* LEE *et al., 2001).*

4.3 *MESSIAS - Method of an Experimental Seismic Site Assessment*

With regard to the different types of site classification schemes, the ones using instrumental data for purpose of comparison and checking prove to be the most reliable. Reliability of an experimental-based site classification primarily depends on the quality and amount of available information about the local subsoil conditions.

As it was already stressed, a detailed acquaintance to local site conditions becomes important in evaluating the site amplification characteristics, and consequently in elaborating the damage potential of seismic ground motion.

Based on the principles of hybrid site classification procedures, a method has been developed that incorporates all available information about the site of interest. The main consequences of the "*MESSIAS*" method can be specified as follows (LANG *et al.*, 2003a):

- estimation of the site transfer function, either in an analytical or instrumental way,
- evaluation of possible "surrogate" subsoil profiles, in cases of missing or only fragmentary subsoil information,
- classification of the site according to a generally accepted code provision scheme,
- estimation of the site spectrum and the level of seismic action, only if required earthquake data is available.

Figure 4.4 illustrates the procedure in terms of a flowchart. The different components will be described in the following sections.
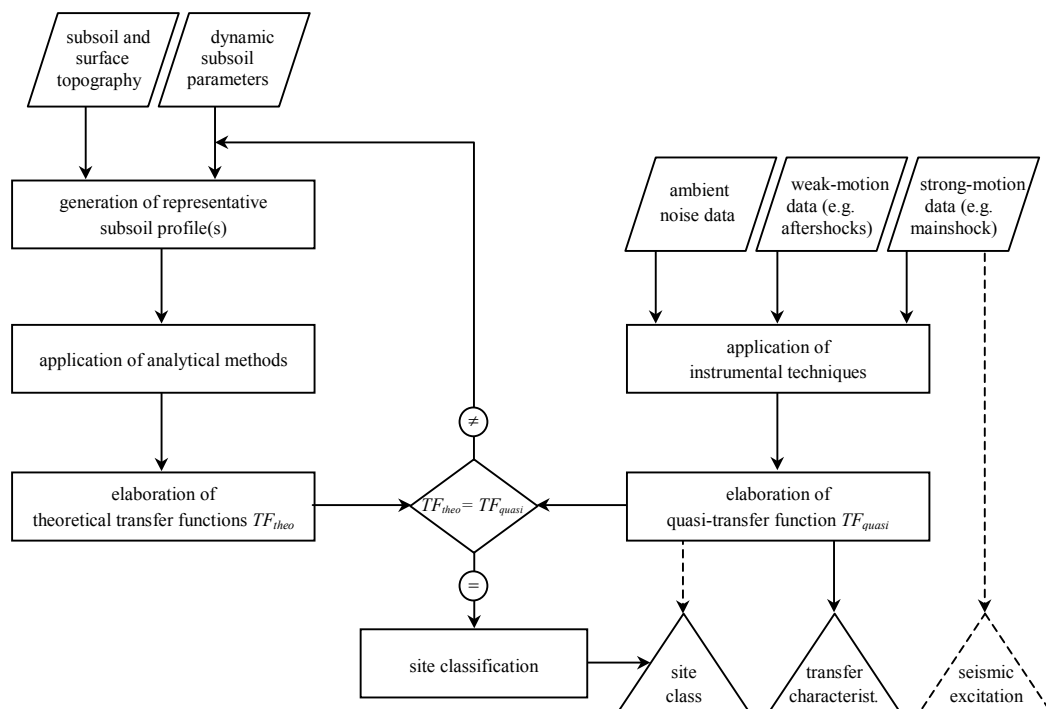
Figure 4.4 Flowchart of MESSIAS - Method of an Experimental Seismic Site Assessment
(LANG *et al.*, 2003a).

4.3.1   Site classification procedure

Since different types of input data are correlated, the site classification scheme incorporated within *MESSIAS* can be denoted as a hybrid. On the basis of theoretical and experimental information, a more refined classification of the subsoil at best can be carried out.

In order to provide a standardization of the explored sites, the site-specific classification scheme was selected that was proposed in the German earthquake code DIN 4149 (DIN, 2002), subdividing it into 6 resp. 7 (SCHWARZ *et al.*, 1999) site-specific subsoil classes (*SC*).

The procedure of site classification described in this work rests mainly upon the conformity between the theoretical transfer function, TF_{theo}, and the experimentally determined quasi-transfer function, TF_{quasi} . The latter usually reflects the spectral H/V-ratio on microtremor data (*HVNR*). Since the shape of a site-characteristic *HVNR* cannot be affected by any means, conformity between both transfer functions can only be obtained by varying the parameters of the subsoil model.

Reliability of site classification strongly depends on the quality and amount of available subsoil information. As experience shows, three different cases regarding the completeness of soil parameters have to be distinguished, namely whether:

- any parameters of soil materials are missing,
- parameters only of the near-surface soil materials are available,
- parameters of the whole soil profile reaching down to bedrock are available.

(a)   (b)
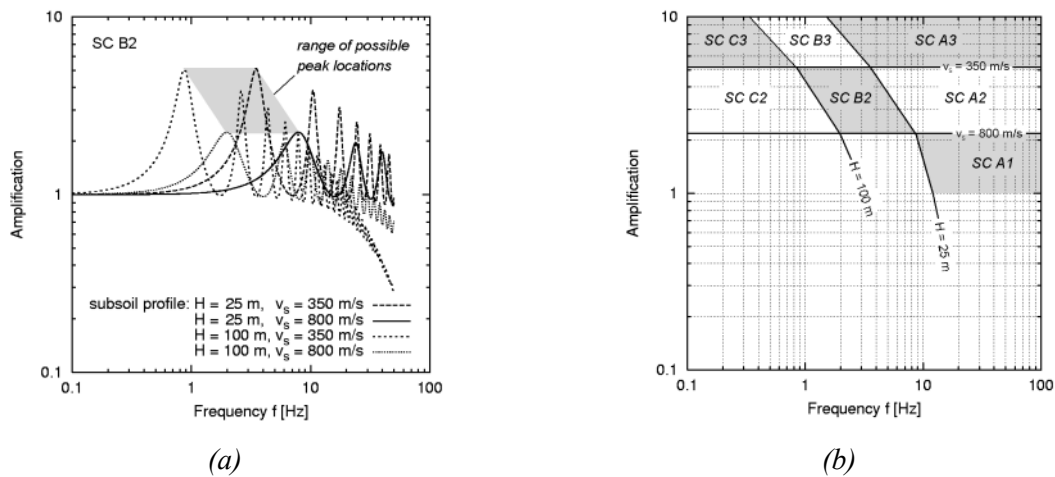
Figure 4.5   Qualitative ranges of possible peak locations of 1-D transfer functions (a) for site-specific subsoil class B2 described by model profiles conforming to the highest and lowest possible soil parameters, and (b) for all subsoil classes on the basis of simplified soil profiles. (Note: Amplification level of depicted transfer functions can only be regarded qualitatively, since a constant damping factor, ξ, was applied for all soil types.)

Given that information on subsoil consistency or single subsoil-describing parameters is missing, subjective site observations (e.g. of the general geology, topography, vegetation, and natural covers) may help for a rough estimate of queueing subsoil conditions.

As Figure 4.5 shows, and according to the rough subsoil information, a variety of simplified (one-dimensional) subsoil profiles are generated that meet the conditions of the German earthquake code provision DIN 4149 (DIN, 2002). In this regard, attention should especially be paid to the upper and lower bounds of ranges for soil stiffness and sediment thickness in order to cover all possible combinations within one site-specific subsoil class.

One-dimensional transfer functions are calculated in the next step for each possible subsoil profile of one site class, using the analytical method described in Section 3.2. Because the location of the predominant peak of one-dimensional transfer functions can be regarded as a function of average soil consistency and total sedimentary thickness, a qualitative range of possible peak locations in the frequency-amplification domain can be evaluated for each subsoil class *SC* (Figure 4.5b). Figure 4.5a illustrates this for site-specific subsoil class B2.

By arranging the quasi-transfer functions, TF_{quasi}, of instrumental data (e.g. *HVNR*) into the shown possible ranges of predominant peak locations, a rough site classification can be carried out. Figure 4.6 presents averaged spectral H/V-ratios on microtremor data allocated into site-specific subsoil classes following the German earthquake code DIN 4149 (DIN, 2002).

The classification of a site by the arrangement of its spectral peak (e.g. of *HVNR*) into determined ranges of site classes (as shown in Figure 4.5b) should be done on a relative basis rather than strictly concentrating on the specified absolute ranges. This is especially true for the limiting values of the amplification demarcating soil condition classes 1, 2, and 3 (in terms of its soil stiffness). The relative amplification level of an H/V-peak should be defined according to a peak's development, i.e. the function's right- and left-handed descent of the peak.

These effects can clearly be observed at H/V-ratios shown in Figure 4.6 and Annex 4. While spectral H/V-functions at stiff soil sites (*SC* A2, B2, C2) are characterized by peaks with moderate amplifications, those at soft soil sites (*SC* A3, B3, C3) clearly exhibit distinct peaks with strong descents of relative amplification.

To check the reliability of results based on the hybrid classification, a comparison with those of stiffness-related classification schemes has been performed in Table 4.9. It can be seen that site classes based on the applied hybrid procedure agree mostly with the stiffness-related site classes (soft soil, stiff soil, rock) as proposed by AMBRASEYS *et al.* (1996).

Once a site-specific subsoil class was allocated, a calibration of an appending model-profile could be achieved. By variations of the average soil stiffness and/or the total sedimentary thickness, an approximation of the theoretical transfer function, TF_{theo}, to the experimentally appointed transfer function, TF_{quasi}, can be performed. This results in a more precise classification of the site, as shown in Figure 4.7.

With regard to a "closer-to-reality" generation of the soil profile, any information about the geological site conditions are valuable. Such information may include detailed geological maps, data of geotechnical (boreholes), or seismic exploration methods (seismic reflection/

refraction). This was accomplished for a variety of recording sites (in Germany and international earthquake regions), of which geological information is available to a greater or lesser extent. Annex 4 illustrates the site classification following the single steps of *MESSIAS* as previously described.
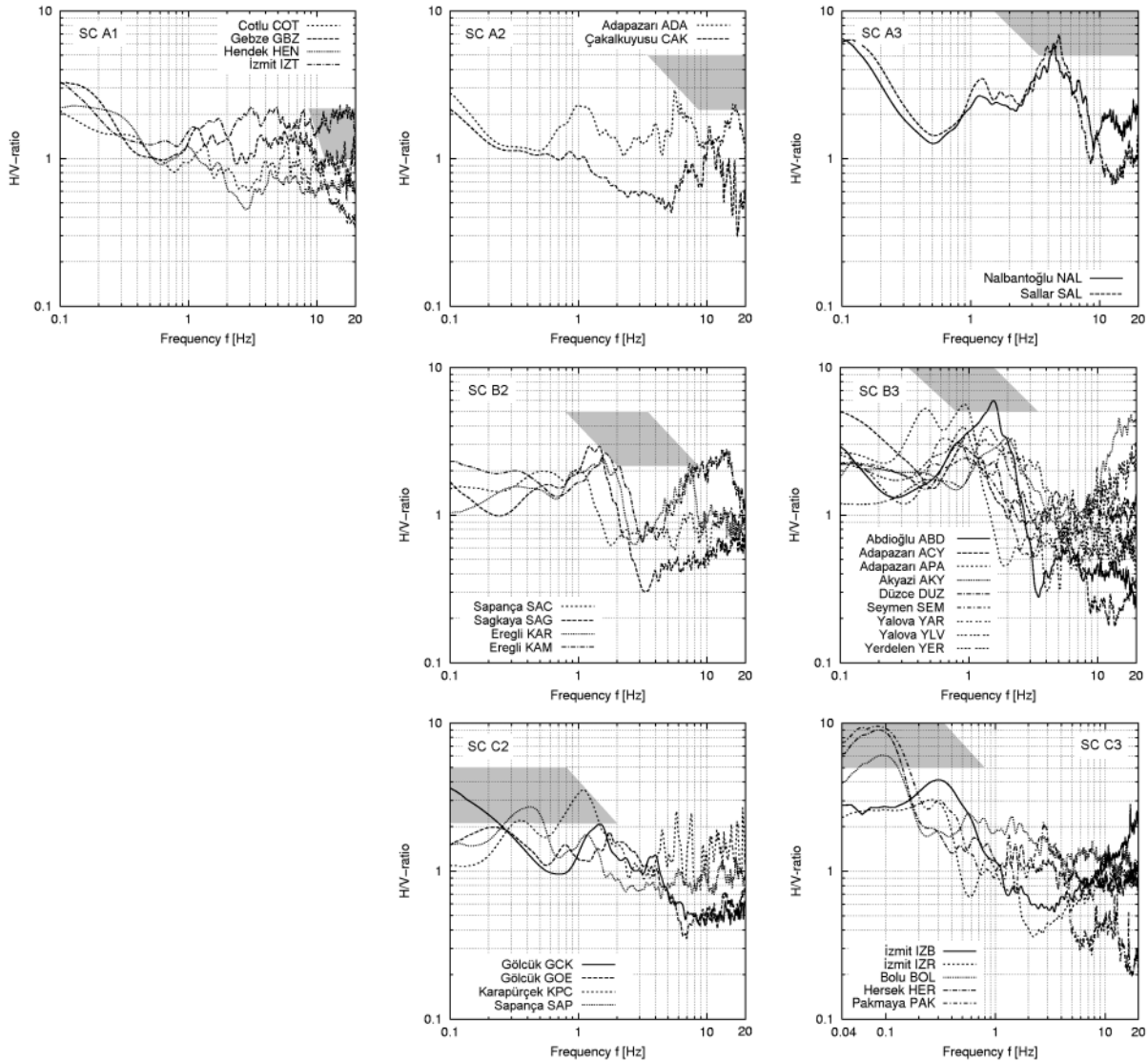
Figure 4.6   Spectral H/V-ratios on microtremors recorded in North- and Southanatolian Türkiye allocated into site-specific subsoil classes following DIN 4149. (Note: Each curve represents the arithmetic mean function of several H/V-spectra for succeeding time periods at the same site.)

Since the near-surface soil conditions of the "German model sites" as described above are mainly based on geological borehole data, site classification should be reliable. An overview of the assigned site classes is given in Table 4.10. In addition to the results that use the hybrid classification schemes of BRAY & RODRÍGUEZ-MAREK (1997) or *MESSIAS*, those of respective stiffness-related classification schemes, which solely depend on the average shear wave velocity, $v_{s,30}$, of the uppermost 30 m, are also confronted. With respect to the near-surface geology and their classification according to the different schemes, remarkable agreements

can be observed. Consistency between both hybrid classification schemes exists to some extent, even though the site classes of BRAY & RODRÍGUEZ-MAREK (1997) do not begin to cover all possible combinations of soil profiles.

Table 4.9 Site classification of strong-motion stations in Northanatolian Türkiye.

Instit. [1]	Station	Index	Station coordinates		Stiffness-related site classification [2]		Hybrid site classification (*MESSIAS*) [4]
			Latitude	Longitude	YOUD *et al.*, 2000	SCHWARZ *et al.*, 2002a [3]	
GTFE	Adapazarı	ADA	40.737°	30.380°	-	rock	A2
GTFE	Adapazarı	APA	40.714°	30.386°	-	soft soil	B3
GTFE	Adapazarı	AZA	40.756°	30.390°	-	stiff soil	A2
GTFE	Akyazi	AKY	40.670°	30.623°	-	soft soil	B3
GTFE	Çaybaşi	CAY	40.690°	30.440°	-	soft soil	A3/B3
GTFE	Düzce	DUZ	40.844°	31.148°	-	soft soil	B3
GTFE	Gebze	GEB	40.782°	29.416°	-	rock	A1
GTFE	Gölyaka	GOY	40.779°	31.003°	-	soft soil	B3
GTFE	Hendek	HEN	40.795°	30.735°	-	rock	A1
GTFE	Eregli	KAR	40.701°	29.672°	-	stiff soil	B2
GTFE	Sapanca	SAP	40.689°	30.257°	-	stiff soil	C2
GTFE	Seymen	SEY	40.710°	29.907°	-	stiff soil	A2
GTFE	Çiftlikköy	YAL	40.661°	29.324°	-	stiff soil	A2
AFET	Düzce	DZC	40.844°	31.148°	soft	soft soil	B3
AFET	Gebze	GBZ	40.786°	29.445°	stiff/rock	rock	A1
AFET	İzmit	IZT	40.761°	29.910°	rock	rock	A1
AFET	Sakarya	SKR	40.737°	30.384°	stiff/rock	rock	A2
AFET	Bolu	BOL	40.746°	31.608°	soft	soft soil	C3

[1]   operators of the station: AFET - General Directorate of Disaster Affairs, GTFE - German TaskForce for Earthquakes
[2]   according to the stiffness-related classification scheme of the near-surface soil layers, e.g. AMBRASEYS *et al.* (1996)
[3]   determined subsoil classification for elaboration of site-dependent attenuation laws
[4]   based on spectral H/V-ratios on microtremors and site classification scheme of DIN 4149 (DIN, 2002)
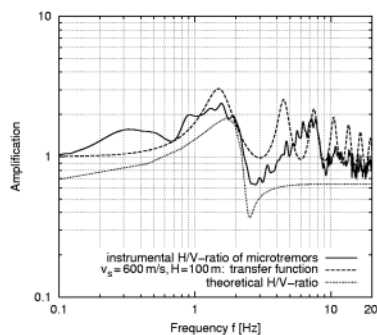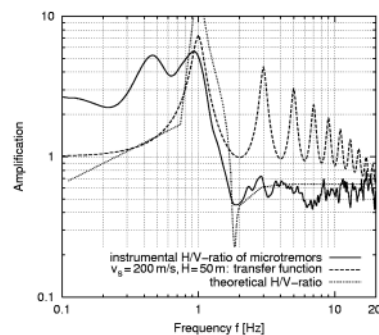
(a) Eregli KAR: SC B2   *(b) Adapazarı APA: SC B3*   *(c) Sapanca SAP: SC C2*
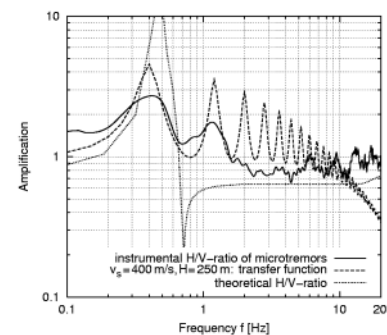
Figure 4.7   Calibration of model profiles for selected recording sites by approximating theoretical transfer functions to instrumental H/V-ratios on microtremors (cf. Figure 4.6).

*Table 4.10 Classification of German model sites using different schemes and input data
(a detailed description of the model sites is given in Annex 4).*

Site	Available subsoil parameters		Predom. frequency	Stiffness-related classification [2]			Hybrid classification	
	$v_{s,30}$ [m/s]	H [m]	f_s [Hz] [1]	AMBRASEYS *et al.*, 1996	HOSSER & KLEIN, 1983	1997-UBC (ICBO, 1997)	BRAY & RODRÍGUEZ-M., 1997 [3]	*MESSIAS*
BWN	260	~ 18.5	4.0	soft	A	D	-	A2-A3
	> 1500	-	-	rock	R	A (B)	A (B)	A1
BWP	211-253	>> 100	0.15	soft	A	D	D-3	C2
BYG	175	~ 7.5	4.0-8.0	very soft	A	E	E-1	A3
BYI	426-445	~ 100	0.8-0.9	stiff	M	C	D-1 ($\neq$)	B2-C2
BYR	404	100-135	1.2	stiff	M	C	D-1 ($\neq$)	B2 (B3)
HNB	310-337	>> 500	0.13	soft	A	D	D-3	C2-C3
SHB	183	> 100	0.5-0.6	very soft	A	E	E-2	C3
				soft	A	D	D-1	C2-C3
SHK	239-397	> 100	0.6-0.7	soft	A	D	D-2	C2
				stiff	A	C	D-2 ($\neq$)	C2
SHS	201	~ 80	0.8	soft	A	D	D-1	B2-B3
SAE	350-400	~ 120	0.9	stiff	A (M)	C (D)	D-2	B3-C3

[1]   predominant peak of representative H/V-ratios on microtremors (*HVNR*) indicating the natural site frequency, f_s

[2]   on the basis of available shear wave-velocities, $v_{s,30}$, of the uppermost 30 m

[3]   according to the 1997-UBC site classes, ranges of total sediment thicknesses, H, and natural site frequency, f_s

4.3.2 *MESSIAS*' significance in an engineering analysis of structural damage

Compared to common classification schemes referred to in international earthquake codes, for example, the hybrid procedure of seismic site classification *MESSIAS* provides some advantages:

-   estimation of the total thickness of overlying sedimentary soil layers, and thus a more realistic classification of the site,
-   verification of available subsoil information, or in case no soil data is present, the evaluation of "surrogate" subsoil profiles,
-   warranty of comparable results, since the experimental component of the procedure (spectral H/V-ratios on ambient seismic noise) can be easily obtained at any site.

Not only is the stiffness of (near-surface) soil layers an important point, but so is their total depth in the seismic design of structures, especially in the long-period range of seismic motion (DOBRY *et al.*, 1976). Site classification procedures incorporating the sedimentary thickness allow the consideration of possible attenuation effects of seismic ground motion. Investigations done by TRIFUNAC & BRADY (1975) and SEED *et al.* (1976) on strong-motion records in the western United States revealed average values of peak ground acceleration

(*PGA*), which were somewhat lower for sites on alluvium than for sites on rock (see Figure 4.3a).

As demonstrated, the value of *MESSIAS* insists on identifying the site class or investigating the transfer characteristics of local subsoil, and thus *a priori* allow for a reliable structural design or damage analysis, rather than directly being involved with.

The main consequences of the procedure can be listed as follows:

- the identification of the local subsoil conditions and transfer characteristics,
- the site classification according to a customary scheme.

Within an engineering analysis of structural damage, these investigation findings may help to perform the following:

- select suitable mainshock data of recording sites having comparable subsoil conditions to the site of interest,
- select alternative weak-motion records (e.g. aftershocks) at the site representing the frequency characteristics of the damaging mainshock and thus applicable for extrapolation to higher levels of ground acceleration,
- provide shapes of site-dependent elastic design spectra representing the theoretical response characteristics of the site during earthquakes.

5 Structural damage and site-dependent seismic action

5.1 Interpretation procedure of structural earthquake damage

5.1.1 Observations of earthquake-induced effects in regions of high seismicity

Based on experiences gained by the German TaskForce during recent field missions into disaster areas (Table 5.1), an attempt has been made to interpret structural earthquake damage. To reach this target, a detailed documentation of structural damage has to be provided. This can be done with different degrees of accuracy in respect to the dimension or scale of the investigation (cf. Section 1.2; Annex 1):

- regional, through macroseismic investigations on different building types in spaciously areas,
- local, by areal investigation of a single building type in urban areas or districts, for example,
- site-specific, concentrated on individual sites or damage cases.

Table 5.1 Effects on residents and building development caused by earthquakes investigated between 1997 and 2003.

Region, earthquake	Magnitude	Death toll (injured)	Structural damage extent	
			destroyed buildings	damaged buildings
Northeastern Venezuela, Cariaco (Casanay) July 9, 1997	M_s 6.8	73 (531)	1,000	few thousands
Southanatolian Türkiye, Adana (Ceyhan) June 27, 1998	M_s 6.2	150 (1,500)	1,100	9,000
Northanatolian Türkiye, İzmit (Kocaeli) August 17, 1999	M_s 7.8	18,000 (42,400)	66,400	146,500
Northanatolian Türkiye, Düzce (Bolu) November 12, 1999	M_s 7.4	765 (5,000)	several hundred	several thousand
Aegean Türkiye, Sultandağı (Afyon) February 3, 2002	M_s 6.5	54 (172)	107	several hundred
Eastanatolian Türkiye, Bingöl May 1, 2003	M_s 6.4	177 (530)	15	3,000 (residential units)

On the basis of selected real existing damage cases in Venezuelan and Turkish earthquake regions, the site-specific way of interpreting structural earthquake damage will be applied here. In doing so, mostly "engineered" building types, that is multistoried, reinforced-concrete frames (furnished with masonry infill walls), will be investigated.

5.1.2   Procedure and basic principles

The interpretation of structural earthquake damage to buildings strongly depends on the integrity and quality of available information regarding each of the following:

- the site,
- the seismic excitation, and
- the structure itself, including the actual pattern of structural damage.

As was already mentioned at the beginning of Chapter 1, a reliable interpretation of earthquake damage can only be performed if the grade of influence for each of the three factors has been previously evaluated. The site and subsoil conditions, the seismic excitation, and the character of the structure may directly or indirectly result in structural damage through one or more of the following:

- local site effects leading to abnormal amplifications of certain frequency ranges,
- local shaking intensity exceeding the design level of seismic excitation of the structure,
- grade of structural vulnerability being influenced by deficiencies of the structural layout or working materials.

In most cases the structural damage is caused by different factors acting together. Since a reliable analysis of structural damage requires both a comprehensive data collection and detailed investigations (which are time- and also cost-consuming), a kind of observation-based procedure should be performed in order to identify damage-supporting factors in the forefront of the intrinsic damage analysis. The suggested procedure is schematically illustrated in Figure 5.1. Without deeper knowledge of the structure, the site, and the seismic excitation, possible reasons for damage can still be isolated and unlikely damage reasons can be excluded. On the basis of in-situ observations of the site conditions, the layout, and the damage characteristics of the treated structure and possibly existing structures in the vicinity, a first estimation of the damage-supporting factors can be achieved.

If direct seismic site effects, e.g. soil liquefaction, landslides or surface rupture, are present at the site and obviously responsible for most of the structural damage, further investigations can be abandoned. In that case, failures in land use management leading to a poor selection of the building site can be considered as the main reason for damage (see Figure 5.1).

A comprehensive compilation and discussion of these effects is included in the Seismic Microzonation Manual (DRM, 2002), which was prepared for earthquake risk mitigation in endangered Turkish regions. Table 5.2 lists the specified direct seismic site effects and gives

information on their causes. Even though some information is available, it cannot be used in any structural analysis to prevent damage to existing structures.

It should be stressed that all the structures treated in this work are not influenced by direct seismic site effects. This can be confirmed through very detailed observations of respective building sites.

Table 5.2 Causes for direct seismic site effects (DRM, 2002).

Effect	Caused by	In consideration of
liquefaction and settlements	- loose granular soil materials - high water table, resulting in saturated soils	detailed knowledge of soil materials and subsurface stratigraphy (borehole data)
landslides, rock fall	- inertial forces, which will cease once shaking stops - loss of strength, which may exist also after shaking ceases	knowledge of the geometry, soil materials, and hydrostatic conditions of the slope
earthquake-related flooding	- tsunamis and seiches - lateral spreading along the coastline	knowledge of bathymetric conditions, and topography of the coastline
surface faulting and tectonic deformation	- vertical displacements - lateral offsets of the earth surface	knowledge of tectonic fault lines

Based on the extent of damage to the surrounding buildings of nearly the same type or with the same number of stories, a classification can be performed into the different possible damage-supporting effects.

Given the presence of similar housing in the surroundings, this procedure can yield feasible results; additional investigations of the site and structures, however, are strongly recommended.

It should be stated that this procedure can only be adopted if buildings of comparable structural type are present in the vicinity where damage occurred. In case the same building type is damaged in the same way, but located at different sites within an earthquake-stricken area, the flowchart in Figure 5.1 cannot be applied. To circumstantiate this, Figure 5.2 shows two examples of typical school buildings in Eastanatolian Türkiye seriously damaged by the 2003 Bingöl earthquake. Within the surrounding villages of Bingöl City, three of the schools suffered exactly the same damage while being situated on different subsoil conditions and at distinct distances to the epicenter. Without further investigations, structural deficiencies of the buildings certainly led to the collapses. Detailed analyses of these structural damages are given by SCHWARZ *et al.* (2004).
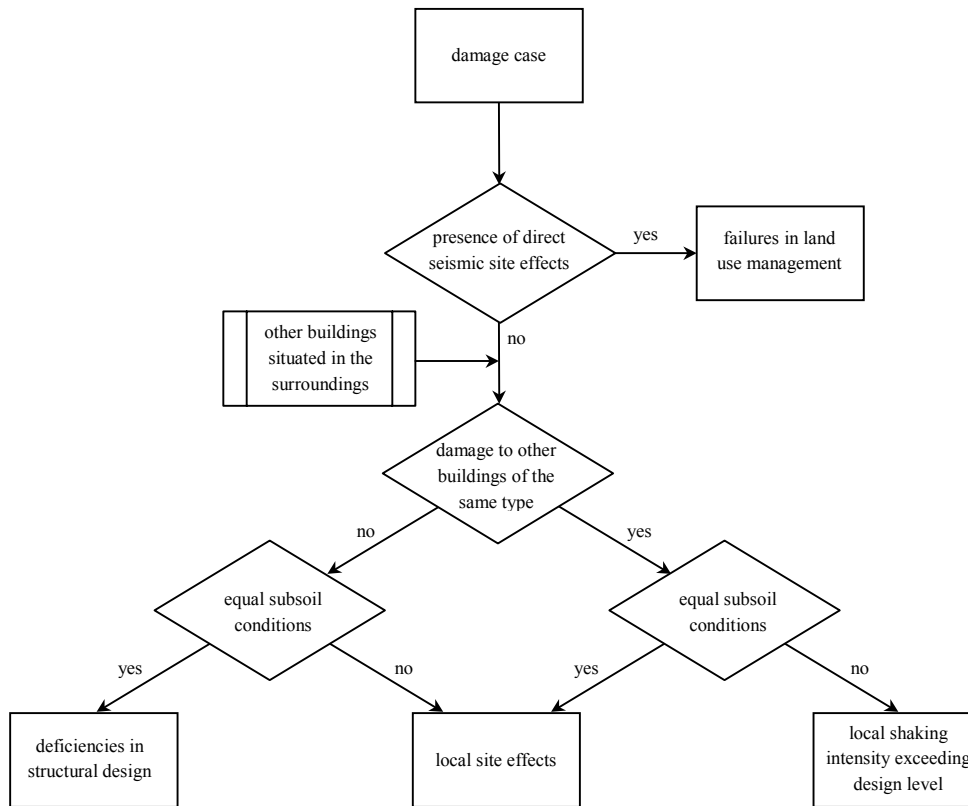
Figure 5.1 Flowchart of observation-based procedure in order to perform a rough estimate of possible reasons for structural earthquake damage.

(a) Çeltiksuyu   *(b) Sarıçiçek*

Figure 5.2 Typical school buildings "İlkokulu" in Eastanatolian Türkiye showing exactly the same structural layout and damage pattern (from SCHWARZ *et al.*, 2004).

Table 5.3 Compilation of information on the seismic excitation, the site, and the structure valuable for the interpretational analysis of structural earthquake damage.

Information on:	such as
seismic excitation	- data of the (damaging) mainshock recorded at the building site - data of the mainshock recorded at sites with comparable subsoil conditions and epicentral distance - aftershock records directly at the building site scaled to the level (and character) of the damaging mainshock - elastic response spectra representing the basis of building design
site and the subsoil conditions	- in-situ site observations (e.g. general geology, topography, vegetation) - information on subsoil stratigraphy or soil-describing parameters - experimental seismic data recorded at the ground level (subsurface)
structural layout	- documentation of the structural dimensions (site survey, working plans) - specifications of material properties and reinforcement detailing - in-situ material testings (e.g. concrete compression strength) - instrumental investigations on the dynamic vibrational characteristics - extent, locations, and characteristics of structural earthquake damage

To recapitulate, the procedure as given in Figure 5.1 should be seen only as an additional check and not as a substitute for detailed damage analysis. In Figure 5.3 an integrated analysis of structural damage will be presented that incorporates all available information on the seismic excitation, the site, and the structure (see Table 5.3).

All of these types of information may represent the input data within the process flow of the analysis procedure. On the basis of selected damage cases, the procedure described here will be applied, combining different types of input data with different analysis methods coming from the scientific fields of engineering seismology, soil dynamics, or structural engineering.

As can be seen in Figure 5.3, the whole procedure for the interpretation of structural damage basically consists of three sectors: the site, the seismic excitation, and the structure, with the latter dealing mainly with the elaboration of the structural model and its capacity spectrum. This will be explained in the following section. The second branch, providing the representative seismic excitation for the structure, will be discussed in the following sections. It must be stressed, that, in the case of missing data of the damaging mainshock recorded directly at the site of interest, a preparation of alternative seismic data (e.g. mainshock records of other sites, design spectra, etc.) can only be carried out if a detailed classification of the site was obtained. As represented by the flowchart's third sector, a site classification on the basis of theoretical as well as experimental investigations will be performed following the procedure of Chapter 4.
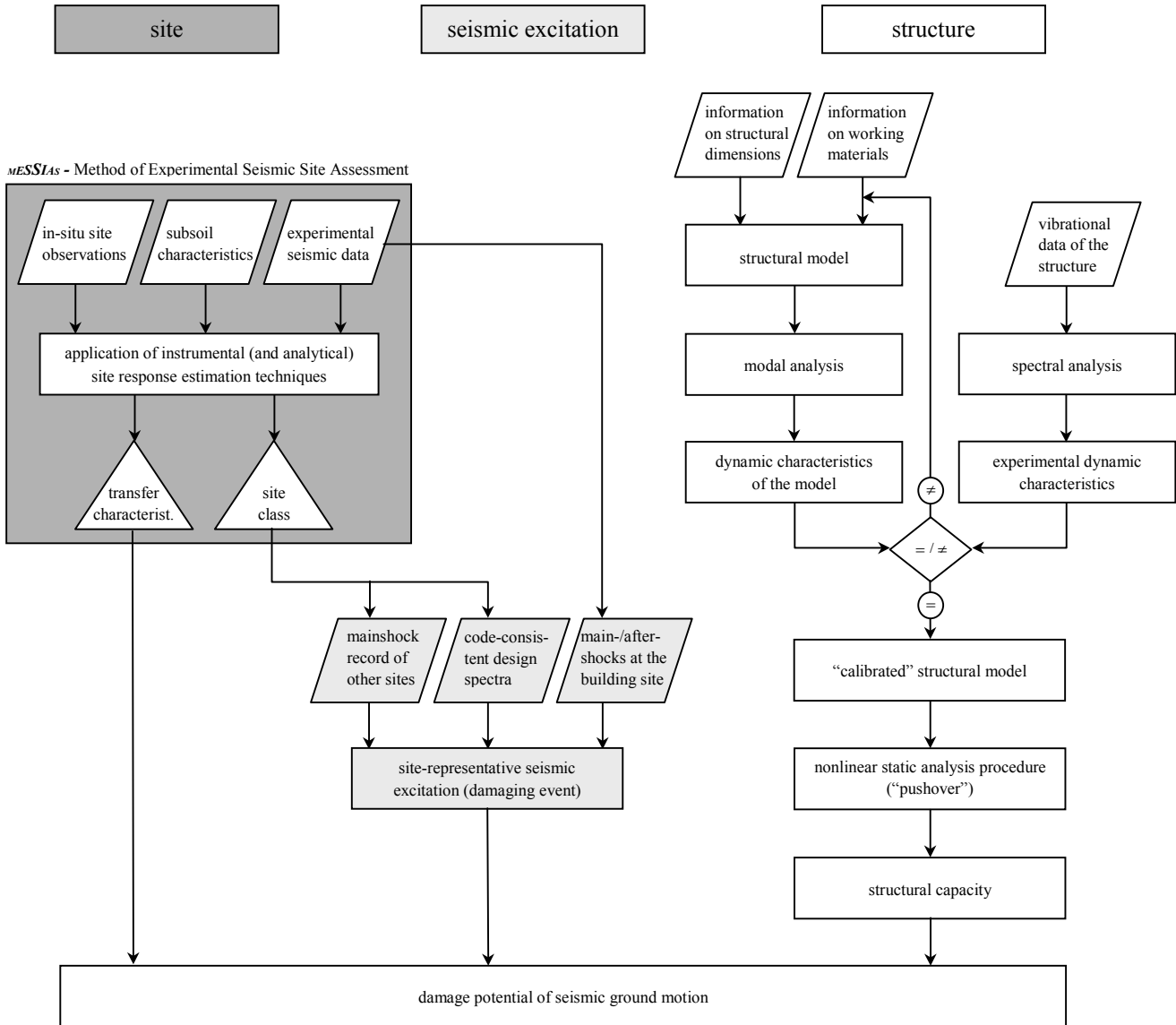
Figure 5.3 Schematic flowchart showing the procedure of damage interpretation on the basis of selected cases.

5.1.3   Selected damage cases for further investigations

As already mentioned, the investigations described here are concentrated on selected damage cases that were documented during recent field-work assignments of German TaskForce for Earthquakes (GTFE) into disaster areas of Türkiye and Venezuela.

All buildings are principally characterized by multistoried (3- to 9-stories), reinforced-concrete frames representing the primary supporting structure. Most of the structures are furnished with masonry infills over all stories, while sometimes infills on the ground level are missing. The construction status of some buildings can be described as purely RC frame skeletons, since no infills have been attached to the structure at the time of the damaging earthquake (see Table 5.4).

Table 5.4 Overview of general information on investigated RC frame structures (detailed structural information is given in Annex 5-3).

Structure	Index	Year of construct.	Structural characteristics [1]				Damage grade [3]
			Story no. [2]	Base-ment	Brick infills	Peculiarities	
Av. Perimetral, Cumaná	AVE	1997	7	○	◖	soft ground story	3
Edif. Toyota, Cumaná	TOY	1997	3	○	◖	eccentric brick infills	3-4
Edif. Miramar, Cumaná	MIR	1978/79	9 (10)	●	●	-	5
Edif. Residencial, Cumaná	EDR	1995/96	9	○	●	-	0
Seymen	SEM	< 1995	4	○	●	-	2
İzmit 1	IZT-1	1999	7	○	○	RC frame skeleton	3
İzmit 2a	IZT-2a	1999	6	○	○	RC frame skeleton	3
İzmit 2b	IZT-2b	1999	6	○	◖	soft ground story	3
İzmit 2c	IZT-2c	2002	4	○	◖	soft ground story	-
Sapanca	SAC	2002	3	○	◖	soft ground story	-
Düzce 1	DUZ-1	1999	4 (5)	●	●	-	0
Düzce 2	DUZ-2	1995/96	5 (6)	●	●	-	2-3
Yavuzlar Fındık, Gölyaka	YZL	1994	4	○	●	-	5
Sultandağı	SUL	2001/02	5	○	○	RC frame skeleton	3

[1] ● present   ◖ partly present   ○ not present
[2] parantheses indicate the total story number, including basements
[3] grade of damage according to the European Macroseismic Scale EMS-1998 (GRÜNTHAL (ed.) *et al.*, 1998)

The following are reasons for selecting this type of structural system:

- the high vulnerability to dynamic loads leading to high damage concentrations,
- its prevalence within the respective earthquake areas,
- the possibility of analyzing buildings having (nearly) similar layout shapes, but different numbers of stories,
- the possibility of analyzing uniform buildings located at different sites with different subsoil conditions.

An overview of all available buildings selected for investigations is given in Table 5.4.
A more detailed description of these buildings, including structural layout and pattern of damage is provided in Annex 5-3.

Since each of the structures possesses different qualities and the completeness of available structural information and experimental data is different for each, a kind of sub-classification must be carried out. This is done according to the Eurocode 8, part 3: "Strengthening and repair of buildings" (CEN, 2003), which, among other things, deals with assessing the earthquake resistance of already existing buildings. Buildings are therefore classified into three different *knowledge levels (KL)* according to "the amount and quality of the information collected", focussing primarily on the following:

- the geometrical properties of the structural system *(geometry)*,
- the amount and detailing of reinforcement *(details)*, and
- the mechanical properties of the constituent materials *(materials)*.

As this classification mainly concentrates on both the in-situ inspection of the geometry or structural detailing and in-situ testing of materials (thus assuming that all of the three subjects are more or less available), a one-to-one adoption of this classification concept on the buildings discussed here may not be promising. On the contrary, this work's classification system is based on the question whether input information, e.g. the reinforcement detailing, is available or not.

Considering the different types of input parameters necessary for an integrated analysis of the selected damage cases, a distinction between the structural information and the information on the seismic action (excitation) has been made. This leads to the following definitions:

- knowledge level structural properties (*KLS*), and
- knowledge level seismic action (*KLA*).

In addition to the provision of these two types of knowledge levels, possible structural damage due to seismic excitation can either be implemented as a parameter to verify the results of the damage interpretation procedure. The so-called "verifying parameter: damage (*VPD*)", then, refers not only to the occurrence of structural damage, but also to the detailed description of damage locations.

Regarding the matrix shown in Figure 5.4, each structure up for investigation can be classified as a combination of *KLS* and *KLA*, and possibly even endorsed by the *VPD*.
While the knowledge level *KLS* is assigned depending on the availability of the structural layout (geometry), its working materials, and its reinforcement detailing, knowledge level *KLA* is appointed according to the known level of seismic action and the ground motion characteristics during the damaging mainshock.

To illustrate this point, if records of the damaging mainshock directly at the building site are available, *KLA-3* must be assigned; but if only records of the mainshock at comparable sites or records of smaller earthquakes (e.g. aftershocks) directly at the building site are available, *KLA-2* must be chosen.

Given that no (*KLA-1*) or only rough information (*KLA-2*) on the earthquake reponse of the building site are obtainable, both the level and characteristics of the seismic ground motion during the mainshock has to be determined in alternative ways. Possible alternative solutions to specifying the seismic demand are provided in Section 5.3. A reliable identification of local subsoil conditions or the classification of the site can therefore be indispensable. Hybrid site classification schemes (Sections 4.2.3 and 4.3) provide an applicable tool in this case, even when subsoil information is missing.

As the matrix in Figure 5.4 illustrates, the availability of both the geometry of the structure itself and the level of seismic excitation at the building site can be considered as two preconditions for the analysis.

Combinations between *KLA* and *KLS* are subdivided into three different groups reflecting the probability of appearance:

- Group 1:   most prevailing case
- Group 2:   occasionally appearing case
- Group 3:   rarely appearing case (ideal case)

Given that both the entire description of the structural properties (including RC detailing) and the ground motion characteristics of the damaging mainshock are available, investigation results will display the highest level of reliability (Group 3).

In contrast, Group 2 represents more probable appearing cases having some missing input information either concerning the description of seismic action or structural properties. In this case greater efforts have to be done in order to achieve a reliable investigation. These may insist in seeking for an alternative seismic excitation through experimental site studies (cf. Section 4.3: MESSIAS; LANG *et al.*, 2003a), or in adopting certain structural pecularities, such as material parameters or reinforcement detailing.

Damage cases of which only structural geometry is known and coarse information on the ground motion characteristics of the mainshock is available, are counted among Group 1. For these damage cases, an identification of damage potential seems to be difficult.

Irrespective of the detailedness of available structural information, an estimation of possible damage-promotive factors can be performed through:

- an evaluation of the structural design, including evident failings in quality and workmanship,
- an identification of site effects, comparing predominant site frequency, f_s, with natural building frequency, f_n, the latter approximately determined by empirical relationships (cf. Table 5.6).

Figure 5.5 categorizes the herein investigated damage cases into the different *KLS-KLA*-combinations. Grey-shaded building indices suggest the presence of structural earthquake damage, hence the availability of the *VPD*.

Not all of the herein presented damage cases will entirely be investigated, particularly when the application of the nonlinear static "pushover" analysis is concerned, as it requires reliable information on the reinforcement detailing (chapter 5.2.2).

Those buildings erected after the damaging events and which consequently suffered no structural damage (damage cases IZT-2c, SAC) will also be excluded from the analysis.

	KLS-1	KLS-2		KLS-3	
	●	●	●	●	geometry
	○	●	○	●	materials
	○	○	●	●	detailing (RC)

KLA-1	●	□	Group 1			
KLA-2	●	◪		Group 2		
KLA-3	●	■			Group 3	
	excitation level (intensity, PGA)	ground motion characteristics				

○ information unavailable   ● information available

□ no information   ◪ rough description
■ more detailed description of the ground motion characteristics of the damaging mainshock at the building site

Figure 5.4   Classification matrix of (existing) structures into combinations of "knowledge level structural properties (KLS)" and "knowledge level seismic action (KLA)".

	KLS-1	KLS-2		KLS-3	
	●	●	●	●	geometry
	○	●	○	●	materials
	○	○	●	●	detailing (RC)

KLA-1	●	□	-	*AVE IZT-1*	-	*EDR MIR* *IZT-2 IZT-2c*
KLA-2	●	◪	-	*SEM YZL* *SAC*	-	*TOY SUL* *DUZ-1*
KLA-3	●	■	-	*DUZ-2*	-	-
	excitation level (intensity, PGA)	ground motion characteristics	*index*	presence of the verifying parameter: damage (VPD)		

○ information unavailable   ● information available

□ no information   ◪ rough description
■ more detailed description of the ground motion characteristics of the damaging mainshock at the building site

Figure 5.5   Classification of selected damage cases into combinations of KLS and KLA that are possibly provided with the "verifying parameter: damage (VPD)".

5.2 Structural performance under dynamic excitation

The processing method used to elaborate on the capacity of already existing structures, and thus to define the fundamentals for interpreting structural earthquake damage, is briefly illustrated in the flowchart in Figure 5.3. The single steps of the procedure will be comprehensively examined in the following order:

- compilation of the structural model on the basis of information available on structural dimensions and working materials (Section 5.2.1),
- experimental identification of the dynamic characteristics of selected structures (Section 5.2.1.2),
- calibration of the structural model according to experimental results (Section 5.2.1.3),
- application of the nonlinear static "pushover" analysis in order to determine the structural capacity of already existing buildings (Section 5.2.2).

Both modeling and dynamic analysis of the damage cases are done by using the program ETABS Nonlinear, Version 8.11 (Computers and Structures, Inc., CSI). As will be subsequently indicated (Annex 5-3), structural models and respective analysis results were partly adopted from SCHOTT *et al.* (2003), and LANG *et al.* (2003b).

5.2.1 Structural modeling

5.2.1.1 Regulations and modeling rules

All structural analyses incorporated in this work were done with ETABS Nonlinear, Version 8.11 (CSI). This includes the compilation of structural models, modal analysis, and the performance of nonlinear static "pushover" analyses.

General rules for the creation of the structural models are briefly summarized here:

- supporting conditions for all primary structural members at the ground floor level have rigid restraints (fixed-base assumption); translations: $u_x, u_y, u_z = 0$; rotations: $r_x, r_y, r_z = 0$;
- basements, i.e. stories below the ground surface level, are not considered in the model;
- roofs, mostly consisting of timber beams and clay tiles, are not modeled; loads coming from the dead weight of its materials are considered by a substitute load uniformly distributed over the top slab;
- columns and beams are defined as rectangular frame elements with rigid restraints at both ends;
- slabs are modeled as shell elements with constant plate thickness, t, and partly as rigid diaphragms (each point on the slab has the same translation, but no rotation);
- masonry infill walls between reinforced-concrete frames are considered by diagonal struts fastened to the RC frame elements;

- on the basis of in-situ tests of concrete compression strength (*SCHMIDT-hammer* testing) and information possibly available on used concrete quality classes, material properties of RC elements are determined; tabular values of concrete strength classes are calculated according to EC 2, Part 1 (CEN, 1992).

In order to perform the nonlinear static "pushover" analysis, nonlinear hinges are to be defined. Their nonlinear force-deformation relationship is based on the following specifications:

- bilinear force-deformation relationship with strength degradation,
- moment-rotation relationship,
- consideration of rotational ductility dependent on actual reinforcement detailing,
- consideration of axial force in columns,
- assignment of material law at either ends of frame elements (beams and columns).

5.2.1.2 *Experimental identification of the dynamic building characteristics*

The only way to check the reliability of the structural model is found in the experimental identification of the dynamic characteristics of the real existing building. This was done during a couple of measuring campaigns for some of the buildings investigated here (LANG *et al.*, 2004).

By the use of a multichannel-acquisition system and several high-sensitive seismic sensors distributed at different stories and layout positions of the building, the simultaneous recording of the buildings dynamic response at different floor levels could be achieved.

Figure 5.6 schematically illustrates the instrumentation of a building. In order to excite the building, not only is ambient noise mainly coming from wind and environmental disturbances applied, but also a type of external excitation. The latter simply consists of people pulling the structure by a rope fixed at a primary structural element (e.g. outer column or beam) from the outside. Compared with noise excitation, Figure 5.7 demonstrates that this technique allows a more reliable identification of the distinct mode frequencies, f_n, and thus of their respective mode shapes. By using this type of excitation, even structural damping factors, ξ, can sometimes be determined.

Table 5.5 summarizes the main results of the instrumental measurements carried out at most of the selected structures. Figure 5.8 correlates the experimentally identified fundamental periods, $T_{n,exp}$, with the number of stories, N. These are overlaid by curves of empirical formulas to calculate the fundamental frequencies of RC frame structures as specified in international building codes (e.g. of Türkiye, Eurocode 8) or other publications (e.g. BAYÜLKE, 1978). Empirical relationships solely based on the story number, N, clearly cannot estimate the fundamental period, T_n, of the assortment of buildings analyzed here. Since the general dimensions of the building, such as its total height, h_n, or its overall length, L, in the direction under consideration, have strong influence on the dynamic shaking characteristics,

Table 5.6 displays the experimental values of the fundamental periods, $T_{n,exp}$, with those calculated by more specified formulas as collected by GOEL & CHOPRA (1996), HAMPE (1985), HAMPE *et al.* (1991).

The investigation results given in Table 5.6 illustrate that empirical formulas incorporating the structures' principal dimensions are apparently more suitable to meet the experimentally identified fundamental periods of the structures, $T_{n,exp}$. Given that no experimental data of buildings are available, these results are of highest interest in order to at least estimate the predominant periods, T_n.

In addition, results presented in Table 5.6 cannot confirm the large differences between the experimental periods, $T_{n,exp}$, for undamaged and pre-damaged structures as being obvious in Figure 5.8. Discrepancies between the experimental and empirical fundamental periods, T_n, of an individual structure may be explained by structural peculiarities (e.g. atypically high overall stiffness by the presence of single shear-walls, low overall stiffness by extremely bad concrete quality) rather than by pre-damaging effects that possibly lead to an enlargement of the fundamental period by a significant decrease in stiffness.

Nevertheless, in cases where moderate damages to primary structural elements occurs, this should be also taken into account with the calibration procedure of the theoretical structural model.
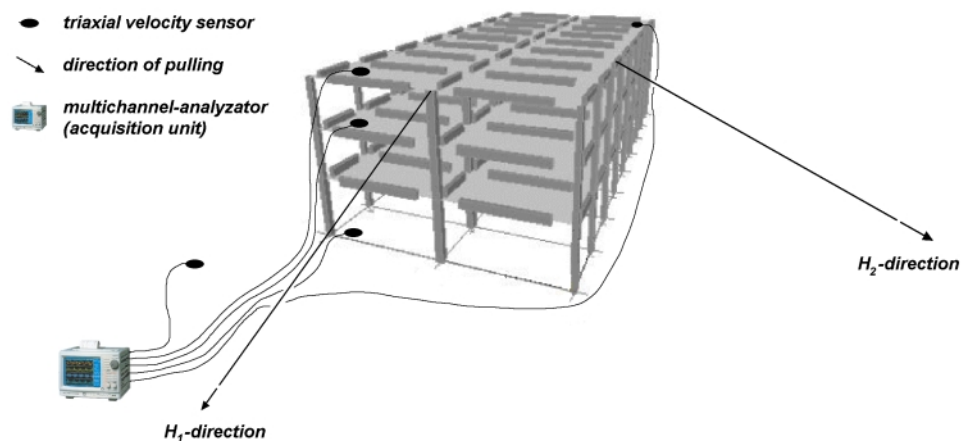
Figure 5.6   Instrumentation scheme for the experimental identification of the dynamic response characteristics and for the principle of rope pulling in both horizontal building axes (H_1, H_2).

(a)   *(b)*
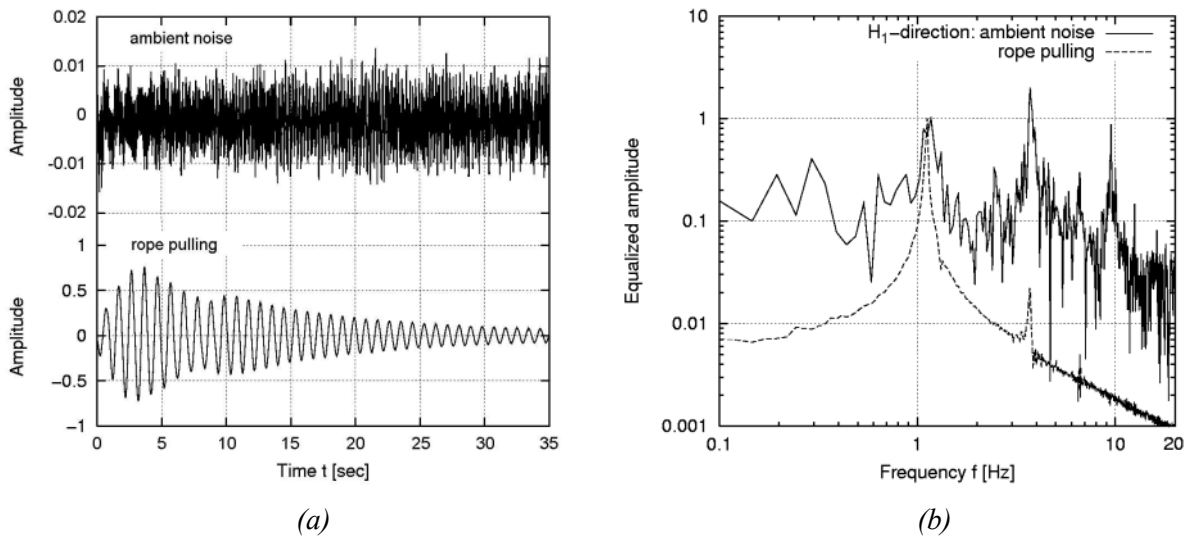
Figure 5.7 Differences between the structural response excited by ambient noise and rope pulling in (a) the time domain, and (b) the frequency domain.

Table 5.5 Main results of the dynamic measurements at RC frame structures in Venezuela and Türkiye for both major building axes.

Index	No. of stories [2]	Brick infills [1]	First mode period, $T_{n,exp}$ [sec]		Damping factor, ξ [%]		Damage grade (DG) [3]
			H_1-direction	H_2-direction	H_1-direction	H_2-direction	
AVE	7	◑	no instrumental tests performed				3
TOY	3	◑	no instrumental tests performed				3-4
MIR	9 (10)	●	no instrumental tests performed				5
EDR	9	●	0.35	0.50	-	-	0
YZL	4	●	no instrumental tests performed				5
IZT-1	7	○	0.68	0.69	6.30	8.10	3
IZT-2a	6	○	0.85	0.66	6.60	6.80	3
IZT-2b	6	◑	0.50	0.73	7.90	8.50	3
IZT-2c	4	◑	0.21	0.23	-	-	-
DUZ-1	4 (5)	●	0.26	0.29	-	-	0
DUZ-2	5 (6)	●	0.47	0.73	-	-	2-3
SAC	3	◑	0.15	0.20	-	-	-
SEM	4	●	0.33	0.40	-	-	2
SUL	5	○	0.89	0.71	6.5	6.9	3

[1]   brackets indicate the total number of stories, including basements

[2]   ● present   ◑ partly present   ○ not present

[3]   grade of damage according to the European Macroseismic Scale EMS-1998 (GRÜNTHAL (ed.) *et al.*, 1998)
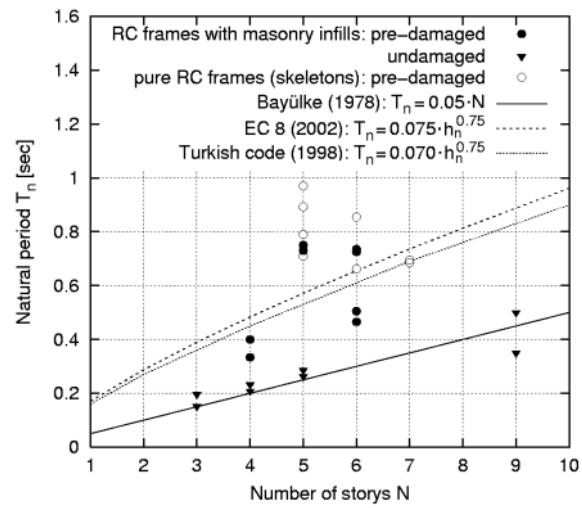
Figure 5.8 Comparison between experimentally identified fundamental periods, $T_{n,exp}$, and empirical formulas specified in different building codes.

Table 5.6 Comparison between experimental and calculated fundamental periods, T_n, of buildings investigated using more accurate empirical formula relationships.

Index	N [2]	Direction	Total height, h_n [m]	Length in direction, L [m]	Experim. identified period, $T_{n,exp}$ [sec] [2]	Period T_n acc. to empirical relationships [2]		
						ICBO (1994) $T_n = 0.09 \cdot N \cdot \sqrt{\frac{h_n}{L}}$	ATC (1978) with infills $T_n = 0.09 \cdot \frac{h_n}{\sqrt{L}}$	no infills $T_n = 0.1 \cdot N$
AVE	7	H_1	20.30	30.70	-	0.51	0.33	-
		H_2		20.70	-	0.62	0.40	-
TOY	3	H_1	11.70	36.00	-	0.15	0.18	-
		H_2		21.60	-	0.20	0.23	-
MIR	9	H_1	24.45	28.00	-	0.76	0.42	-
		H_2		14.90	-	1.04	0.57	-
EDR	9	H_1	25.65	19.40	**0.35**	*0.82*	0.46	-
		H_2		12.00	**0.50**	*1.07*	0.60	-
YZL	4	H_1	19.00	32.10	-	0.28	0.30	-
		H_2		14.60	-	0.41	0.45	-
IZT-1	7	H_1	19.60	20.25	**0.68**	0.62	-	0.70
		H_2		13.15	**0.69**	0.77	-	
IZT-2a	6	H_1	16.90	19.00	**0.85**	*0.51*	-	0.60
		H_2		19.80	**0.66**	0.50	-	
IZT-2b	6	H_1	16.90	19.00	**0.50**	0.51	0.35	-
		H_2		19.80	*0.73*	*0.50*	*0.34*	-
IZT-2c	4	H_1	11.30	18.90	**0.21**	0.28	0.23	-
		H_2		19.75	**0.23**	0.27	0.23	-
DUZ-1	4	H_1	11.40	18.00	**0.26**	0.29	0.24	-
		H_2		12.63	**0.29**	0.34	0.29	-
DUZ-2	5	H_1	17.15	11.65	**0.47**	0.55	0.45	-
		H_2		14.45	**0.73**	0.49	0.41	-
SAC	3	H_1	8.70	10.55	**0.15**	0.25	0.24	-
		H_2		9.40	**0.20**	0.26	0.26	-
SEM	4	H_1	12.20	12.50	**0.33**	0.36	0.31	-
		H_2		9.70	**0.40**	0.40	0.35	-
SUL	5	H_1	15.50	15.53	*0.89*	*0.45*	-	*0.50*
		H_2		15.35	*0.71*	*0.45*	-	

[1]   number of stories excluding basements
[2]   low consistencies between experimental and calculated periods are *italicized*

5.2.1.3 *Calibration of the structural model*

Experimental results provide a good opportunity to calibrate the structural models to their modal analysis results. The main criterion for this is the agreement of the first translational modes in both principal building directions (*x, y* respectively H_1, H_2).

Since the mass of the structure or its structural elements can be seen as a fixed parameter, calibration will mainly be done on the structural stiffness (ABRAHAMCZYK *et al.*, 2004).

By the stepwise reduction of Young's modulus, E, of building materials (reinforced concrete), fundamental periods of the model, $T_{n,i}$, will be adjusted to the experimental periods, $T_{n,exp,i}$.

As the investigations show (Table 5.7), factors for reducing Young's modulus, E, of the primary structural elements (reinforced concrete) are between 40 and 60% for pre-damaged structures. Given that concrete elements are not supposed to be cracked, no reduction of the characteristic strength values needs to be conducted.

These findings are closely associated with the provisions of the present draft of the Eurocode 8 (CEN, 2003):

"Unless a more accurate analysis of the cracked elements is performed, the elastic flexural and shear stiffness properties of concrete and masonry elements may be taken equal to one-half of the corresponding stiffness of the uncracked elements."

Table 5.7 Correlation between experimental and modal analysis results for selected buildings.

Index	Experimental results		Modal analysis results			Calibration of RC elements
	Direction	Period, $T_{n,exp,i}$ [sec]	Mode	Direction	Period, $T_{n,i}$ [sec]	Reduction factor of Young's modulus, E
IZT-1	-	-	1	z ↻	0.79	
	x ↔	0.69	2	x ↔	0.73	50 %
	y ↕	0.68	3	y ↕	0.69	
IZT-2a	-	-	1	z ↻	0.87	
	x ↔	0.85	2	x ↔	0.67	60 %
	y ↕	0.66	3	y ↕	0.65	
IZT-2b [1]	x ↔	0.73	1			
	-	-	2			
	y ↕	0.51	3			
IZT-2c	-	-	1	z ↻	0.211	
	x ↔	0.23	2	x ↔	0.201	0 %
	y ↕	0.21	3	y ↕	0.168	
SAC	-	-	1	z ↻	0.171	
	x ↔	0.19	2	x ↔	0.132	0 %
	y ↕	0.15	3	y ↕	0.119	
DUZ-1	x ↔	0.29	1	x ↔	0.29	
	-	-	2	z ↻	0.28	50 %
	y ↕	0.26	3	y ↕	0.26	
DUZ-2 [1]	x ↔	0.73	1			
	-	-	2			
	y ↕	0.47	3			
SEM	x ↔	0.40	1	x ↔	0.44	
	-	-	2	z ↻	0.36	40 %
	y ↕	0.33	3	y ↕	0.32	
SUL	x ↔	0.89	1	x ↔	0.89	
	-	-	2	z ↻	0.73	55 %
	y ↕	0.71	3	y ↕	0.71	

[1] at the present state of investigation, structures were not yet modeled

5.2.2   Nonlinear static "pushover" analysis

A broad variety of analysis methods both elastic (linear) and inelastic (nonlinear), are available for the design of future buildings or for checking structures that already exist. Since the most customary inelastic analysis procedure insists in the nonlinear time history analysis, which is regarded as impractical and time-consuming, simplified nonlinear analysis procedures provide a more manageable tool. Even though nonlinear time history analyses are considered to provide more exact results, simplified nonlinear procedures are believed to produce satisfactory results for many particular tasks.

The analysis procedure as applied in this work is known as the *capacity spectrum method* (CSM), bringing together the capacity ("pushover") curve of the structure and a reduced (critically damped) response spectrum representing the (damaging) seismic excitation or the seismic demand. By superpositioning the structural capacity and seismic action (demand), the performance of the structure under lateral impact can be estimated (ATC, 1996; FAJFAR, 2000; FREEMAN, 1998; FREEMAN *et al.*, 1975).

5.2.2.1   *Structural capacity*

The main component of the nonlinear static analysis procedure is the elaboration of the capacity ("pushover") curve. The capacity curve represents the lateral displacement of any structural point dependent on the total base shear, V. The most convenient way to plot the force-displacement relationship is by tracking the roof displacement, δ, and the base shear, V.

The procedure for finding the structural capacity curve is explained below. Consideration is taken of the single elements shown in Figure 5.9:

Before executing the actual pushover procedure, a modal analysis has to be carried out assuming a two- or three-dimensional computer model ① following the modeling rules in Section 5.2.1.1. In case of pre-damaged buildings, potential loss in element stiffness should be regarded through reduced Young's modulus of the working materials (as previously explained).

The main element of the pushover procedure is the application of an incrementally increasing horizontal force ② to the structure until it reaches a limit state. The decision about the shape of load distribution over height ③ should be made in accordance with mass distribution and the fundamental mode shape in respect to lateral direction.

Plotting the roof displacement, δ against the lateral force or base shear, $V,$ generates the capacity curve ④ of the structure, which approximates how structures behave after exceeding their elastic limits. The inelastic part of the curve indicates the single points of progressive structural yielding up until the total failure of the building. As shown also in Figure 5.9, thresholds of different damage states ⑤ according to HAZUS®99 (FEMA, 1999) indicate the level of structural earthquake damage.
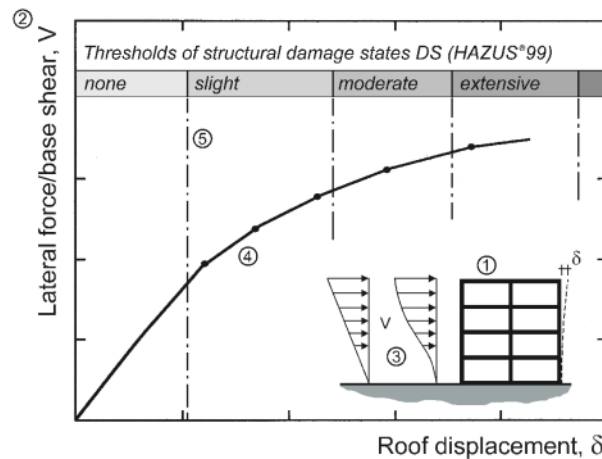
Figure 5.9 Capacity or "pushover" curve representing the lateral displacement, δ, as a function of the lateral force, V, applied to the structure.

In order to allow a comparison between structural capacity and seismic demand, both have to be plotted in the same domain. One possibility is to depict both in the spectral acceleration versus spectral displacement domain. To convert the capacity ("pushover") curve to the capacity spectrum, a point-by-point transformation of each $δ$-V-value into a S_a-S_d-format has to be carried out regarding the modal mass coefficients, $α$, and the participation factors of the fundamental mode, PF_1. The detailed conversion of the capacity curve into the so-called acceleration-displacement response spectra format (SASD) is comprehensively explained in the ATC-40 provision (ATC, 1996).

Capacity spectra shown in Figure 5.10 are plotted in the spectral acceleration-displacement domain. The following observations can be made:

- like the capacity curve, the capacity spectrum is also characterized by an elastic and inelastic part, the latter showing the yield points of single or group of elements; consequently each yield point/analysis step is interrelated to the partial or complete failure of single structural elements;
- lines radiating from the origin of an SASD have constant periods T; consequently the linear part of the capacity spectrum reflects the elastic period of the structure, T_n, whereas the period, T_n, lengthens as the structure undergoes inelastic displacement.

In general, the lengthening of the period T_n can be explained both by the stiffness degradation during the progressive failure of single structural elements, and by the cracking of concrete and the emerging nonlinear hinges.
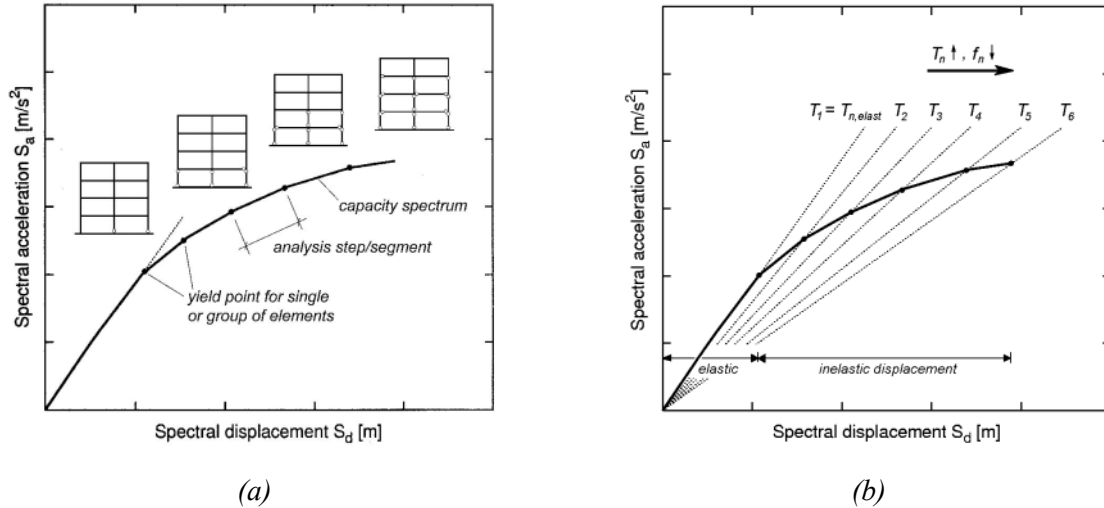
Figure 5.10 Capacity spectrum in the acceleration-displacement (SASD) range (a) indicating the distinct yield points for single or group of structural elements and (b) illustrating the lengthening of (elastic) natural period, T_n, as the structure undergoes inelastic displacement.

5.2.2.2 Seismic demand

Usually the seismic demand in terms of a critically damped response spectrum or an elastic design spectrum is available, as given, for example, in code provisions. To convert these spectra from the standard S_a vs T format into the S_a vs S_d (SASD) format, the $S_{d,i}$ values for each spectral acceleration, $S_{a,i}$ (T_i), must be calculated using equation (5.1).

$$S_{d,i} = \frac{1}{\omega^2} \cdot S_{a,i} = \frac{T_i^2}{4 \cdot \pi^2} \cdot S_{a,i} \tag{5.1}$$

The main task of the capacity spectrum method as applied here is to determine a displacement along the capacity curve that is consistent with the seismic demand. Consequently, a point on the capacity spectrum also has to be found lying on the response spectrum, which in turn is reduced for nonlinear effects. The reduction of the seismic demand spectrum is carried out through the "equivalent" damping, ξ_{eq}, which depends on both, the structure's material and the hysteretic behavior of the structure under dynamic impact:

$$\xi_{eq} = \xi_0 + \xi = \xi_0 + 0.05 \tag{5.2}$$

where: ξ -   viscous damping inherent in the structure (assumed to be constant)

                ξ_0 -   hysteretic damping (equivalent viscous damping)

Determining the performance point, $d_p \, a_p$, can only be done iteratively. Using the theoretical background as indicated in the ATC-40 document (ATC, 1996), Figure 5.12 schematically illustrates this procedure.
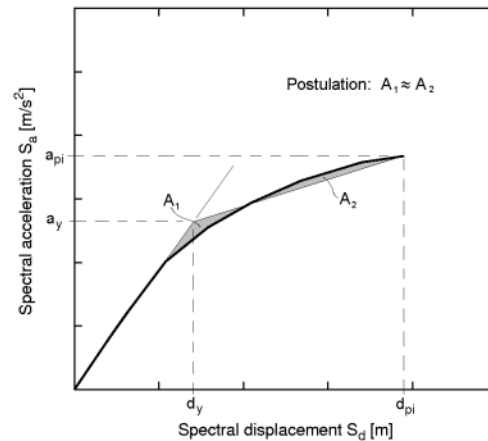
Figure 5.11 Bilinear representation of structural capacity spectrum defining inflexion point d_y, a_y and trial performance point d_{pi}, a_{pi} being chosen at the end of the capacity spectrum.

The following aspects must be considered:

- the bilinear representation of the capacity curve should meet the requirement of having equal areas, A_1 and A_2, between the capacity spectrum and its bilinear representation line; this directly determines the effective structural damping, ξ, as well as the location of the trial performance point, d_{pi} a_{pi} (Figure 5.11);

- reducing the demand response spectrum by damping factor, ξ, results in the displacement intersection point, d_i a_i; if this point does not match with the estimated trial performance point, d_{pi} a_{pi}, a new d_{pi} a_{pi} point has to be selected; the iteration has to be repeated until both points are nearly equal (Figure 5.12);

- given that displacement intersection point and trial performance point sufficiently agree with each other, the performance point, d_p a_p, is found; the displacement value, d_p, represents the maximum structural displacement expected for the regarded seismic demand (ATC, 1996).

(a)   *(b)*
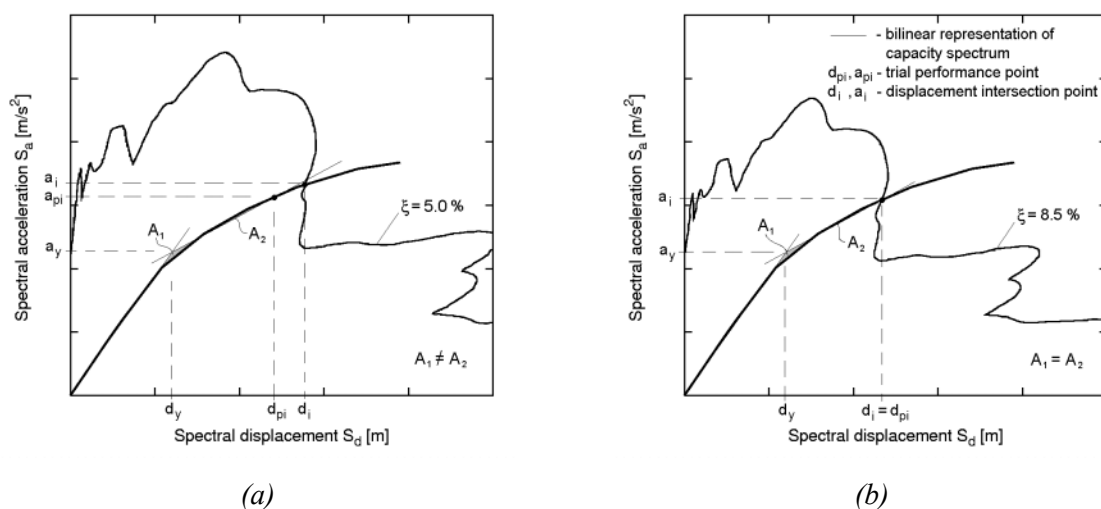
Figure 5.12 Step-by-step procedure to identify the performance point, d_p a_p.

The demand spectrum representing the seismic excitation at the building site can either be based on a real earthquake record (usually in terms of ground acceleration, a_g) or an elastic design spectrum; both are syntonized to the local site and subsoil conditions.

For the sake of completeness, both types of seismic demand will be applied for the capacity spectrum procedure. The selection of suitable earthquake records, their conformance to varied conditions (e.g. level of peak ground acceleration, *PGA*), and the generation procedure of appropriate elastic design spectra will be comprehensively described in Section 5.3.

5.3 Specification of the seismic demand

Seismic data of the damaging mainshock recorded directly at the site of interest, i.e. the site of the damaged structure, is usually not available. Because of this an alternative seismic excitation reflecting the level and characteristics of the damaging earthquake has to be provided.

Types of substitute seismic excitation could be comprised of the following:

- records of smaller earthquakes (e.g. aftershocks) at the site,
- records of the same mainshock or comparable-magnitude earthquakes at adjacent stations having (nearly) the same subsoil conditions,
- elastic response spectra generated for the building site (design spectrum) according to the valid code provision, for example, which represents the sites' subsoil conditions and the level of the damaging event (damage-inducing seismic demand).

In either case the seismic input selected for further analysis should agree with the impact of the damaging event at the building site regarding the following:

- the frequency characteristics (considerably dominated by the local subsoil conditions), and
- the amplitude level of seismic ground motion (e.g. peak ground acceleration, *PGA*).

The identification of local subsoil conditions was already comprehensively described in the preceding chapter (cf. MESSIAS procedure; LANG *et al.*, 2003a). Site classification according to relevant schemes will be subsequently summarized for the sites of the different damage cases. In contrast, the damage-inducing demand level can only be roughly estimated, given that no mainshock records directly at the building site are available. Different ways of deriving the level of seismic demand will therefore be checked concerning three points:

- records of earthquake ground motion at adjacent sites,
- attenuation relationships of peak ground acceleration, *PGA*, valid for the regarded region,
- correlation relationships between intensity and *PGA*.

5.3.1 Identification of local subsoil conditions

With respect to the flowchart shown in Figure 5.3, the identification and the classification of local subsoil can be regarded as an essential precondition to providing an alternative seismic excitation. Additional investigations of any mainshock recording station situated in the affected earthquake area thus have to be carried out.

Own site classification results on the basis of instrumental surveys at several strong-motion stations in Northanatolian Türkiye are listed in Table 4.9. As a result, a more reliable selection of suitable mainshock records for structural analysis can be achieved.
Sites of the selected buildings as well as sites of adjacent mainshock recording stations are classified using the hybrid site assessment procedure *MESSIAS* (LANG *et al.*, 2003a).

A detailed description of the subsoil classification at the building sites that is dependent on investigated regions is given in Annex 5-1. Table 5.8 summarizes the site classification results and allocates the respective site class according to the national seismic codes.

Table 5.8 Subsoil classification of the different building sites based on experimental investigations and available information.

Structure	Index	Experimental classification		Classified into site classes following	
		AMBRASEYS *et al.* (1996)	*MESSIAS*	Venezuelan code (MDU, 1990)	Turkish code (TMPS, 1998)
Av. Perimetral, Cumaná	AVE	(very) soft	B3	S_3	-
Edif. Toyota, Cumaná	TOY	stiff (soft)	C2	S_2	-
Edif. Miramar, Cumaná	MIR	(very) soft	B3	S_3	-
Edif. Residencial, Cumaná	EDR	soft	B3	S_2	-
Seymen	SEM	(very) soft	B3	-	Z4
İzmit 1	IZT-1	soft	C3	-	Z4
İzmit 2a	IZT-2a	soft	C3	-	Z4
İzmit 2b	IZT-2b	soft	C3	-	Z4
İzmit 2c	IZT-2c	soft	C3	-	Z4
Sapanca	SAC	stiff (soft)	B2	-	Z2
Düzce 1	DUZ-1	soft	B3	-	Z3-Z4 (Z3 [1])
Düzce 2	DUZ-2	soft	B3	-	Z3-Z4 (Z3 [1])
Yavuzlar Fındık, Gölyaka	YZL	soft	B3	-	Z3
Sultandağı	SUL	stiff	A2-B2	-	Z2

[1] according to information in AKKAR & GÜLKAN (2002)

5.3.2   Damage-inducing demand level

5.3.2.1   *Recordings of earthquake ground motion*

Since no records of the damaging earthquake are available directly at the site of interest, an alternative is to use those records at adjacent sites. To ensure a certain degree of reliability, both the recording site and the site of interest should agree in subsoil conditions, surface topography, and, to a certain extent, epicentral or fault distance.

For the investigated damage cases situated in Venezuela and Türkiye, available records for their respective mainshocks at neighboring stations are listed in Tables 5.9 and 5.10.

The queueing subsoil conditions need to be checked, whether those records are adaptive to the sites of the different damage cases. Recorded levels of peak ground acceleration, *PGA,* will be compared to predicted ones based on correlation relationships of *PGA* in dependence on source distance, *d*, and local shaking intensity, *I*.

For further analysis, it is common practice to scale available mainshock records to the predicted level of peak ground acceleration, *PGA*.

Table 5.9 Peak ground accelerations at recording stations due to the Cariaco earthquake.

Station	Index	Site class (*MESSIAS*)	Peak ground acceleration, *PGA* [%g]		
			H_1-comp.	H_2-comp.	*V*-comp.
Cumaná Corporiente[1]	COP	A1	11.0	17.0	7.0
Cumaná Universidad de Oriente	UDO	B2	9.2	4.8	3.4

[1]   since station COP is an analog operating station, digital records of the mainshock are missing

Table 5.10 Peak ground accelerations and corresponding closeset damage cases at relevant recording stations due to the İzmit (top rows) and Sultandağı (lowest row) earthquakes.

Station	Index	Site class (*MESSIAS*)	Peak ground acceleration, *PGA* [%g] [1]			Closest damage cases		
			H_1-comp.	H_2-comp.	*V*-comp.			
Düzce	DZC	B3	32.1	38.6	48.0	DUZ-1	DUZ-2	YZL
Gebze	GBZ	A1	26.5	14.1	19.8			
İzmit [2]	IZT	A1	17.9	23.5	14.6	IZT-1	IZT-2	SEM
Sakarya	SKR	A2	-	42.2	26.2	SAC		
Yarimca	YPT	C3	29.8	24.7	24.2	IZT-1	IZT-2	SEM
Afyon	AFY	-	11.3	9.5	3.6	SUL		

[1] H_1 - normal, H_2 - parallel
[2]   recording station IZT is not considered representative due to its hillside location (see Annex 4)

5.3.2.2 Ground motion prediction through attenuation laws

A common tool for the prediction of seismic ground motion lies in the elaboration of attenuation relationships of peak ground accelerations, *PGA*, and the spectral accelerations, S_a. Reliability of these relationships increases with the amount of available data, i.e. earthquake records of different magnitude ranges, *M*, and epicentral distances, R_e, or fault distances, *D*.

Because of the large amount of mainshock- and aftershock records in the Northanatolian region available for the year 1999, the elaboration of attenuation laws representative for this seismic region was possible. Results were published by LANG *et al.* (2000), HABENBERGER *et al.* (2001), SCHWARZ *et al.* (2002a), SCHWARZ *et al.* (2002b), and SCHWARZ *et al.* (2003).

In order to estimate ranges of horizontal peak ground accelerations, *PGA*, at the sites of the different damage cases in Northanatolian Türkiye, the recently published attenuation law (SCHWARZ *et al.*, 2003) was applied:

$$\log_{10}(a_H) = C_1 + C_2 \cdot M_L + C_4 \cdot \log_{10}(R) + \sigma \cdot P \tag{5.3}$$

This attenuation model is based on the ground motion model identical to that published by AMBRASEYS *et al.* (1996), whereas parameter *R* displays the following relationship:

$$R = \sqrt{d^2 + h_0^2} \tag{5.4}$$

While h_0 can be regarded as the focal depth, parameter *d* embodies either the epicentral distance, R_e, or fault distance, *D*.

A two-stage regression analysis has to be performed to determine the coefficients C_1, C_2, and C_4. Since the applied attenuation law is based on a dataset mainly consisting of mainshocks and aftershocks recorded at soft soil stations, and damage cases are all situated on soft soil sites, no distinction of subsoil conditions was performed.

Attenuation functions of predicted peak ground accelerations, *PGA*, separated for epicentral distances, R_e, and fault distances, *D*, are shown in Figure 5.13. Corresponding values of peak ground acceleration, *PGA*, are given in Table 5.11. Both, epicentral distances, R_e, and fault distances, *D*, were calculated using the epicentral coordinates and the regional fault rupture map provided by EERI (YOUD *et al.*, 2000).

(a)

(b)
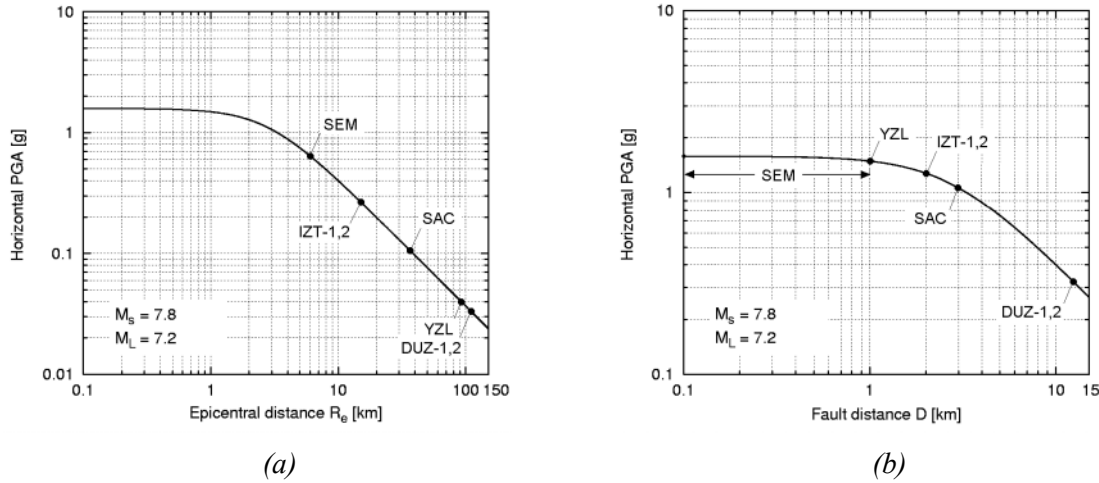
Figure 5.13 Predicted horizontal PGA at the sites of the different damage cases calculated for the magnitude of the 1999 İzmit earthquake (M_s 7.8, M_w 7.4, M_L 7.2) dependent on (a) epicentral distance, R_e, and (b) fault distance, D.

Table 5.11 Predicted peak ground accelerations at the sites of the different damage cases dependent on epicentral and fault distances based on the model by SCHWARZ *et al.* (2003).

Damage case	Epicentral distance, R_e [km] [1]	Predicted peak ground acceleration, PGA_{Re} [%g]	Fault distance, D [km] [1]	Predicted peak ground acceleration, PGA_D [%g]
IZT-1,2	15	26.6	2	128
SEM	6	64.0	0-1	149-158
SAC	36	10.6	3	106
DUZ-1,2	110	3.3	13	30.8
YZL	92	4.0	1	149

[1]   based on epicentral coordinates and mapping of the fault rupture provided by EERI (YOUD *et al.*, 2000)

It can be seen from the values given in Table 5.11 that the attenuation law elaborated by SCHWARZ *et al.* (2003) is obviously misleading for this case. The over-estimation of *PGA* especially for small epicentral or fault distances ($d ≤ 2$ km) is probably due to a large number of weaker aftershocks used for the equation by SCHWARZ *et al.* (2003).

In order to check ranges of *PGA*, additional estimations of *PGA* were carried out using an attenuation model based on near-field records ($D ≤ 15$ km) of earthquakes with $5.8 ≤ M_s ≤ 7.8$, published by AMBRASEYS & DOUGLAS (2003). The corresponding equation has the following form:

$$\log_{10}(a_H) = b_1 + b_2 \cdot M_s + b_3 \cdot D + b_A \cdot S_A + b_S \cdot S_S \tag{5.5}$$

where: $b_{1,2,3,A,S}$ -   regression coefficients

M_s -   surface wave magnitude

D -   distance to the surface projection of rupture plane

S_A, S_S -   coefficient considering soil conditions

(soft: $S_A = 0$, $S_S = 1$; stiff: $S_A = 1$, $S_S = 0$; rock: $S_A = S_S = 0$;).

Attenuation curves representing both the 1999 İzmit earthquake (M_s 7.8, soft soil), and the 2002 Sultandağı earthquake (M_s 6.5, stiff soil), are illustrated in Figure 5.14. Their respective values of predicted peak ground acceleration, *PGA*, are listed in Table 5.12.
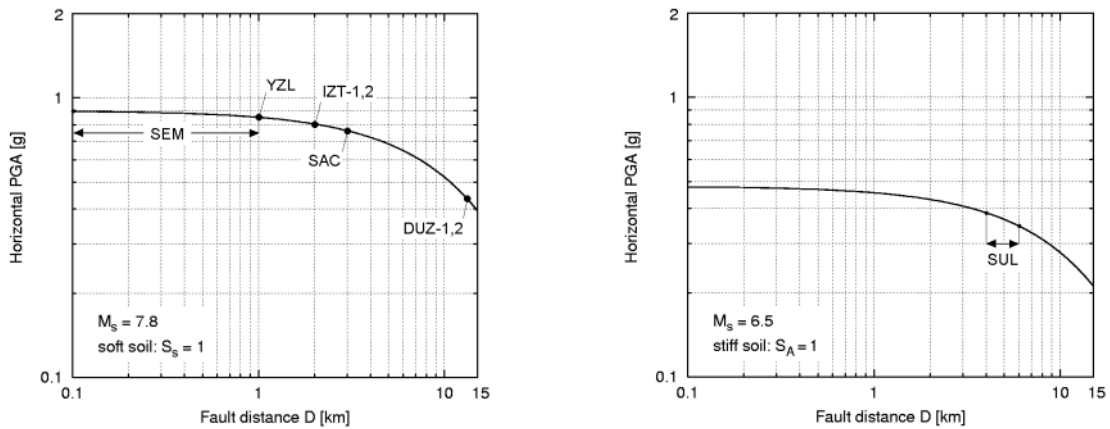
(a) *Northanatolian Türkiye: 1999 İzmit earthquake*   (b) *Aegean Türkiye: 2002 Sultandağı earthquake*

Figure 5.14   Attenuation curves of horizontal peak ground acceleration based on the model by AMBRASEYS & DOUGLAS (2003) *elaborated for different Turkish regions.*

Table 5.12 Predicted peak ground accelerations at the sites of different damage cases dependent on fault distance; based on the model by AMBRASEYS & DOUGLAS (2003).

Damage case	Fault distance D [km]	Predicted peak ground acceleration PGA_D [%g]
IZT-1,2	2 [1]	80.6
SEM	0-1 [1]	85.1 - 89.4
SAC	3 [1]	76.3
DUZ-1,2	13 [1]	44.1
YZL	1 [1]	85.1
SUL	4-6 [2]	34.6 - 38.6

[1]   based on epicentral coordinates and mapping of the fault rupture provided by EERI (YOUD *et al.*, 2000)
[2]   based on epicentral coordinates provided by UNITED STATES GEOLOGICAL SURVEY (USGS)

5.3.2.3   Intensity correlation relationships

If instrumental recordings of the seismic ground motion are missing, seismic intensity is still often the only observed parameter from which to quantify the level of ground shaking (WALD *et al.*, 1999b). Seismic intensity on the basis of macroseismic intensity scales can be regarded as a means to estimate the level of occurred peak ground acceleration (*PGA*), reflecting the complexity of ground motion characteristics at the site. The investigations in this work are related to the twelve-tiered (12-stage) intensity scales, denoted as:

-   Modified Mercalli Intensity Scale MMI (WOOD & NEUMANN, 1931),
-   Medvedev-Sponheuer-Karnik Scale MSK (SPONHEUER & KARNIK, 1964),
-   European Macroseismic Scale EMS (GRÜNTHAL (ed.) *et al.*, 1993; 1998).

Since lower seismic intensities cannot cause observable damages to buildings, intensities lower than VI are assigned on felt accounts of humans. Conversely, higher intensities are defined by the damage extent to buildings as well as by the impacts on the natural environment.

Many correlations between observed seismic intensities and instrumentally determined parameters of peak ground motion are available (e.g. GUTENBERG & RICHTER, 1956; MEDVEDEV & SPONHEUER, 1969; TRIFUNAC & BRADY, 1975; MURPHY & O'BRIEN, 1977). WALD *et al.* (1999a, b) recently developed correlation relationships between Modified Mercalli Intensity, I_{mm}, and ranges of peak ground accelerations (*PGA*) as well as peak ground velocities (*PGV*), which are thought to be more reliable. Detailed relationships are based on observed ranges for the *PGA* of Californian earthquakes and the corresponding Modified Mercalli Intensities, I_{mm} (see Table 5.13).

The formula expressions of WALD *et al.* (1999a) for calculating values of I_{mm} are given by the following equations dependent on intensity ranges:

for $I_{mm} < V$:
$$I_{mm} = 2.20 \cdot \log(PGA) + 1.00 \tag{5.6}$$

for $V < I_{mm} < VIII$:
$$I_{mm} = 3.66 \cdot \log(PGA) - 1.66 \tag{5.7}$$

A *PGA* to intensity relationship particularly relevant for northern Türkiye has also been established by BOMMER *et al.* (2002). It incorporates damage data from surveys in proximity to strong ground-motion instruments, and to their recorded *PGA*. The correlation relationship between macroseismic intensities, I_{EMS}, and *PGA* is presented in equation (5.8). It is valid only for intensities $V \leq I_{EMS} \leq X$.

for $V \leq I_{EMS} \leq X$:
$$\log(PGA) = 0.146 \cdot I_{EMS} + 1.258 \exists 0.164 \cdot \# \tag{5.8}$$

where: $\#$ - standard normal variable

In dependence on the respective type of intensity, Table 5.13 compares values of *PGA* provided by WALD *et al.* (1999a) and those calculated on the basis of the relationship formula by BOMMER *et al.* (2002).

For intensities $I_{mm} > VIII$ (8), values of *PGA* given by WALD *et al.* (1999a) seem to be unrealistically high. This is probably because they were not able to include intensity IX (or larger) values. Due to the evidence of amplitude saturation, the values of *PGA* listed here are not representative.

In contrast, calculated values of *PGA* using the BOMMER *et al.* (2002) relationship even for intensities larger than VIII prove to be more reliable, since they could be confirmed by own observations.

Table 5.13 Instrumentally observed and calculated values of peak ground accelerations for Modified Mercalli Intensities I_{mm} (adapted from WALD et al., 1999a; BOMMER et al., 2002).

Intensity I_{mm} resp. I_{EMS}	I	II-III	IV	V	VI	VII	VIII	IX	X
Instrumentally observed *PGA* [%g] (WALD *et al.*, 1999a)	< 0.17	0.17-1.4	1.4-3.9	3.9-9.2	9.2-18	18-34	34-65	65-124	> 124
Calculated *PGA* [%g] (BOMMER *et al.*, 2002)	-	-	-	9.9	13.9	19.4	27.2	38.1	53.3

The values of local shaking intensities at the building sites of interest can either be assigned by available intensity maps or by in-situ observations of possible shaking effects on the building stock and natural environment; the latter leads to a small-scale intensity assignment for the neighboring area.

Specified shaking intensities according to different available maps are given in Tables 5.14 and 5.15 for the building sites in Cumaná (Venezuela), and Northanatolian provinces (Türkiye), respectively. Local shaking intensities at the building sites are extracted from different intensity maps (Annex 5-2) and presented with each other. Based on own "small scale" observations at respective sites, representative intensities are given additionally.

Table 5.14 Local shaking intensities at the building sites in Cumaná (Venezuela) due to the 1997 Cariaco earthquake (compare with Annex 5-2, Table A5-2.1).

Structure	Index	I_{MMI} (FUNVISIS, 1997)	I_{EMS} (SCHWARZ *et al.*, 2000)	Representative intensity, *I*
Av. Perimetral, Cumaná	AVE		V-VI	V-VI
Edif. Toyota, Cumaná	TOY	VI-VII	-	VII [1]
Edif. Miramar, Cumaná	MIR		VII	VII
Edif. Residencial, Cumaná	EDR		V-VI	V-VI

[1]   intensity was assigned in accordance with local damage occurrence

Table 5.15 Local shaking intensities at the building sites in Northanatolian provinces (Türkiye) due to the 1999 İzmit earthquake (compare with Annex 5-2, Table A5-2.2).

Structure	Index	I_{MSK} (ÖZMEN, 2000)	I_{MMI} (YOUD *et al.*, 2000)	I_{EMS} (RASCHKE, 2001)	Representative intensity, *I*
Seymen	SEM	X	IX	X	IX
İzmit 1	IZT-1	IX	VIII	IX-X	VIII
İzmit 2a	IZT-2a	IX	VIII	IX-X	VIII
İzmit 2b	IZT-2b	IX	VIII	IX-X	VIII
İzmit 2c	IZT-2c	IX	VIII	IX-X	VIII
Sapanca	SAC	VIII	X-XI	VIII-IX	VIII
Düzce 1	DUZ-1	IX	VIII	VIII	VI
Düzce 2	DUZ-2	IX	VIII	VIII	VIII
Yavuzlar Fındık, Gölyaka	YZL	X	X-XI	VIII	VIII

Table 5.16 Local shaking intensity at the building site SUL in Aegean Türkiye due to the 2002
Sultandağı earthquake (compare with Annex 5-2, Table A5-2.3).

Structure	Index	I_{EMS} (ERDIK *et al.*, 2000)	Representative intensity, I
Sultandağı	SUL	VII	VII

5.3.3 Code-consistent demand level

If no information on the level of seismic excitation at the building site is available, the level of the seismic design can be used instead. Even if the building was not designed according to an anti-seismic code provision, it can provide a first hypothesis on the seismic impact at the site. In common code provisions, the seismic impact on the structure is considered by the description of a 5 % damped (elastic) design spectrum. This can be done either for the elastic or the inelastic case, the latter incorporating seismic load reduction factors, *R*, accounting for the specific nonlinear behavior of the structural system during earthquake.

The shape of the spectrum as well as its level of ground acceleration is determined by different parameters depending on the seismic hazard of the site (zonation), the building's structural system and type of use, and the local subsoil conditions.

Because the investigations performed here are concentrated on buildings in Turkish and Venezuelan earthquake areas, design spectra will be supplied according to their respective code provisions:

- Venezuela, COVENIN (Provisional) 1756-82 (MDU, 1990),
- Türkiye, Specifications for Structures to be built in Disaster Areas (TMPS, 1998).

Both provisions specify different ways of elaborating the design spectra and will therefore be treated separately in the following sections.

5.3.3.1 *Design spectra according to the Venezuelan seismic code*

For each of the four Venezuelan buildings selected for an engineering analysis, Table 5.17 lists the parameters required for a compilation of the elastic design spectra. The subscription of parameters as well as their allocated values are done in accordance with the code provision COVENIN (Provisional) 1756-82 (MDU, 1990). All necessary parameters are available as tabular values depending on the given conditions of the site and the structure.

The actual shape of the design spectrum strongly depends on the subsoil conditions, i.e. the site class S_1 to S_3 (cf. Figure 5.15), which first has to be identified. Connected to the site class are the soil amplification factor β, the corner period T^*, and the spectral exponent *p*.

Elastic design values for spectral accelerations, A_d, can be determined using equations (5.8) to (5.10):

for $T < 0.15$ s :
$$A_d = \alpha \cdot A_0 \cdot \left(1 + \frac{T}{0.15} \cdot (\beta - 1) \right) \tag{5.8}$$

for $0.15 \leq T < T^*$:
$$A_d = \alpha \cdot \beta \cdot A_0 \tag{5.9}$$

for $T \geq T^*$:
$$A_d = \alpha \cdot \beta \cdot A_0 \cdot \left(\frac{T^*}{T} \right)^p \tag{5.10}$$

Table 5.17 Parameters for the preparation of elastic design spectra according to the Venezuelan code provision COVENIN 1756-82 (MDU, 1990).

Structure	Index	Zonation		Type of use		Allocated subsoil class	
		Seismic zone	effect. acc. A_0	Building class	Import. factor α	given in project plans	based on exp. data [1]
Av. Perimetral, Cumaná	AVE	4	0.30g	B	1.0	-	S_3
Edif. Toyota, Cumaná	TOY	4	0.30g	B	1.0	S_2 or S_3	S_2
Edif. Miramar, Cumaná	MIR	4	0.30g	B	1.0	-	S_3
Edif. Residencial, Cumaná	EDR	4	0.30g	B	1.0	-	S_2

[1] allocated subsoil classes according to the Venezuelan code COVENIN 1756-82 for respective site-specific subsoil classes, which were identified by applying *MESSIAS* (see Chapter 4)
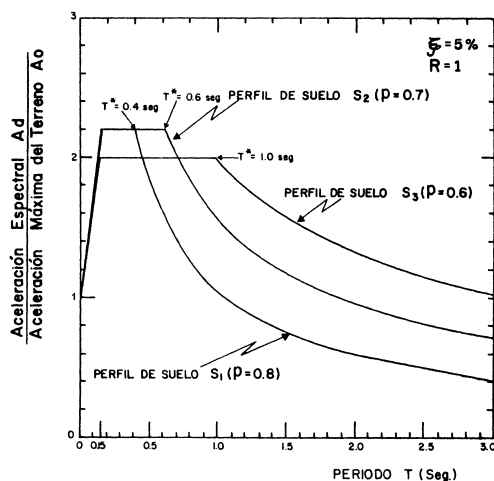
Site class	amplif. factor β [-]	corner period T^* [sec]	exponent p
S_1	2.2	0.4	0.8
S_2	2.2	0.6	0.7
S_3	2.0	1.0	0.6

Figure 5.15 Shape of elastic design spectra and spectrum-describing parameters for site classes S_1 to S_3 according to the Venezuelan seismic code COVENIN 1756-82.

5.3.3.2 Design spectra according to the Turkish seismic code

Parameters necessary for the elaboration of design spectra for the Turkish structures are found in Table 5.18 (TMPS, 1998). It can be seen that the Turkish procedure is somewhat similar to the Venezuelan procedure.

After classification of the local subsoil conditions into site classes Z1 to Z4 (cf. Figure 5.16), elastic design spectra can be generated. The period-dependent Spectral Acceleration Coefficient, $A(T)$, shall be computed by equations (5.11) to (5.13):

for $T < T_A$:
$$A(T) = A_0 \cdot I \cdot \left(1 + 1.5 \cdot \frac{T}{T_A}\right) \tag{5.11}$$

for $T_A < T \le T_B$:
$$A(T) = 2.5 \cdot A_0 \cdot I \tag{5.12}$$

for $T > T_B$:
$$A(T) = 2.5 \cdot A_0 \cdot I \cdot \left(\frac{T_B}{T}\right)^{0.8} \tag{5.13}$$

Table 5.18 Parameters for the preparation of elastic design spectra according to the Turkish code provisions (TMPS, 1998).

Structure	Index	Zonation		Type of use		Allocated subsoil class
		Seismic zone	effect. acc. A_0	Building class	Import. factor I	based on experimental investigations [1]
Seymen	SEM	1	0.40g	4	1.0	Z4
İzmit 1	IZT-1	1	0.40g	4	1.0	Z4
İzmit 2a	IZT-2a	1	0.40g	4	1.0	Z4
İzmit 2b	IZT-2b	1	0.40g	4	1.0	Z4
İzmit 2c	IZT-2c	1	0.40g	4	1.0	Z4
Sapanca	SAC	1	0.40g	4	1.0	Z2
Düzce 1	DUZ-1	1	0.40g	1	1.5	Z3-Z4
Düzce 2	DUZ-2	1	0.40g	4	1.0	Z3-Z4
Yavuzlar Fındık, Gölyaka	YZL	1	0.40g	4	1.0	Z3
Sultandağı	SUL	1	0.40g	4	1.0	Z2

[1]   allocated subsoil classes according to the Turkish seismic code (TMPS, 1998) for respective site-specific subsoil classes, which were identified by applying *MESSIAS* (see Chapter 4)
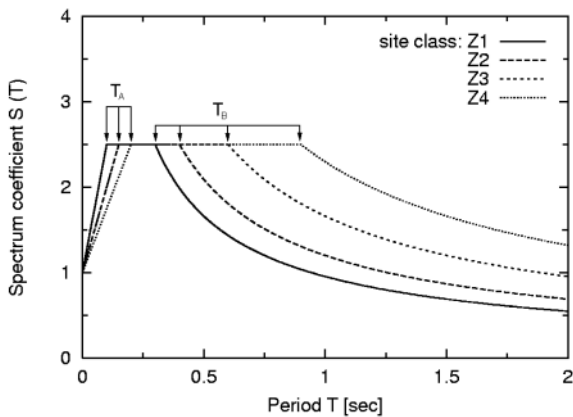
Site class	corner period T_A [sec]	corner period T_B [sec]
Z1	0.10	0.30
Z2	0.15	0.40
Z3	0.15	0.60
Z4	0.20	0.90

Figure 5.16 Shape of elastic design spectra and spectrum-describing parameters for site classes Z1 to Z4 according to the Turkish seismic code (TMPS, 1998).

5.3.3.3 Design spectra according to the German seismic code

Based on the provisions of German seismic code DIN 4149 (DIN, 2002), the design spectra corresponding to the type of site classification used in this work can be generated from equations (5.14) to (5.17). It becomes obvious after looking at Table 5.19 that the 6 (respectively 7) spectra for site-specific subsoil classes vary in both amplitude and spectral shape. The first is caused by soil parameter S, the latter by corner periods T_B, T_C.

SCHWARZ, LANG & GOLBS (1999) recommended an additional subsoil class C2, which contains stiff soil conditions with mighty layer thicknesses (cf. Figure 4.2). Though this subsoil class is not incorporated in the present draft of DIN 4149 (DIN, 2002), parameters as suggested by SCHWARZ, LANG & GOLBS (1999) are included in Table 5.19.

Since values for effective accelerations, a_g, as indicated in DIN 4149 are exclusively related to the seismicity of Germany's earthquake regions, they will not be alluded to here.

for $T_A \leq T \leq T_B$:
$$S_e(T) = a_g \cdot S \cdot \left(1 + \frac{T}{T_B} \cdot (\% \, \beta_0 - 1)\right) \qquad (5.14)$$

for $T_B \leq T \leq T_C$:
$$S_e(T) = a_g \cdot S \cdot \% \, \beta_0 \qquad (5.15)$$

for $T_C \leq T \leq T_D$:
$$S_e(T) = a_g \cdot S \cdot \% \, \beta_0 \cdot \frac{T_C}{T} \qquad (5.16)$$

for $T \geq T_D$:
$$S_e(T) = a_g \cdot S \cdot \% \, \beta_0 \cdot \frac{T_C \cdot T_D}{T^2} \qquad (5.17)$$

whereas:

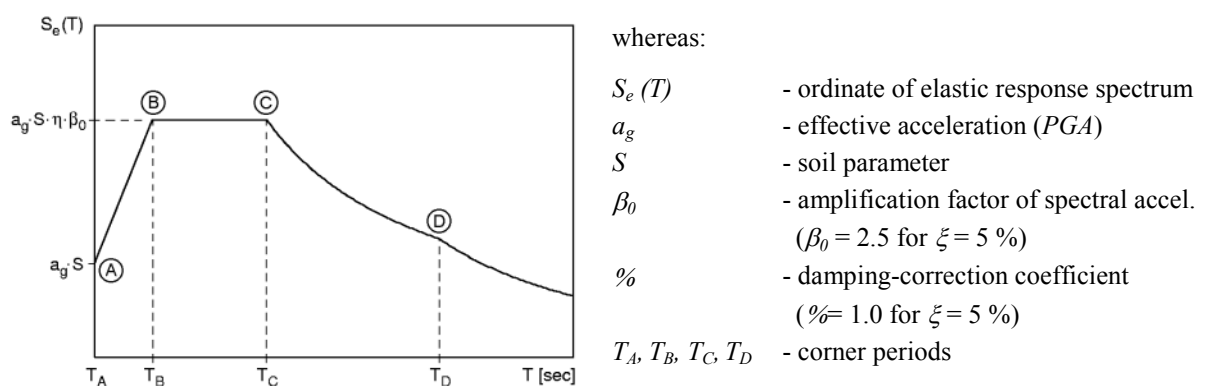|	
$S_e(T)$	- ordinate of elastic response spectrum
a_g	- effective acceleration (*PGA*)
S	- soil parameter
β_0	- amplification factor of spectral accel. ($\beta_0 = 2.5$ for $\xi = 5$ %)
$\%$	- damping-correction coefficient ($\% = 1.0$ for $\xi = 5$ %)
T_A, T_B, T_C, T_D	- corner periods

Figure 5.17 Shape of design spectrum according to the German code DIN 4149 (DIN, 2002).

Table 5.19 Parameters describing the design spectra of DIN 4149 (DIN, 2002).

Site class	Soil parameter S	Corner periods		
		T_B [sec]	T_C [sec]	T_D [sec]
A1	1.00	0.05	0.20	2.00
A2	1.25	0.05	0.25	2.00
A3	1.50	0.05	0.30	2.00
B2	1.00	0.10	0.30	2.00
B3	1.25	0.10	0.40	2.00
C2 [1)]	0.75	0.10	0.50	2.00
C3	0.75	0.10	0.50	2.00

[1)] subsoil class C2 is not adopted in the present draft of DIN 4149 (DIN, 2002); parameters were taken from SCHWARZ, LANG & GOLBS (1999)

5.3.4   Compilation of seismic demand level for the different damage cases

Table 5.20 summarizes the possible levels of peak ground acceleration (*PGA*) that supposedly occurred during the mainshocks and that are thus responsible for possible damage.
Levels of possible *PGA* are compiled regarding the following:

-   recordings of the mainshock at the closest stations,
-   empirical attenuation laws,
-   intensity correlation relationships.

Effective accelerations, A_0 resp. a_g, as provided by the national seismic design codes are given in Table 5.20. These values represent the maximum values of *PGA*.

Table 5.20 Compilation of peak ground accelerations [% g] determined on various ways.

Structure	Closest mainshock record		Attenuation laws adapted from			Intensity correlation relationsips adapt. from		Seismic design (national code)
	H_1	H_2	SCHWARZ *et al.* (2003)		AMBRASEYS & DOUGLAS (2003)	WALD *et al.* (1999a)	BOMMER *et al.* (2002)	
			R_e	D				
AVE	11	17	-	-	-	6.7-12.6	9.9-13.9	30
TOY	11	17	-	-	-	18-34	19.4	30
MIR	11	17	-	-	-	18-34	19.4	30
EDR	11	17	-	-	-	6.7-12.6	9.9-13.9	30
SEM	29.8	24.7	64.0	149-158	85.1-89.4	65-124	38.1	40
IZT-1	29.8	24.7	26.6	128	80.6	34-65	27.2	40
IZT-2a	29.8	24.7	26.6	128	80.6	34-65	27.2	40
IZT-2b	29.8	24.7	26.6	128	80.6	34-65	27.2	40
IZT-2c	29.8	24.7	26.6	128	80.6	34-65	27.2	40
SAC	-	42.2	10.6	106	76.3	34-65	27.2	40
DUZ-1	32.1	38.6	3.3	30.8	44.1	9.2-18	13.9	40 (60)
DUZ-2	32.1	38.6	3.3	30.8	44.1	34-65	27.2	40
YZL	32.1	38.6	4.0	149	85.1	34-65	27.2	40
SUL	11.3	9.5	-	-	34.6-38.6	18-34	19.4	40

5.4 Classification of structural damage

The quantification of earthquake damage to buildings can be classified in different ways. Numerous different concepts can be found in several provisions, such as in macroseismic intensity scales (e.g. the European Macroseismic Scale EMS-98; GRÜNTHAL *et al.*, 1998).

The classification of effects on structural elements can be done either descriptively or empirically: the former by a more or less detailed description of damage indicators, the latter by the definition of certain thresholds of building motion parameters, e.g. interstory drift ratio $\&_{dr,i}$, spectral displacement S_d, spectral acceleration S_a.

An empirically-based classification of structural damage requires a detailed model of the structure as well as its structural analysis.

Since these available concepts on damage classification are usually not precise enough to describe the actual damage pattern, their ability to derive the strength of shaking during the damaging earthquake is constricted. Some of the available parameters to quantify structural damage will be briefly discussed below.

It should be explicitly stated that the following discussion will focus only on reinforced-concrete (RC) frame structures furnished with masonry infill walls between the frame members.

5.4.1 The descriptive concept of the EMS-98

The European Macroseismic Scale 1998 (GRÜNTHAL (ed.) *et al.*, 1998) defines five different damage grades (*DG*) in order to classify structural earthquake damage. For reinforced-concrete structures, Table 5.21 reproduces the definition of each damage grade separately on the extents to structural and nonstructural elements.
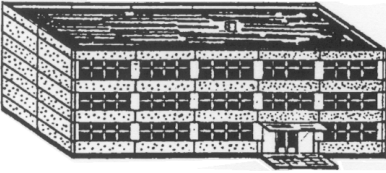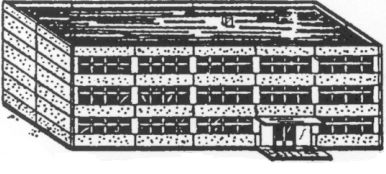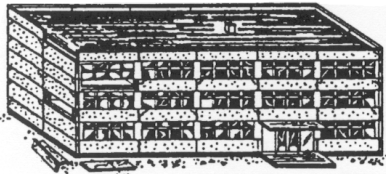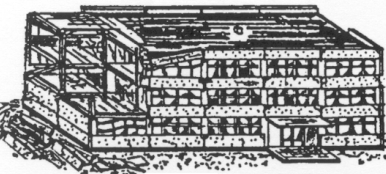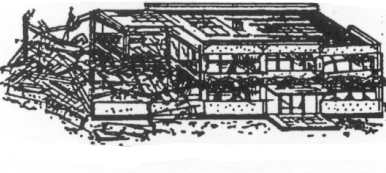
As annotated in the EMS-98, "damage grades are also something of a compromise": they intend to ideally represent a linear increase in the strength of shaking. Looking at the illustrative pictures given in Table 5.21, only the visible amount of structural (and nonstructural) damage to the building is decisive in order to assign the grade of damage (*DG*). However, with the objective of assessing the damage potential of seismic ground motion, the classification procedure may have some deficiencies. For example, the classification concept alone does not consider any of the following:

- structural differences (e.g. quality of materials, structural layout, grade of antiseismic design) strongly influencing the response and failure mechanisms,
- the number of structural elements suffering a certain degree of damage (no classification is done that accounts for the quantity of cracks or yielded elements),
- damage to those structural elements that are not directly observable (e.g. not visible due to architectural finishes or fireproofing).

One should also bear in mind that the assessment of the damage grade strongly depends on the subjective view of the operator, since well-defined limits of each damage grade do not exist.

As a result, the classification concept as proposed by the EMS-98 may lead to under- or overestimations of the actual damage pattern. This in turn is produced by a rough, step-like subdivision into five damage grades that do not incorporate the structural peculiarities and thus its particular structural performance.

Table 5.21 Classification of damage to reinforced-concrete buildings into damage grades (DG) according to the EMS-98 (GRÜNTHAL (ed.) *et al.*, 1998).

Definition of Damage Grade (*DG*)	Extent of	
	structural damage	nonstructural damage
Grade 1: Negligible to slight damage	none	slight: Fine cracks in plaster over frame members or in walls at the base. Fine cracks in partitions and infills.
Grade 2: Moderate damage	slight: Cracks in columns and beams of frames and in structural walls.	moderate: Cracks in partition and infill walls; falling of brittle cladding and plaster. Falling mortar from the joints of wall panels.
Grade 3: Substantial to heavy damage	moderate: Cracks in columns and beam column joints of frames at the base and at joints of coupled walls. Spalling of concrete cover, buckling of reinforced rods.	heavy: Large cracks in partition and infill walls, failure of individual infill panels.
Grade 4: Very heavy damage	heavy: Large cracks in structural elements with compression failure of concrete and fracture of rebars; bond failure of beam reinforced bars; tilting of columns. Collapse of a few columns or of a single upper floor .	-
Grade 5: Destruction	very heavy: Collapse of ground floor or parts (e.g. wings) of buildings.	-

A quantification of the different damage grades (*DG*) on structural performance during lateral loading was presented by K. LANG (2002). Using the nonlinear static "pushover" analysis, K. LANG connected the damage grades (*DG*) of the EMS-98 (GRÜNTHAL (ed.) *et al.*, 1998) to different points on the capacity curve at which the building enters the next damage grade. Each of these points is determined by a certain roof displacement, $Э_i$, and its corresponding base shear, $V_{b,i}$ (Figure 5.18). The indicators for when the building enters the next damage grade (*DG*) are given in Table 5.22. Since these investigations are constricted to RC shear wall buildings, no direct adoption of these findings to the herein concerned RC moment resisting frame structures can be carried out. On the basis of own damage observations and analysis results, a definition of damage grade indicators needs to be found.
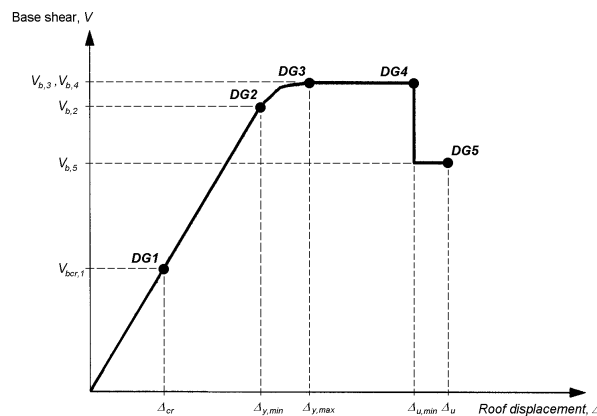
Figure 5.18   Allocation of damage grades (DG) following the EMS-98 on the capacity curve according to K. LANG *(2002).*

Table 5.22 Indicators of damage grades (DG) for RC shear wall buildings (K. LANG, 2002).

Damage grade (EMS-98)	Indicators (K. LANG, 2002)	Point in *Fig. 5.18*
DG1	point of onset of cracking (before it the building is considered to be undamaged) → tensile stress at the extreme tensile fibre of the wall section reaches the tensile strength of concrete	$Э_{cr}$, $V_{bcr,1}$
DG2	behavior of the building becomes nonlinear, the stiffness of the building starts to reduce → yielding of the first wall	$Э_{y,min}$, $V_{b,2}$
DG3	increased nonlinear behavior of the building, the stiffness of the building tends to zero → yielding of the last wall	$Э_{y,max}$, $V_{b,3}$
DG4	→ ultimate displacement of the first wall, determined either by compression failure of concrete or fracture of the reinforcing bars	$Э_{u,min}$, $V_{b,4}$
DG5	→ drop of the base shear of the building V_b below $2/3 \cdot V_{bm}$	$Э_u$, $V_{b,5}$

5.4.2   The empirical concept in HAZUS®99

In order to empirically classify structural and nonstructural earthquake damage, one must simply turn to HAZUS®99 (FEMA, 1999). Here a subdivision into structural damage states (*DS*), referred to as *slight, moderate, extensive,* and *complete*, is carried out. Each of them are demarcated by its respective threshold of damage state and, represents values of drift ratios, $\&_{dr,i}$ (Figure 5.19), as well as spectral displacement, S_d. (Note: Thresholds of damage states dependent on spectral displacement values, S_d, are not applied here.)

Thresholds of damage states are provided which depend on the following characteristics:

- the structural building type (e.g. concrete moment frame, concrete shear walls),
- the building height or number of stories (low-, mid-, and high-rise), and
- the seismic design level (pre-, low-, moderate-, and high-code).

With regard to the last criterion, it becomes obvious that this concept is intended for the prediction of damage to known buildings rather than assessing the level of damage at buildings with missing input information. Given that no detailed information on the structural peculiarities (e.g. reinforcement detailing) can be obtained, a reliable evaluation of the seismic design level proves to be difficult in hindsight.

Figure 5.19a schematically illustrates the shape of capacity curves that correlate to the building's seismic design level. Figure 5.19b displays any given capacity curve with thresholds of damage states for the different seismic design levels. Indicators for structural damage states (*DS*) are given in Table 5.23. Since thresholds of damage states show large variations and sizeably differ in respect to the seismic design level, a classification of damage can only be achieved if the required details on the structure are available.

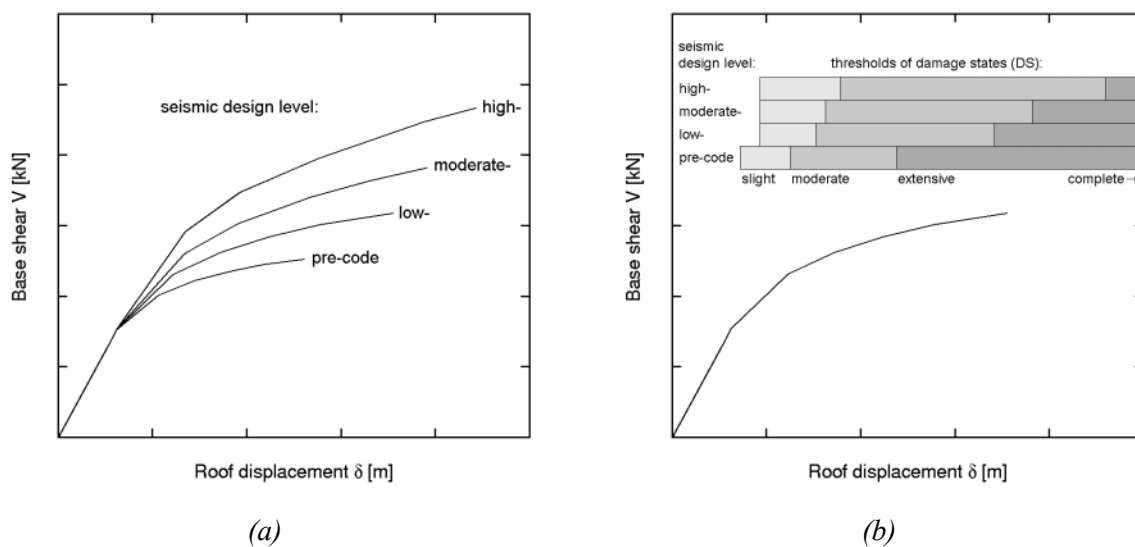*(a)*   *(b)*

Figure 5.19   The influence of (a) the seismic design level on the shape of structural capacity curve, and (b) on the definition of thresholds of damage states (HAZUS®99).

Figure 5.19a shows that seismic design level is associated with structural ductility and thus with its vulnerability. Analogies to the vulnerability classes of the EMS (GRÜNTHAL (ed.) *et al.*, 1998) exist.

In contrast to the definition of damage grades within the EMS-98 (GRÜNTHAL (ed.) *et al.*, 1998), the damage classification proposed here is quantified on the number (*few, some, most*) of affected elements. However, since a reliable description of damage occurrence depends on the detailed knowledge of the structural layout (including the seismic design level) and on the results of structural (pushover) analysis, this concept is somewhat disadvantageous for engineering practice.

Table 5.23 Indicators for structural damage states (DS) for selected structural building types as defined in HAZUS®99 (FEMA, 1999)

Structural damage state (*DS*)	Reinforced-concrete moment resisting frames (C1)	Concrete frame buildings with unreinforced masonry infill walls (C3)
slight	Flexural or shear type hairline cracks in some beams and columns near joints or within joints.	Diagonal (sometimes horizontal) hairline cracks on most infill walls; cracks at frame-infill interfaces.
moderate	Most beams and columns exhibit hairline cracks. In ductile frames some of the frame elements have reached yield capacity indicated by larger flexural cracks and some concrete spalling. Nonductile frames may exhibit larger shear cracks and spalling.	Most infill wall surfaces exhibit larger diagonal or horizontal cracks; some walls exhibit crushing of brick around beam-column connections. Diagonal shear cracks may be observed in concrete beams or columns.
extensive	Some of the frame elements have reached their ultimate capacity indicated in ductile frames by large flexural cracks, spalled concrete and buckled main reinforcement; nonductile frame elements may have suffered shear failures or bond failures at reinforcement splices, or broken ties or buckled main reinforcement in columns which may result in partial collapse.	Most infill walls exhibit large cracks; some bricks may dislodge and fall; some infill walls may bulge out-of-plane; few walls may fall partially or fully; few concrete columns or beams may fail in shear resulting in partial collapse. Structure may exhibit permanent lateral deformation.
complete	Structure is collapsed or in imminent danger of collapse due to brittle failure of non-ductile frame elements or loss of frame stability. Approximately 20% (low-rise), 15% (mid-rise) or 10% (high-rise) of the total area of Cl buildings with complete damage is expected to be collapsed.	Structure has collapsed or is in imminent danger of collapse due to a combination of total failure of the infill walls and nonductile failure of the concrete beams and columns. Approximately 25% (low-rise), 20% (mid-rise) or 15% (high-rise) of the total area of C3 buildings with complete damage is expected to be collapsed.

5.4.3   The concept of states of structural damage pattern (*DP*)

It could be shown that the available concepts can definitely classify the extent of structural damage, although they do not suffice for accurately describing the actual damage pattern.
Since damage grades or other damage classification parameters should ideally represent a linear increase of earthquake shaking strength, the capacity curve derived from the nonlinear static analysis procedure provides a suitable tool. The application of an incrementally increasing lateral load is directly associated with the severity of damage to the structural and nonstructural elements.

Since each analysis step on the "pushover" capacity curve is connected to a certain damage pattern indicating the locations of yielding elements as well as their respective state of plastification, structural damage will be quantified on the capacity curve and respective states of damage pattern (*DP*).

Figure 5.20 schematically depicts the capacity curve of an exemplary RC frame structure and the locations of yielded elements at the different steps of analysis (1-6). Indices at the different elements (*B, IO, LS, CP, C, D, E*) characterize different "structural performance levels", as provided by FEMA 273 (FEMA, 1997) and ATC-40 (ATC, 1996). Figure 5.21 illustrates the different yield conditions of the element and the locations of structural performance levels (*SPL*) on a generalized load-deformation curve.
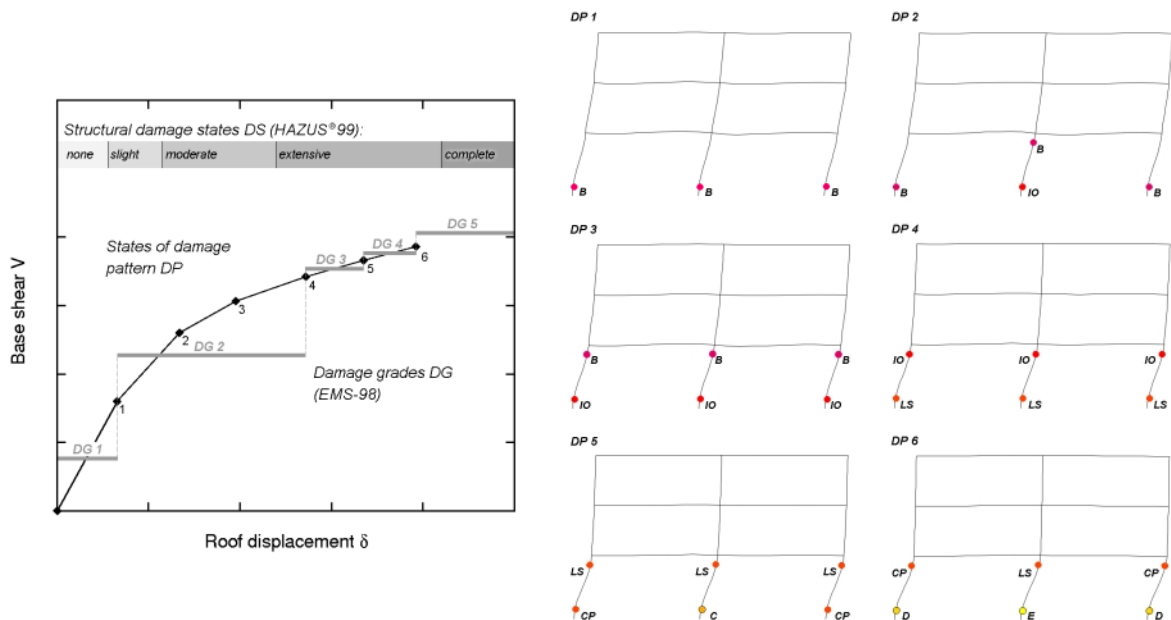
Figure 5.20   Comparison between conventional damage parameters (DS, DG) and states of actual damage pattern DS.
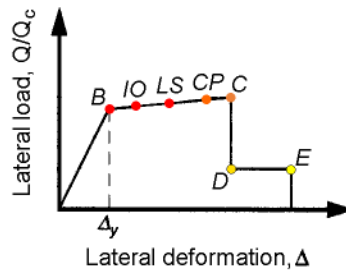
Figure 5.21   Generalized load-deformation relationship for structural components indicating structural performance levels (modified figure taken from ATC-40).

In order to visualize the differences between the damage classification concepts already discussed, both structural damage states (HAZUS®99) and damage grades (EMS-98) were superimposed onto the structural capacity curve, and thus to states of damage pattern (Figure 5.20). While thresholds of *DS* are provided as a fixed measure of roof displacement, δ, ranges of *DG* were specified according to agreements between their respective damage indicators on primary structural elements (Table 5.24).

It can be seen in Figure 5.20 that both structural damage states and damage grades cannot describe the specific pattern of structural damage. As long as it is concentrated on the analysis of several buildings, damage classification should be done more accurately by considering the states of damage pattern. This also assumes the detailed modeling, structural analysis of the building, and the thoroughly documentation of actual damage.

In addition to this method of classifying damage, SWAIN & SCHWARZ (2004) quantified damage grades of the EMS-98 on the damaging effects on structural columns. On the basis of finite element (FEM) models and the results of dynamic stress analysis, damage grades were defined in relation to the percentage of affected columns. Figure 5.22 illustrates the allocation of damage grades (*DG*) on the capacity curve of an exemplary RC frame structure. As seen from the sketches below, each stage of damage grades is connected to a certain stress distribution in the structural RC elements, which also represents the state of damage pattern (*DP*).

Table 5.24 Comparison of structural performance levels and damage grades according to agreements in damage indicators on primary structural elements (FEMA 273, ATC-40, EMS-98).

Structural performance levels *SPL* (FEMA 273, ATC-40)		Damage grades *DG* (EMS-98)	
B	Very little damage.	*DG 2*	Cracks in columns and beams of frames and in structural walls.
IO	Very limited flexural and shear cracking with no spalling; no permanent offset.		
LS	Hinges have formed in the lower parts of the building, causing spalling above and below beam-column joints.	*DG 3*	Cracks in columns and beam column joints of frames at the base and at joints of coupled walls. Spalling of concrete cover, buckling of reinforced rods.
CP	The building remains standing, but only barely; any other damage or loss is acceptable.	*DG 4*	Large cracks in structural elements with compression failure of concrete and fracture of rebars; bond failure of beam reinforced bars; tilting of columns. Collapse of a few columns or of a single upper floor .
C	Hinges have formed in the lower parts of the building causing significant spalling above and below beam-column joints and pulverizing of concrete within the core.		
D	Initial failure of components, maybe associated with phenomena such as fracture of longitudinal reinforcement, spalling of concrete, or sudden shear failure following initial yield.		
E	Collapse.	*DG 5*	Collapse of ground floor or parts (e.g. wings) of buildings.

DG 1 (starting point)   DG 1 (end point)   DG 2 (starting point)

DG 2 (end point)   DG 3 (starting point)   DG 3 (end point)

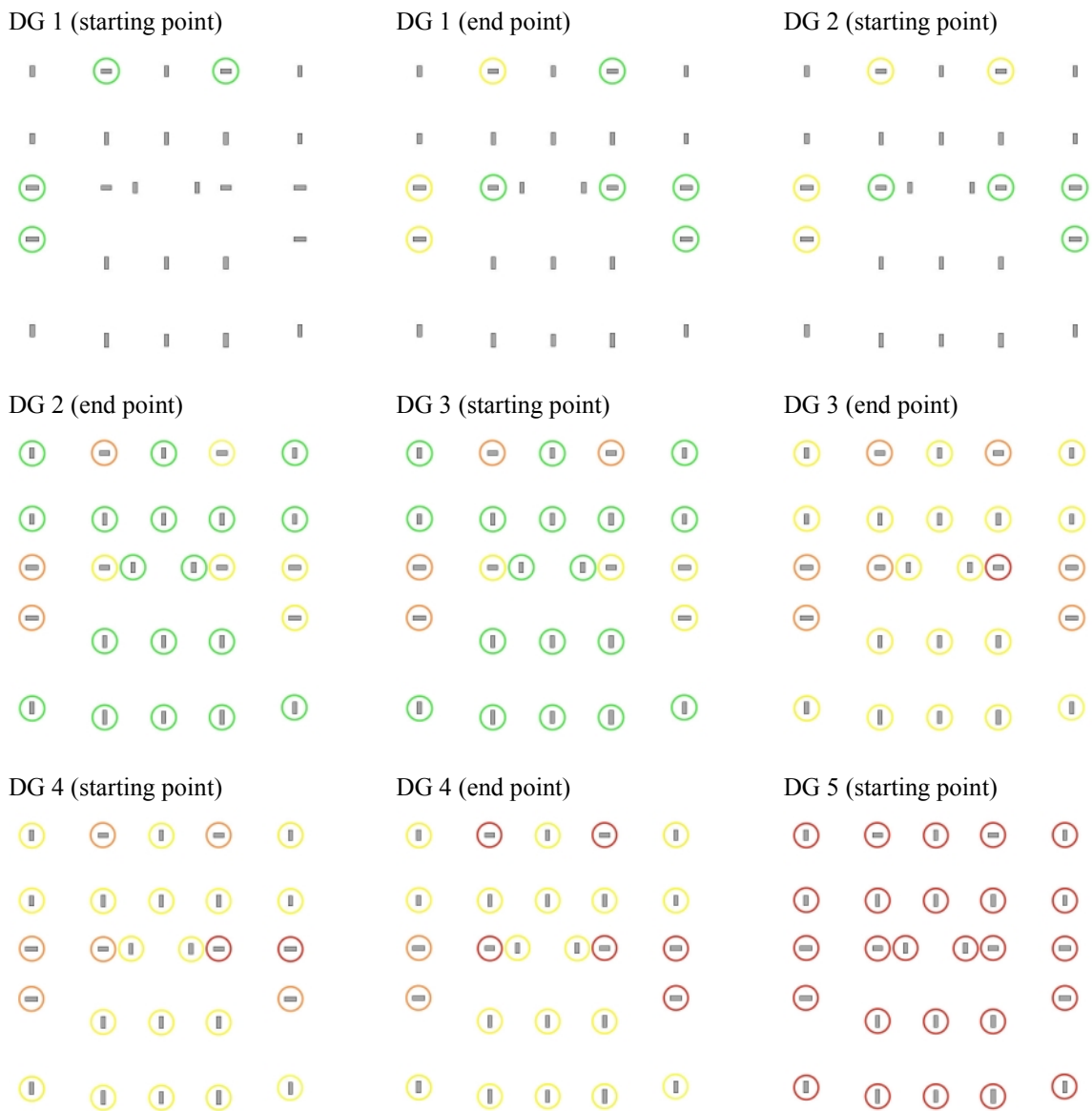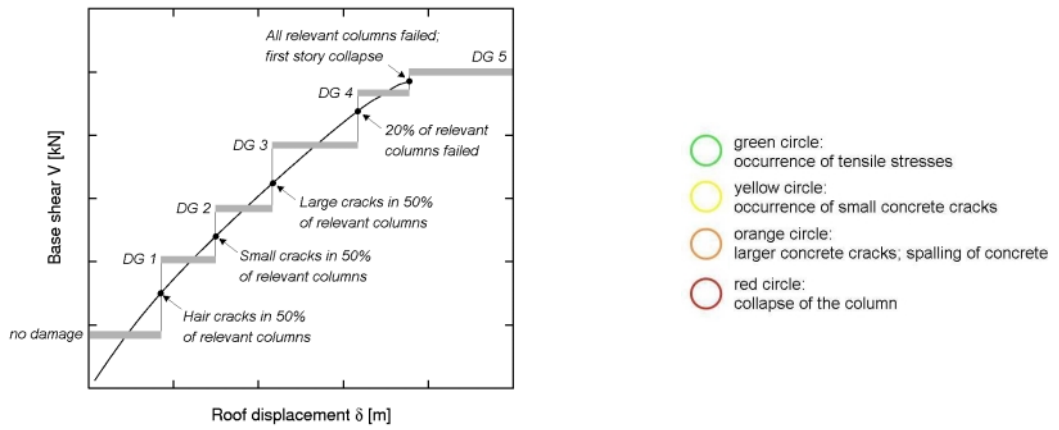DG 4 (starting point)   DG 4 (end point)   DG 5 (starting point)

Figure 5.22 Allocation of damage grades (DG) on the capacity curve; based on results of dynamic stress analysis for an exemplary reinforced-concrete frame structure (SWAIN & SCHWARZ, 2004).

5.5 Establishing the damage potential of seismic ground motion

The quantification of the damage potential of seismic ground motion is of particular interest for the interpretation of structural damage and even of structural design.

As mentioned already at the beginning of this work, the damage potential of seismic ground motion can be defined in different ways. Irrespective of the term's nature, it is common knowledge that the damage potential of seismic ground motion depends not only on the seismic demand, but also on the structural capacity.

However, experience gained from past earthquakes has shown that the engineering profession has not yet succeeded in defining ground motion parameters that correlate well with observed damage.

Since both seismic ground motion and structural capacity are complex phenomena depending on several influencing factors, the damage potential of seismic ground motion certainly cannot be quantified to a single parameter.

Methods of defining and concepts of identifying damage potential of seismic ground motion according to different scientific groups will now be briefly discussed.

5.5.1 Customary concepts

When SEED & IDRISS (1969) first investigated the influence of local soil conditions on building damage potential during strong earthquakes, they predicated their concept of damage potential on the "estimation of forces and motions that are induced in structures of any type during earthquakes, and the effects of this dynamic response on structural performance." Although acceleration values of recorded ground motion allow for maximum lateral forces to be determined that are inflicted upon to the structure during the earthquake, damaging effects cannot be accounted for.

In addition, MOORE (1979) stated that not only the maximum values, but also the frequency characteristics of seismic ground motion influenced by the subsoil conditions at the building site should be regarded. A distinction between different structural building types must also be ensured that considers the type of framing or quality of materials. A quantification of damage potential is achieved by indices F_r and D_r, comparing induced lateral forces with design lateral forces:

$$F_r = \frac{V_{max}}{V_{design}} = \frac{W \cdot S_a}{g \cdot V_{design}} = \frac{W \cdot S_a}{g \cdot K \cdot W} = \frac{S_a}{g \cdot K} \qquad (5.18)$$

or

$$D_r = \frac{S_v}{K} \qquad (5.19)$$

where: V_{max} - max. induced dynamic lateral force (base shear)

V_{design} - static design lateral force

S_a, S_v - spectral acceleration, spectral velocity

W - weight of the SDOF (total dead load)

K - horizontal force factor

RAHNAMA & KRAWINKLER (1991) used the term *damage potential* "to denote the potential of earthquake ground motion to inflict damage to manmade structures." The damage potential consequently depends on the severity of ground shaking and the structure's ability to resist this shaking. The superposition of structural capacity and seismic demand is realized in the frequency domain, where strength capacity curves, $F_y(g)$, of code-designed buildings are compared with elastic, $F_{y,e}$ ((= 1), and inelastic ((= 2, 3, 4) strength demand spectra, $F_y(()$. This leads to the requirement of ductility demands, (, in order to bring strength demand spectra, $F_y(()$, under capacity curves, $F_y(g)$.

In contrast to these ideas, the recent approach published by SUNASAKA *et al.* (2003) incorporated both the level and characteristics of damage. According to them, *damage potential* is defined as a spectrum of strength demand required to maintain a damage index less than or equal to a tolerable damage index value, D. For example, damage index D proposed by PARK & ANG (1985) can be determined as follows:

$$D = \frac{\delta_m}{\delta_u} + \beta \cdot \int \frac{dE}{(Q_y \cdot \delta_u)}$$

(5.20)

where: δ_m - maximum response deformation

δ_u - ultimate deformation under static loading

β - coefficient for cyclic loading effect

dE - incremental dissipation hysteretic energy

Q_y - yield strength, maximum base shear

Using the above premise, for a single-degree-of-freedom (SDOF) system with a predefined bilinear force-deformation characteristic, the strength demand for a specified ground motion can be calculated. Strength demand representing the damage potential of a SDOF system, is defined in turn to be yield strength ratio, R_y:

$$R_y = \frac{Q_y}{W}$$

(5.21)

where: W - weight of SDOF (total dead load)

Table 5.25 Distinguishing features of the different concepts.

Author	Mechanical principle	Dimension
SEED & IDRISS (1969)	force + displacement	-
MOORE (1979)	force	global
RAHNAMA & KRAWINKLER (2003)	strength	structural type-dependent
SUNASAKA *et al.* (2003)	deformation + energy [1]	local (on single structural elements), global application

[1]   using the damage index proposed by PARK & ANG (1985)

5.5.2   Formulation of an alternative concept for damage potential estimation

In order to identify the damage potential of seismic ground motion, an objective assessment of the different components possibly contributing to the damaging process has to be obtained. It is the author's opinion that damage potential of seismic ground motion can only be regarded as the case arises. Therefore no general statements about the damage potential related to a particular earthquake event, subsoil, or structural building type will be given here.

Table 5.25 compares the different concepts presented in the preceding chapter to the mechanical principle of damage models and to the dimension of the investigations. They are either only roughly defined with no distinction of structural types or building sites on a general scale, or they are concentrated on a very small dimension, dealing with the local damage models of single structural elements.

Conversely, a more case-dependent procedure was worked out (cf. Table 5.4) and applied to selected damage cases (Annex A5-3).

The damage potential of seismic ground motion should generally be defined as the capability of a supposed seismic excitation, representative in frequency content and amplitude level for the given building site, to induce structural damage to the building. This encompasses both the vulnerability of the buildings as well as subsoil conditions of the site.

The damage potential of seismic ground motion can only be assessed by a thorough investigation of all components, including the (damaging) seismic excitation, structural layout, site and subsoil conditions, and, if present, pattern of structural damage.

Even though the detailed description of occurred structural damage yields higher accuracy, an assessment of damage potential can also be done prospectively, e.g. in the structural design process.

Since the available structural information of some damage cases (Table 5.4, Annex A5-3) do not admit the creation of a reliable structural model and thus the performance of structural analyses, an entire identification of the damage potential of seismic ground motion cannot be carried out.

Given that experimental results of the structure's dynamic characteristics (i.e. experimental identified natural periods of the structure, $T_{n,exp}$) are disposable, a rough evaluation of the

damage potential of seismic ground motion can be performed. By comparing the ranges of natural building periods, $T_{n,exp}$, with those of the predominant site periods, T_s, an initial statement on the possible occurrence of resonance effects between site and structure can be made. It should be noted that these surveys are solely related to the elastic range of structural performance and site response.

The flowchart depicted in Figure 5.23 describes a procedure that will be applied, step-by-step, to determine the damage potential of seismic ground motion. This scheme can be regarded as the continuation of the flowchart shown in Figure 5.3, adopting the results of the *MESSIAS* procedure (identification of subsoil conditions at the building site, selection of representative seismic excitation) and those of the structural analysis (identification of structural capacity).
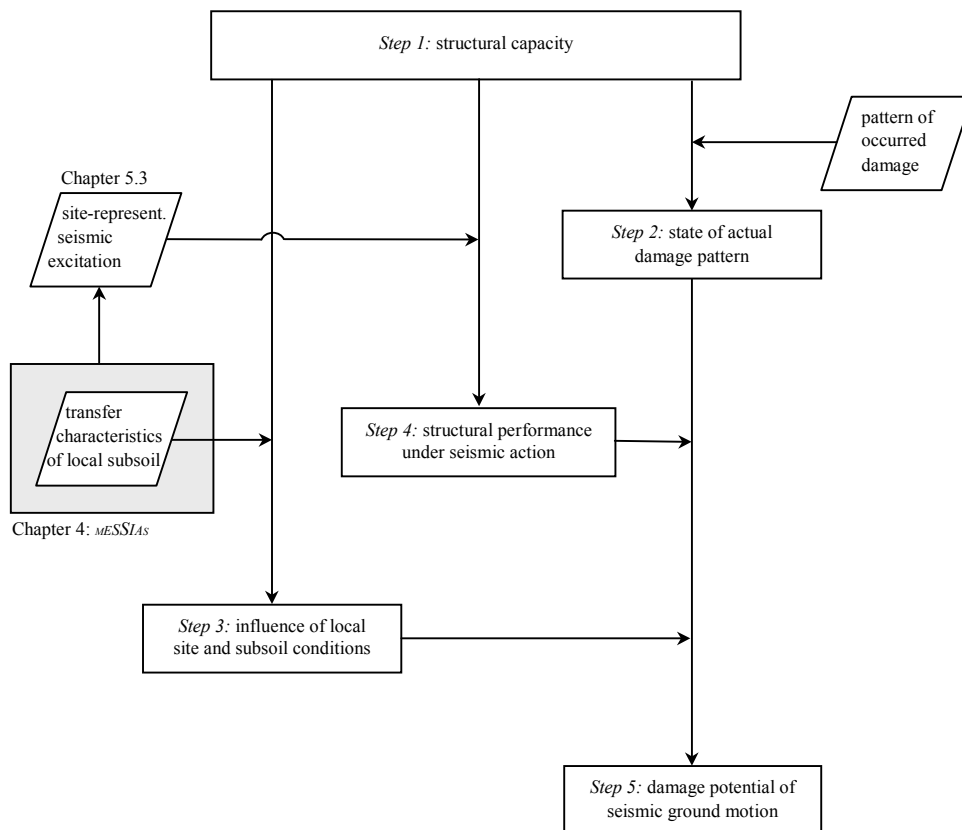

*Figure 5.23 Flowchart indicating the procedure to determine the damage potential
of seismic ground motion.*

Steps of the procedure shown in Figure 5.23 can be structured as follows:

- *Step 1:* The structural capacity for certain levels of material stiffness is worked out in order to account for different levels of structural design or different damage states (Section 5.2.1).
- *Step 2:* The capacity range correlating with the actual building state (Section 5.2.1) is specified, as well as the quantification of actual damage into states of actual damage pattern (*DS*); Section 5.4.
- *Step 3:* Possible influence of local subsoil conditions as identified by the experimental site investigation MESSIAS is surveyed using available information on the site (Chapter 4).
- *Step 4:* The performance point $d_p\,a_p$ (Section 5.2.2) is determined for different types and levels of seismic demand representative for the given site (Section 5.3).

Once all of these steps are processed, the damage potential of seismic ground motion for the specific damage case will be assessed.

5.5.2.1   Step 1: Structural capacity

As it was comprehensively described in Section 5.2.2.1, structural capacity of a modeled building can be obtained by applying the nonlinear static "pushover" analysis. By using the program ETABS Nonlinear, Version 8.11 (Computers and Structures, Inc., CSI), modeling of the structure, performance of the modal analysis and the nonlinear "pushover" analysis can be carried out.

To put it more simply, structural capacity can be seen to reflect a structure's ability to withstand lateral loads. This strongly depends on the stiffness of the building, and this in turn depends on the elasticity of the building materials as expressed by Young's modulus, *E*.

As the lateral force incrementally imposed on the building increases, the structure will begin to yield after exceeding its elastic limits (cf. Figure 5.9). This again causes a stiffness degradation of the structure and consequently a variation of structural capacity.

In order to account for the effects of stiffness degradation during the analysis, three different models, each having a certain range of Young's modulus, *E*, will be investigated (Table 5.26).

Table 5.26 Investigated types of models representing different states of damage
for nonlinear static "pushover" analysis.

Level of Young's modulus, *E*	Comment	State of damage
100%	characteristic values of Young's modulus as supplied in the code provisions	undamaged
40-60%	reduction of Young's modulus as experienced during the calibration of the selected structural models (Table 5.7), accounting for the cracking of concrete elements	slight to moderate
25%	further reduction of Young's modulus considering structural damage progression	extensive (pre-collapse)

5.5.2.2 *Step 2: State of actual damage pattern*

Since each point on the capacity curve directly represents the horizontal displacement of the structure, *δ,* under an increasing lateral load, *V*, it is also a measure of damage extent. Each of the calculated yield points, as given by the program ETABS Nonlinear, is connected to a certain pattern of damage, which indicates the number and locations of yielded elements as well as their state of plastification (Section 5.4).

By comparing those hypothetical patterns of element yielding at the different "pushover" analysis steps on the capacity curve with pattern of real occurred damage, the capacity range of the actual damage or building state can be identified (Figure 5.24). This alone already provides useful information on the following topics:

- the (range of the) structure's maximum lateral displacements reached during the dynamic excitation,
- the expected amplitude level of the seismic event inducing the actual damage state,
- the structure's frequency behavior shifting to longer periods (lower frequencies) in the course of structural yielding (damaging process).
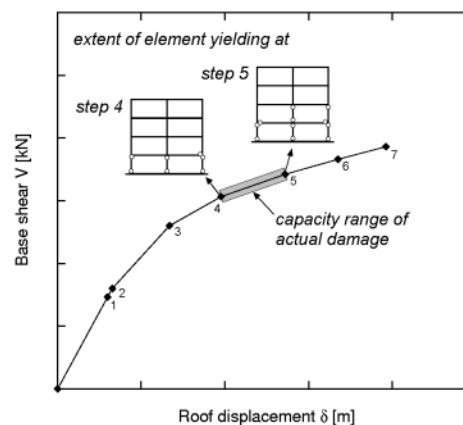
Figure 5.24   Determination of the affected capacity range through comparison between element yielding at the different steps of the "pushover" analysis (step 1-7) and actual damage pattern.

With regard to Section 5.4 the quantification of structural earthquake damage into a classification scheme can be achieved in different ways. However, it should be remembered that the conventional classification schemes, such as damage grades (EMS-98) or states of structural damage (HAZUS®99), can only roughly describe the actual state of damage pattern. This is because their classes cover a broad range of damage extent, thus leading to the unreliability of these conventional concepts used for damage classification to estimate the strength of the damaging earthquake.

Given that locations and pattern of real occurred damage are thoroughly documented, pushover analysis results precisely indicating the locations and level of element yielding at

each analysis step can be applied to identify the capacity range of the building with high accuracy.

In practice, "damage-corresponding" capacity range will be described by two analysis steps. For the determination of these steps, the actual damage pattern must be classified according to the criteria presented in Table 5.24. In this table a more or less precise description of damage effects (structural performance levels *SPL*) ready for practical application is presented. The selection of damage-corresponding analysis steps can be easily performed based on this description.

5.5.2.3 Step 3: Influence of local site and subsoil conditions

As comprehensively discussed in Chapters 2 and 3, local site and subsoil conditions can have a wide influence on earthquake ground motion.
With regard to the selected procedure, however, not all influences coming from the site conditions can be accounted for. It was already addressed that direct seismic site effects cannot be considered in the procedure of structural analysis (Section 5.1.2).
In addition, effects resulting from surface topography or nonlinear soil behavior can only be roughly described if recordings of the damaging event directly at the site of interest are missing. Given that alternative seismic recordings are available, such as the data of weak-motion earthquakes or microtremors, a more or less precise evaluation of these effects can be carried out (Chapter 4, *MESSIAS*).

It can be checked in the SASD domain whether a building's natural frequencies, f_n, fall into ranges of predominant site frequencies, f_s, thus leading to possible interaction (resonance) effects of site and structure.
Figure 5.25 illustrates a transformed capacity spectrum and the possible ranges of predominant site frequencies, f_s. Since the capacity spectrum also reflects the shifting of the structure's fundamental frequency, f_n, during progressive structural yielding, possible interaction effects between site and structure can be identified in the SASD.
In principle, (parts of) the capacity spectrum may intersect different ranges of predominant subsoil frequency, f_s, at the building site, such as:

- area I-a or area I-b: Either the range of natural site frequency f_s is higher than the (elastic) natural building frequency $f_{n,elast}$ (area I-a: $f_{s,I-II} > f_{n,elast}$), or lower than the (inelastic) natural building frequency $f_{n,inelast}$ (area I-b: $f_{s,III-I} < f_{n,inelast}$).
- area II: The (elastic) fundamental frequency of the structure $f_{n,elast}$ agrees with the range of predominant site frequency f_s ($f_{s,I-II} < f_{n,elast} < f_{s,II-III}$).
- area III: Parts of the inelastic section of the capacity spectrum, especially the capacity range of actual damage pattern, are located within the range of natural site frequency f_s ($f_{s,II-III} < f_{n,inelast} < f_{s,III-I}$).
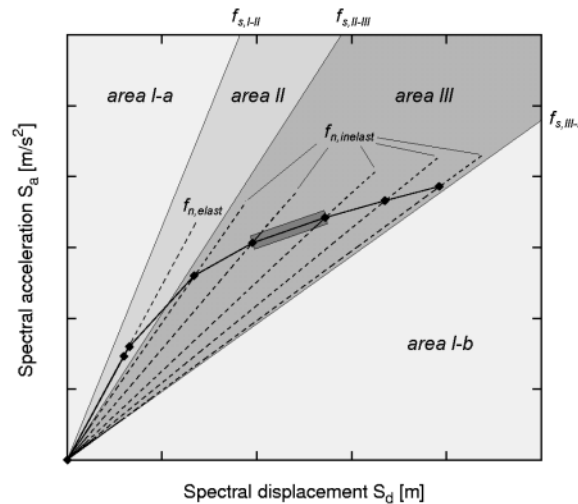
Figure 5.25 Sketch illustrating different areas of predominant site frequencies f_s and their possible influence on structural capacity. (Lines radiating from the origin have constant frequencies, f. The larger the gradient of the curve, the higher the characterized frequency, f.)

In order to evaluate the influence of possible interaction effects between subsoil and structure, the following comments can be made on the different areas of natural site frequencies, f_s:

- area I-a, area I-b: Any interaction effects due to frequency-dependent resonance between site and structure can be excluded.
- area II: High probability that interaction effects between site and structure occur even at low ground motion amplitudes, possibly leading the structure into the inelastic range and thus increasing the amount of structural damage.
- area III: Resonance effects first appear at higher level of ground motion, when progressive structural yielding under lateral loading has already started. Even though resonance effects may increase the amount of structural damage, it surely cannot fully be ascribed to these effects. In contrast, reasons for driving the structure into the inelastic range play the main role in the damage process.

In addition to these investigations, the topographical situation of the building should be regarded, as it can possibly alter (amplify) the ground motion of the damaging mainshock (cf. Section 3.1.3). However, all buildings investigated here were situated on plane terrain, so that topographical effects can be excluded.

5.5.2.4   Step 4: Structural performance under seismic action

Besides the evaluation of the structural vulnerability through comparison with predicted damage levels and possible influence of local site effects, the major part of the procedure consists of identifying structural performance under seismic action. It is a matter of particular interest then whether the actual damage pattern can really be ascribed to hypothetical seismic impact scaled to possible levels of ground motion amplitudes.

For this purpose, the analysis procedure as introduced in Section 5.2.2.2 provides an applicable tool. Through the iterative capacity spectrum method (CSM), the performance of the structure under a given seismic impact is elaborated. While structural performance is represented by its capacity spectrum, seismic impact can either be expressed in time (time-series of earthquake ground motion) or frequency domain (response spectra).

To investigate the impact of different seismic excitation on structural performance, and thus to identify the damage potential of respective seismic ground motion, the following steps must first be carried out:

- identification of structural capacity (step 1; Section 5.2.2.1),
- assortment of the seismic excitation (e.g. recorded time-histories, generated design spectrum) suitable for respective site and subsoil conditions (Section 5.3),
- specification of the seismic demand level likely to occur at the respective site (Section 5.3.4, Table 5.20),
- determination of structural performance for distinct values of seismic demand level (Section 5.2.2.2).

After a comparison of calculated performance points for different levels of seismic ground motion (usually peak ground acceleration, *PGA*) is made with the capacity range of the actual damage pattern (*CRAD*), a first estimation on the damage potential of respective seismic input can be found.

Figure 5.26 illustrates different cases of structural performance in response to an assumed seismic ground motion scaled to different levels of *PGA*. Each of the four schemes indicates different ranges of performance points d_p a_p , i.e. locations of the intersection point between structural capacity spectrum and seismic demand scaled to possible ranges of *PGA*.

Areas shaded light-gray indicate ranges of seismic demand (*ADRS*) bounded by the upper and lower level of expected *PGA*.

Given that the range of actual damage pattern is known, the following comments on cases 1-4 can be made:

- Case 1: *ADRS << CRAD*
  Respective seismic demand can only activate the linear branch of the capacity spectrum, but is not responsible for actual damage (*CRAD*).
- Case 2: *ADRS < CRAD*
  Seismic demand (*ADRS*) can in fact cause structural damage to a certain extent; however, it is not strong enough to induce the actual damage pattern (*CRAD*).
- Case 3: *ADRS ≈ CRAD*
  Scaled seismic demand can assuredly cause the actual damage pattern, since *CRAD* agrees with the range of seismic demand (*ADRS*).
- Case 4: *ADRS > CRAD*
  Expected seismic demand at the building site (*ADRS*) would be able to produce even higher extents of structural damage than the observed pattern reflects.

As already described in Section 5.2.2.2, the calculation of the performance point, especially in the inelastic range of capacity spectrum, is strongly connected to an increase of structural damping due to the hysteretic behavior of the structure. This means that each point on the inelastic branch of the capacity spectrum is combined with a different "equivalent" damping factor, ξ_{eq}, thus reducing the amplitudes of the *ADRS* that represents the seismic demand.

Consequently, values of equivalent damping, ξ_{eq}, that reduces the response spectra of seismic demand should also be regarded when judging the structural performance.
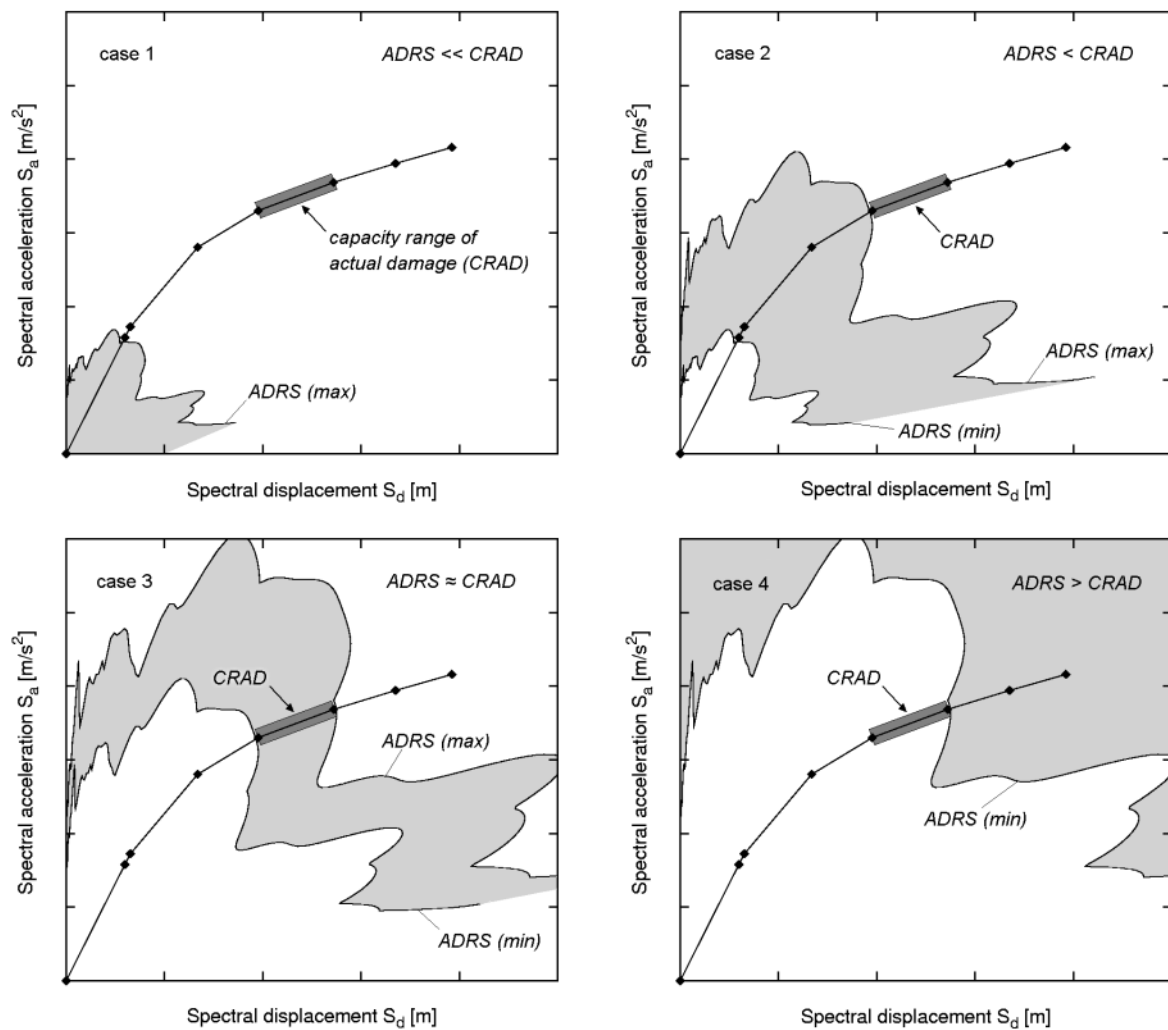

Figure 5.26 Possible combinations of structural capacity, range of actual damage pattern, and seismic demand scaled to distinct levels of peak ground acceleration (represented by light-gray areas bounded by the upper and lower level of expected PGA).

5.5.2.5 *Step 5: Specification of the damage potential*

As represented by the flowchart in Figure 5.23, the specification of the damage potential of seismic ground motion should not be obtained until all of the possible influencing factors are carefully investigated.

The damage potential of seismic ground motion as proposed here using the nonlinear pushover analysis can be determined either if an earthquake struck the relevant building or not. In other words, the possibility of assigning the damage potential of seismic ground motion exists not only for the purpose of damage interpretation, but also in the forefront of future earthquakes (e.g. in the process of structural design, strengthening, or retrofitting). As indicated by Eurocode 8 (CEN, 2002), the nonlinear static "pushover" analysis "may be applied to verify the structural performance of newly designed and of existing buildings for the following purposes:

- to verify or revise the overstrength ratio values,
- to estimate expected plastic mechanisms and the distribution of damage,
- to assess the structural performance of existing or retrofitted buildings (..), (..)."

The concept of damage potential estimation presented here will be proved on the basis of existing damage cases. In doing so, all available information on the site, structure, and expected seismic demand (possibly damaging the structure) will be incorporated.
The processing sequence of available damage cases in Turkish and Venezuelan earthquake regions will be governed by available information on the site and the structure (cf. classification scheme of Section 5.1.3, Figures 5.4 and 5.5).

On the basis of the capacity curves and its identified ranges of actual (building or) damage state (*CRAD*), the procedure provides the opportunity to investigate up to which extent seismic ground motion can cause the extent of occurred damage. The influence of local subsoil conditions and the level of seismic action as well as structural deficiencies are also thereby considered and incorporated.

Given that all of these aspects are examined, the damage potential of seismic ground motion can be identified. This holds for the following:

- the particular structure,
- its position on respective soil conditions,
- under selected seismic excitation scaled to possible amplitude level.

6 Damage potential of seismic ground motion

6.1 Overview of case studies

During performed missions of German TaskForce into disaster areas of Venezuela and Türkiye (cf. Table 1.2) a comprehensive stock of damage cases could be collected. As it was presented in Chapter 5, a selection of those damage cases will be a matter of subject within the present work.

In Figures 5.4 and 5.5 a classification of the selected damage cases was performed according to their available information on the structural layout and the damaging seismic action, referred to as "knowledge level structural properties (*KLS*)" and "knowledge level seismic action (*KLA*)", respectively.

Experimental investigations of the dynamic structural characteristics enabling the generation of a calibrated structural building model were only realized at some of these structures. This also involving a certain difference of the knowledge about the structure.

In a first step of elaboration, the damage potential of seismic ground motion was assessed for those buildings of which instrumental information on the structural behavior could not be obtained.

The itemized damage cases illustrate the necessity of instrumental investigations in order to clearly identify the structures' dynamic behavior and vulnerability. Given that this information is missing, a definite interpretation of structural earthquake damage is hard to assess.

Table 6.1 Evaluation of the causes for structural damage of selected damage cases discussed during previous investigations (LANG & SCHWARZ, 2001).

Case study	Damage case	Proportionate cause for damage	
		Site effects	Structural vulnerability
01	Escuela R. Martinez, Cariaco		
02	Escuela V. Valiente, Cariaco		
03	Edificio Miramar, Cumaná		
07	Yavuzlar Fındık, Gölyaka		
08	Gölcük, inner-city zone		

100%   75%   50%   25%   25%   50%   75%   100%

On the basis of structural layout, either documented on site or by the thorough survey of building plans, and results of instrumental site investigations (e.g. strong-motion and/or microtremor records), a more or less rough evaluation of the damage-provoking factors was performed. Table 6.1 summarizes some of these case studies, being published by LANG & SCHWARZ (2001). Since all of these structures totally collapsed during their respective mainshock, instrumental investigations on them could not be achieved.

Consequently, further studies will only concentrate on those buildings of which the dynamic behavior could be identified on the experimental way.

As stated above, the reliability of investigation results strongly depend on the available information on the site, the seismic excitation, and the structure itself (including the actual damage pattern). This in turn is connected to the defined "knowledge levels" *KLA* and *KLS*, as well as to the "verifying parameter: damage *VPD*" (Section 5.1.3).

Due to missing structural information (e.g. RC detailing), some of the different damage cases (Table 5.4) are not suitable for the entire procedure of damage potential identification. For those damage cases that are at least experimentally investigated (Section 5.2.1.2), a comparison between natural building periods, $T_{n,exp}$, and predominant site periods, T_s, can be performed.

As Table 6.2 and Figure 6.1 illustrate, no clear agreement between the natural building periods, $T_{n,exp}$, and (first) predominant site periods, $T_{s,i}$, can be observed in the different damage cases.

Table 6.2 Comparison of natural building periods, $T_{n,exp}$, and predominant site periods, T_s,
for instrumentally investigated damage cases in Türkiye.

Index	Natural building period, $T_{n,exp}$ [sec]		Predominant site periods, $T_{s,i}$ [sec] (on the basis of *HVNR*, Annex A5-1)			Concurrence [1] between $T_{n,exp}$ and $T_{s,i}$
	H_1-direction	H_2-direction	1st peak	2nd peak	3rd peak	
IZT-1	*0.68*	*0.69*	2.5 - 5.0	1.0 - 1.1	*0.67*	◑ 3rd peak of *HVNR*
IZT-2a	0.85	0.66	3.3 - 4.0	1.0 - 1.25	-	○
IZT-2b	0.50	0.73	3.3 - 4.0	1.0 - 1.25	-	○
IZT-2c	0.21	0.23	3.3 - 4.0	1.0 - 1.25	-	○
DUZ-1	0.26	0.29	1.25 - 1.7	0.67 - 1.0	-	○
DUZ-2	0.47	*0.73*	1.1 - 1.4	*0.6 - 0.7*	-	◑ 2nd peak of *HVNR*
SAC	0.15	0.20	0.9 - 1.25	-	-	○
SEM	0.33	0.40	0.9 - 1.4	-	-	○
SUL	0.89	0.71	0.4 - 0.5	0.2 - 0.25	-	○

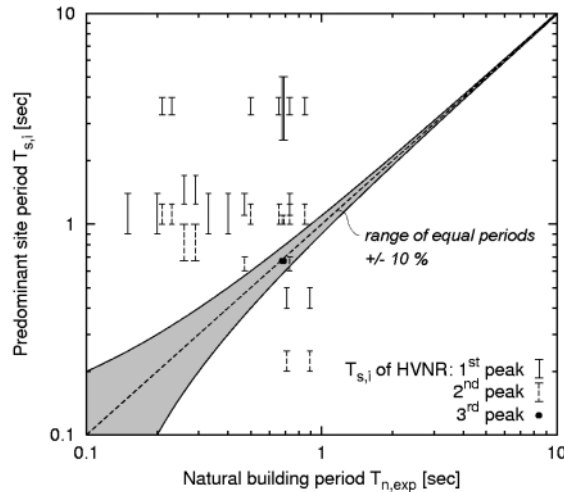[1]   ● high   ◑ with restriction   ○ no

Figure 6.1 Graphic illustration of natural building periods, $T_{n,exp}$, and predominant site periods, $T_{s,i}$, at the instrumentally investigated damage cases. (The dashed line indicates equal periods, $T_{n,exp} = T_{s,i}$. Gray-shaded area represents +/− 10% variation.)

For the buildings discussed here, resonance effects between site and structure may not have contributed to the extent of structural damage.

These buildings represent the prevalent type of residential buildings in Türkiye that suffered the highest rates of structural damage during recent earthquakes. It can be assumed that similar buildings were also located at sites having nearly equal predominant site periods, T_s. As Figure 6.1 shows, natural periods of the buildings, T_n, are shorter than 1 second, whereas the respective predominant site periods, T_s, are mostly longer.

Whether interaction effects between site and structure may lead to an increase of structural damage may be investigated through microzonation studies in affected areas. The urban areas of Adapazarı, Gölcük, or Düzce, for example, were heavily destroyed by the 1999 earthquakes. Within these areas, comprehensive instrumental investigations were carried out by engineering group of German TaskForce in order to identify predominant site periods, T_s, especially at those sites showing damage concentrations to multistoried RC frame structures (Annex 3). The spectral H/V-ratios (*HVNR*) of some of these recording sites are comprised in Figure 4.6.

For a reliable analysis of possible interaction effects between site and structure, however, additional information on the building stock and the occurrence of structural damage has to be available. Since the task of the present work is to identify the damage potential of seismic ground motion of single damage cases, a statistical analysis of possible interaction effects between site and structure will not be given here.

As the flowchart in Figure 5.23 illustrates, the procedure of damage potential identification adopted here regards possible interaction effects between the site and the structure. Damage cases SUL (Sultandağı) and IZT-2a (İzmit-2a) will be subjected below to the entire procedure that considers all possible causes for structural damage. Both damage cases were selected

because their input information (with respect to *KLA*, *KLS*, *VPD*) provides a high level of reliability and completeness. Finally, the modeling of pure RC frame structures without masonry infill walls minimizes failures in the structural analysis.

Specifications on the local site and subsoil conditions, seismic input (e.g. the damaging mainshock), structural properties, and possible occurred structural damage can be taken from the Annexes.

6.2 Case study: Sultandağı (SUL)

Structural layout of the 5-story RC frame can be taken from Annex 5, Table A5-3.1.
With regard to the classification scheme in Figures 5.4 and 5.5, damage case Sultandağı can be classified into a combination of the following:

- KLS-3: signifies a high reliability of the structural model, since high-detailed information on the building's geometry, materials, and reinforcement detailing are available, and
- KLA-2: representing a rough description of the damaging mainshock effects at the building site.

A documentation of the damage locations within the building could also be conducted (presence of the verifying parameter: damage, *VPD*).

6.2.1   Step 1: Structural capacity

For a better understanding of the analysis results, Figure 6.2 schematically illustrates the orientation of both horizontal building axes. It can be seen that clear differences exist between the structural capacity of the two main building axes. Stiffness in *y*-direction is clearly higher than in the *x*-direction, mainly being provoked by the arrangement and orientation of RC columns.
The differences in structural stiffness can be also observed in the experimentally detected natural periods, $T_{n,exp}$, of the building, which are 0.89 sec in $x(H_1)$-, and 0.71 sec in $y(H_2)$-direction (Table 5.5).

Figure 6.2 presents the capacity curves (*V-δ*-domain) determined for distinct values of concrete Young's modulus, *E*. As discussed in Section 5.5.2.1, regarded levels of Young's modulus, *E*, should ideally represent different stages of the building during the damaging process. The "45%-capacity curve" reflects the results of the experimental calibration, thus representing the actual state of the building after sustaining the 2002 Sultandağı mainshock.
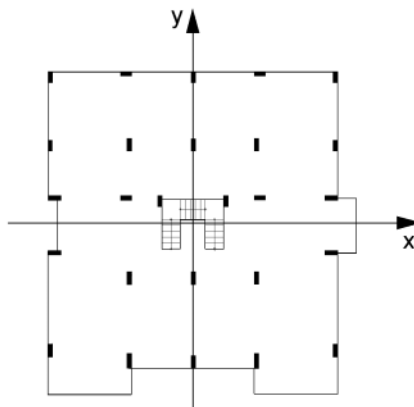

Figure 6.2 Sketch of the building with column arrangement illustrating the model's axis orientation.

The qualitative comparison of capacity curves in both principal building axes indicates quite a different behavior, which is connected with different structural stiffnesses. In the *x*-direction, smaller lateral loads, *V*, cause even larger horizontal displacements than in the *y*-direction, thus correlating to an increase of structural damage.

(a) x-direction   *(b) y-direction*
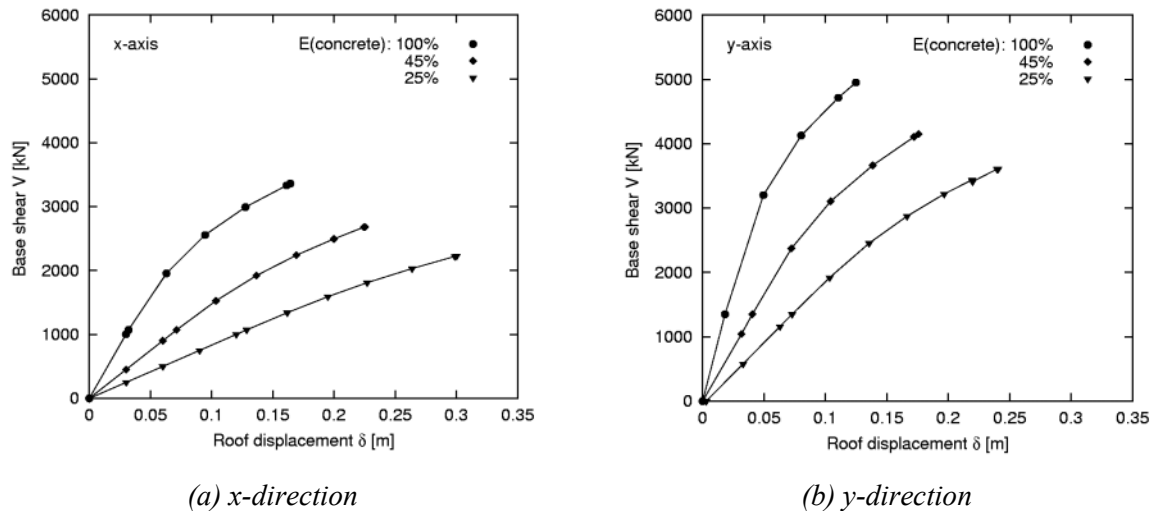
Figure 6.3   Capacity curves for different types of structural models with varying Young's modulus, E, of concrete.

6.2.2   Step 2: State of actual damage pattern

In order to identify the capacity range which corresponds to the actual damage pattern of the building, a detailed documentation of occurred damage has to be available that includes the locations and patterns of damaged elements.

A short description of the damage pattern can be taken from Annex 5, Table A5-3.1.
A descriptive classification of real occurred damage can be made based on these observations:

-   damage grade *DG* 3 (European Macroseismic Scale EMS-98), cf. Table 5.21,
-   structural performance level *"Life Safety" LS* (FEMA 273, ATC-40), cf. Table 5.24.

Table 6.3 marks the actual state of damage pattern on the capacity curve for both horizontal building axes. Corresponding plots indicating the locations of element yielding (as provided by the calculation program ETABS Nonlinear, CSI) are given for the upper and lower bound of the capacity range concerned here.

Thresholds of damage states (*DS*) as provided in the HAZUS®99 documents (FEMA, 1999), are also plotted to the capacity curves of both principal building axes (Figure 6.4). In order to allow the comparison of the results for different buildings, capacity curves are normalized by dividing the base shear, *V*, over the total building weight, *W*, and by dividing the roof displacement, *δ*, over the total building height, h_n.

As described comprehensively in Section 5.4, thresholds of damage states (*DS*) represent tabular values (HAZUS®99) for model building type C1M (mid-rise concrete moment frame) and a "low-code" seismic design level.

Figure 6.4 shows that capacity ranges of the actual damage pattern hold up very well to the thresholds of structural damage states (*DS*). Their respective indicators for RC moment resisting frames are given in Table 5.23.

Table 6.3 Steps of element yielding corresponding to the actual state of damage pattern (CRAD) separated for both horizontal building axes.

	x-direction	y-direction
	Capacity curves of the actual building state (calibrated structural model)	
	Yielding of structural elements corresponding to the actual state of damage pattern (*CRAD*)	
lower bound		
upper bound		

(a) x-direction *(b) y-direction*
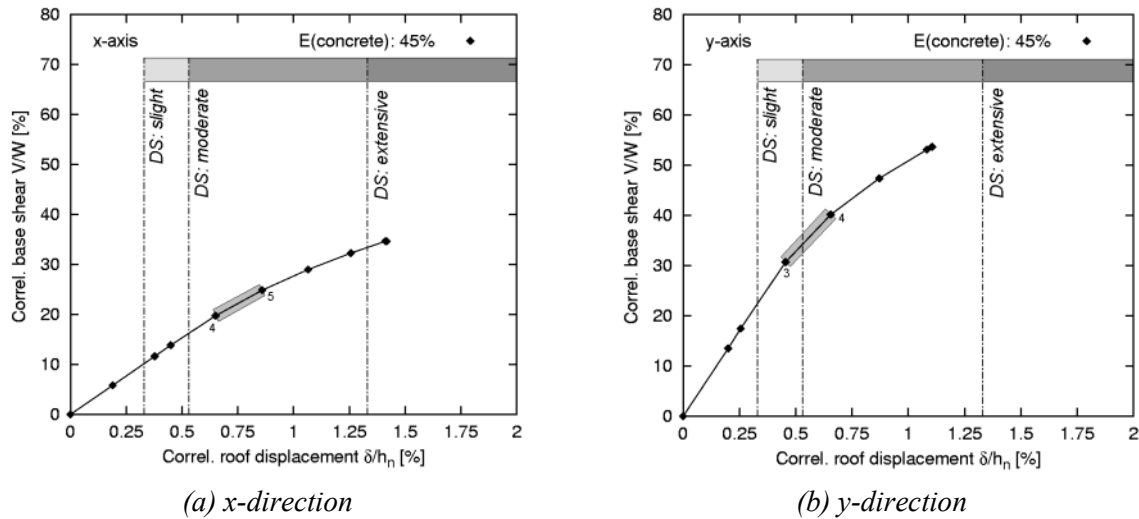
Figure 6.4 Capacity curves with range of actual damage pattern and thresholds of damage states DS (Fema, 1999).

6.2.3   Step 3: Influence of local site and subsoil conditions

To investigate the influence of local subsoil conditions on the linear and nonlinear structural behavior, a frequency- or period-dependent domain must be assumed. The structural capacity curve must therefore be transferred into the S_a-S_d-domain (SASD).

Local subsoil conditions are represented by plotting the ranges of predominant site frequencies, f_s, and their respective predominant site periods, T_s. These can be taken from spectral H/V-ratios on microtremors recorded at the building site (Annex 5, Table A5-1.3). Similarly, H/V-ratios at station SUL show amplified frequency ranges from 2.0-2.5 Hz and 4.0-5.0 Hz. These are plotted in the SASD-domain with structural capacity spectra (Figure 6.5).

It is becoming obvious from Figure 6.5 that none of the capacity spectra intersects the ranges of predominant site frequency, f_s, in any way. Both ranges of predominant site frequencies, f_s, are even higher than the elastic natural building frequencies, $f_{n,elast}$, of all investigated models (compare to Figure 5.25, area I-a).
Consequently, any interaction effects due to frequency-dependent resonance between site and structure can be excluded.

(a) x-direction   *(b) y-direction*
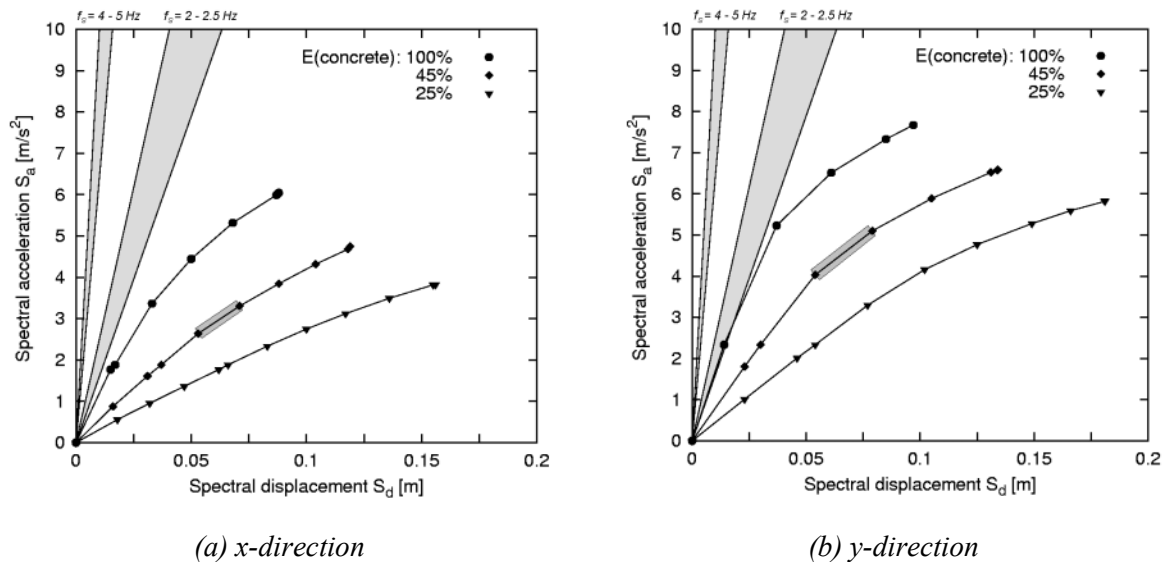
Figure 6.5   Capacity spectra overlaid with ranges of predominant site frequencies, f_s, derived from H/V-ratios on microtremors at station SUL.

6.2.4   Step 4: Structural performance under seismic action

By applying the iterative capacity spectrum method (CSM), structural performance under estimated seismic action can be investigated. Since no records are available for the damaging 2002 Sultandağı mainshock directly at the building site, alternative records have to be selected complying with the subsoil conditions and level of ground motion at the building site.

The only near-field recording station of the 2002 Sultandağı mainshock was located within the city of Afyon. Although this strong-motion station (AFY) was situated in a larger epicentral distance than the Sultandağı structure (Annex 5, Table A5-2.3), their geological conditions fortunately seem to be comparable (Annex 5, Table A5-1.3).

Figure 6.6 shows both horizontal acceleration time-histories of the mainshock recorded at station AFY and their corresponding response spectra ($\xi = 5\%$).

(a)   *(b)*   *(c)*
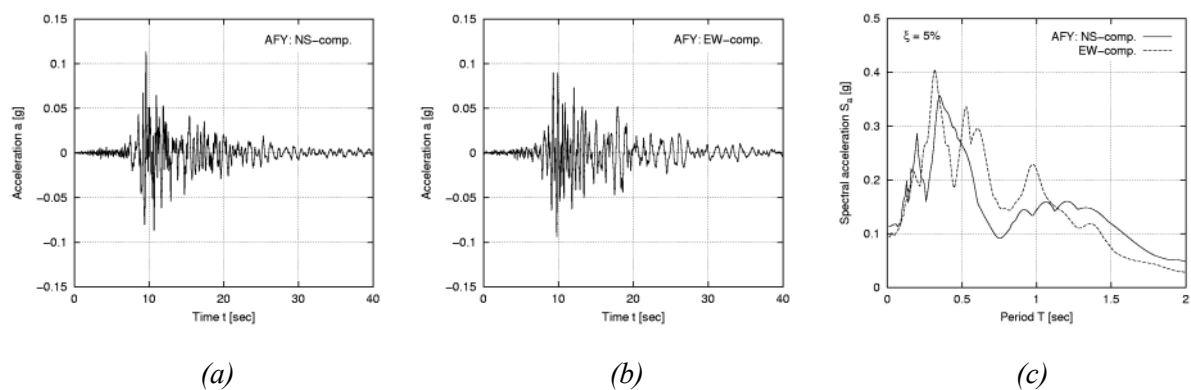
Figure 6.6   Ground motion records of the 2002 Sultandağı earthquake at station Afyon (AFY): (a) and (b) horizontal time-histories, (c) response spectra ($\xi = 5\%$).

As seen in Section 5.3, different ways of deriving the level of seismic demand, and more precisely the level of peak ground acceleration (*PGA*), were checked. Results are summarized in Table 5.20, indicating a possible range of *PGA* at the building site SUL during the Sultandağı mainshock between 18 and 40% g.

Figure 6.7 presents the results of the capacity spectrum method for both principal building axes and both horizontal components of the AFY-record, scaled to values of *PGA* between 18 and 40% g. Gray-shaded areas represent the lower (18% g) and upper bound (in fact 40% g) of scaled seismic demand. One of the main prerequisites for the capacity spectrum method is having an intersection point between the capacity spectrum and the response spectrum. Seismic demands with higher *PGA* in particular fail sometimes to fulfill this without being attenuated by unrealistic high damping values, *ξ*.

(a) x-direction   (b) y-direction
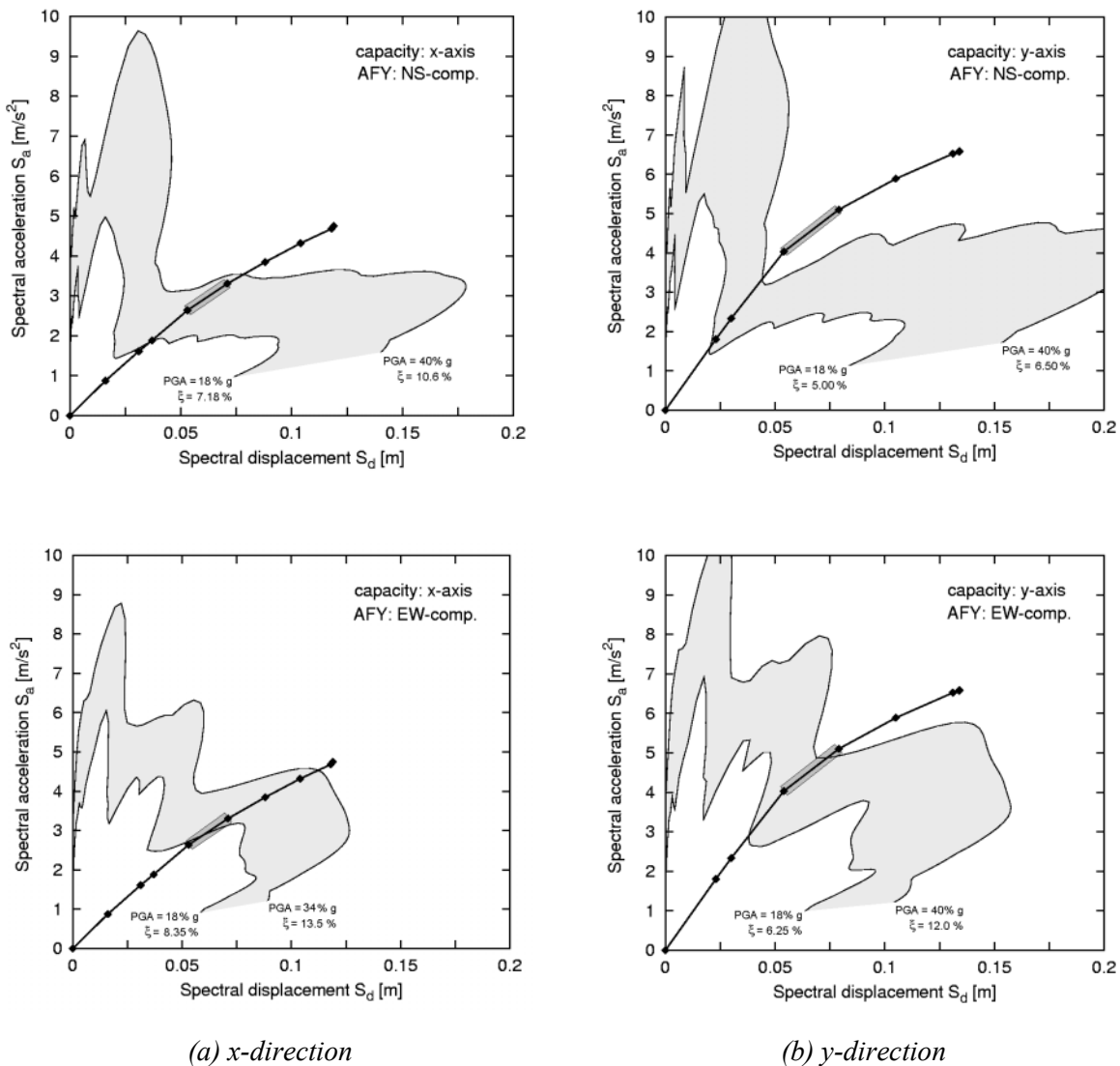
Figure 6.7 Structural performance in both principal building axes for selected seismic demand scaled to a certain range of PGA.

With regard to the evaluation scheme in Section 5.5.2.4, Table 6.4 summarizes the results for each capacity-demand combination given in Figure 6.7. It can be seen that seismic demand (*ADRS*) agrees with the capacity range of actual damage (*CRAD*), except for its performance in *y*-direction and the *NS*-component of the seismic demand.

Table 6.4 Capacity-demand combinations for scaled mainshock record at station AFY and damage case Sultandağı (SUL).

| Capacity	Demand	Lower bound		Upper bound		Case
		PGA [%g]	ξ [%]	*PGA* [%g]	ξ [%]	(Section 5.2.2.4)
x-axis	*NS*-comp.	18	7.18	40	10.6	Case 3: *ADRS* ≈ *CRAD*
	EW-comp.	18	8.36	34	13.5	Case 3: *ADRS* ≈ *CRAD*
y-axis	*NS*-comp.	18	5.00	40	6.50	Case 2: *ADRS* < *CRAD*
	EW-comp.	18	6.25	40	12.0	Case 3: *ADRS* ≈ *CRAD*

6.2.5   Step 5: Specification of the damage potential

To reiterate, damage potential of seismic ground motion should be specified according to all available information on the site, the structure, and the damaging seismic excitation.
The following aspects can be summarized from the results of the analysis steps 1-4:

Step 1:
- structural capacity is quite different for both principal building axes, being produced by prominent structural deficits, for example by arrangement and orientation of columns, and non-compliance of a regular beam grid (Annex 5, Table A5-3.1);
- capacity curves indicate a higher vulnerability to lateral loads in the *x*-direction, since smaller lateral loads induce larger deformations in this direction.

Step 2:
- the observed damage pattern is consistent with the results released by the analysis program (*CRAD*), endorsing the compliance of the structural model and its assumptions (Table 6.3);
- the comparison between the *CRAD* and structural damage states (*DS*, HAZUS®99) for low-code seismic design level displays a high agreement in the damage indicators (Figure 6.4).

Step 3:
- since capacity spectra for both principal building axes (and thus their elastic and inelastic natural building frequencies, $f_{n,elast}$ resp. $f_{n,inelast}$), do not intersect the ranges of predominant site frequencies, f_s, a direct interaction effect due to frequency-dependent resonance between site and structure can be precluded (Figure 6.5),

- on the basis of the experimental site classification (*MESSIAs*, Chapter 4) stiff soils with a total layer thickness of several tens of meters are expected at the building site (Annex 5, Table A5-1.3); consequently, even the occurrence of nonlinear soil behavior during strong ground shaking can be excluded;
- topographical effects leading to remarkable ground motion amplifications can also be excluded, since the topographic slope at the building site is too small.

Step 4:
- the spectral characteristics of the selected seismic excitation (record of the 2002 Sultandağı earthquake at station AFY) show a high compatibility with the SUL site;
- observations of the vicinity around the Sultandağı structure directly after the mainshock revealed a local intensity I_{EMS} = VII, which agrees with the intensity assignment as given in ERDIK *et al.*, 2000 (Table 5.16; Annex A5-2.3);
- the possible range of peak ground acceleration, *PGA* = 18-40% g, complies to different ways of deriving the level of seismic excitation (Section 5.3);
- the application of the capacity spectrum method (CSM) to the mainshock record at station Afyon (AFY) scaled to determined levels of *PGA* (see Figure 6.7) demonstrates:
  - the ability of both horizontal components (*NS, EW*) to generate the actual state of structural damage in the "more vulnerable" *x*-direction (*ADRS* $\approx$ *CRAD*);
  - the ability of the *EW*-component to induce the actual state of damage pattern in the stronger *y*-direction (*ADRS* $\approx$ *CRAD*);
  - the incapacity of the *NS*-component to cause the actual state of damage pattern in the *y*-direction (*ADRS* < *CRAD*); even seismic demand scaled to the lower level of *PGA* = 18%g cannot drive the structure into the inelastic range (ξ = 5%);

To assess the damage potential of seismic ground motion for the damage case Sultandağı (SUL), the state of actual structural damage can surely be ascribed to the structural vulnerability, especially in the building's *x*-direction. This being mainly affected by poor quality of workmanship and materials, as well as by the structural deficiencies mentioned above.
On the basis of derived results, the influence of local site effects can be completely excluded.

Referring to the flowchart of the observation-based procedure that performs a rough estimation of the reasons for structural earthquake damage (cf. Figure 5.1), structural vulnerability should also be regarded as the main damaging factor in the damage case Sultandağı (SUL).

6.3 Case study: İzmit-2a (IZT-2a)

Structural layout of the 5-story RC frame can be taken from Annex 5, Table A5-3.3.
With regard to the classification scheme in Figures 5.4 and 5.5, damage case İzmit-2a can be classified into a combination of the following

- KLS-3: signifies a high reliability of the structural model, since high-detailed information is available on the building's geometry, materials, and reinforcement detailing, and
- KLA-1: shows no information on the damaging mainshock at the building site.

Locations of structural damages within the building could also be documented, leading to the presence of the "verifying parameter: damage, *VPD*".

6.3.1   Step 1: Structural capacity

It can be seen from the building's sketch in Figure 6.8 that stiffness in the *x*-direction is somewhat higher than in the *y*-direction. This is caused mainly by the orientation of RC columns. The experimentally identified natural periods of the building, $T_{n,exp}$, amount to 0.85 sec in $x(H_1)$-, and 0.66 sec in $y(H_2)$-direction (Table 5.5).
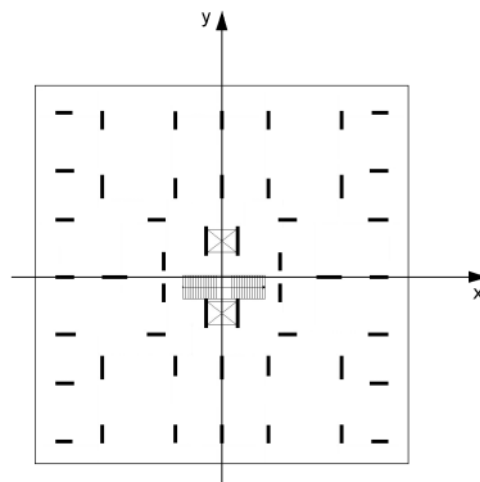
Figure 6.8 Sketch of the building with column arrangement illustrating the model's axis orientation.

Capacity curves (*V-δ*-domain) for distinct values of concrete Young's modulus, *E*, are given in Figure 6.9. Analysis results for the "40% *E*-model", as worked out above, comply with experimental results.
Although natural building periods, T_n, are different for both principal building axes, their capacity curves show comparable characteristics.

(a) x-direction   *(b) y-direction*
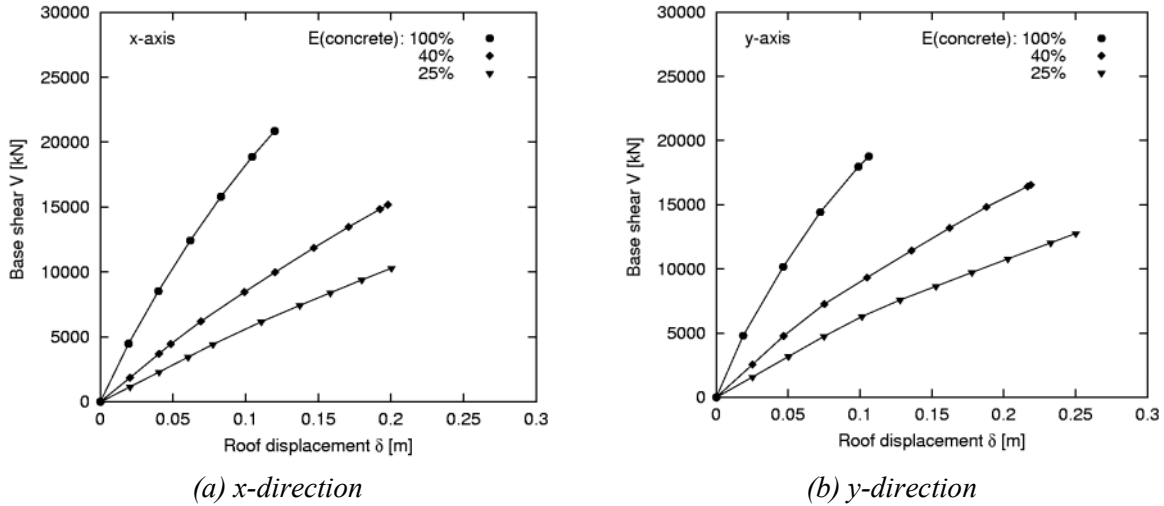
Figure 6.9 Capacity curves for different types of structural models with varying Young's modulus, E, of concrete.

6.3.2   Step 2: State of actual damage pattern

On the basis of in-situ observations, real occurred damage can be classified into the following:

- damage grade *DG* 3 (European Macroseismic Scale EMS-98), cf. Table 5.21,
- structural performance level *"Life Safety" LS* (FEMA 273, ATC-40), cf. Table 5.24.

Following the procedure of the previous section, Table 6.5 marks the actual state of damage pattern on the capacity curve for both horizontal building axes and gives the corresponding plots indicating the locations of element yielding.

(a) x-direction   *(b) y-direction*
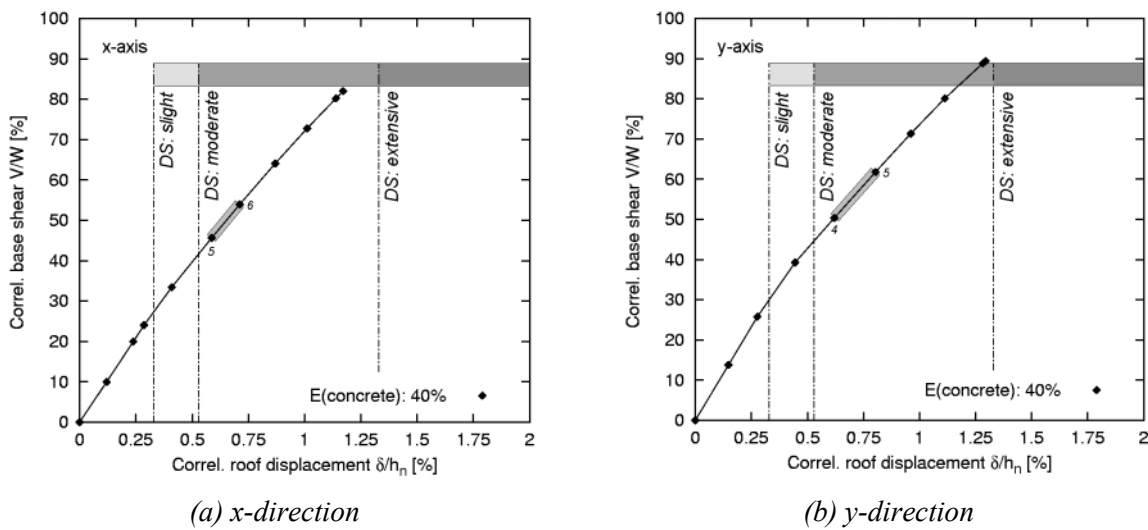
Figure 6.10 Capacity curves with range of actual damage pattern and thresholds of damage states DS (HAZUS®99).

Table 6.5 Steps of element yielding corresponding to the actual state of damage pattern separated for both horizontal building axes.

	x-direction	y-direction
	Capacity curves of the actual building state (calibrated structural model)	
	Yielding of structural elements corresponding to the actual state of damage pattern (*DG*)	
lower bound		
upper bound		

The capacity range of actual damage (*CRAD*) can be allocated to structural damage state "moderate" (HAZUS®99; cf. Figure 6.10). According to the information from structural plans, thresholds of damage states are calculated for "low-code" seismic design level (model building type C1M).

An exemplarily check if observed damage pattern really can be described by the calculated locations of element yielding is given in Figure 6.11. It can be seen, that the spalling of concrete at the columns' base agrees with the calculated level of element yielding as a result of the pushover analysis using the program ETABS Nonlinear (CSI).
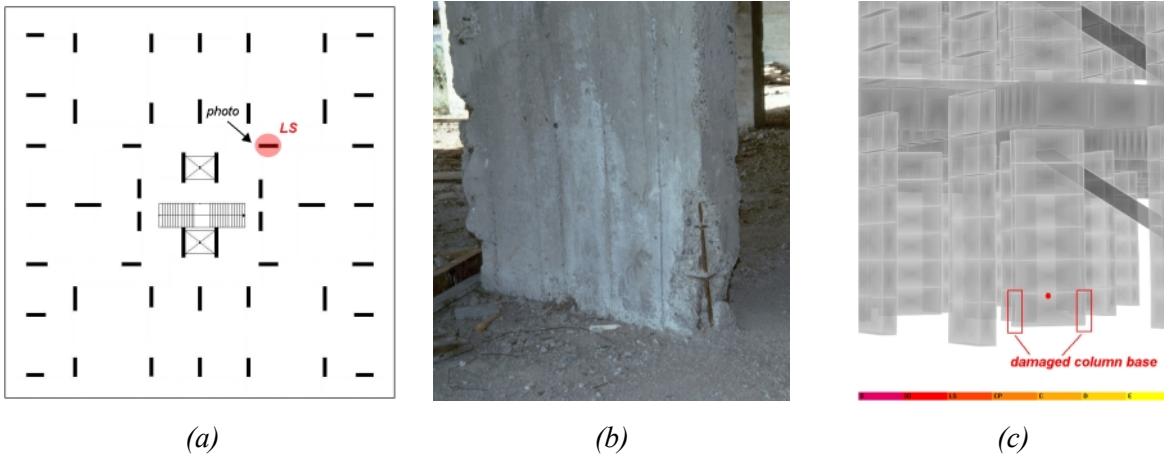
Figure 6.11 Exemplary comparison between actual damage pattern and calculated element yielding, (a) column plan of ground floor indicating the location of the damaged column shown in (b), (c) detail of the affected column with calculation results of the pushover analysis (x-axis, step 6).

6.3.3 Step 3: Influence of local subsoil conditions

Capacity spectra (S_a-S_d-domain) are overlaid with ranges of predominant site amplification (Annex 5, Table A5-1.2, station IZT-2) in Figure 6.12.

It is evident that no intersection between capacity spectra and ranges of site frequency, f_s, occurs. Even capacity spectra for the "25% *E*-model" representing a stronger damage state, do not fall into the identified ranges.

Consequently, local site effects possibly contributing to the damaging process can be excluded.

(a) x-direction   *(b) y-direction*
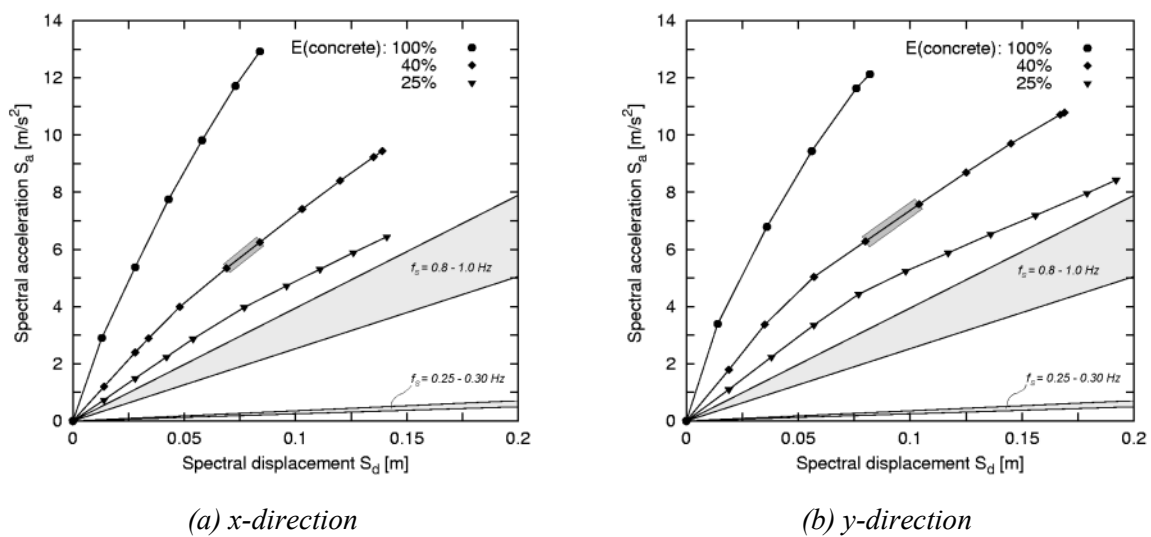
Figure 6.12 Capacity spectra overlaid with ranges of predominant site frequencies, f_s, derived from H/V-ratios on microtremors at station IZT-2.

6.3.4 Step 4: Structural performance under seismic action

Since no recording stations of the mainshock are situated in the surroundings of damage case IZT-2a, an alternative record has to be selected. The closest recording station of the 1999 İzmit mainshock was situated at the northern coastline of İzmit Bay (Yarimca YPT), at a distance of about 25 km to damage case IZT-2a (Annex 5, Table A5-1.2).

Available information on the subsoil at station YPT indicates comparable conditions than those at IZT-2a. Figure 6.13 shows both horizontal acceleration time-histories of the mainshock record at station YPT as well as their corresponding response spectra ($\xi = 5\%$). Peak ground accelerations reached 29% and 24% g, for the *NS*- and *EW*-component, respectively.

Regarding available intensity shaking maps (Annex 5, Table A5-2.2) and empirical data of *PGA*, the range of *PGA* possibly occurring at the building site is between 24% and 65% g (cf. Table 5.20). Figure 6.14 presents the results of the capacity spectrum method using the YPT-records scaled to these ranges of *PGA*.
Table 6.6 summarizes the results for each capacity-demand combination given in Figure 6.14.

(a)   *(b)*   *(c)*
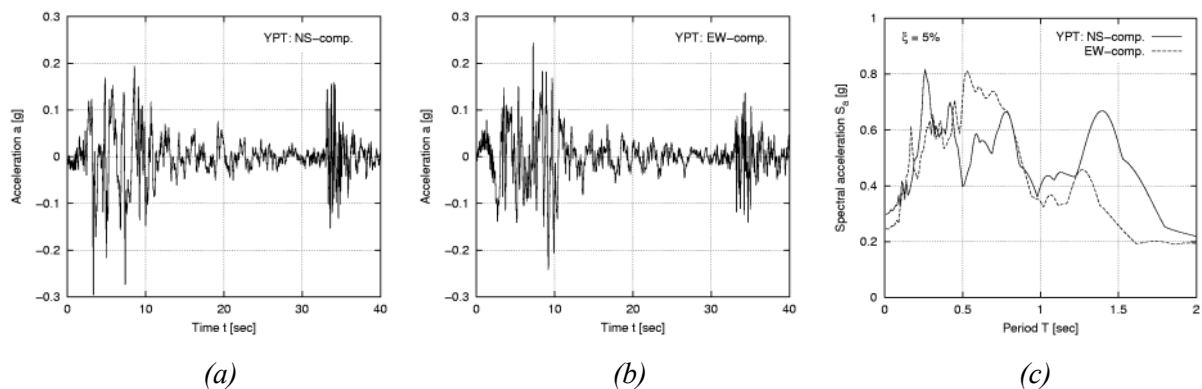
Figure 6.13 Ground motion records of the 1999 İzmit earthquake at station Yarimca (YPT): (a) and (b) horizontal time-histories, (c) response spectra ($\xi = 5\%$).

Table 6.6 Capacity-demand combinations for scaled mainshock record at station YPT and damage case İzmit-2a (IZT-2a).

Capacity	Demand	Lower bound		Upper bound		Case
		PGA [%g]	ξ [%]	*PGA* [%g]	ξ [%]	(Section 5.2.2.4)
x-axis	*NS*-comp.	29	7.76	54	10.38	Case 3: *ADRS* $\approx$ *CRAD*
	EW-comp.	24	9.07	44	10.39	Case 3: *ADRS* $\approx$ *CRAD*
y-axis	*NS*-comp.	29	7.72	54	13.45	(Case 3: *ADRS* $\approx$ *CRAD*)
	EW-comp.	24	9.95	54	13.79	Case 3: *ADRS* $\approx$ *CRAD*

(a) x-direction   (b) y-direction
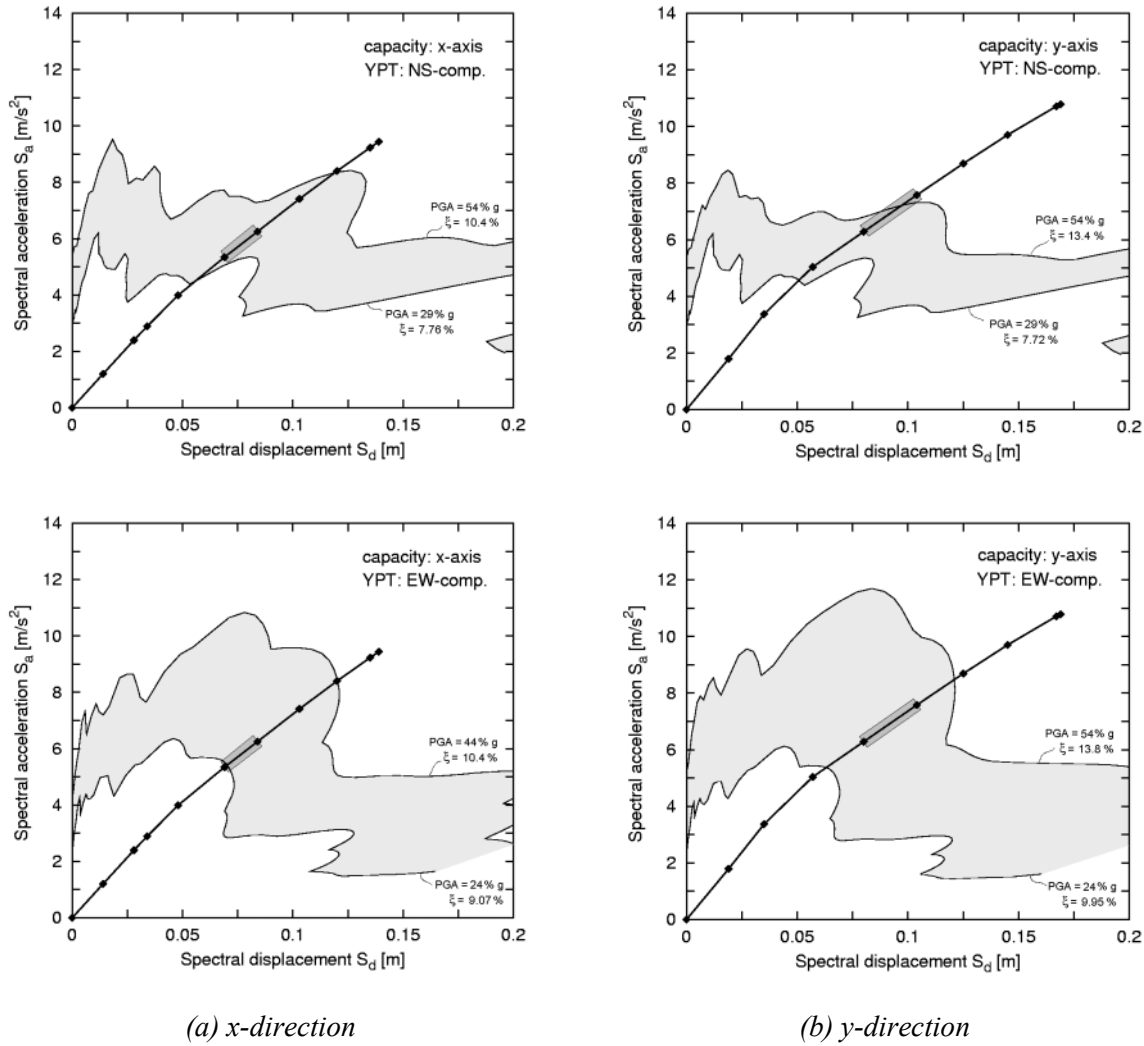
Figure 6.14   Structural performance in both principal building axes for selected seismic demand scaled to a certain range of PGA.

6.3.5   Step 5: Specification of the damage potential

For each analysis step, worked out above, the following can be stated:

Step 1:
- structural capacity can be compared for both principal building axes; due to the orientation and arrangement of columns (Annex 5, Table A5-3.3);
- capacity curves indicate a higher deformability to lateral loads in the *y*-direction.

Step 2:
- the observed damage pattern is consistent with the results released by the analysis program (*CRAD*), endorsing the compliance of the structural model and its assumptions (Table 6.5);
- the comparison between the *CRAD* and structural damage states (*DS*, HAZUS®99) for low-code seismic design level displays a high agreement in the damage indicators (Figure 6.10).

Step 3:

- no intersection between the ranges of predominant site frequencies, f_s, and the capacity spectra can be observed, thus any direct interaction effect due to frequency-dependent resonance between site and structure can be precluded (Figure 6.12),
- on the basis of the experimental site classification (*MESSIAS*, Chapter 4) soft soils with a total layer thickness of about 200 m are expected at the building site (Annex 5, Table A5-1.2);
- due to the plane terrain of the site, topographical effects leading to remarkable ground motion amplifications can be excluded.

Step 4:

- the applicability of the YPT-record is high in respect to the epicentral distance, the general geological conditions of both sites, recording station YPT, and site of damage case IZT-2a;
- assigned intensities for the building site vary between I = VIII - X (Table 5.15; Annex A5-2.2); with respect to own observations at the surroundings of the damage case, a representative intensity I_{EMS} = VIII was determined for further analysis (Table 5.15);
- the possible ranges of peak ground acceleration, PGA = 29-65% g, resp. 24-65% g, complies to different ways of deriving the level of seismic excitation (Section 5.3);
- applying the capacity spectrum method (CSM) to the mainshock record at station Yarimca (YPT), which is scaled to specific levels of PGA (cf. Figure 6.14), demonstrates the following:
  - both horizontal components (*NS, EW*) can generate the actual state of structural damage in both principal building axes (*ADRS* $\approx$ *CRAD*), irrespective of connected damping values, ξ;
  - damping values, ξ, for the upper bound of seismic demand can be seen to exceed the range of plausibility, especially for the building's *y*-direction; this means that respective seismic demand should not be used for further statements concerning the damage potential of seismic ground motion;

In case of the İzmit-2a structure, occurred structural damage can be attributed to the assumed level of seismic excitation, and surely to the structural vulnerability. Since damage case IZT-2a was not yet furnished with infill masonry walls, it should have sustained the effects of the 1999 İzmit mainshock without any damages.

The assumed high level of peak ground acceleration, *PGA*, within the concerned area, however, could not be absorbed by the structure without any damages to the primary structural elements.

Based on results of the site investigations and the fact, that deep layers of sediments tend to attenuate ground motion amplitudes, the influence of local site effects can be excluded.

7 Summary and conclusions

The present work can be regarded as an attempt to approach the scientific fields of engineering seismology and structural engineering. The work's arguments and conclusions rest upon data collected during comprehensive field investigations of the German TaskForce group into Venezuelan and Turkish earthquake regions (Table 1.2).

The available data can roughly be subdivided into a sizeable database of seismic recordings such as mainshocks, aftershocks, or microtremors (Table 2.5, Table 2.6) and a variety of documented multistoried RC frame structures. Some of them have been heavily damaged or destroyed during recent earthquakes in Venezuela and Türkiye (Table 5.1).

In order to identify probable reasons for structural earthquake damage to "engineered", multistoried RC frame buildings, a procedure was developed that incorporates possible influences coming from the site, the seismic excitation, and the structure itself.
For this purpose, detailed knowledge of the following is required:

- the site and subsoil conditions,
- the (damaging) seismic excitation, and
- the structural capacity.

The flowchart given in Figure 5.23 depicts these subjects as the starting points from which to derive the *damage potential of seismic ground motion*. The single steps in which these subjects explain this term and way they interact with each other are illustrated by Figure 5.3.
Experimental investigations play a major role in this work. An important section is devoted to instrumental site response estimation techniques in order to derive parameters useful for engineering purposes. As numerous investigations of other scientific groups revealed, problems appear when trying to implicate instrumental site investigations and structural damage (Section 1.2). As Table 1.1 summarizes, results of site response estimation techniques in most cases are applied only to identify the local site conditions. A correlation between the results of site studies and structural damage data is usually missing.

Contrary to most papers so far published on this topic, results of instrumental investigations of both the site and the structure establish the main basis for the procedure of damage potential identification.

As the procedure's flowchart illustrates (Figure 5.3), instrumental investigations of the site are used for three main tasks:

-   the identification of the transfer characteristics of local subsoil,
-   the assignment of a site class according to a generally accepted code provision scheme (here: DIN 4149, 2002),
-   the selection of the seismic excitation suitable for the given site and subsoil conditions.

These represent the main output from the *Method of an Experimental Seismic Site Assessment*, MESSIAS (LANG *et al.*, 2003a; Section 4.3).

Instrumental investigations were also carried out at selected multistoried RC structures (representing the typical building type in the regarded regions) in order to identify their dynamic characteristics, and thus to calibrate the building models for further structural analyses.

By applying the nonlinear static "pushover" analysis to the calibrated structural models and the capacity spectrum method (CSM), the structural performance under seismic action is assessed.

Consequently, damage potential of seismic ground motion is identified by evaluating the following:

-   the state of actual damage,
-   the structural performance under seismic action, and
-   the influence of local site and subsoil conditions.

The following conclusions can be summarized about the single steps of the work finally contributing to the identification of the damage potential of seismic ground motion:

-   According to the work of numerous research groups, the influence of local site effects causing strong amplifications of the seismic waves can be regarded as the main reason for structural damage.
-   In contrast to this keen assumption, whose task is probably to divert from structural deficiencies, an interpretation of structural earthquake damage should not be carried out neglecting the structural characteristics entirely. Since structural earthquake damage is the final result of the (dynamic) interaction between soil and structure, the vibrational characteristics of the structure must urgently be investigated (MOORE, 1979).
-   Structural earthquake damage in general can be ascribed to effects coming from the seismic excitation, the site and subsoil conditions, and from the structure. Consequently, all of these factors have to be thoroughly investigated in order to identify the damage potential of seismic ground motion.
-   Given that no precise information on the (damaging) seismic event or the local subsoil conditions are available, instrumental site investigations sometimes provide the only alternative to obtain further information, and thus to allow a reliable damage analysis.

- In most cases recordings of strong (damaging) earthquakes at the site of interest are not available. If so, other types of seismic signals, such as ambient seismic noise (microtremors) or records of smaller earthquakes, can be applied to describe the seismic ground motion characteristics at the recording site.

- Although each of these "alternative" types of ground motion data shows pronounced differences to strong-motion earthquake data in respect to amplitude and frequency characteristics, they do provide some advantages regarding its applicability for identifying the site amplification.

- Through the application of a number of currently available site response estimation techniques on different types of instrumental ground motion data, it can be shown that they can derive parameters useful for engineering purposes.

- With regard to the identification of the predominant site frequency, f_s, the level of site amplification, and the "quasi" transfer function of the site, TF_{quasi}, spectral H/V-ratio method on ambient seismic noise data (HVNR) yields the most reliable and stable results.

- Comparisons between the results of instrumental methods (e.g. HVNR) with those of theoretical techniques based on available subsoil information demonstrate their reliability.

- To derive parameters suitable for structural design (design spectrum), the elaboration only of normalized response spectra, S_a/a, on earthquake data should be performed. No direct correlations to the results of spectral ratio methods exist.

- A practical application of site response estimation techniques exists in site classification schemes. As conventional schemes for site categorization can only be applied if soil material parameters are present, a hybrid procedure of site classification was developed primarily based on spectral H/V-ratios on microtremors recorded at the ground surface. The classification of the subsoil conditions into site classes (*SC*) following the German earthquake code provision DIN 4149 (DIN, 2002) can be achieved according to their shape.

- Based on the instrumental investigation of several sites for which detailed information on the subsoil conditions is available, reliability of the *Method of an Experimental Seismic Site Assessment, MESSIAS* (LANG *et al.*, 2003a), is evident (Annex 4).

- In contrast to conventional site classification schemes usually restricted to the uppermost 30 m of soil layers (e.g. AMBRASEYS *et al.*, 1996; HOSSER & KLEIN, 1983; ICBO, 1997), the classification scheme used here accounts for both stiffness and total depth of sedimentary layers overlying the geological basement. This allows a more realistic evaluation of the local subsoil conditions.

- Consequently, the elaborated site classification procedure (*MESSIAS*) helps to provide reliable seismic loads for engineering analysis. These are suitable for the given site and subsoil conditions, even when detailed subsoil information is missing.

- The presented procedure of damage potential assessment is related to multistoried RC frame buildings, which seem to be representative for their respective earthquake regions.

By conducting instrumental investigations at some of these buildings, the dynamic characteristics, such as the natural building frequencies, $f_{n,exp}$, or structural damping factors, ξ, can clearly be determined.

- By the variation of material stiffness (Young's modulus, E) a calibration of the structural model on the experimental results is performed. As the analyses show, reduction factors of Young's modulus of concrete elements strongly depend on the structure's state of damage. While no stiffness reduction has to be regarded at undamaged buildings (e.g. IZT-2c, SAC), reduction factors of 40 to 60 % must be applied in order to adjust the models of structures suffering slight to moderate structural damage. Findings agree with the provisions of the present draft of Eurocode 8 (CEN, 2003).

- Structural performance of the calibrated models is appointed by comparing structural capacity (pushover analysis) with seismic demand representative in frequency content and amplitude level for the given site. Since each point on the capacity curve is connected to a certain degree of element yielding, the capacity range correlating with the actual damage pattern can be accurately determined.

- Plotting structural capacity in the S_a-S_d-domain allows a direct examination of whether the expected seismic demand can provoke the actual state of damage pattern, or whether interaction effects between the site and the structure can occur.

- Investigation results of all damage cases observed in this paper showed that local site effects (those that lead to resonance phenomena between the site and the structure and thus represent the main reason for structural damage) can be entirely excluded.

- As the detailed analyses of two RC frame structures (SUL, IZT-2a) demonstrated, the reason for structural damage can be regarded as a result of structural vulnerability, and, to some extent, the level of seismic input.

- With regard to aforementioned definitions, the established damage potential of seismic ground motion is explicitly related to the seismic excitation assumed to inflict structural damage to a certain building (type) located on a specific subsoil.

Prospects on further investigations

The procedure for damage potential identification in this work was applied to selected RC frame structures without masonry infill walls. Acceleration data of the respective damage-causing mainshocks was taken from adjacent recording stations.

Further application of this procedure is intended using the available assemblage of preprocessed input data, which consists of seismic ground motion data (Annex 3) and structural information on multistoried RC frame buildings (Annex 5-3). This may include some or all of the following:

- the structural analysis of RC frame buildings with masonry infill walls, which would require a realistic failure model of the (nonstructural) wall elements and their interaction with structural RC frame elements,
- the calibration of the structural models according to the locations and grade of actual damage, this comprising the reduction of material stiffness only to those reinforced-concrete elements that sustained damage,
- the provision of different types of seismic demand, such as code design spectra (see Section 5.3.3) or (spectrum-compatible) synthetically generated accelerograms, whether suitable seismic recordings are not available.

Beyond this, investigation results of the types of buildings discussed here and located on different site and subsoil conditions may be applied to future studies on damage prediction or loss scenarios. This implies making recommendations for future code development and engineering design practice (strengthening, retrofitting measures), as well as for land use management and urban planning.

Weimar, February 2004

D.H. Lang

Symbols and abbreviations

a	acceleration
a_g	effective acceleration, peak ground acceleration
a_H	horizontal acceleration
A	area
A_0	effective acceleration
A_d	design spectral acceleration
A_g	amplification factor of the ground (NAKAMURA, 2000)
$A(T)$	spectral acceleration coefficient
b_1, b_2, b_3, b_A, b_S	regression coefficients
C_1, C_2, C_4	regression coefficients
d	source distance
$d_p a_p$	performance point
$d_y a_y$	inflexion point
D	fault distance, damage index (PARK & ANG, 1985)
D_r	damage potential indicator (MOORE, 1979)
DG	damage grade according to the EMS-98
DS	structural damage states according to HAZUS®99
E	modulus of elasticity (Young's modulus)
E_{dyn}	dynamic modulus of elasticity (dynamic Young's modulus)
f	cyclic frequency
f_g	predominant frequency of earthquake ground motion
f_s	natural/predominant site frequency
f_n	natural frequency of the structure, first mode frequency
$f_{n,elast}$	elastic natural frequency of the structure, first mode frequency
$f_{n,inelast}$	inelastic natural frequency of the structure
$f_{n,exp}$	experimental identified natural frequency of the structure
$F(\omega)$	transfer function of soil profile
F_r	damage potential indicator (MOORE, 1979)
$F_y(g)$	strength capacity curves
$F_y(()$	strength demand spectra
g	acceleration of gravity (9.81 m/s²)
G	shear modulus
G_{dyn}	dynamic shear modulus
$G(\gamma)$	strain-dependent shear modulus
G_{max}	shear modulus for smallest shear strains
H_1, H_2	horizontal building axes, horizontal component of ground motion

h_i	thickness of soil layer i
h_0	focal depth
h_n	total building height
H	thickness of soil layer (total sediment thickness)
i	integer
I	local shaking intensity, building importance factor
I_{mm}	Modified Mercalli Intensity
I_{MMI}	Modified Mercalli Intensity
I_{MSK}	Medvedev-Sponheuer-Karnik Intensity
I_{EMS}	Macroseismic Intensity according to the EMS-98
k	stiffness, wave number in x- direction (P & S_V)
k_s^*, k_r^*	complex wave numbers of the sediment or bedrock motion
K	horizontal force factor
K_g	vulnerability index of the ground (NAKAMURA, 2000)
L	principal building dimension (length) in affected direction
L_g	Love wave
m	mass, integer, wave number in z-direction (P)
m_b	body wave magnitude
M	magnitude
M_d	duration magnitude
M_L	local magnitude, Richter magnitude
M_s	surface wave magnitude
M_w	moment magnitude
n	integer, wave number in z-direction (S_V)
N	number of stories, standard penetration resistance of soil, integer
N_{SPT}	standard penetration resistance of soil
p	spectral exponent
P	primary waves, compressional waves
$P\uparrow, P\downarrow$	P propagator term either in the up- ($\uparrow$) or downward ($\downarrow$) direction
PF_i	participation factors of ith mode
PI	plasticity index
Q_y	yield strength, maximum base shear
r_x, r_y, r_z	rotations around the x-, y-, and z-axis
$\vec{r}(z)$	stress motion vector
R	(seismic source) distance parameter, seismic load reduction factor
R_e	epicentral distance
R_g	Rayleigh waves
R_y	yield strength ratio
S	secondary waves, shear waves, soil parameter
S_a	spectral acceleration
S_d	spectral displacement
S_v	spectral velocity
$S\uparrow, S\downarrow$	S propagator term either in the up- ($\uparrow$) or downward ($\downarrow$) direction
S_a/a	normalized response spectra, amplification function
$S_e(T)$	ordinate of elastic response spectrum
S_A, S_S	coefficient considering soil conditions

S_H	hoizontal shear waves
S_V	vertical shear waves
t	time, plate thickness
T	period
T^*	corner period
T_A, T_B	corner periods
T_B, T_C	corner periods describing the plateau range of a design spectrum
T_G	predominant period of earthquake ground motion
T_s	natural/predominant site period
T_n	natural period of the structure, first mode period
$T_{n,exp}$	experimental identified natural period of the structure
u_s	ground motion at the free surface, undrained shear strength
u_r	ground motion at halfspace
u_x, u_y, u_z	translations in x-, y-, and z-direction
v_p	compressional wave velocity
v_s	shear wave velocity
$v_{s,30}$	average shear wave velocity of the uppermost 30 m soil layers
v_R	Rayleigh wave velocity
V	vertical component of ground motion, base shear
V_b	base shear, lateral force
V_{design}	static design lateral force
V_{max}	max. induced dynamic lateral force (base shear)
W	weight of the SDOF (total dead load)
z	(soil) depth
α	constant, angle, modal mass coefficient, building importance factor
α_z	impedance contrast
α_z^*	complex impedance contrast
β	constant, angle, coefficient for cyclic loading effect, amplification factor
β_0	amplification factor of spectral acceleration
γ	shear strain
γ_{ref}	reference shear strain
$\delta, \ni$	roof displacement
δ_m	maximum response deformation
δ_u	ultimate deformation under static loading
#	standard normal variable
)	wave length
%	damping-correction coefficient
(	ductility factor
v	Poisson's ratio
ξ	damping factor, viscous damping inherent in the structure
ξ_0	hysteretic damping (equivalent viscous damping)
ξ_{eq}	"equivalent" damping
ρ	mass density
$\rho_i \cdot v_{s,i}$	impedance of a soil material i

σ	normal stress, standard deviation
τ	topographic amplification factor, shear stress
ϕ	phase angle, aperture angle, wedge angle of surface topography
$\vartheta_{dr,i}$	interstory drift ratio desribing damage state i
ω	angular (circular) frequency

ADRS	spectral acceleration-spectral displacement response spectrum
CP	Collapse Prevention (*SDL* in FEMA 273)
CRAD	capacity range of actual damage pattern
CSM	capacity spectrum method
DG	Damage Grade (EMS-98)
DP	States of Damage Pattern
DS	Structural Damage States (HAZUS®99)
FAS	Fourier amplitude spectrum
FFT	Fast-Fourier-Transformation
HVNR	Horizontal-to-vertical noise ratio
HVSR	Horizontal-to-vertical spectral (earthquake) ratio
IO	Immediate Occupancy (*SDL* in FEMA 273)
KLA	knowledge level seismic action
KLS	knowledge level structural properties
LS	Life Safety (*SDL* in FEMA 273)
PGA	peak ground acceleration
PGV	peak ground velocity
RC	reinforced concrete
SASD	spectral acceleration-spectral displacement domain
SBSR	surface-borehole spectral ratio
SC	site class, subsoil class (site-specific subsoil class according to DIN 4149)
SDOF	single degree of freedom system
SPL	Structural Performance Level (as defined in FEMA 273)
SPT	Standard Penetration Test
SRET	site response estimation technique
SRSR	sediment-rock spectral ratio (*SSR*)
SRSS	square root of the sum of squares
SSR	standard spectral ratio (*SRSR*)
TF	transfer function of local subsoil profile
TF_{theo}	theoretical transfer function
TF_{quasi}	experimental ("quasi") transfer function
VPD	verifying parameter: damage

References

ABEKI, N., K. SEO, I. MATSUDA, T. ENOMOTO, D. WATANABE, M. SCHMITZ, H. RENDON & A. SÁNCHEZ (1998a): Microtremor observation in Caracas City, Venezuela. In: IRIKURA, KUDO, OKADA & SASATANI (eds.): *Proceedings* of the Symposium on the Effects of Surface Geology on Seismic Motion, Yokohama, October 1998.

ABEKI, N., D. WATANABE & J. AVENDANO (1998b): Microtremor observation in Cumaná City, Venezuela. In: IRIKURA, KUDO, OKADA & SASATANI (eds.): *Proceedings* of the Symposium on the Effects of Surface Geology on Seismic Motion, Yokohama, October 1998.

ABRAHAMCZYK, L., C. SCHOTT, T.M. SWAIN & J. SCHWARZ (2004): Vulnerability of RC frame structures in Turkish earthquake regions (Part 2): Modeling and analysis. In preparation. *Proceedings* of the 13th World Conference on Earthquake Engineering, Vancouver/Canada, 2004.

AFET (1998): The Adana, Turkey, earthquake of June 28, 1998: duration magnitudes (M_d) and localization of aftershocks. *Internal document.* AFET İşleri Genel Müdürlüğü, Deprem Araştırma Dairesi Başkanlığı, Ankara/Türkiye, 1998.

AKI, K. (1957): Space and time spectra of stationary stochastic waves, with special reference to microtremors. *Bulletin of the Earthquake Research Institute Tokyo* **35** (1957), pp. 415-456.

AKI, K. (1988): Local site effects on strong ground motion. *Proceedings* of the Geotechnical Engineering Division, American Society of Civil Engineers (ASCE), New York, 1988.

AKKAR, S. & P. GÜLKAN (2002): A critical examination of near-field accelerograms from the Sea of Marmara Region earthquakes. *Bulletin of the Seismological Society of America* **92**, 1, pp. 428-447, February 2002.

AMBRASEYS, N.N., K.A. SIMPSON & J.J. BOMMER (1996): Prediction of horizontal response spectra in Europe. *Earthquake Engineering and Structural Dynamics* **25**: 371-400, 1996.

AMBRASEYS, N.N., P. SMIT, R. BERARDI, D. RINALDIS, F. COTTON & C. BERGE (2000): Dissemination of European Strong-Motion-Data, CD-ROM-Collection, 2000.

AMBRASEYS, N.N. & J. DOUGLAS (2003): Near-field horizontal and vertical earthquake ground motions. *Soil Dynamics and Earthquake Engineering* **23** (2003), pp. 1-18.

ANSARY, M.A., M. FUSE, F. YAMAZAKI & T. KATAYAMA (1995): Use of microtremors for the estimation of ground vibration characteristics. *Proceedings* of the Third International Conference on Recent Advances in Geotechnical Earthquake Engineering and Soil Dynamics, April 2nd - 7th, 1995, Volume II, St. Louis/Missouri.

ARAI, H. & K. TOKIMATSU (1998): Evaluation of local site effects based on microtremor H/V spectra. In: IRIKURA, KUDO, OKADA & SASATANI (eds.): The Effects of Surface Geology on Seismic Motion. Balkema, Rotterdam, 1998.

ARAI, H., H. HIBINO, Y. OKUMA, M. MATSUOKA, T. KUBO & F. YAMAZAKI (2000): Estimation of ground motion characteristics and damage distribution in Golcuk, Turkey, based on microtremor measurements. *Proceedings* of the Sixth International Conference on Seismic Zonation (6th ICSZ), Earthquake Engineering Research Institute (EERI), Palm Springs/CA, 2000.

ATHANASOPOULOS, G.A., P.C. PELEKIS & E.A.LEONIDOU (1998): Effects of surface topography and soil conditions on the seismic ground response - including liquefaction - in the Egion (Greece) 15/6/1995 earthquake. *Proceedings* of the Eleventh European Conference on Earthquake Engineering (11th ECEE), Paris/France, 1998.

BAKIR, B.S., H. SUCUOGLU & T. YILMAZ (2002): An overview of local site effects and the associated building damage in Adapazari during the 17 August 1999 Izmit earthquake. *Bulletin of the Seismological Society of America* **92**, 1, pp. 509-526, February 2002.

BARD, P.-Y. (1995): Effects of surface geology on ground motion: Recent results and remaining issues. *Proceedings* of the 10th European Conference on Earthquake Engineering, Vienna, Austria. Balkema Rotterdam, G. Duma (Ed.), 1995.

BARD, P.-Y. & A. WIRGIN (1995): Effect of built environment on "free-field" motion for very soft, urbanised sites. *Proceedings* of the Third International Conference on Recent Advances in Geotechnical Earthquake Engineering and Soil Dynamics, Volume II, Paper No. 7.04, pp. 549-555, St. Louis/Missouri, 1995.

BARD, P.-Y. (1997): Local effects on strong ground motion: Basic physical phenomena and estimation methods for microzoning studies. Advanced Study Course on Seismic Risk (SERINA), 21st-27th September 1997, Thessaloniki/Greece.

BARD, P.-Y. (1998): Microtremor measurements: A tool for site effect estimation? Second International Symposium on the Effects of Surface Geology on seismic Motion - ESG98. Yokohama, Japan, December 1998.

BAYÜLKE, N. (1978): Tuğla yığma yapıların depremlerdeki davranışı, Deprem Araştrıma Enstitüsü Bülteni, **6** (22), pp. 26-41, 1978.

BELTRAN, C. & J.A. RODRIGUEZ (1995): Ambientes de sedimentacion fluvio-deltaica y su influencia en la magnificación de danos por sismos en la ciudad de Cumaná, Venezuela. II Coloquio Internacional de "Microzonificacíon Sísmica", V Reunión de Cooperación Interamericana, Corporiente, Cumaná, Venezuela, 1995.

BOATWRIGHT, J., J.B. FLETCHER & T.E. FUMAL (1991): A general inversion scheme for source, site and propagation characteristics using multiply recorded sites of moderate-sized earthquakes. *Bulletin of the Seismological Society of America* **81**, No. 5, pp. 1754-1782, October 1991.

BOLT, B.A. (1976): Nuclear Explosions and Earthquakes: The Parted Veil. Freeman, San Francisco, 1976.

BOLT, B.A., W.H. FREEMAN and COMPANY (1988): Earthquakes. Freeman, New York.

BOMMER, J., R. SPENCE, M. ERDIK, S. TABUCHI, N. AYDINOGLU, E. BOOTH, D. DEL RE & O. PETERKEN (2002): Development of an earthquake loss model for Turkish catastrophe insurance. *Journal of Seismology* **6**: 431-446, 2002.

BONAMASSA, O. & J.E. VIDALE (1991): Directional site resonances observed from aftershocks of the 18 October 1989 Loma Prieta earthquake. *Bulletin of the Seismological Society of America* **81**, No. 5, pp. 1945-1957, October 1991.

BONNET, G. & J.F. HEITZ (1995): Non-linear seismic response of a soft layer. *Proceedings* of the 10th European Conference on Earthquake Engineering, 1995.

BORCHERDT, R. (1970): Effects of local geology on ground motion near San Francisco Bay. *Bulletin of the Seismological Society of America* **60**, No. 1, pp. 29-61, February 1970.

BORCHERDT, R., G. GLASSMOYER, M. ANDREWS & E. CRANSWICK (1989): Effect of site conditions on ground motion and damage. *Earthquake Spectra* – Special Supplement: Armenia Earthquake Reconnaissance Report, August 1989.

BOUDEN-ROMDHANE, N., P. MECHLER, A.M. DUVAL, P. MÉNEROUD & S. VIDAL (2000): Microzoning the city of Tunis using both background noise and weak motions. *Proceedings* of the 12th World Conference on Earthquake Engineering, Auckland/New Zealand 2000.

BRAY, J.D. & A. RODRÍGUEZ-MAREK (1997): Geotechnical site categories. *Proceedings* of the First PEER-PG&E Workshop on Seismic Reliability of Utility Lifelines, San Francisco/CA, 1997.

BUDNY, M. (1984): Seismische Bestimmung der bodendynamischen Kennwerte von oberflächennahen Schichten in Erdbebengebieten der niederrheinischen Bucht und ihre ingenieurseismologische Anwendung. *Dissertation*. Geologisches Institut der Universität zu Köln, Sonderveröffentlichung Nr. **57**, 1984.

BUTTKUS, B. (1991): Spektralanalyse und Filtertheorie in der angewandten Geophysik. Springer-Verlag, 1991.

CAMELBEECK, T., T. VAN ECK, R. PELZING, L. AHORNER, J. LOOHUIS, H.W. HAAK, P. HOANG-TRONG & D. HOLLNACK (1994): The 1992 Roermond earthquake, the Netherlands, and its aftershocks. *Geologie en Mijnbouw* **73**, pp. 181-197, Kluwer Academic Publishers, 1994.

CELEBI, M., C. DIETEL, J. PRINCE, M. ONATE & G. CHAVEZ (1987): Site amplification in Mexico City (determined from 19 September 1985 strong-motion records and from recordings of weak motions). In: A.S. CAKMAK (ed.): Developments in Geotechnical Engineering **44**: Ground Motion and Engineering Seismology, Elsevier, 1987.

ÇELEBI, M. (2000): Revelations from a single strong-motion record retrieved during the 27 June 1998 Adana (Turkey) earthquake. *Soil Dynamics and Earthquake Engineering* **20** (2000), pp. 283-288.

ÇELEBI, M. (2003): Identification of site frequencies from building records. *Earthquake Spectra* **19**, No. 1, pp. 1-23, February 2003.

CHÁVEZ-GARCÍA, F.J. & P.-Y. BARD (1994): Site effects in Mexico City eight years after the September 1985 Michoacan earthquakes. *Soil Dynamics and Earthquake Engineering* **13** (1994), pp. 229-247.

CHÁVEZ-GARCÍA, F.J. & J. CUENCA (1998): Site effects and microzonation in Acapulco. *Earthquake Spectra* **14**, No. 1, pp. 75-93, February 1998.

CHÁVEZ-GARCÍA, F.J., G. PEDOTTI, D. HATZFELD & P.-Y. BARD (1990): An experimental study of site effects near Thessaloniki (Northern Greece). *Bulletin of the Seismological Society of America* **80**, No. 4, pp. 784-806, August 1990.

CHÁVEZ-GARCÍA, F.J., D. RAPTAKIS, K. MAKRA & K. PITILAKIS (2000): Site effects in Euroseistest: A comparison between observations and modeling. *Proceedings* of the 12th World Conference on Earthquake Engineering, Auckland/New Zealand, 2000.

CHAVÉZ-GARCIA, F.J., L.R. SÁNCHEZ & D. HATZFELD (1996): Topographic site effects and HVSR. A comparison between observations and theory. *Bulletin of the Seismological Society of America* **86**, No. 5, pp. 1559-1573, October 1996.

CHEN, C.-H. & L.-Y. CHEN (1995): Ground periods of Taipei basin. In: K. ISHIHARA (ed.): *Proceedings* of the 1st International Conference on Earthquake Geotechnical Engineering, IS-Tokyo 1995. Balkema Rotterdam, **1**, pp. 543-548, 1995.

CHERRY, S. & P.E. SALT (1971): A preliminary investigation of microtremor spectra in British Columbia. *Proceedings* of the First Canadian Conference on Earthquake Engineering, Vancouver/Canada, 1971.

CLOUGH R.W. & J. PENZIEN (1993): Dynamics of structures. Second edition. McGraw-Hill, 1993.

COMPUTERS AND STRUCTURES, INC. (CSI): ETABS Nonlinear, Extended Analysis of Building Systems, Version 8.11.

CRUZ, E.F., R. RIDDELL, L. FERNANDEZ & D. VALDIVIA (2000): A study of site amplification effects in Santiago based on earthquake records obtained from the Smasch Array. *Proceedings* of the 12th World Conference on Earthquake Engineering, Auckland/New Zealand, 2000.

CALIFORNIA STRONG-MOTION PROGRAM CSMIP: ftp://ftp.convsr.ca.gov/pub/dmg/csmip/. California Geological Survey.

DOBRY, R., I. OWEIS & A. URZUA (1976): Simplified procedures for estimating the fundamental period of a soil profile. *Bulletin of the Seismological Society of America* **66**, No. 4, pp. 1293-1321, August 1976.

DOBRY, R. & I.M. IDRISS (1978): Duration characteristics of horizontal components of strong-motion earthquake record. *Bull. Seism. Soc. Am.* **68** (1978) 5, pp. 1487-1520.

DOLŠEK, M. & P. FAYFAR (2001): Soft storey effects in uniformly infilled reinforced concrete frames. *Journal of Earthquake Engineering* **5**, No. 1 (2001), 1-12.

DUBOS, N., A. SOURIAU, M. SYLVANDER, C. PONSOLLES, G. SENECHAL, J.-F. FELS & S. CHEVROT (2002): Site effects in the city of Lourdes (France) and elements of seismic risk evaluation. Poster presentation at the 27th General Assembly of the European Geophysical Society (EGS), Nice/France, 2002.

DURVILLE, J.-L., J.-P. MÈNEROUD, P. MOUROUX & J.-M. SIMON (1985): Evaluation de l'aléa sismique local – Microzonage. In: Génie Parasismique, V. Davidovici ed., Presses des Ponts-et-Chaussées, pp. 239-264.

DUVAL, A.-M., J.-P. MÉNEROUD, S. VIDAL & P.-Y. BARD (1994): Usefulness of microtremor measurements for site effect studies. *Proceedings* of the 10th European Conference on Earthquake Engineering, Balkema Rotterdam, 1995.

DUVAL, A.-M., P.-Y. BARD, J.-P. MÉNEROUD & S. VIDAL (1995): Mapping site effect with microtremors. *Proceedings* of the 5th International Conference on Seismic Zonation, Nice/France, Vol. **II**, pp. 1522-1529, 1995.

DUVAL, A.-M., J.-P. MÉNEROUD, S. VIDAL & A. SINGER (1998): Relation between curves obtained from microtremor and site effects observed after Caracas 1967 earthquake. *Proceedings* of the 11th European Conference on Earthquake Engineering. Balkema Rotterdam, 1998.

EDUPRO CIVIL SYSTEMS, INC.: ProShake, Version 1.1. User's manual, 53 pp. Redmond/Washington.

ELTON, D.J. & J.R. MARTIN II (1989): Dynamic site periods in Charleston, SC. *Earthquake Spectra* **5**, No. 4, 1989.

ENDE, C. (2000): Development of a program for ground response analysis with respect to SASW and the Nakamura method. *Project work* **00:1**, Division of Soil and Rock Mechanics, Dept. of Civil and Environmental Eng., Royal Institute of Technology, Stockholm/Sweden, 2000.

ENDE, C. (2001): Präzisierung ingenieurseismologischer Kenngrößen auf der Grundlage von Bodenunruhemessungen und Nachbebenregistrierungen. *Diplomarbeit*. Bauhaus-Universität Weimar, Institut für Konstruktiven Ingenieurbau, 2001.

ENOMOTO, T., T. KURIYAMA, N. ABEKI, T. IWATATE, M. NAVARRO & M. NAGUMO (2000): Study on microtremor characteristics based on simultaneous measurements between basement and surface using borehole. *Proceedings* of the 12th World Conference on Earthquake Engineering, Auckland/New Zealand, 2000.

ERDIK, M., K. SESETYAN, M.B. DEMIRCIOĞLU, U. ÇELEP, Y. BIRO & E. UCKAN (2002): Sultandağı Earthquake – Turkey. Report by the Department of Earthquake Engineering, Kandilli Observatory and Earthquake Research Institute, Boğaziçi University. http:\\www.koeri.boun.edu.tr .

FÄH, D., C. IODICE, P. SUHADOLC & G.F. PANZA (1993): A new method for the realistic estimation of seismic ground motion in megacities: the case of Rome. *Earthquake Spectra* **9**, No. 4, pp. 643-649, 1993.

FÄH, D. & G.F. PANZA (1994): Realistic modelling of observed seismic motion in complex sedimentary basins. *Annali di Geofisica* **37**, No. 6, pp. 1771-1797, December 1994.

FÄH, D., P. SUHADOLC, ST. MUELLER & G.F. PANZA (1994): A hybrid method for the estimation of ground motion in sedimentary basins: Quantitative modelling for Mexico City. *Bulletin of the Seismological Society of America* **84**, No. 2, pp. 383-399, April 1994.

FÄH, D. & P. SUHADOLC (1994): Application of numerical wave-propagation techniques to study local soil effects: The case of Benevento (Italy). *PAGEOPH* **143**, No. 4, pp. 513-536, 1994.

FÄH, D., T. NOACK, P. KRUSPAN & E. RÜTTENER (1996): Microzonation of the city of Basel (Switzerland) based on numerical simulations and in-situ measurements. *Proceedings* of the 11th World Conference on Earthquake Engineering, Mexico City, 1996, Paper No. 727.

FÄH, D. & F. KIND & D. GIARDINI (2001): A theoretical investigation of average H/V ratios. *Geophys. J. Int.* (2001) **145**, pp. 513-536.

FAJFAR, P. (2000): A nonlinear analysis method for performance based seismic design. *Earthquake Spectra* **16**, No. 3, pp. 573-592, August 2000.

FAUST, L.Y. (1951): Seismic velocity as a function of depth and geologic time. *Geophysics: a Journal of general and applied Geophysics* **16**, 1951.

FARBIARZ, J., J.D. JARAMILLO & M.R. VILLARRAGA (2000): Microzonation of the city of Medellín. *Proceedings* of the 12th World Conference on Earthquake Engineering, Auckland/New Zealand, 2000.

FIELD, E.H. & K.H. JACOB (1993): The theoretical response of sedimentary layers to ambient seismic noise. *Geophysical Research Letters* **20**, No. 24, pp. 2925-2928, December 1993.

FIELD, E.H., K.H. JACOB & S.E. HOUGH (1992): Earthquake site response estimation: A weak-motion case study. *Bulletin of the Seismological Society of America* **82**, No. 6, pp. 2283-2307, December 1992.

FIELD, E.H. & K.H. JACOB (1995): A comparison and test of various site-response estimation techniques, including three that are not reference-site dependent. *Bulletin of the Seismological Society of America* **85**, No. 4, pp. 1127-1143, August 1995.

FIELD, E.H., A.C. CLEMENT, K.H. JACOB, V. AHARONIAN, S.E. HOUGH, P.A. FRIBERG, T.O. BABAIAN, S.S. KARAPETIAN, S.M. HOVANESSIAN & H.A. ABRAMIAN (1995): Earthquake site-response study in Giumri (formerly Leninakan), Armenia, using ambient-noise observations. *Bulletin of the Seismological Society of America* **85**, No. 1, pp. 349-353, February 1995.

FIELD, E.H., S.E. HOUGH & K.H. JACOB (1990): Using microtremors to assess potential earthquake site response: A case study in Flushing Meadows, New York City. *Bulletin of the Seismological Society of America* **80**, No. 6, pp. 1456-1480, December 1990.

FLESCH, R. (1993): Baudynamik: praxisgerecht. Bd.1. Berechnungsgrundlagen. Unter Mitarb. von Horst Pacht. Bauverlag GmbH, Wiesbaden und Berlin, 1993.

FRANNTI, G.E. (1963): The nature of high-frequency earth noise spectra. *Geophysics* **28**, No. 4, pp. 547-562, August 1963.

FREEMAN, S.A. (1998): Development and use of capacity spectrum method. *Proceedings* of the 6th U.S. National Conference on Earthquake Engineering, Seattle, 1998.

FREEMAN, S.A., J.-P. NICOLETTI & J.V. TYRELL (1975): Evaluations of existing buildingsfor seismic risk – A case study of Puget Sound Naval Shipyard, Bremerton, Washington. *Proceedings* of the 1st U.S. National Conference on Earthquake Engineering, Berkeley/CA, 1975.

FUJIWARA, T., Y. SUZUKI & K. FUKUMOTO (2000): Response characteristics of soil and structures obtained from observation networks. *Proceedings* of the 12th World Conference on Earthquake Engineering, Auckland/New Zealand, 2000.

FUKUWA, N. & J. TOBITA (2000): Examination of estimated surface layer profiles based on soil data and microtremor records using observed seismic ground motions. *Proceedings* of the 12th World Conference on Earthquake Engineering, Auckland/New Zealand, 2000.

GALLIPOLLI, M.R., M. MUCCIARELLI, M. ARCIERI & V. LAPENNA (2002): Stability of HVSR from earthquakes and microtremors. Oral presentation at the 27th General Assembly of the European Geophysical Society (EGS), Nice/France, 2002.

GAULL, B.A., H. KAGAMI & H. TANIGUCHI (1995): The microzonation of Perth, western Australia, using microtremor spectral ratios. *Earthquake Spectra* **11**, No. 2, pp. 173-191, 1995.

GÉLI, L., P.-Y. BARD & B. JULLIEN (1988): The effect of topography on earthquake ground motion: a review and new results. *Bulletin of the Seismological Society of America* **78**, pp. 42-63, 1988.

GEOMATRIX CONSULTANTS (1993): Compilation of geotechnical data for strong-motion stations in the western United States. Report to Lawrence Livermore National Laboratory, Project No. 2256.

GHAYAMGHAMIAN, M.R., H. KAWAKAMI & H. MOGI (1995): Microtremor data analysis for seismic microzonation in north of Tehran. In: K. ISHIHARA (ed.): *Proceedings* of the 1st International Conference on Earthquake Geotechnical Engineering, IS-Tokyo 1995. Balkema Rotterdam, Vol. 1, pp. 561-566, 1995.

GIBBS, J.F. & E.F. ROTH (1989): Seismic velocities and attenuation from borehole measurements near the Parkfield prediction zone, central California. *Earthquake Spectra 5*, No. 3, 1989.

GOEL, R.K. & A.K. CHOPRA (1996): Evaluation of code formulas for fundamental period of buildings. *Proceedings* of the Eleventh World Conference on Earthquake Engineering, Acapulco/Mexico. Paper No. 1127, 1996.

GONZÁLEZ, J., M. SCHMITZ, F. AUDEMARD, R. CONTRERAS, A. MOCQUET, J. DELGADO & F. DE SANTIS (2002): Site and induced effects associated to the 1997 Cariaco earthquake. – intended to be published in *Tectonophysics* (Special Volume).

GRAIZER, V., A. SHAKAL & P. HIPLAY (2000): Recent data recorded from downhole geotechnical arrays. SMIP2000 – Seminar on Utilization of Strong-motion Data, *Proceedings*, pp. 23-38, Sacramento/CA.

GRÜNTHAL, G. (ed.), R. MUSSON, J. SCHWARZ & M. STUCCHI (1993): European Macroseismic Scale 1992 (updated MSK-scale). Cahiers du Centre Européen de Geodynamique et de Séismologie, Volume 7, Luxembourg, 1993.

GRÜNTHAL, G. (ed.), R. MUSSON, J. SCHWARZ & M. STUCCHI (1998): European Macroseismic Scale 1998. Cahiers du Centre Européen de Geodynamique et de Séismologie, Volume 15, Luxembourg, 1998.

GÜLKAN, P. & E. KALKAN (2002): Attenuation modeling of recent earthquakes in Turkey. *Journal of Seismology* **6**, pp. 397-409, 2002.

GÜLKAN, P., G. ÖZCEBE, H. SUCUOĞLU, S. BAKIR, Ö. ÇETIN, T. TANKUT, U. AKYÜZ, T. YILMAZ, A. PEKÖZ, S. BAYILI, V. AYDOĞAN, M. BARAN & U. YAZGAN (2002): 3 Şubat 2002 Sultandağı ve Çay Depremleri Mühendislik Raporu. Published on the internet: http://www.metu.edu.tr, 2002.

GÜRBÜZ, M., A. APAK, E. YARAR & T. KURU (2000): İvme-Yerel Zemin Kosulları Araşindaki İliski. In: DEMIRTAS, R. (ed.): 17 Ağustos 1999 İzmit Körfezi Depremi Raporu. Bayındırlık ve İskan Bakanlığı, AFET İşleri Genel Müdürlüğü, Ankara, Oktober 2000, 175-203.

GÜRBÜZ, M. & T. KURU (1998): Investigation results of seismic refraction measurements at the strong-motion sites that were established after the Adana-Ceyhan earthquake on June 27, 1998. AFET İşleri Genel Müdürlüğü, Deprem Araştırma Dairesi Başkanlığı, Ankara, 1998.

GUILLIER, B., K. ATAKAN, A.-M. DUVAL, M. OHRNBERGER, R. AZZARRA, F. CARA, J. HAVSKOV, G. ALGUACIL, P. TEVES-COSTA, N. THEODULIDIS & THE SESAME PROJECT WP02-TEAM (2002): Influence of instruments on H/V spectra of ambient noise. Poster presentation at the 27th General Assembly of the European Geophysical Society (EGS), Nice/France, 2002.

GURLER, E.D., Y. NAKAMURA, J. SAITA & T. SATO (2000): Local site effects of Mexico City based on microtremor measurement. *Proceedings* of the Sixth International Conference on Seismic Zonation. Earthquake Engineering Research Institute (EERI), Palm Springs/CA, 2000.

GUTENBERG, B. & C.F. RICHTER (1956): Earthquake magnitude, intensity, energy and acceleration. *Bulletin of the Seismological Society of America* **46**, pp. 105-145.

GUTIERREZ, C. & S.K. SINGH (1992): A site effect study in Acapulco, Guerrero, Mexico: Comparison of results from strong-motion and microtremor data. *Bulletin of the Seismological Society of America* **82**, No. 2, pp. 642-659, April 1992.

HABENBERGER, J., D. LANG & J. SCHWARZ (2001): Antwortspektren auf der Grundlage der Starkbeben-messungen im Erdbebengebiet der Türkei. *Thesis*, Wissenschaftliche Zeitschrift der Bauhaus-Universität Weimar, 1./2. Heft 2001, 47. Jahrgang, pp. 70-79, 2001.

HAMPE, E. (1985): Bauwerke unter seismischen Einwirkungen, Teil 2. Studienmaterial des Instituts für Aus- und Weiterbildung im Bauwesen, 1. Auflage, Leipzig, 1985.

HAMPE, E., C. RIEDEL & J. SCHWARZ (1990): Ergebnisse von Experimenten und Berechnungen zur Boden-Bauwerk-Wechselwirkung, Teil 1. Hochschule für Architektur und Bauwesen Weimar, Juli 1990.

HAMPE, E., R. GOLDBACH & J. SCHWARZ (1991): Verhalten von Bauwerken unter seismischen Einwirkungen. *Bautechnik* **68** (1991), H. 7.

HARDIN, B.O. & V.P. DRNEVICH (1970): Shear modulus and damping in soils II: design equations and curves. Technical report of University of Kentucky UKY, No. 26-2770CE2, Soil Mechanics Series, 1970.

HARDIN, B.O. & V.P. DRNEVICH (1972): Shear modulus and damping in soil: measurements and parameter effect. *Journal of the Soil Mechanics and Foundations Division*, ASCE, **98**: 603-624.

HARTZELL, S.H. (1992): Site response estimation from earthquake data. *Bulletin of the Seismological Society of America* **82**, No. 6, pp. 2308-2327, December 1992.

DE HERNÁNDEZ, M. & A. DE BARCIA (1999): Estudio comparativo entre sismos pequenos y registros de vibracion ambiental, para la determinacion de frequencias del suelo. VI Congreso Venezolano de Sismologia e Ingenieria Sismica, Mérida/Venezuela, Mayo 1999.

HILLER, D. (1985): Makroseismische Wirkungen des Albstadt-Bebens vom 3. September 1978 in Baden-Württemberg. *Dissertation*. Institut für Geophysik der Universität Stuttgart, 1985.

HOSSER, D. & K. KLEIN (1983): Realistische seismische Lastannahmen für Bauwerke mit erhöhtem Sekundärrisiko. Technical report, Kömnig & Heunisch, Frankfurt/M., 1983.

HOUGH, S.E., L. SEEBER, A. ROVELLI, L. MALAGNINI, A. DECESARE, G. SELVEGGI & A. LERNER-LAM (1992): Ambient noise and weak-motion excitation of sediment resonances: Results from the Tiber Valley, Italy. *Bulletin of the Seismological Society of America* **82**, No. 3, pp. 1186-1205, June 1992.

IBS-VON SEHT, M. (1996): Die seismische Bodenunruhe als Werkzeug zur Erkundung des geologischen Untergrundes. *Dissertation*. Aachener Geowissenschaftliche Beiträge, Band 16, 1996.

IDRISS, I.M. (1990): Response of soft soil during soil earthquakes. *Proceedings* of the H. Bolton Seed Memorial Symposium, pp. 273-290.

IKEMOTO, T., M. MIYAJIMA & M. KITAURA (2000): Inverse analysis of dynamic soil parameters using acceleration records. *Proceedings* of the 12th World Conference on Earthquake Engineering, Auckland/New Zealand, 2000.

IMPROTA, L., G. DI GULIO & A. ROVELLI (2002): Local site effects in the city of Benevento (Southern Italy) using weak-motion and microtremor recordings. Poster presentation at the 27th General Assembly of the European Geophysical Society (EGS), Nice/France, 2002.

JAFARI, M.K. (2000): Microtremor studies in South of Tehran. *Proceedings* of the 12th World Conference on Earthquake Engineering, Auckland/New Zealand, 2000.

JONGMANS, D. (1990): L'influence des structures géologiques sur l'amplification des ondes sismiques - measures in situ et modélisation. Université de Liège, Faculté des Sciences Appliquées, 1991.

JONGMANS, D. & M. CAMPILLO (1990): The 1983 Liège earthquake: Damage distribution and site effects. *Earthquake Spectra* **6**, No. 4, pp. 713-728, 1990.

KANAI, K. (1983): Engineering Seismology. University of Tokyo Press, 1983.

KANAI, K., T. TANAKA & K. OSADA (1954): Measurement of the micro-tremor. *Bulletin of the Earthquake Research Institute of Tokyo Univ.* **32**, pp. 199-209, 1954.

KANNO, T., K. KUDO, M. TAKAHASHI, T. SASATANI, S. LING & H. OKADA (2000): Spatial evaluation of site effects in Ashigara valley based on S-wave velocity structures determined by array observations of microtremors. *Proceedings* of the 12th World Conference on Earthquake Engineering, Auckland/New Zealand, 2000.

KATAOKA, S., M. MATSUI & T. SATO (1994): Using the microtremors to estimate the natural frequency of the site: A case study at Kuno, Ashigara valley blind prediction site (KS2) in Japan. In: G. DUMA (ed.): *Proceedings* of the 10th European Conference on Earthquake Engineering, Vienna/Austria. Balkema Rotterdam, 1995.

KIND, F., D. FÄH, F. STEIMEN, F. SALAMI & D. GIARDINI (2000): On the potential of microtremor measurements. *Proceedings* of the 12th World Conference on Earthquake Engineering, Auckland/New Zealand 2000.

KLIMIS, N.S., B.N. MARGARIS & P.K. KOLIOPOULOS (1999): Site-dependent amplification functions and response spectra in Greece. *Journal of Earthquake Engineering* **3**, No. 2 (1999) 237-270.

KOKUSHO, T., J. TOHMA, H. YAJIMA, Y. TANAKA, M. KANATANI & N. YASUDA (1994): Seismic response of soil layer and its dynamic properties. *Proceedings* of the 10th World Conference on Earthquake Engineering. Balkema Rotterdam, 1994.

KRAMER, S.L. (1996): Geotechnical Earthquake Engineering. *Prentice-Hall civil engineering and engineering mechanics series,* New Jersey, 1996.

KUDO, K. (1996): Practical estimates of site response; state-of-art report. *Proceedings* of the Fifth International Conference on Seismic Zonation, Volume III, pp. 1878-1907.

KUDO, K. & Z. WANG (1992): A preliminary analysis of strong motion in Ashigara valley test site; and errata. In: *Int. Symp. Effects of Surf. Geol. on Seismic Motion*, ESG 1992, Odawara/Japan, **3**, pp. 15-18.

KUDO, K., T. KANNO, H. OKADA, O. ÖZEL, M. ERDIK, T. SASATANI, S. HIGASHI, M. TAKAHASHI & K. YOSHIDA (2002): Site-specific issues for strong ground motions during the Kocaeli, Turkey, earthquake of 17 August 1999, as inferred from array observations of microtremors and aftershocks. *Bulletin of the Seismological Society of America* **92**, 1, pp. 448-465, February 2002.

KURAMA, Y., B. MORGEN & Q. SHEN (2000): Stress-strain behavior of Turkish reinforcing bars from the November 12, 1999 Duzce earthquake. *Technical Note*, Department of Civil Engineering and Geological Sciences, University of Notre Dame, Notre Dame/IN, February 2000, 12 pp.

KURITA, T., M. KAWAHARA, T. ANNAKA & S. TAKAHASHI (2000): Evaluation of local site effects in the Kanto district based on observation records. *Proceedings* of the 12th World Conference on Earthquake Engineering, Auckland/New Zealand, 2000.

KURIYAMA, T., T. ENOMOTO & T. MOCHIZUKI (2000): Microzoning of seismic intensity distribution considering site effects due to irregularity of subsurface soil structures. *Proceedings* of the 12th World Conference on Earthquake Engineering, Auckland/New Zealand, 2000.

LACHET, C. & P.-Y. BARD (1994): Numerical and theoretical investigations on the possibilities and limitations of Nakamura's technique. *J. Phys. Earth* **42**, pp. 377-397, 1994.

LACHET, C., M. BOUCHON, N. THEODULIDIS & P.-Y. BARD (1994): Horizontal to vertical spectral ratio and geological conditions. In: G. DUMA (ed.): *Proceedings* of the 10th European Conference on Earthquake Engineering, Vienna, Austria. Balkema Rotterdam, 1995.

LANG, K. (2002): Seismic vulnerability of existing buildings. *Dissertation*. Institute of Structural Engineering, Swiss Federal Institute of Technology (ETH) Zurich, 2002.

LANG, D. H. & J. SCHWARZ (2000): A comparison of site response estimation techniques: Case studies in earthquake-affected areas. *Proceedings* of the 6th International Conference on Seismic Zonation, Palm Springs/USA, 2000.

LANG, D.H., J. SCHWARZ & J. HABENBERGER (2000): Strong-motion data recorded during missions of German TaskForce. *Oral presentation.* 17th General Assembly of the European Seismological Commission (ESC), Lisbon/Portugal, 2000.

LANG, D.H. & J. SCHWARZ (2001): Herausarbeitung lokaler Standorteffekte auf der Grundlage von Nachbebenregistrierungen und Aufzeichnungen der seismischen Bodenunruhe. *Thesis*, Wissenschaftliche Zeitschrift der Bauhaus-Universität Weimar, (2001) Heft **1/2**, pp. 100-116.

LANG, D.H., J. SCHWARZ & C. ENDE (2002): The reliability of site response estimation techniques. 12th European Conference on Earthquake Engineering, London/UK, 2002.

LANG, D.H., J. SCHWARZ & C. ENDE (2003a): Subsoil classification of strong-motion recording sites in Turkish earthquake regions. *Schriftenreihe* der Bauhaus-Universität Weimar **116**, 2003.

LANG, D.H., M. RASCHKE & J. SCHWARZ (2003b): The Cariaco, Venezuela, earthquake of July 09, 1997: strong-motion recordings, site response studies and macroseismic investigations. *Schriftenreihe* der Bauhaus-Universität Weimar **116**, 2003.

LANG, D.H., C. ENDE & J. SCHWARZ (2004): Vulnerability of RC frame structures in Turkish earthquake regions (Part 1): Instrumental testing. In preparation. *Proceedings* of the 13th World Conference on Earthquake Engineering, Vancouver/Canada, 2004.

LANGER, H. (1986): Seismotektonische Herdparameter und Ausbreitungseffekte bei Mikroerdbeben im Bereich der westlichen Schwäbischen Alb. *Dissertation*. Institut für Geophysik der Universität Stuttgart, 1986.

LANGSTON, C.A. (1977): Corvallis, Oregon, crustal and upper mantle receiver structure from teleseismic P and S waves. *Bull. Seis. Soc. Am.* **67**, pp. 713-724.

LANGSTON, C.A. (1979): Structure under Mount Rainier, Washington, inferred from teleseismic body waves. *J. Geophys. Res.* **84**, pp. 4749-4762.

LAY, T. & T.C. WALLACE (1995): Modern global seismology. Volume 58 in the International Geophysics Series. Academic Press, 1995.

LEE, C.-J., C.-L. LIOU & B.-R. WU (1995): Microtremor measurements within the Taipei Basin. In: K. ISHIHARA (ed.): *Proceedings* of the 1st International Conference on Earthquake Geotechnical Engineering, IS-Tokyo 1995. Balkema Rotterdam, Vol. 1, pp. 567-572, 1995.

LEE, C.-T., C.-T. CHENG, C.-W. LIAO & Y.-B. TSAI (2001): Site classification of Taiwan free-field strong-motion stations. *Bulletin of the Seismological Society of America* **91**, 5, pp. 1283-1297, October 2001.

LERMO, J. & F.J. CHÁVEZ-GARCÍA (1993): Site effect evaluation using spectral ratios with only one station. *Bulletin of the Seismological Society of America* **83**, No. 5, pp. 1574-1594, October 1993.

LERMO, J. & F.J. CHÁVEZ-GARCÍA (1994): Are microtremors useful in site response evaluation? *Bulletin of the Seismological Society of America* **84**, No. 5, pp. 1350-1364, October 1994.

LERMO, J., M. RODRIGUEZ & S.K. SINGH (1988): The Mexico earthquake of September 19, 1985 – Natural period of sites in the valley of Mexico from microtremor measurements and strong motion data. *Earthquake Spectra* **4**, No. 4, pp. 805-814, 1988.

LÜDELING, R. (1976): Bodendynamische Untersuchungen des Baugrundes nach dem seismischen Aufzeitverfahren. *Geologisches Jahrbuch,* Reihe C, 12, Stuttgart, 1976.

LUSSOU, P., Y. FUKUSHIMA, P.-Y. BARD & F. COTTON (2000): Seismic design regulation codes: A proposal for improving site effect evaluation. *Proceedings* of the Sixth International Conference on Seismic Zonation. Earthquake Engineering Research Institute (EERI), Palm Springs/CA, 2000.

MALAGNINI, L., A. ROVELLI, S.E. HOUGH & L. SEEBER (1993): Site amplification estimates in the Garigliano Valley, Central Italy, based on dense array measurements of ambient noise. *Bulletin of the Seismological Society of America* **83**, No. 6, pp. 1744-1755, December 1993.

MARTIROSYAN, A., U. DUTTA, N. BISWAS, A. PAPAGEORGIOU & R. COMBELLICK (2002): Determination of site response in Anchorage, Alaska, on the basis of spectral ratio methods. *Earthquake Spectra* **18**, No. 1, pp. 85-104, February 2002.

MARUYAMA, Y., F. YAMAZAKI & T. HAMADA (2000): Microtremor measurements for the estimation of seismic motion along expressways. *Proceedings* of the Sixth International Conference on Seismic Zonation. Earthquake Engineering Research Institute (EERI), Palm Springs/CA, 2000.

MASAKI, K., K. SAGUCHI & A. SÁNCHEZ (1998): On the 1997 Cariaco earthquake and microtremor observation in Cariaco City, Venezuela. *Proceedings* of Hayama Seminar on Bul. Countries, Yokohama, 1998.

MASAKI, K., J. GONZÁLEZ, F. DE SANTIS, M. SCHMITZ, A. PERNÍA, A. SÁNCHEZ, K. SAGUCHI & H. DUQUE (1999): Characterización de los suelos de Cariaco mediante mediciones de ruido ambiental, sísmica de refraccíon y análisis de información geotécnica. VI Congreso Venezolano de Sismologia e Ingenieria Sismica, Mérida/Venezuela, Mayo 1999.

MAYER-ROSA, D. & M.-J. JIMÉNEZ (2000): Seismic Zoning. State-of-the-art and recommendations for Switzerland. *Geologische Berichte Landeshydrologie und -geologie* **26**, Bern, 2000.

MENKE, W., L. LERNER-LAM, B. DUBENDORFF & J. PACHECO (1990): Polarization and coherence of 5 to 30 Hz seismic wave fields at a hard-rock site and their relevance to velocity heterogeneities in the crust. *Bulletin of the Seismological Society of America* **80**, pp. 430-449.

MESKOURIS, K., H. SADEGH-AZAR, M. BÉRÉZOWSKY, H. DÜMLING & R. FRENZEL (2001): Schnellbewertung der Erdbebengefährdung von Gebäuden. *Bauingenieur* **76**, Heft 7/8 (2001), pp. 370-376.

MIRANDA, E. (2001): Estimation of inelastic deformation demands of SDOF systems. *Journal of Structural Engineering*, September 2001, pp. 1005-1012.

MOGI, H., H. KAWAKAMI & M.R. GHAYAMGHAMIAN (1995): Probability distributions of spectral ratios. In: K. ISHIHARA (ed.): *Proceedings* of the 1st International Conference on Earthquake Geotechnical Engineering, IS-Tokyo 1995. Balkema Rotterdam, Vol. **1**, pp. 573-578, 1995.

MOORE, F. (1979): Relationship between ground condition and earthquake damage to structures. Individual studies by participants at the International Institute of Seismology, 1979, pp. 279-312.

MADEN TETKIK VE ARAMA GENEL MÜDÜRLÜGÜ MTA (2002): Geological maps of the Republic of Türkiye (1:500.000), compiled by Z. Ternek, http://www.mta.gov.tr, 2002.

MUCCIARELLI, M. (1998): Reliability and applicability of Nakamura's technique using microtremors: An experimental approach. *Journal of Earthquake Engineering* **2**, No. 4 (1998), pp. 625-638, Imperial College Press.

MURPHY, J.R., A.H. DAVIS & N.L. WEAVER (1971): Amplification of seismic body waves by low-velocity surface layers. *Bulletin of the Seismological Society of America* **61**, No. 1, pp. 109-145, February 1971.

NAKAJIMA, Y., N. ABEKI & D. WATANABE (2000): Study on the stability of H/V spectral ratio of microtremor in short period range for the estimation of dynamic characteristics of surface geology. *Proceedings* of the 12th World Conference on Earthquake Engineering, Auckland/New Zealand, 2000.

NAKAMURA, Y. (1989): A method for dynamic characteristics estimation of subsurface using microtremor on the ground surface. *QR of RTRI* **30**, No. 1, February 1989.

NAKAMURA, Y. (1996): Real time information systems for seismic hazard mitigation UrEDAS, HERAS and PIC. *Quarterly Report of RTRI* **37**, No. 3, pp. 112-127.

NAKAMURA, Y. (2000): Clear identification of fundamental idea of Nakamura's technique and its applications. *Proceedings* of the 12th World Conference on Earthquake Engineering, Auckland/New Zealand, 2000.

NAKAMURA, Y., T. SATO & M. NISHINAGA (2000): Local site effects of Kobe based on microtremor measurement. *Proceedings* of the Sixth International Conference on Seismic Zonation (6th ICSZ). Earthquake Engineering Research Institute (EERI), Palm Springs/CA, 2000.

NAKAO, Y., K. TAMURA & S. KATAOKA (2000): Effects of earthquake source parameters on estimated ground motions. *Proceedings* of the 12th World Conference on Earthquake Engineering, Auckland/New Zealand, 2000.

NEWMARK, N.M. & W.J. HALL (1982): Earthquake spectra and design. Engineering Monographs on Earthquake Criteria, Structural Design, and Strong Motion Records. Earthquake Engineering Research Institute, 1982.

NOGOSHI, M. & T. IGARASHI (1971): On the amplitude characteristics of microtremor (Part 2*). Jour. seism. Soc. Japan* **24**, pp. 26-40 (in Japanese with English abstract).

ÖZEL, O., E. CRANSWICK, M. MEREMONTE, M. ERDIK & E. SAFAK (2002): Site effects in Avcilar, west of Istanbul, Turkey, from strong- and weak-motion data. *Bulletin of the Seismological Society of America* **92**, 1, pp. 499-508, February 2002.

ÖZMEN, B. (2000): Eş-şiddet haritası. In: R. DEMIRTAŞ (ed.): 17 Ağustos 1999 İzmit Körfezi Depremi Raporu. AFET İşleri Genel Müdürlüğü, Deprem Araştırma Dairesi Başkanlığı. Ankara/Türkiye, 2000.

OGAWA, Y., K. SHIMIZU, J. EJIRI & D. MAEJIMA (2000): Local site amplification of peak horizontal ground velocity based on microtremors. *Proceedings* of the 12th World Conference on Earthquake Engineering, Auckland/New Zealand, 2000.

OHMACHI, T., Y. NAKAMURA & S. NAKAMURA (1991a): Ground motion characteristics with reference to damage by the Philippine earthquake of July 16, 1990. *Proceedings* of the First International Conference on Seismology and Earthquake Engineering, Tehran/Islamic Republic of Iran, Vol. **I**, 1991.

OHMACHI, T., Y. NAKAMURA & T. TOSHINAWA (1991b): Ground motion characteristics of the San Francisco bay area detected by microtremor measurements. *Proceedings* of the Second International Conference on Recent Advances in Geotechnical Earthquake Engineering and Soil Dynamics, Paper No. LP08, pp. 1643-1648, St. Louis/Missouri, 1991.

OHTA, Y., H. KAGAMI, N. GOTO & K. KUDO (1978): Observation of 1- to 5-second microtremors and their application to earthquake engineering. Part I: Comparison with long-period accelerations at the Tokachi-Oki earthquake of 1968. *Bulletin of the Seismological Society of America* **68**, No. 3, pp. 767-779, June 1978.

OTANI, S. & T. MATSUMORI (1997): Correlation of damage and Analysis: Experience from the 1995 Kobe Earthquake. In: *Proceedings* of the 7th Int. Conf. on Computing in Civil and Build. Eng., Seoul/Korea, August 1997, pp. 19-21.

PARK Y.J. & A.H.-S. ANG (1985): Mechanistic seismic damage model for reinforced concrete. *Journal of Structural Engineering* **111** (4), pp. 740-754, 1985.

PAVLENKO, O.V. (2001): Nonlinear seismic effects in soils: Numerical simulation and study. *Bulletin of the Seismological Society of America* **91**, 2, pp. 381-396, April 2001.

PETERSEN, C. (1996): Dynamik der Baukonstruktionen. Friedr. Vieweg & Sohn Verlagsgesellschaft mbH, Braunschweig/Wiesbaden, 1996.

PLATE, E.J. & B. MERZ (eds.) (2001): Naturkatastrophen – Ursachen, Auswirkungen, Vorsorge. E. Schweizerbart'sche Verlagsbuchhandlung (Nägele u. Obermiller), Stuttgart, 2001.

RAHNAMA, M. & H. KRAWINKLER (1991): Analysis of damage potential of earthquake ground motions. *Proceedings* of the First International Conference on Seismology and Earthquake Engineering, Tehran/Islamic Republic of Iran, Vol. **I**, 1991.

RAPTAKIS, D., N. THEODULIDIS & K. PITILAKIS (1998): Data analysis of the Euroseistest strong motion array in Volvi (Greece): Standard and horizontal-to-vertical spectral ratio techniques. *Earthquake Spectra* **14**, No. 1, pp. 203-223, February 1998.

RASCHKE, M. (2001): Makroseismische Effekte des Kocaeli/Izmit (Türkei)-Erdbebens vom 17. August 1999. *Thesis*, Wissenschaftl. Zeitschrift der Bauhaus-Universität Weimar, 1./2. Heft 2001, 47. Jahrgang, 2001.

RATHJE, E.M., K.H. STOKOE II & B. ROSENBLAD (2003): Strong motion station characterization and site effects during the 1999 earthquakes in Turkey. *Earthquake Spectra* **19**, No. 3, pp. 653-675, August 2003.

RODRIGUEZ, V.H.S. & S. MIDORIKAWA (2000): Applicability of microtremor in evaluating site conditions of ground motion. *Proceedings* of the Sixth International Conference on Seismic Zonation. Earthquake Engineering Research Institute (EERI), Palm Springs/CA, 2000.

RODRÍGUEZ-GRANADOS, E.E., J. NIVIA, J. ALVARO & G. GONZALEZ (2000): Seismic wave amplification by local effects in Santa Fe de Bogota and Armenia, Colombia. Proceedings of the 12th World Conference on Earthquake Engineering, Auckland/New Zealand, 2000.

RODRÍGUEZ-MAREK, A., J.D. BRAY & N.A. ABRAHAMSON (2001): An empirical geotechnical seismic site response procedure. *Earthquake Spectra* **17**, No. 1, pp. 65-87, February 2001.

ROVELLI, A., S.K. SINGH, L. MALAGNINI, A. AMATO & M. COCCO (1991): Feasibility of the use of microtremors in estimating site response during earthquakes: Some test cases in Italy. *Earthquake Spectra* **7**, No. 4, pp. 551-561, 1991.

SAKAJIRI, N. (2000): Site amplification in Hachinohe observation site, Aomori, Japan: A comparison of S-waves, coda and microtremors spectral ratio. *Proceedings* of the 12th World Conference on Earthquake Engineering, Auckland/New Zealand, 2000.

DE SANTIS, F. & R. HERNÁNDEZ (1999): Caracterización de los suelos que liquaron durante el sismo del 9 de Julio de 1997 en Cariaco, Estado Sucre. VI Congreso Venezolano de Sismología e Ingeniería Sísmica, Mérida, 12-14 de Mayo de 1999, 10 pp.

SATO, K., S. HIGASHI, S. SASAKI & H. YAJIMA (2000): Effects of radiation pattern in local site effects of sedimentary basin. *Proceedings* of the 12th World Conference on Earthquake Engineering, Auckland/New Zealand, 2000.

SATOH, T., H. KAWASE & S. MATSUSHIMA (2001a): Estimation of S-wave velocity structures in and around the Sendai basin, Japan, using array records of microtremors. *Bulletin of the Seismological Society of America* **91**, 2, pp. 206-218, April 2001.

SATOH, T., H. KAWASE & S. MATSUSHIMA (2001b): Differences between site characteristics obtained from microtremors, S-waves, P-waves and codas. *Bulletin of the Seismological Society of America* **91**, 2, pp. 313-334, April 2001.

SATOH, T., H. KAWASE, T. IWATA, S. HIGASHI, T. SATO, K. IRIKURA & H.-C. HUANG (2001c): S-wave velocity structure of the Taichung basin, Taiwan, estimated from array and single-station records of microtremors. *Bulletin of the Seismological Society of America* **91**, 5, pp. 1267-1282, October 2001.

SCHERBAUM, F. (1993): Basic concepts in digital signal processing for seismologists. *Lecture Notes in Earth Sciences* **53**. Springer-Verlag, 1993.

SCHERBAUM, F., J. RIEPL, B. BETTIG, M. OHRNBERGER, F. COTTON & P.Y. BARD (2000): Dense array measurements of ambient vibrations in the Grenoble basin to study local site effects. 60. Jahrestagung der Deutschen Geophysikalischen Gesellschaft, München, 2000.

SCHMITZ, M. & J. GONZÁLEZ (1998): A review on seismic microzonation studies in Venezuela and changes in the new seismic building code. Contribution to: Workshop on "Joint Study on Seismic Microzonation in Earthquake Countries", Yokohama/Japan, 1998.

SCHOTT, C., T.M. SWAIN & J. SCHWARZ (2003): Calibration of nonlinear force-deformation relationships for RC frame systems with or without masonry infill walls and application of the Pushover analysis: Case studies on the basis of multistory RC structures representative for Turkish earthquake regions. *Unpublished technical report*, Earthquake Damage Analysis Center, Bauhaus-Universität Weimar, November 2003.

SCHWARZ, J., D.H. LANG & CH. GOLBS (1999): Erarbeitung von Spektren für die DIN 4149-neu unter Berücksichtigung der Besonderheiten deutscher Erdbebengebiete und der Periodenlage von Mauerwerksbauten. *Forschungsbericht* im Auftrage der Deutschen Gesellschaft für Mauerwerksbau e.V., Erdbebenzentrum am Institut für Konstruktiven Ingenieurbau der Bauhaus-Universität Weimar, Juli 1999 (1. Entwurf), September 1999 (Endfassung).

SCHWARZ, J., D. H. LANG, M. RASCHKE, H.-G. SCHMIDT, F. WUTTKE, M. BAUMBACH & J. ZSCHAU (2000): Lessons from Recent Earthquakes – Field Missions of German Task Force. *Proceedings* of the 12th World Conference on Earthquake Engineering, Auckland/New Zealand, 2000.

SCHWARZ, J., D.H. LANG & M. RASCHKE (2000): Die Erdbeben in der Türkei am 17.08.1999 und 12.11.1999. Ein Beitrag zur Ingenieuranalyse der Erdbebenschäden. *Bautechnik* **77**, Heft 5, Mai 2000.

SCHWARZ, J., C. ENDE, J. HABENBERGER, D.H. LANG & M. RASCHKE (2002a): Engineering analysis of strong-motion data recorded during German TaskForce missions to Turkey (1998-2000). *Poster presentation.* 27th General Assembly of the European Geophysical Society (EGS), Nice/France, 2002.

SCHWARZ, J., C. ENDE, J. HABENBERGER, D.H. LANG, M. BAUMBACH, H. GROSSER, C. MILKEREIT, S. KARAKISA & S. ZÜNBÜL (2002b): Horizontal and vertical response spectra on the basis of aftershock recordings from the 1999 Izmit (Turkey) earthquake. *Poster presentation.* 28th General Assembly of the European Seismological Commission (ESC), Genoa/Italy, 2002.

SCHWARZ, J., C. ENDE, J. HABENBERGER & D.H. LANG (2003): Site-dependent spectra from the 1999 Turkey earthquakes considering different sets of strong-motion data. *Poster presentation.* EGS-AGU-ESC Joint Assembly, Nice/France, 2003.

SCHWARZ, J. & H. MAIWALD (2003): Analytische Standortuntersuchungen im Vergleich zu den Registrierungen in seismisch instrumentierten Tiefenbohrungen. *Schriftenreihe* der Bauhaus-Universität Weimar **116**, 2003.

SCHWARZ, J., L. ABRAHAMCZYK, D.H. LANG & H. MAIWALD (2004): Ingenieuranalyse von Erdbebenschäden: Das Bingöl (Türkei) Erdbeben vom 1. Mai 2003. *Bautechnik* **81**, Heft 6, Juni 2004.

SEED, H.B. & I.M. IDRISS (1969): Influence of local soil conditions on building damage potential during earthquakes. *EERC* 69-15, 1969.

SEED, H.B. & I.M. IDRISS (1982): Ground motions and soil liquefaction during earthquakes. Earthquake Engineering Research Institute, Berkeley/CA, 1982.

SEED, H.B., I.M. IDRISS & F.W. KIEFER (1969): Characteristics of rock motions during earthquakes. *Journal of the Soil Mechanics and Foundations Devision,* ASCE, **95**, No. SM5, pp. 1199-1218, 1969.

SEED, H.B., C. UGAS & J. LYSMER (1976): Site-dependent spectra for earthquake-resistant design. *Bulletin of the Seismological Society of America* **66**, pp. 221-243, 1976.

SEO, K., (1997): Comparison of measured microtremors with damage distribution. JICA Research and Development Project on Earthquake Disaster Prevention, pp. 306-320.

SEO, K., H. YAMANAKA, K. KURITA, K. MOTOKI, K. ETO, M. TERASAKA & H. KOBAYASHI (2000): A joint research on microtremors in Fukui basin, Japan – For site effects evaluation during the 1948 Fukui (Japan) earthquake. *Proceedings* of the 12th World Conference on Earthquake Engineering, Auckland/New Zealand, 2000.

SILVA, W. (1991): Site geometry and global characteristics. *Proceedings* of thee NSF/EPRI workshop on dynamic soil properties and site characterization, EPRI NP-7337, **1**, pp. 6.1-6.80.

SMIT, P. (1996): Datenerfassung und Bestimmung der Abminderung der Bodenbewegung bei Erdbeben in der Schweiz. *Dissertation.* Publikationsserie des Schweizerischen Erdbebendienstes No. 108, Eidgenössische Technische Hochschule Zürich, 1996.

SOKOLOV, V., C.-H. LOH & K.-L. WEN (2000): Empirical study of sediment-filled basin response: The case of Taipei City. *Earthquake Spectra* **16**, No. 3, August 2000.

SPONHEUER, W. & V. KARNIK (1964): Neue seismische Skala. In: Sponheuer, W., (Ed.), *Proc.* 7th Symposium of the ESC, Jena, 24-30 Sept. 1962, Veröff. Inst. f. Bodendyn. u. Erdbebenforsch. Jena d. Deutschen Akad. d. Wiss., No 77, pp. 69-76.

STEINMÜLLER, B. (1987): Seismische Übertragungsfunktionen für typische Sedimentfolgen in Baden-Württemberg. *Dissertation.* Institut für Geophysik der Universität Stuttgart, 1987.

STEINWACHS, M. (1974): Systematische Untersuchungen der kurzperiodischen seismischen Bodenunruhe in der Bundesrepublik Deutschland. *Geologisches Jahrbuch Reihe E* (Geophysik), Heft 3, Hannover 1974.

STEPHENSON, W.R. (2000): The dominant resonance response of Parkway basin. *Proceedings* of the 12th World Conference on Earthquake Engineering, Auckland/New Zealand, 2000.

STROHBACH, K. (1955): Zum Studium der mikroseismischen Bodenunruhe in Hamburg. *Zeitschrift für Geophysik* **21**, pp. 190-214, 1955.

STROHBACH, K. (1969): Über die Natur der elastischen Wellen der Seegangs-Mikroseismik. *Zeitschrift für Geophysik* **35**, pp.113-132, 1969.

STUDER, J. & A. ZIEGLER (1986): Bodendynamik. Springer Verlag, Berlin - Heidelberg - New York, 1986.

SWAIN, T.M. & J. SCHWARZ (2004): Formulation of a concept for assignment of damage grades according to the EMS-98 by consideration of associated damage patterns. *Internal technical report.* Earthquake Damage Analysis Center, Bauhaus-Universität Weimar, Januar 2004.

TABER, J.J. (2000): Comparison of site response determination techniques in the Wellington region, New Zealand. *Proceedings* of the 12th World Conference on Earthquake Engineering, Auckland/New Zealand, 2000.

TEVES COSTA, P. & M.L. SENOS (2000): Estimation of site effects using microtremor measurements and analytical modelling – Application to the Lower Tagus Valley, Portugal. *Proceedings* of the 12th World Conference on Earthquake Engineering, Auckland/New Zealand, 2000.

THEODULIDIS, N.P. & P.-Y. BARD (1995): Horizontal to vertical spectral ratio and geological conditions: an analysis of strong motion data from Greece and Taiwan (SMART-1*). Soil Dynamics and Earthquake Engineering* **14** (1995), pp. 177-197.

TOKIMATSU, K. (1995): Geotechnical site characterization using surface waves. In: K. ISHIHARA (ed.): *Proceedings* of the 1st International Conference on Earthquake Geotechnical Engineering, IS-Tokyo 1995. Balkema Rotterdam, Vol. 3, pp. 1333-1365, 1995.

TRIFUNAC, M.D. & A.G. BRADY (1975): On the correlation of seismic intensity scales with the peaks of recorded strong ground motion. *Bulletin of the Seismological Society of America* **65**, pp. 139-162, 1975.

TRIFUNAC, M.D. & M.I. TODOROVSKA (2000): Can aftershock studies predict site amplification factors? Northridge, CA, earthquake of 17 January 1994. *Soil Dynamics and Structural Engineering* **19** (2000), pp. 233-251.

TSUBOI, S., M. SAITO & Y. ISHIHARA (2001): Verification of horizontal-to-vertical spectral-ratio technique for estimation of site response using borehole seismographs. *Bulletin of the Seismological Society of America* **91**, No. 3, pp. 499-510, June 2001.

TSURUGI, M., M. TAI, A. KOWADA, Y. TATSUMI & K. IRIKURA (2000): Estimation of empirical site amplification effects using observed records. *Proceedings* of the 12th World Conference on Earthquake Engineering, Auckland/New Zealand, 2000.

TUCKER, B.E., J.L. KING, D. HATZFELD & I.L. NERSESOV (1984): Observations of hard-rock site effects. *Bulletin of the Seismological Society of America* **74**, No. 1, pp. 121-136, February 1984.

UDWADIA, F.E. & M.D. TRIFUNAC (1973): Comparison of earthquake and mircrotremor ground motions in El Centro, California. *Bulletin of the Seismological Society of America* **63**, pp. 1227-1253.

UETAKE, T. & K. KUDO (2000): The ground motion characteristics of Ashigara Valley, Japan. *Proceedings* of the 12th World Conference on Earthquake Engineering, Auckland/New Zealand, 2000.

ULUSAY, R., Ö. AYDAN, H. KUMSAR & H. SÖNMEZ (2000): Engineering geological characteristics of the 1998 Adana-Ceyhan earthquake, with particular emphasis on liquefaction phenomena and the role of soil behaviour. *Bulletin of the Engineering Geology Environment* (2000) **59**: 99-118, Springer-Verlag, 2000.

VUCETIC, M. & R. DOBRY (1991): Effect of soil plasticity on cyclic response. *Journal of Geotechnical Engineering,* ASCE, **117** (1), pp. 89-107.

WAGNER, J.-J., C. FRISCHKNECHT, P. ROSSET, M. SARTORI, C. SCHINDLER, C. BEER, D. MAYER-ROSA, E. RÜTTENER & P. SMIT (2000): Contribution au zonage sismique dans la vallée du Rhône, entre Sion et Brigue. Beitrag zur seismischen Zonierung des Rhonetals zwischen Sitten und Brig. *Geologische Berichte Landeshydrologie und -geologie* **25**, Bern, 2000.

WALD, D.J., V. QUITOIANO, T.H. HEATON & H. KANAMORI (1999a): Relationships between Peak Ground Acceleration, Peak Ground Velocity, and Modified Mercalli Intensity in California. *Earthquake Spectra* **15**, No. 3, August 1999.

WALD, D.J., V. QUITORIANO, L. DENGLER & J.W. DEWEY (1999b): Utilization of the Internet for rapid community seismic intensity maps. *Seismological Research Letters* **70**, No. 6, pp. 680-697.

WANG, J. G.Z.Q. & K.T. LAW (1994): Siting in earthquake zones. A.A. Balkema/Rotterdam/Brookfield, 1994.

WATABE, M., K. DAN, T. SATO & T. OKUMURA (1994): Microzonation and disaster mitigation. *Proceedings* of the 10th World Conference on Earthquake Engineering. 1994 Balkema Rotterdam, pp. 6535-6549.

WEISSENBURG, S. (1995): Beitrag zur Untersuchung der Standortabhängigkeit der Bodenbewegung bei Erdbeben infolge des Effektes der Bodenverstärkung. *Dissertation*, Hochschule für Architektur und Bauwesen Weimar, 1995.

WEN, K.-L., H.-Y. PENG, Y.-B. TSAI & K.-C. CHEN (2001): Why 1G was recorded at TCU129 site during the 1999 Chi-Chi, Taiwan, earthquake. *Bulletin of the Seismological Society of America* **91**, 5, pp. 1255-1266, October 2001.

WESSEL, P. & W.H.F. SMITH (2002): GMT - The Generic Mapping Tools, Version 3.4.1: http://gmt.soest.hawaii.edu.

YAMANAKA, H., M. DRAVINSKI & H. KAGAMI (1993): Continuous measurements of microtremors on sediments and basement in Los Angeles, California. *Bulletin of the Seismological Society of America* **83,** No. 5, pp. 1595-1609, October 1993.

YAMANAKA, H., N. YAMADA, H. SATO, S. OIKAWA, Y. OGATA, K. KURITA, K. SEO & Y. KINUGASA (2000): Exploration of basin structure by microtremor array technique for estimation of long-period ground motion. *Proceedings* of the 12th World Conference on Earthquake Engineering, Auckland/New Zealand, 2000.

YAMAMOTO, A. & Y. INAGAKI (1995): A site response analysis in Kushiro City during the 1993 Kushiro-Oki earthquake. In: K. ISHIHARA (ed.): *Proceedings* of the 1st International Conference on Earthquake Geotechnical Engineering, IS-Tokyo 1995. Balkema Rotterdam, Vol. 1, pp. 537-542, 1995.

Yang, J., T. Sato & X.-S. Li (2000): Nonlinear site effects on strong ground motion at a reclaimed island. *Canadian Geotechnical Journal* **37**, pp. 26-39 (2000).

YOUD, T.L., J.-P. BARDET, J.D. BRAY (eds.) (2000): *Earthquake Spectra* - Supplement A to Volume 16: Kocaeli, Turkey, Earthquake of August 17, 1999 reconnaissance report. Earthquake Engineering Research Institute (EERI), Publication Number 2000-03.

ZASLAVSKY, Y., A. SHAPIRA & A.A. ARZI (1998): Site response study in the Dead Sea area using earthquake and microtremors data. *Proceedings* of the 26th General Assembly of the European Seismological Commission (ESC) in Tel Aviv/Israel, pp. 258-262, 1998.

ZASLAVSKY, Y. & A. SHAPIRA (1998): The influence of topographical effects on seismic ground motion. *Proceedings* of the 26th General Assembly of the European Seismological Commission (ESC) in Tel Aviv/Israel, pp. 241-245, 1998.

ZHANG, W. & K. MATSUNAMI (2000): A comparison of site-amplification estimated from different methods using a strong motion observation array in Tangshan, China. *Proceedings* of the 12th World Conference on Earthquake Engineering, Auckland/New Zealand, 2000.

ZHAO, B., M. HORIKE & Y. TAKEUCHI (2000): Analytical study on reliability of seismic site-specific characteristics estimated from microtremor measurements. *Proceedings* of the 12th World Conference on Earthquake Engineering, Auckland/New Zealand, 2000.

ZHENZHONG, Z. & L. RUOQI (1995): The microzonation method reflecting earthquake disaster characteristics in loess deposit area. In: K. ISHIHARA (ed.): *Proceedings* of the 1st International Conference on Earthquake Geotechnical Engineering, IS-Tokyo 1995. Balkema Rotterdam, Vol. 1, pp.555-559, 1995.

Standards and guidelines

APPLIED TECHNOLOGY COUNCIL ATC (1978): Tentative Provisions for the Development of Seismic Regulations for Buildings. Report No. ATC3.06, 1978.

APPLIED TECHNOLOGY COUNCIL ATC (1996): ATC-40 – Seismic Evaluation and Retrofit of Concrete Buildings, Volume 1. Report No. SSC 96-01, Redwood City/CA, November 1996.

ASSOCIATION FRANCAISE DU GENIE PARASISMIQUE AFPS (1990): Recommendations AFPS-90 pour la redaction des regles relatives aux ouvrages et installations a realiser dans les regions sujettes aux seismes. Presse des Ponts et Chaussées, Paris/France, 1990.

DEUTSCHES INSTITUT FÜR NORMUNG DIN (2002): DIN 4149, Bauten in deutschen Erdbebengebieten. Berlin, 2002.

WORLD INSTITUTE FOR DISASTER RISK MANAGEMENT DRM (2002): Seismic Microzonation Manual, Microzonation for Earthquake Risk Mitigation Project in Turkey (DRM-MERM). J. Studer (ed.), Zürich, 2002.

EUROPEAN COMMITTEE FOR STANDARDIZATION CEN (1992): ENV 1992-1-1, Eurocode 2: Design of Concrete Structures. Part 1.1: General Rules: General Rules and Rules for Buildings. 1992.

EUROPEAN COMMITTEE FOR STANDARDIZATION CEN (2002): prEN 1998-1:200x, Eurocode 8: Design of structures for earthquake resistance, Part 1: General rules, seismic actions and rules for buildings. Draft No. 5, May 2002. Doc CEN/TC250/SC8/N317. Brussels, 2002.

EUROPEAN COMMITTEE FOR STANDARDIZATION CEN (2003): prEN 1998-3:200x, Eurocode 8: Design of structures for earthquake resistance, Part 3: Strengthening and repair of buildings. Draft No. 4, July 2003. Doc CEN/TC250/SC8/N371. Brussels, 2003.

FEDERAL EMERGENCY MANAGEMENT AGENCY FEMA (1997): NEHRP Guidelines for the Seismic Rehabilitation of Buildings (FEMA 273). FEMA Publication 273. Federal Emergency Management Agency and National Institute of Building Sciences, Washington D.C., 1997.

FEDERAL EMERGENCY MANAGEMENT AGENCY FEMA (1999): HAZUS®99 – Earthquake Loss Estimation Methodology. Federal Emergency Management Agency and National Institute of Building Sciences, Washington, D.C., 1999.

INTERNATIONAL CONFERENCE OF BUILDING OFFICIALS ICBO (1997): 1997 Uniform Building Code (1997-UBC). Whittier/CA, United States of America, 492 pp., 1997.

JAPAN ROAD ASSOCIATION (1980): Specification for highway bridges, Part V –Earthquake Resistant Design. Japan Road Association, 207 pp., 1980.

MINISTERIO DEL DESARROLLO URBANO MDU (1990): COVENIN (Provisional) 1756-82, Norma Venezolana - Edificaciónes Antisísmicas, CDU 721:550.34. Funvisis, Caracas/Venezuela, 1990.

TURKISH MINISTRY OF PUBLIC WORKS AND SETTLEMENT TMPS (1998): Specification for Structures to be built in Disaster Areas. Part III – Earthquake Disaster Prevention (Chapter 5-13). Effective from 1.1.1998. English translation, 84 pp., 1998.